CREEP CRACK GROWTH IN CAST STEAM TURBINE CASING STEELS

William Laidler

Thesis presented to the University of Aston in Birmingham for the degree of Doctor of Philosophy.

December 1978.

Creep Crack Growth in Cast Steam Turbine Casing Steels

William Laidler. Ph.D. December 1978

Summary

The creep rupture properties of cast ½Cr½Mo¼V and 1Cr1Mo¼V alloy steel used in the manufacture of power station steam generating plant, have been investigated. The effects of constraint and geometry on the creep rupture properties are also considered.

The validity of various criteria controlling macroscopic creep crack growth in cast CrMoV alloys has been examined. It is found that neither the stress intensity factor nor reference stress correlate satisfactorily the creep crack growth rates at the test temperature of 550°C. Certain minimum displacements must be achieved for crack initiation and propagation. It is found that this displacement as measured by crack opening displacement or crack aspect ratio, is the same in both compact tension and centre-cracked panel geometries, is invariant with crack length and decreases with increasing constraint. The effect of constraint on creep crack growth rate in the two geometries is less conclusive.

A new model describing creep crack growth in cast CrMoV alloy steels has been developed. The model is based on the results from a numerical finite element creep analysis of the relaxation and redistribution of stress ahead of an incubating creep crack. It is found that macroscopic creep crack growth in a material undergoing either plane stress or plane strain deformation can be described by a fracture stress which is based on the Von Mises equivalent stress. It has been shown that this model is capable of rationalising all of the experimental crack velocity data from the cast CrMoV alloys. The resultant degree of data correlation is far superior to that obtained when using the stress intensity factor or reference stress.

A cumulative damage creep fracture model based upon the results from the numerical analysis has been developed. It is found that the model is capable of predicting the behaviour of propagating creep cracks in cast CrMoV alloys from smooth bar creep rupture data.

Key Words. Creep Crack Growth. CrMoV Steel. Fracture Mechanics. Stress Analysis. Fracture Model.

CONTENTS

CHAPTER 1

Introduction

1.1 The Generation of Electricity

The Central Electricity Generating Board is required by law to provide a reliable and economic supply of electricity to the industrial and domestic user. The peak demands for electricity often approach the total generating capacity and supply can only be guaranteed by maintaining a high level of plant availability in those power stations with high output generating units. The development of the steam turbine from the 30MW sets of 30 years ago to the more efficient 500 and 600MW sets of today, has been achieved primarily because of better mechanical design. Improvements in steelmaking practice, fabrication techniques, quality control and alloy design, have also contributed to the development of the modern steam turbine and its immediate ancillary equipment namely, steam chests and steam control valve bodies (Figure 1). These factors are discussed in some detail in the following sections.

1.2 Turbine Technology

The purposes of turbine technology are to extract the maximum quantity of energy from the working fluid (water) and to convert it into work with maximum efficiency by means of plant having maximum reliability, minimum running cost and minimum starting time. The steam power station uses a closed cycle to enable the working fluid to be recycled, to allow the final pressure at which heat is rejected to be below atmospheric and to consume the heat in the condensate. The cycle used is the Rankine Cycle modified to include superheating, regenerative feedwater heating and, on modern stations, reheating. For maximum efficiency the temperature at which heat is added should be as high as possible and the temperature at which heat is rejected should be as low as possible. A higher pressure in the boiler

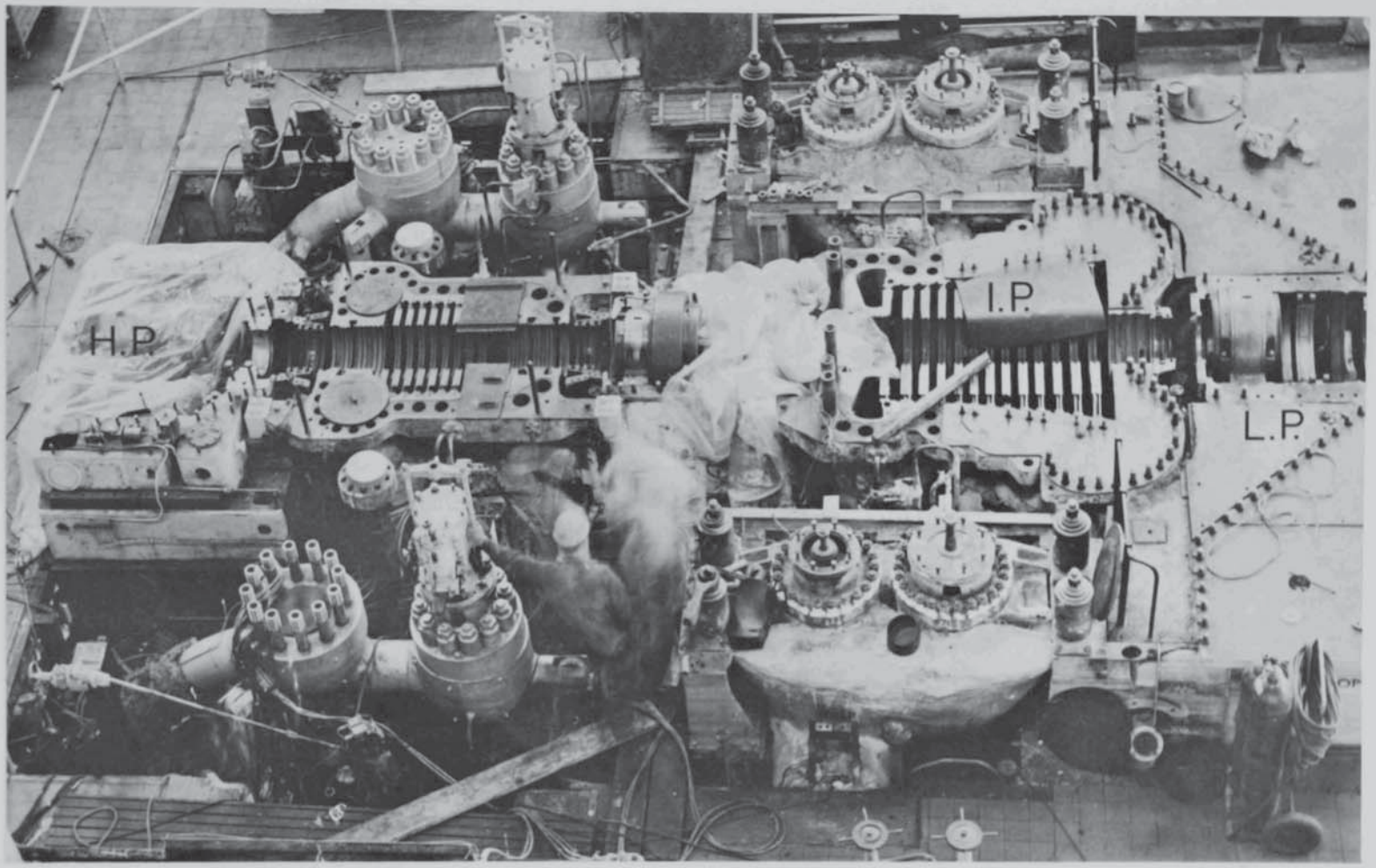

FIG. 1 A 120 MW STEAM TURBINE

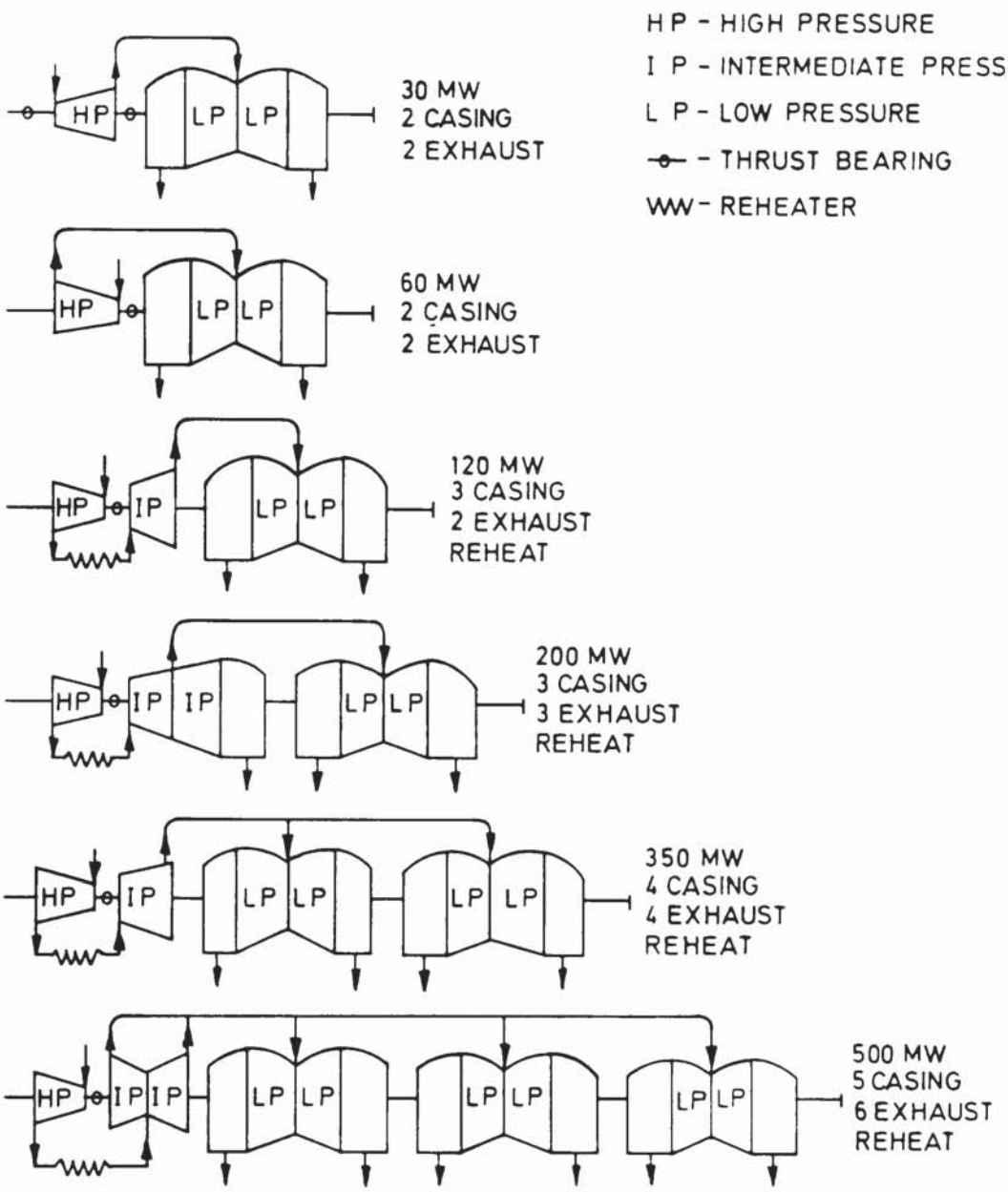

FIG. 2 TYPICAL TURBINE LAYOUTS

for example, raises the temperature at which latent heat is added thus increasing the cycle efficiency. However, it also has the effect of increasing the moisture content at the exhaust end of the turbine. This can have a detrimental effect on the integrity of the blades in the low pressure (L.P.) stage of a turbine. Thus, there is a limit to the pressure which can be used with a given steam temperature. A further method of increasing cycle efficiency is by increasing the mean temperature at which superheat is added. In addition, if the pressure of the steam remains unaltered, the effect on the turbine will be to cause a smaller part of the expansion to be in the wet region, giving a further improvement in turbine efficiency. Thus, superheat is doubly beneficial. The temperature of steam entering the turbine is, however, limited by the properties of the materials from which casings, steam chests and valves bodies are constructed. For ferritic steels the present limit is 550 to 565^{o}C.

In order to obtain full benefit from high steam conditions, large turbines are used; partly because of manufacturing savings and partly because losses become proportionately smaller. In these large turbines (greater than 100MW) it becomes economic to increase the cycle efficiency by using reheat. By returning partially expanded steam to a reheater and by expanding this reheated steam through the remaining stages of the turbine, the exhaust wetness is reduced. This has the effect of reducing the rate of erosion of the L.P. turbine blades.

1.3 Turbine Casings

A turbine casing is essentially a pressure vessel designed to withstand hoop stresses and to be very stiff in the longitudinal direction in order to maintain clearances between rotors and stators. A turbine may have one casing or if the length is such that additional bearings are required to support the shaft, it may have several casings. Figure 2 shows various typical turbine layouts. It can be observed that on larger sets where higher temperature steam is used, the

H.P. casing is reversed so as to minimise differential expansion. Where the steam conditions are high the H.P. casing is generally of a double shell design in which steam at exhaust pressure fills the space between the shells, enabling each shell to be designed for a relatively small pressure differential. The reduced shell thickness together with the increased area of contact between steam and metal, permits quicker warming up of the turbine when starting. Also, the work of the steelfounder is simplified, resulting in sounder castings. H.P. and I.P. casings are normally CrMoV creep resistant steel castings but L.P. casings, where temperature never exceeds 230°C, are sometimes made of cast iron. This is generally the case on non-reheat machines. On large reheat turbines however, the temperature of steam entering the L.P. stage may be more than 230°C. In this case, carbon steel castings or mild steel plates are used.

1.4 Steam Chests

Steam is admitted to a turbine from the superheater outlet via the high pressure main to the steam chest. This component houses the emergency stop valves and governing valves. The chest is normally made from a low alloy steel casting or in the case of very high steam conditions, from a solid forging. In some turbine designs the portion containing the governing valves may be contained in the H.P. casing. Unfortunately, such a component can be difficult to manufacture because of its complicated shape. The normal method of manufacture is to cast in two parts and then weld together. Although a proven design for low steam conditions, this type of multi-valve integral steam chest is unsuitable for steam temperatures above 480°C. Above this temperature, high surface and through thickness thermal stresses interacting with stress concentrations can cause cracking. Modern steam chests operating in high steam conditions are more simple in design and as a consequence, are less prone to thermally induced cracking.

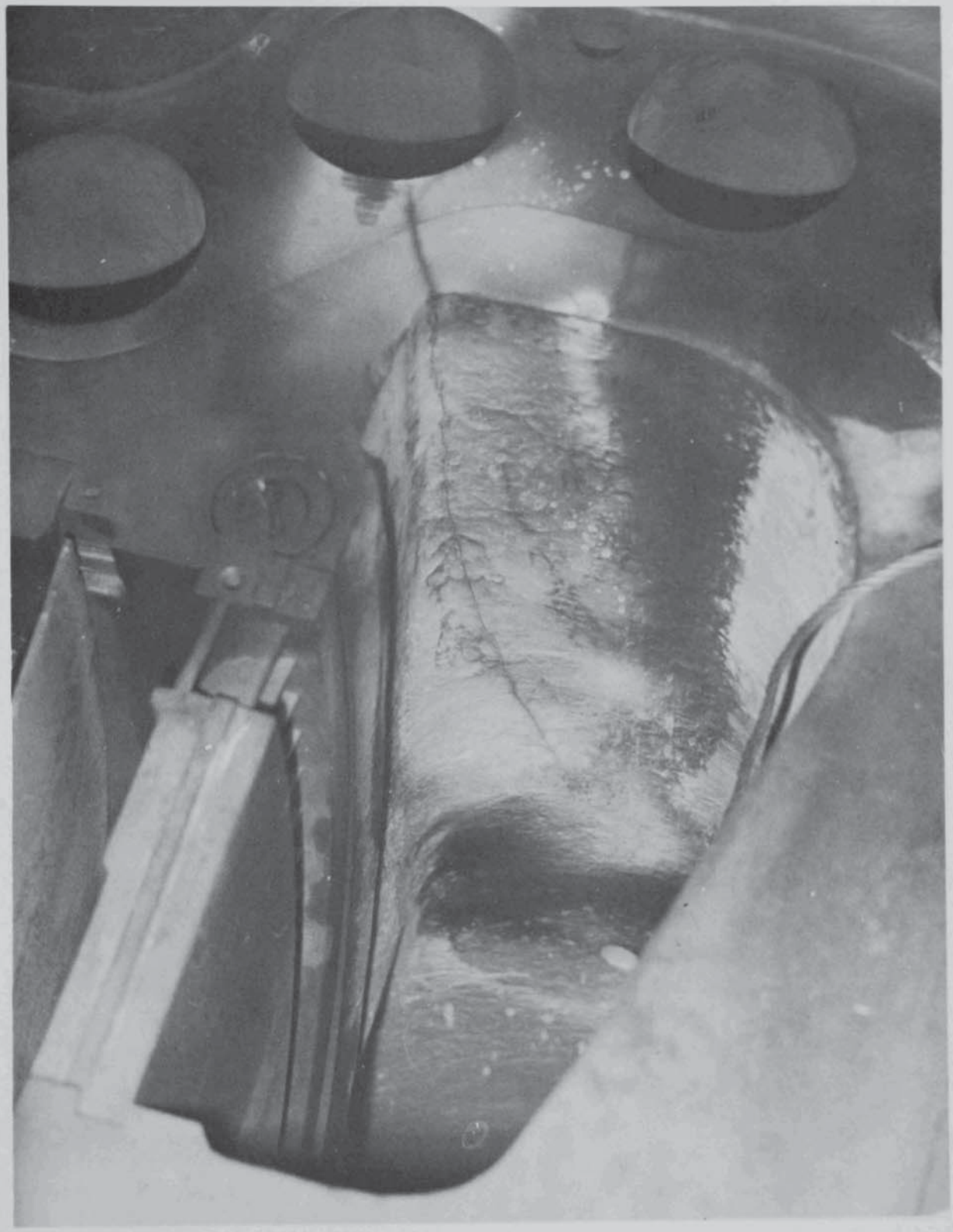

FIG. 3 CRACK IN I.P. CASING INLET STEAM BELT

1.5 Operating Conditions

The Grid system, which interconnects the generating stations, permits the stations to be loaded selectively to achieve the minimum cost of production at all times. Thus, the plant which is cheapest to operate runs continuously at full load (base load operation) and the stations which are more expensive to run operate at progressively lower load factors. The most expensive plant may operate for only a few hours during the peak load period (two-shift operation). As far as possible new stations of advanced design are so located geographically as to reduce to a minimum fuel delivery costs. They are likely therefore, to operate on base load for the initial part of their life. However, because of technological development these stations are eventually superseded by others which are more efficient and it is not unusual for a new station to be relegated to two-shift operation some five years after commissioning. The consequences of moving from base load to two-shift operation is that repeated thermal cycling can lead to the initiation and growth of thermal fatigue cracks in casings, steam chests and valve bodies. This can lead to a reduction in their operational life. Superimposed creep damage can also aggravate this problem particularly when steady-state thermal conditions are reached during two-shifting, or when turbines are returned to base load operation. An example of cracking in the inlet steam belt of an I.P. casing following base load and two-shift operation is shown in Figure 3. Creep damage alone is also known to reduce the integrity of components operating purely under base load conditions.

The high availability of efficient generating plant is of the greatest importance and much effort has been devoted to understanding the mechanisms of crack development in pressure vessels. The ultimate aim of this is the production of a defect acceptance standard so designed as to thoroughly test the fitness for purpose of the defective component. It is in this context that the present investigation on creep crack growth in cast CrMoV ferritic steels has been initiated.

1.6 Relevance of Present Work

The application of linear elastic fracture mechanics to describe creep crack growth in components undergoing time dependent deformation has been the subject of much debate during recent years. Many workers have argued the case for the stress intensity approach when material creep ductility is low and where constraint to deformation is high. Alternatively, post yield fracture mechanics concepts such as crack opening displacment, or general engineering concepts that include net section stress or reference stress, have been applied to more ductile materials. In general, design documents or defect acceptance standards covering macroscopic creep crack growth have been based on the stress intensity factor primarily because it provides a pessimistic and hence, safe life assessment. However, on the occasions where undue pessimism is built into standards, unnecessary rejection of material and loss of plant availability can result. This situation can only be improved by a more thorough understanding of the true crack tip stress distribution and of the events leading to the growth of creep cracks, neither of which are completely explained by linear elastic, post yield or general engineering fracture concepts. It is the aim of this Thesis to develop further the theoretical understanding of creep crack growth in low alloy steels and to examine the applicability of the above fracture concepts. This has been done by varying geometry, initial crack length and applied load, and the degree of crack tip constraint in laboratory specimens manufactured from two cast CrMoV alloys. These variables are particularly important because it is known that stress fields ahead of cracks in steam plant can contain both direct and bending components the proportion of which can vary as creep cracking develops. It is also known that bulk creep ductility of defect free materials can vary with applied load and with the degree of constraint to deformation; it was thought the same may also be true for local creep fracture events in the region ahead of macroscopic creep cracks. The experimental programme has been supported by a numerical and analytical analysis of the stress distribution ahead of incubating and growing creep cracks.

Literature Review

A brief account is given of the design of creep resisting steels and the philosophy behind their selection for high temperature cast steel turbine casings and steam chests. The design and fitness-for-purpose of these vessels is then discussed by referring to codes of practice and material standards.

The integrity of pressure vessels operating in the creep range can deteriorate with time; the conditions required for this are given together with examples of failures. The micro-mechanisms of creep and the effect of notches on creep rupture behaviour are then reviewed. Finally, after describing the development and limitations of fracture mechanics, its applicability to macroscopic creep crack growth is considered.

2.1 Alloy Design and Selection

Prior to the 1960's, high temperature steam turbine steel castings were manufactured from Mo bearing C/Mn steels. The addition of Mo to ferritic steels is known to be essential when good creep resistance is required above 450°C (Jamieson et al. 1972). Glen and Barr (1966) have shown that the addition of Mo increases the 10^5 hour creep rupture strength, the greatest increase in strength occurring with the first small additions. Creep experiments on normalised ½Mo and 1Mo steels tested at 550°C have shown that most of the initial strength comes from the Mo in solid solution (Jamieson et al. 1972; Johnson and Glen, 1972). Beyond 1000 hours however, a depletion of Mo in solid solution due to the precipitation of Mo carbides and nitrides can result in a reduction in creep strength.

Further alloy development has shown that in order to develop and maintain high creep strengths for times in excess of 10^5 hours and at temperatures around 565°C, both Cr and V must be added to the melt. Cr improves creep strength and ductility primarily by the mechanism of solid

solution strengthening (Baird et al. 1972), while V improves creep strength by the formation of very fine stable carbides in the matrix and along grain boundaries (Smith and Nutting, 1957; Dunlop and Honeycombe, 1976; 1977). Diehl et al. (1975) have demonstrated that Mo is still a very important constituent in creep resisting ferritic steels. From their observations on the effect of variable Mo content on the 30000 hour creep behaviour of a 1Cr½V steel at 550°C, Diehl and his co-workers concluded that optimum creep properties are attainable with 0.55% Mo.

The stability of carbides in ascending order, from studies during the tempering of quenched steels, are considered to be as follows (Sellars, 1972):-

$$Fe_3C < M_3C < M_{23}C_6, M_6C < M_7C_3 << VC, MO_2C$$

Dunlop (1972) considered the contribution of carbide dispersions to creep strength and ductility, and showed that the development of the optimum properties depends on many interrelated factors;

(1) The state of matrix dispersion; whether it is uniform, located on a dislocation network or banded due to precipitation during a parent phase transformation.

(2) Precipitation on prior austenite or ferrite grain boundaries.

(3) Precipitate free regions particularly near grain boundaries.

(4) Dynamic precipitation during service.

(5) High temperature stability of the dispersion in the matrix and the grain boundary.

Plumbridge and Miller (1972) considered that either solute drag or precipitate interaction was responsible for the creep strength of CrMoV alloys. The optimum creep strength was conferred by a fine and uniform distribution of vanadium carbide.

The heat treatment procedure normally adopted to develop a stable and finely dispersed carbide structure in CrMoV castings consists of a homogenising treatment followed by normalising and tempering. The actual temperatures and cooling rates are dependent upon the alloy composition and size of

casting. A casting may also be re-tempered following repair or cosmetic welding during the final stages of fabrication.

A statistical analysis of cast steels by Hoznek (1967), revealed that creep strength is partly dependent on the cleanliness of the steel. A major cause of poor creep properties is the presence of sulphide inclusions. These have been known to reduce the creep strength of grain boundaries (Roes and Witte, 1967) and the matrix (Baker and Charles, 1973). Baker and Charles observed that interconnected colonies of Type II MnS precipitating as extensive arrays of fine rods in an interdendritic eutectic distribution, provided an easy path for cracks. Similar observations on the deleterious effect of sulphides on creep properties have been made by McCann (1973) for a 500 MW 1CrMoV rotor forging.

The presence of certain trace elements (Sb, As etc.) are also known to reduce the creep properties of CrMoV steels (Tipler and Hopkins, 1976). These authors demonstrated that both creep ductility and the creep life of the steels when operating at 550^{o}C can be improved by reducing the level of trace elements.

The improvement in creep strength and maintenance of creep ductility offered by the CrMoV steels enabled a second generation of cast turbine components to be produced. The chosen steel was the 1Cr1Mo¼V low carbon alloy in the normalised and tempered condition. This alloy had adequate castability and weldability. Its relatively high creep strength also enabled wall thicknesses to be reduced thereby lowering thermal stresses. A disadvantage in using this alloy was its inability to produce a homogeneous microstructure in large sectioned castings following heat treatment. For example Kolorz and Orths (1965) observed a deterioration of mechanical properties in a cast CrMo and CrMoV steel with increasing distance from the surface of 300mm castings and with increasing wall thickness. The importance of a uniform structure in CrMoV castings was also recognised by Mirkin et al. (1965) and Murphy and Branch (1969). The shortcomings of the

1CrMoV alloy were also adequately demonstrated by Branch et al. (1973). They showed that mixed ferrite/bainite structures could form throughout the section in 50 to 500 MW turbine castings, following a conventional normalising treatment. These authors also demonstrated that the orientation of a casting affected the cooling rate. A casing for example, when normalised in the flange down position contained 5-7% bainite throughout.

An alternative steel capable of providing a homogeneous microstructure and possessing the necessary creep properties, is the ½Cr½Mo¼V alloy. This alloy has been chosen for the present generation of large turbine castings. When normalised from 950-980°C and tempered at 690-710°C, this alloy provides an improvement in creep ductility at little cost to creep strength. Economies in steelmaking are also obtained. A constant cooling transformation (C.C.T.) diagram of the ½Cr½Mo¼V and 1Cr1Mo¼V steels (Figures 4a and 4b) indicates that the ½Cr alloy should provide a more consistent transformation microstructure following normal heat treatment procedures. This has been verified by Branch et al. (1973) for a ½Cr½Mo¼V casing wall and flange.

2.2 Pressure Vessel Codes, Design Criteria and Material Standards

Current design codes and material specifications are concerned mostly with assessing the basic scantlings. They evolve normally from many years of experience of material and component behaviour, and are based on sound engineering practice. The codes in common use in the United Kingdom are provided by the British Standards Institution (B.S.), the American Society of Mechanical Engineers (A.S.M.E.) and the International Standards Organisation (I.S.O.).

There are many British Standards covering the design and manufacture of pressure vessels for use at elevated temperatures (Findlay, 1973). Standards covering fusion welded pressure vessels constructed from carbon and low alloy steels for conventional (B.S.1500:1958 and B.S.1515:1965) and

FIG 4a C.C.T. DIAGRAM FOR A TYPICAL $^{1}/_{2}$ CR $^{1}/_{2}$ Mo $^{1}/_{4}$ V CASING

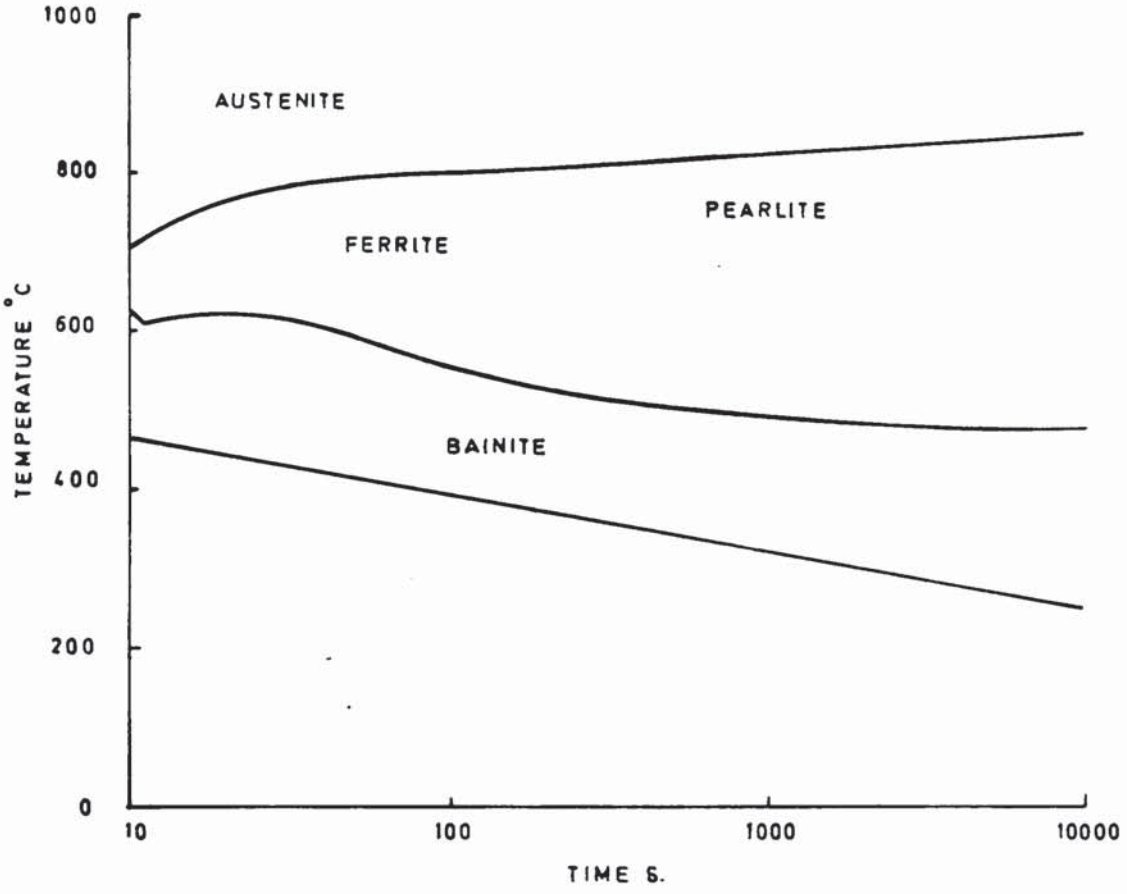

FIG 4b C.C.T. DIAGRAM FOR A TYPICAL 1 CR 1 Mo $^{1}/_{4}$V CASING

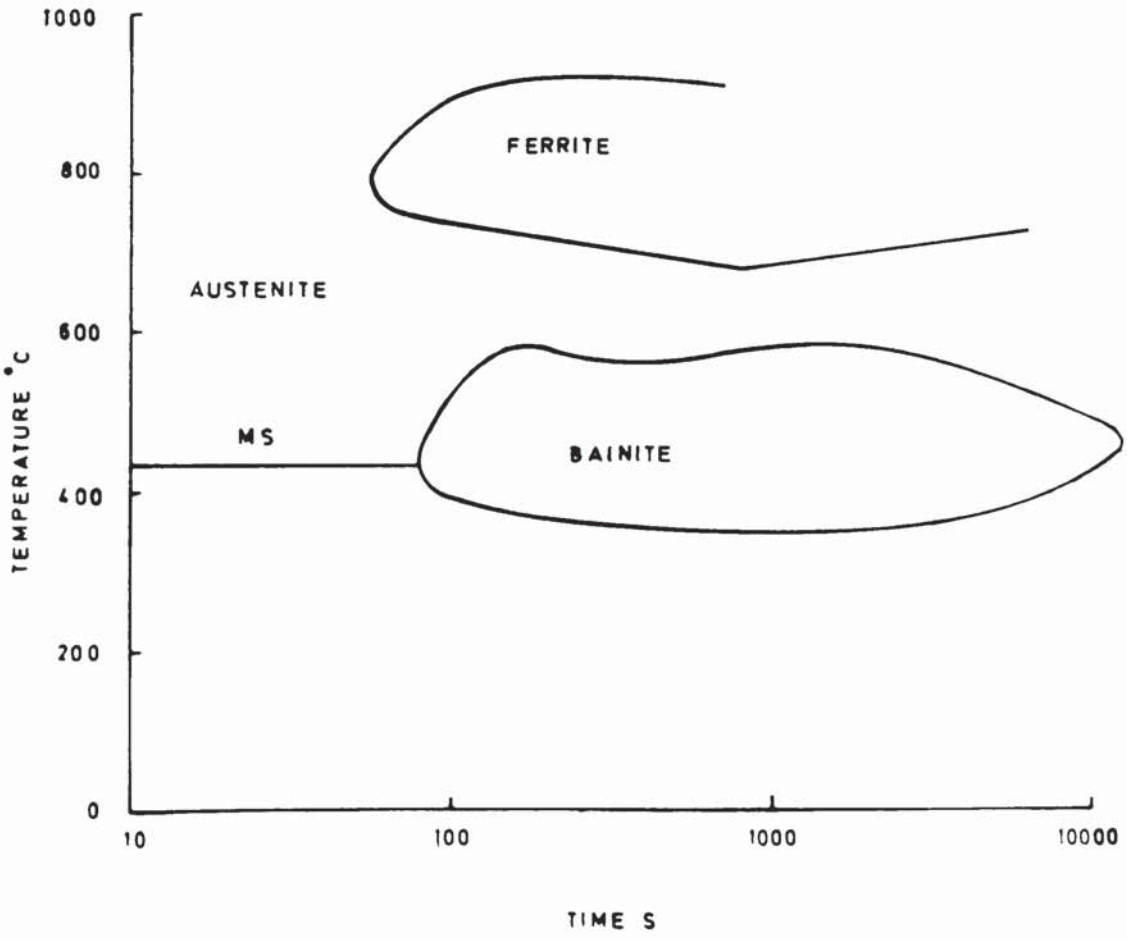

nuclear power installations (B.S.3915:1965), provide design criteria for calculating creep lives. Creep rupture lives are only considered when the operating temperature exceeds 350°C (B.S.3915:1965) and are based on stress levels from known creep rupture data at the relevant temperature. Suitable safety factors are then introduced to allow for uncertainties associated with the experimental data and the extrapolation techniques. This method of calculating permissible stress levels is adopted by all B.S. and A.S.M.E. codes. The magnitude of the safety factor differs according to the class of pressure vessel and the creep life criterion used.

The creep life criterion used in B.S. codes is either:-

(a) average stress to produce rupture in 10^5 hours at the design temperature

or (b) average stress to produce a total creep strain of 1% in 10^5 hours at the design temperature.

The nominal design strength f_F is then calculated from;

$$f_F = \frac{S_{RT}}{1.3} \qquad (1)$$

where S_{RT} is the mean stress for rupture or 1% strain at 10^5 hours (B.S.5500:1976). The S_{RT} properties generally correspond to those agreed by ISO/TC 17/SC 10.

In the A.S.M.E. codes, minor changes occur in the definition of the creep life criterion and the magnitude of the safety factor. The creep life criterion is based on:-

(a) average stress to produce a secondary creep rate of 10^{-5}% per hour at the design temperature,

or (b) average stress to produce rupture in 10^5 hours at the design temperature,

or (c) minimum stress to produce rupture in 10^5 hours at the design temperature,

whilst the level of the safety factor depends on the choice of creep life

criterion, and can vary from 1.0 to 1.67 (Tuppeny, 1963).

British Standards referring specifically to steel castings include B.S.3100:1976, and B.S.1504:1976. Both standards cover a wide range of ferritic and austenitic cast steels and provide information on heat treatment procedures and acceptable levels of mechanical properties. International design codes and material standards on cast steels are also being issued through the International Standards Organisation. A recent issue (I.S.O.3755-1976) specifies requirements for four grades of cast steel for general engineering purposes.

The variability in steel casting quality and its effect on design stress levels is catered for in British Standards by B.S.5500:1976, and in the C.E.G.B. by Standard 66011:1974. Both standards recognise that some defects are inevitable, but the standards of acceptance must be related to the intended working conditions of the casting. The design code B.S.5500:1976 allows design stresses for static casings of 70% of the nominal design stress unless a thorough non-destructive testing procedure has been conducted and potentially harmful defects removed, in which case 90% of the nominal design stress is allowed. The character of potentially harmful defects for CrMoV steel turbine casings are recorded in the C.E.G.B. Standard 66011:1974. This standard regards any crack-like defect having a measurable size normal to the surface of the casting as being unacceptable. The rectification of unacceptable castings involves the removal of defects, followed by repair welding and post-weld heat treatment. The welds are then in turn, examined for unacceptable defects.

2.3 Service Experience of Cast Steel High Temperature Steam Turbine Pressure Vessels

Service defects have been found occasionally in high temperature cast steel vessels such as turbine casings, steam chests and emergency stop valves. The introduction of two-shift operation of steam turbines has resulted in a higher incidence of thermal fatigue cracking in single

cylinder casings of 60 and 120 MW units (Featherstone, 1973), cylinder flanges (Sinton, 1960), steam chests (Neate et.al. 1976) and valve chests (Martin and Blomfield, 1974). These cracks are known to have initiated at stress concentrations (Mellor, 1975) and propagated under the combined action of thermal fatigue and creep (Money and Neate, 1971; Laidler, Whatmough and Gray, 1974). Neate (1975) has deduced that cracks can also propagate from stress concentrations in a period of essentially base-load operation.

A review of power plant failures by Toft and Yeldham (1976) showed that creep failures occur when:-

(a) primary and secondary service stresses exceed the design stress levels,

(b) the time dependent properties of the steel are poor,

(c) the steel was defective prior to going into service.

Welding repairs on defective castings can, if carried out incorrectly, reduce the operational life of high temperature plant. Heat affected zone cracking has been observed in 1CrMoV steam chest to ½CrMoV loop pipe welds (Toft and Yeldham, 1976). Toft and Yeldham showed that cracks formed during the post weld stress relief heat treatment, and then grew in service by creep. Final failure occurred by a transgranular fast fracture. Cracking has also been reported (Jackson, 1973; Neate et.al. 1976) in defective welds in ½CrMoV, 3CrMoVW and 1CrMoV steam chests and valve bodies. The two high Cr Alloys were particularly prone to weld repair cracking.

2.4 Micro-Fracture Mechanisms in Creep

It has been established that creep in metals operating at temperatures in excess of half of their absolute melting point (T_m) deform primarily by a diffusion controlled process. The most familiar process arises from the stress directed diffusion of vacancies from sources in grain boundaries to sinks in orthogonal

grain boundaries. This process can either be through the grains (Narbarro-Herring creep) or along the grain boundaries (Coble creep). In the development of the model of Nabarro-Herring creep (Nabarro, 1948; Herring, 1950) the authors considered the probability of finding a vacancy a short distance from a grain boundary and showed that for a single cubic grain subjected to a biaxial stress system of σ_{11} and $-\sigma_{22}$ a concentration gradient will be established across the grain. As a result, vacancies will flow from the tensile to the compressive grain faces or conversley atoms will flow in the opposite direction. This will lead to the lengthening of the grain in the tensile direction and a contraction in the compressive direction. This form of creep is characterised by a lattice diffusion activation energy and a d^{-2} dependence of creep rate upon grain size d, whereas Coble creep (Coble, 1963) has a grain boundary diffusion activation energy and a d^{-3} grain size dependence of creep rate. Although the Nabarro-Herring model can be criticised on the grounds that it ignores both variations in σ_{ij} across grain faces, and alternative vacancy diffusion paths, several workers (Greenhough, 1952; Pranatis et al., 1955; Price et al., 1964) have obtained a satisfactory agreement between theoretical predictions and experiment. Originally, both Nabarro-Herring and Coble creep were thought to have creep rates directly proportional to the applied stress σ but recent work suggests that the operative stress should in fact be $(\sigma - \sigma_o)$ where σ_o is a threshold stress (Greenfield and Vickers, 1967; Crossland, 1975). The character of σ_o is not fully understood but is considered to arise from an inhibition of the efficiency of vacancy sources and sinks. This can be affected by second phase particles (Sautter and Chen, 1968) and grain boundary defects (Ashby, 1969). To a first approximation, Nabarro-Herring and Coble creep are independent processes. Consequently, the total creep rate can be considered as being the sum of the two contributions with Nabarro-Herring creep dominating at relatively high temperatures and large grain sizes, and the reverse for Coble creep. Both creep processes, because

of their low stress dependence, are also expected to predominate over dislocation creep at low stresses.

Alternative vacancy diffusion creep mechanisms are possible. One is the flow of vacancies between edge dislocations possessing orthogonal Burgers vectors (Nabarro, 1967), and another is where flow occurs between adjacent grain boundaries (Harris, Tucker and Greenwood, 1974). These mechanisms in common with Nabarro-Herring and Coble creep must, according to Hirth (1972) and several other workers, be accompanied by grain boundary sliding in order to maintain material coherency. The question therefore arises of whether sliding can control the deformation rate. Ashby (1972) in considering the relative viscosities of the two basic processes has shown that such a case is possible for perfectly smooth grain boundaries. However, for the more realistic case of imperfect grain boundaries Ashby, Raj and Gifkins (1970), and Raj and Ashby (1971), have argued that diffusion creep will be the dominant process as it will always possess a relatively higher viscosity and as a consequence be rate controlling. They concluded that a combined diffusion/sliding creep process is best thought of as diffusion creep controlled. This conclusion however, may be subject to modification if boundaries contain particles with low interfacial diffusion coefficients or if the particle-matrix interface is not a good vacancy source or sink (Bolton, 1977). In either case, it may be easier for grain accommodation to occur by dislocation creep in which case the strain rate would have a greater than linear dependence on the stress.

The study of creep processes at low values of $\frac{T}{T_m}$ did not gain momentum until the 1940-50 period when Jenkins, Bucknall and Jenkinson (1944), and Greenwood (1952), realised that the cavities they had observed in creep deformed non-ferrous alloys were a significant factor in the process of creep rupture. In a later study of creep in copper and α brass, Greenwood, Miller and Suiter (1954) observed that spheroidal cavities formed at an

early stage of deformation and nucleated predominently on grain boundaries transverse to the applied stress. They concluded that intergranular cracks were formed by the growth and linkage of these cavities and that creep rupture was in turn, dependent on the linkage of these cracks. Further evidence of the formation of cavities on transverse grain boundaries was provided by Jenkins (1954). The formation of cavities in the primary stage of creep has also been demonstrated adequately through the use of accurate density measuring techniques by Brookes, Kirby and Burke (1959-60), Boettner and Robertson (1961), Ratcliffe and Greenwood (1965), and Bowring, Davies and Wilshire (1968).

A study of the creep behaviour of a Nimonic 80A alloy over a wide range of stress and temperature by McLean (1957), revealed that the micro-fracture creep processes occurring in a material could be far more complicated than described previously by Jenkins, Greenwood and their co-workers. McLean (1957) agreed that transverse grain boundaries were good sites for nucleation of cavities but considered that conditions for the nucleation of spheroidal cavities were ideal only when the stress was low and the temperature high. At high stresses and low temperatures however, McLean contended that wedge shaped cavities would be nucleated in preference to the spheroidal form. Intermediate stresses and temperatures would result in the nucleation of both forms of cavities. This work was also supported by Gifkins (1959), who adopted the notation 'r' and 'w' when referring to the rounded and wedge shaped cavities respectively. This notation will be used throughout this Thesis.

The existence of two types of cavities forming in different temperature and stress ranges has led to the development of two basic models to explain their existence. One involves a diffusion process and the other a deformation mechanism.

2.4.1 Void Nucleation

Greenwood (1952) proposed that cavities formed by the condensation of vacancies generated within the grains by plastic deformation. He also proposed that cavities nucleated homogeneously on grain boundaries. Baluffi and Seigle (1955) and Machlin (1956) have shown however, that vacancy supersaturation is not sufficient on its own to cause homogeneous nucleation. An alternative model of cavity nucleation was proposed initially by Ivanova and Oding (1955) and then developed by McLean (1957). These authors proposed that pre-existing holes in the matrix would be suitable sites for nucleation providing they exceeded a critical size. Holes less than the critical size were considered to be unstable and would sinter up. Gifkins (1965) and Garofalo (1965) argued against this model on the grounds that holes were never observed. They also criticised the model on the grounds that it would favour 'r' type cavities at all temperatures and thus would be at variance with the observations from numerous experiments.

A considerable amount of experimental evidence exists to suggest that precipitates on grain boundaries, grain boundary triple points, and sub-grain boundary/grain boundary intersections are important factors in the nucleation of cracks.

Jenkins, Bucknall and Jenkinson (1944) proposed that cavity nucleation occurred on particles or precipitates, whilst Ivanova and Oding (1955) suggested that nucleation could be assisted by non-wetting inclusions. Evidence of cavity nucleation at precipitates on grain boundaries in copper and nimonic alloys has been provided by Resnick and Seigle (1955), Baluffi and Seigle (1957) and Weaver (1958); and by Boniszewski and Eaton (1969) in the heat affected zones of CrMoV steels. In the latter case, voids were seen to be associated with VC particles lying on prior austenite grain boundaries.

Following some creep experiments on copper bicrystals, Chen and Machlin (1956) showed that cavity nucleation was dependent upon grain boundary sliding. In a development of this work by Intrater and Machlin (1959), it

was shown that the number of voids that formed in copper bicrystals between 680°C and 900°C under the action of a shear stress, was proportional to the amount of grain boundary sliding and independent of temperature. Intrater and Machlin concluded that the vacancy condensation mechanism for void nucleation in their tests was inoperative.

The phenomenon of grain boundary sliding and its effect on the integrity of polycrystals was first considered in depth by Zener (1948). Zener proposed that large tensile stresses would develop at a grain boundary triple point due to shear stresses acting along the grain boundaries. These tensile stresses could lead to fracture. Zener's model was developed by Eborall (1954), who suggested that viscous sliding of grains could produce the necessary fracture stress at triple points. Chang and Grant (1956) also considered triple point cracking. They proposed several methods by which cracks would form as a result of grain boundary sliding (Figure 5).

Servi and Grant (1951), Chang and Grant (1956), and Grant (1971), have considered the accommodation of strain developed at a triple point by the surrounding matrix. They showed that stress dispersal can occur by plastic folding in the grain ahead of the triple point. This plastic folding may consist of either slip or kinking. Servi and Grant (1951) did suggest however, that any grain hardening mechanism could prevent plastic folding and hence promote intergranular fracture.

A quantitative analysis of the conditions for fracture along a sliding interface was considered first by Eshelby et al. (1951), and then in more detail by Stroh (1954). Stroh proposed that the conditions for fracture at the end of a sliding interface L, under the action of a shear stress τ in an elastic body, would be attained when:

$$\tau > \left[\frac{12 \mu \gamma_s}{\pi L}\right]^{\frac{1}{2}} \qquad (2)$$

Here, μ is the shear modulus and γ_s the crack surface energy. This equation predicts that low values of γ_s and large slip band lengths L will promote fracture.

FIG 5 WEDGE CRACK FORMATION (CHANG AND GRANT, 1956)

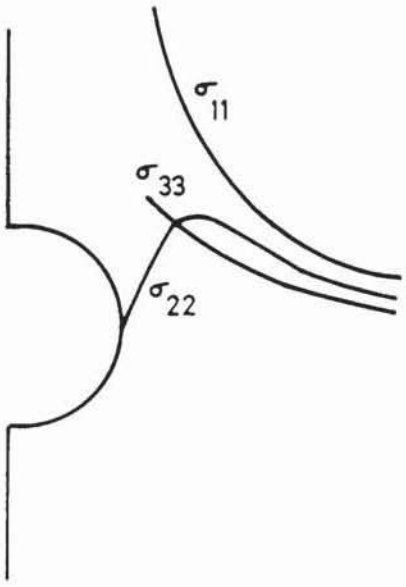

FIG 6 ELASTIC STRESS DISTRIBUTION AHEAD OF A NOTCH

McLean (1957a; 1957b) applied Stroh's fracture concept to the fracture of copper and Nimonic 80A, and obtained moderate success. Additional work on the nimonic alloy by Weaver (1959-60), showed that the introduction of precipitates along grain boundaries reduced the creep rupture life of the alloy. Weaver equated the precipitate spacing with the length of the sliding interface L and obtained the expected value for the crack surface energy. Eborall (1961) and Smith and Barnby (1967b) however, criticised the way Weaver had analysed his results. They argued that the model of blockage of grain boundary sliding by discrete particles was not consistent with the semi-infinite model for triple point cracking.* Also, because of the restricted sliding of the grain boundaries (small value for L) the attainment of the critical value of the shear stress may be preceeded by the fracture of the precipitate. A more sophisticated model for triple point cracking at a double pile-up (Figure 5b) by Smith and Barnby (1967a), has shown that crack nucleation can occur at stresses considerably lower than predicted by Stroh's single pile-up model (Figure 5a). Smith and Barnby (1967a) suggested that for nucleation, the shear stress τ must exceed a critical value given by:

$$\tau > \left[\frac{2\,\mu\,\gamma_s}{\pi(1-\nu)L}\right]^{\frac{1}{2}} \qquad (3)$$

Further evidence of the importance of grain boundary sliding in the nucleation process has been provided by Ratcliffe and Greenwood (1965) and Skelton (1967). These authors have shown that the number of voids nucleated on grain boundaries is proportional to creep strain. Gittins (1970) has gone a stage further and suggested that the contribution of grain boundary sliding to the nucleation process has a positive strain rate dependence, whilst the contribution of the diffusion mechanism to the cavitation process increases as the strain rate decreases.

Alternative mechanisms for producing cavities on sliding grain boundaries have been proposed by Gifkins (1956) and Chen and Machlin (1956). These authors suggested that the intersection of slip bands with sliding

(*There is also an arithmetic error of a factor of 10 in Weaver's work)

grain boundaries could produce ledges or jogs in these boundaries. The ledges and jogs could then obstruct grain boundary sliding and produce stress concentrations high enough to break atomic bonds. Further grain boundary sliding could then open up the fractured bonds.

Davies and Wilshire (1961) have suggested that the intersection of secondary slip systems with sliding grain boundaries could produce a string of isolated cavities along the boundary which could link up and form a stepped wedge crack.

Experimental support for these intersection slip models has been produced by Greenwood, Miller and Suiter (1954), who showed that the cavity spacing in their copper test specimens could be linked to the slip band spacing. McLean (1963) also provided some evidence of ledge formation in iron creep specimens. Voids were also seen to be associated with grain boundary serrations in Al/Mg alloys (Mullendore and Grant, 1961b). Mullendore and Grant suggested that the serrations represented the intersection of a subgrain boundary with the sliding grain boundary. Such a configuration would then enable the Zener mechanism for triple point cracking to operate. The association of cavities with obstacles lying on sliding grain boundaries has also been observed in creep tested copper specimens by Johannesson and Tholen (1972). These authors suggested that the interaction of a sliding grain boundary and a triple point or kink, could produce a stress concentration of 10^3 which could be sufficient to break atomic bands.

The conclusions of many other investigations on creep in both ferrous and non-ferrous alloys have shown overwhelming support for the grain boundary/particle interaction mechanism of cavity nucleation [Weaver (1959-60); Harris (1965); Greenwood (1969); Tipler et al. (1970); Venkiteswaran et al. (1973); Tipler et al. (1976); Sikka et al. (1977)]. Gifkins (1965) however, has suggested that such conclusions could be erroneous. He argues that it is not always possible to determine whether a cavity has nucleated at a particle, or nucleated at some point away from the particle and then grown until encountering it.

In a report by the British Steel Corporation (1970), it was proposed that grain boundary precipitates having a high misfit with the matrix would be very effective nucleation sites for 'r' type cavities. More recently, Hondros and McLean (1976) examined the phenomenon of grain boundary fragility in ferrous and non-ferrous alloys, and showed that there was strong evidence that the segregation of impurity elements to grain boundaries would assist in the de-cohesion of matrix/particle interfaces. They showed for example, that carbide/ferrite interfaces in steels can be weakened by segregated antimony and that high oxygen contents can increase fracture transition temperatures. Similar conclusions on the effect of segregated impurities on the fracture of grain boundaries were reached by Bleakney (1952). Hondros and McLean (1976) did point out however, that even the most gravely weakened grain boundary would still be strong unless the local stress was magnified. Such a high stress could be generated by the intimate interaction of a slip band and a hard particle lying on a grain boundary. Hondros and McLean proposed that under these conditions either the particle/matrix interface would crack under the action of the tensile component of the stress concentration or, the hard particle would fracture. A similar mechanism for particle fracture has been proposed by Rukweid (1972). Tipler and Hopkins (1976) have shown that under these circumstances, a reduction in certain trace elements in CrMoV steels can improve creep ductility and creep life. Tipler and Hopkins concluded that the improvement in creep properties was associated with the delay in cavitation and the reduction in the number of cavities.

2.4.2 Void Growth

The development of models of void growth and microscopic creep crack growth, has been vigorously persued by many workers involved in the study of void nucleation. Both diffusion and deformation mechanisms have been used to produce models of void and crack growth in ferrous and non-ferrous alloys. Although there appears to be two well defined growth mechanisms,

sufficient experimental evidence exists to suggest that both material and test conditions can be varied to favour either one particular mechanism or a combination of the two.

2.4.2.1 Diffusion Mechanism

Cottrell (1961) pointed out that if the magnitude of the local stress at a cavity remains below the critical Griffith value, the local stress can cause the cavity to grow by the process of atoms migrating from the ends to the sides of the cavity. When this occurs the cavity volume remains constant. Alternatively, the cavity can grow with changing volume by atoms migrating from the ends along the grain boundary or into the grain. With continued growth the cavities then either link with neighbouring cavities and cause spontaneous intergranular fracture or, as Cocks and Taplin (1969) have suggested, they can interact with neighbouring cavity groups on different grain boundaries to produce failure by plastic tearing. Initial support for the diffusion mechanism of void growth came from Greenwood (1952; 1954) who considered that sufficient vacancies could be generated by plastic deformation within the grains. These vacancies could then migrate to the grain boundaries to aid void growth.

One of the first attempts at providing a theoretical analysis of the growth of a void in the presence of a stress, was that by Baluffi and Seigle (1955). They considered the chemical potential associated with taking an atom from the surface of a void lying on a grain boundary, to the grain boundary. They showed that the critical tensile stress σ at which a void of radius r would grow by accepting vacancies from the grain boundary was

$$\sigma = \frac{2\gamma}{r \cos^2 \theta} \qquad (4)$$

where θ was the angle between the stress axis and the cavitated grain boundary, and γ the void surface energy. The model predicts a strong dependence of the critical stress on the orientation of the grain boundary. Baluffi and Seigle (1957) considered that the most probable source of vacancies was from grain boundaries with tensile stresses across them.

This view was consistent with experimental observations of the high density of voids on transverse grain boundaries in tension creep tests and on longitudinal grain boundaries in compression creep tests.

The work of Baluffi and Seigle (1955, 1957) received considerable attention by other investigators, notably Hull and Rimmer (1959). Hull and Rimmer developed and applied the original theory (Equation 4) to the creep of copper between 400°C and 500°C. They examined the relative contributions to void growth by lattice diffusion and grain boundary diffusion, and showed that the grain boundary diffusion was the dominant mechanism. They then proceeded to analyse the growth of a spherical void by assuming that growth occurred by vacancies diffusing along grain boundaries orientated normal to the stress axis. Surface diffusion was assumed to be sufficiently rapid to maintain the spherical shape of the void during its growth. Under these conditions, Hull and Rimmer showed that the rate of growth of a void $\frac{dr}{dt}$ under the action of a stress σ, at a temperature T (°K), could be obtained from the expression:

$$\frac{dr}{dt} \alpha \frac{Dg\ \delta z\ \sigma\ \Omega}{2\ k\ T\ a\ r} \qquad (5)$$

Dg is the grain boundary diffusion coefficient, δ_z the width of the grain boundary along which the vacancies migrate, Ω the atomic volume, K is Boltzmann's constant, and a and r are the void spacing and radius respectively. Hull and Rimmer observed in their experiments that part of the creep rupture process consisted of the growth and linkage of voids to form grain boundary cracks. By rearranging and integrating Equation 5, the authors obtained a reasonable fit between actual and predicted rupture lives for their tests. They also noticed that the application of a hydrostatic pressure (σ_H) reduced the rate of void growth and suggested that the active pressure was in fact the sum of $\sigma - \sigma_H$.

A development of Hull and Rimmer's theory based on an improved vacancy concentration profile around the growing voids, has been presented by Speight and Harris (1967). The authors, having fixed the vacancy

concentration to zero at a point mid-way between the voids proceeded to use Fick's Laws on Diffusion to calculate the increase in vacancy concentration as the void surface was approached. They showed that void growth rates could be much greater than those predicted by the Hull and Rimmer theory particularly when voids were forming or when void spacings were large.

Dobes and Cadek (1970) have criticised this work by Speight and Harris (1967) on the grounds that both bulk diffusion effects and varying rates of vacancy generation were ignored. Dobes and Cadek re-analysed the problem and included the effect of bulk diffusion on grain boundary vacancy concentration. They showed that void growth rates would be much faster than predicted by previous theories if void spacings were greater than 25 times the void radius. Weertman (1973) agreed with the analysis technique adopted by Dobes and Cadek (1970) but pointed out errors in their results. He showed that the correct solution to the rate of void growth would be several orders of magnitude greater than originally predicted. Further work by Weertman (1974) has indicated that bulk diffusion or vacancy generation within the grains has little effect on the growth of 'r' type voids, but could constitute the major source of vacancies for the growth of 'w' type voids. Further modifications to the Hull and Rimmer theory have been presented by Vitovec (1972) and Harris, Tucker and Greenwood (1973). They showed that the inclusion of an increasing net section stress effect as voids grew together, would predict higher void growth rates than given by the original theory.

Support for the grain boundary mechanism of vacancy diffusion has come from Hirth (1972), who considered that the mechanism was analogous to Coble creep. In Coble creep, the creep strain is directly proportional to the product of the grain boundary diffusivity and the applied stress, and inversely proportional to the cube of the grain diameter (Coble, 1963). Also, Speight and Beere (1975) have presented a model of diffusional void growth in which vacancy production and the concomittant production of atoms causes adjacent grains

to move apart and so increase the volume of the voids. Similar work by Harris, Tucker and Greenwood (1973; 1974) has shown that specimen creep strain and rupture time are very dependent upon the initial void spacing. They also pointed out that in accelerated creep tests the dominant mode of deformation was usually the non-conservative motion of dislocations. Under these circumstances, the stress dependence of the secondary creep rate can be considerably greater than that for an intergranular mechanism of creep. This fact, together with the activation energy for grain boundary self diffusion being approximately half that for lattice self diffusion, implies that deformation due to void growth will dominate at low stresses and temperatures.

Skelton (1975) developed the latter model by Harris et al. to allow for continuous nucleation of voids. The effect of increasing net stress was not considered. Under these conditions, Skelton calculated that for similar rupture times the fracture strains would be lower than predicted by the Harris et al. model.

Experimental support for the diffusion model has come from several areas of work. Boettner and Robertson (1961) found in their study of copper that void growth began near the specimen surface and worked its way inwards. They considered that the principal diffusion path was along grain boundaries. Ratcliffe and Greenwood (1965), have shown from their work on magnesium, that the application of a hydrostatic pressure reduced the rate of nucleation and growth of cavities. The presence of a hydrostatic pressure was also seen to increase the creep fracture ductility and retard the development of tertiary creep but had no effect on the creep rate. Ratcliffe and Greenwood concluded that the growth of cavities occurred by vacancy diffusion and was independent of a shear deformation mechanism. Similarly, the work of Cane (1974) on creep in a 2¼CrMo steel has shown that the growth of cavities was associated with a tensile stress component and was not due to significant amounts of grain boundary sliding. In addition, Raj and Ashby (1975) have presented an expression for the time

to fracture based on the growth of a constant population of voids by grain boundary and volume diffusion. They assumed that nucleation and growth of voids occurred continuously and simultaneously, primarily at second phase particles.

Support for the Coble Theory of grain boundary diffusion creep has come from the work of Crossland and Clay (1977) on a stainless steel. They looked at the low stress mechanism of creep in this steel at a temperature of approximately half its 'absolute melting point', and observed that its creep behaviour was consistent with the Coble Theory when the strain was less than 2×10^{-5}. At strains approaching 3×10^{-2} however, the creep rates were less than predicted by the theory.

Most theories on diffusion creep assume that the migration of vacancies and atoms is sufficiently fast to maintain a spherical void during the growth process. Early studies by Presland and Hutchinson (1961; 1962; 1963) on void formation in magnesium attributed the 'r' type of void to vacancy diffusion and the 'w' type to grain boundary sliding. Ashby and Raj (1975), in considering the shape of growing voids have suggested that their shape is determined by the kinetics of the atom migration process at the voids surface. They also stated that, 'whilst there is strong evidence to suggest that void nucleation is dependent on a sliding mechanism and thus on the deviatoric part of the stress tensor, they are fairly certain that void growth depends on the maximum principal stress'. In contrast, Davies, Davies and Wilshire (1965) have proposed that the growth of cavities in their Ni/Co alloy was dependent on a shear mechanism and not simply on a diffusion mechanism. They concluded that cavity growth was independent of a microscopic normal stress.

The apparent inability of the diffusion theories of cavity growth to satisfactorily explain all of the foregoing experimental results, has in part lead to the development of an alternative growth mechanism based on a shear process. Due consideration has however, been given to the fact that void growth can under certain conditions occur by both processes. Mullendore

and Grant (1954) for example, have suggested that void growth in an Al/Mg alloy can occur by a diffusional and shear mechanism. Similarly, McLean (1957) proposed that voids can join together either by shear or diffusion processes to form 'w' type cracks.

2.4.2.2 Deformation Mechanism

Early criticisms of the diffusion mechanism came from the work of Kramer and Machlin (1958) and Intrater and Machlin (1959). Kramer and Machlin observed that the grain boundary area occupied by cracks and voids in their nickle specimens was proportional to the creep strain. They contended that the cracks had generated by shear. Similar observations were made by Intrater and Machlin in copper specimens. These authors also found that the area of visible voids was independent of temperature and argued that this was clear evidence of the absence of a diffusion mechanism. Linearity between void volume and creep strain was also observed by Bowring, Davies and Wilshire (1968), and Hensler and Cullen (1964), in a series of magnesium alloys.

The creep behaviour of nickle alloys under the influence of a stress reversal has been cited by Davies and Wilshire (1965) as further evidence of deformation controlled growth. They noted that the introduction of a compressive stress during the tertiary stage of a tensile creep test did not affect the subsequent tensile tertiary creep rate. The authors argued that if void growth occurred by a diffusion mechanism, then compressive creep should have caused void shrinkage. However, as tertiary creep deformation was still in evidence they concluded that void shrinkage had not occurred. Thus, void growth was not diffusion but deformation controlled. In a development of this work, Davies and Dutton (1966) reasoned that an intermediate compressive stress may only stop void growth but not necessarily cause shrinkage. However, if grain boundary sliding were the dominant process then a stress reversal would simply reverse the sliding direction and cause void shrinkage. Alternatively, the introduction of a compressive

stress at 90° to the original applied stress should maintain the initial sliding direction and not affect the growth of voids. Davies and Dutton observed this behaviour in a copper alloy.

Criticism of the stress reversal work has come from Taplin and Gifkins (1967) who argued that void closure due to sintering governed by vacancy release could explain Davis and Duttons (1966) results, but does not prove that void growth had occurred by a diffusion or sliding mechanism. They regarded the case as non-proven. Gittins (1967) has also shown that void sintering can occur on reversed stressing at room temperature. Consequently, grain boundary sliding is not a prerequisite.

Further support for deformation controlled creep has come from Evans (1969) following his observations of void growth in a Mg/Al alloy. Evans observed that void growth rates were directly related to the grain boundary sliding rate. He attributed a ductility minimum to a maximum in the void growth rate and the concomittant maximum grain boundary sliding rate.

Taplin and Barker (1966), having studied the formation of irregularly shaped voids in copper using the electron microscope, concluded that their formation was due to grain boundary sliding. Angular cavities have also been observed by Presland and Hutchinson (1962) in magnesium, by Harris, Haddrell and Rickards (1962) in Magnox, and by Williams (1967) in an Al/Zn alloy. Williams (1967) considered the growth of 'w' type voids lying on grain boundaries oriented at various angles to the applied stress axis, and showed that growth along grain boundaries normal to the stress axis was proportional to the amount of grain boundary sliding. A similar model was proposed by Soderberg (1969).

Continuing the study of void shapes, Wingrove and Taplin (1969) found that the ductility minimum in their iron specimens was associated with both grain boundary sliding and the existence of dendritic type voids. Davies and Williams (1969) presented a mechanism for the formation of the dendritic void. They proposed that these voids would form by a combination of grain boundary shear and triple point cracking. A succession of these events

would then produce a dendritic shaped cavity.

The significance of the distribution of cavities with respect to the axis of the applied stress, has been studied by several workers with reference to both void nucleation and growth. Taplin (1965; 1969) has observed that in fine grained materials, sliding of grain boundaries encourages the growth of cavities lying on boundaries orientated at approximately 45° to the applied stress. In contrast, coarse grained materials encouraged cavity growth on boundaries lying normal to the stress axis. Rao, Rao and Pandey (1973), and Fleck, Beers and Taplin (1975) have observed a similar grain size dependence of cavity orientation in an austenitic stainless steel and copper. Gittins and Williams (1967) however, have demonstrated that the magnitude of the applied stress can influence cavitational behaviour. They observed that high stresses promoted the development of 'r' type cavities on 45° boundaries whereas at low stresses, 90° boundaries were favoured.

Recently, Williams (1975) attempted to rationalise the previous observations on void location by suggesting that their varying orientations could be produced by grain boundary sliding alone. By adopting the Chang and Grant (1956) model of crack formation (Figure 5), Williams has shown that the optimum grain boundary angles for fracture are 45°, 70° and 90° relative to the stress axis.

The effect of a hydrostatic stress on microscopic fracture mechanisms has been studied by several workers. Waddington and Williams (1967) have noted that the application of a hydrostatic pressure equal to the applied stress increased the rupture life and ductility of an Al/Zn alloy and also reduced the crack density. These authors proposed that the latter was due to a reduction in the number of cracks that had grown to a visible size. The total crack population was considered to be unaltered. The reduction in crack growth rate was thought to have been the result of the hydrostatic pressure reducing the effective crack tip stress. Waddington and Williams proposed that the existence of cracks in a specimen subjected to a hydro-

static pressure, was good evidence that the fracture mechanisms were dominated by a deformation process. Waddington and Williams (1967) were unable to strengthen their case due to the absence of grain boundary sliding data. Needham and Greenwood (1975) however, have measured the effect of a hydrostatic pressure on grain boundary sliding. They showed that grain boundary sliding in copper at 500°C decreased when a hydrostatic pressure was present, showing that fracture resulting from a deformation process was not entirely independent of hydrostatic pressure.

In recent times, Dyson, McLean and their co-workers have participated in a comprehensive series of experimental creep programmes designed to investigate the relative effects of the deviatoric and maximum principal stress on the nucleation and growth of creep cavities. Although they only concentrated on creep damage processes in Nimonic alloys, sufficient evidence exists to suggest that their conclusions on material behaviour can be used to rationalise in general terms the behaviour of other alloys, particularly the ferrous alloys considered in this Thesis. Dyson and McLean (1972) in keeping with the general findings of Greenwood (1977), have observed that under pure tension, cavities form very early in the creep life of Nimonic 80A and that their volume increases linearly with time. From this work, Dyson and McLean concluded that cavities nucleate continuously and steadily as creep strain develops. In a development of this theme Dyson, Gibbons and McLean (1975) following the work of Greenwood (1973), have shown that a simple material failure law based on the proportion of total grain boundary area occupied by cavities, and the applied uniaxial stress, can provide a reasonable prediction of fracture life. Unfortunately, the theory cannot account for material behaviour under multiaxial loading as the uniaxial stress component is not defined. In an attempt to rectify this shortcoming, Dyson and McLean (1977a) have studied the dependence of fracture lifetime on what is considered to be the significant failure stress components

namely, $\bar{\sigma}$ and σ_{11}.* By varying the tension/torsion stress ratio in Nimonic 80A specimens at 750°C, Dyson and McLean were able to show that fracture time depended upon both $\bar{\sigma}$ and σ_{11}. Low material creep rates favoured a σ_{11} dependence while high creep rates favoured $\bar{\sigma}$. In deriving the basic constitutive relations covering equivalent creep rate and cavity volume, the authors used a Norton type law to describe material behaviour which perhaps is unfortunate, as its use implies a dominant second stage of creep deformation. As a consequence, they effectively ignore the early formation of creep damage, and the stress dependence of the creep exponent. This apart, the ability of the model to rationalise in general terms the fracture behaviour of materials whose overall deformation is controlled by $\bar{\sigma}$ and this includes low alloy CrMoV steels (Section 2.8), is encouraging. For the case of multiaxial creep, Dyson and McLean (1977a, 1977b) considered that cavitation would be favoured by high values of the stress state parameter $\frac{\sigma_{11}}{\bar{\sigma}}$. Using a thermodynamic argument (Equation 4), Dyson and McLean reasoned that a high σ_{11} would increase the overall stability of cavities thereby enabling a greater proportion of newly created cavities to grow to form microcracks and eventually macrocracks. This theory has been confirmed by the experimental work of Dyson and Rodgers (1977a). They observed a positive relationship between the number of cracked boundaries and the level of the stress state parameter in notched creep specimens.

* $\bar{\sigma}$ is a deviatoric stress and σ_{11} is the maximum principal stress.

2.5 Notched Creep Rupture Testing

2.5.1 Stress Distribution At A Stress Concentration

It has been shown in Section 2.3 that the presence of stress concentrations in high temperature pressure vessels can seriously undermine their integrity and fitness for purpose. Improvements in plant safety and economics can be achieved by a more complete understanding of the effect of stress concentrations on material behaviour. Perhaps the first comprehensive study of stress concentrations was by Kirsch in 1898. He considered the limiting case of the stress distribution around a circular hole in an infinite plate. The more general case, that of the stress distribution around an elliptically shaped hole, was considered later by Kolosoff (1910) and in more detail by Inglis (1913).

Inglis (1913) derived an expression for the magnitude of the stress σ_{11} at the tip of an elliptically shaped crack in an infinite plate with its major axis normal to a remotely applied tensile stress. He showed that the magnitude of σ_{11} could be calculated from the expression;

$$\sigma_{11} = \sigma \left(1 + \frac{2a}{b}\right) \qquad (6)$$

where σ is the level of the remotely applied stress, and a and b are the respective semi-major and semi-minor axes of the ellipse. In the limit, when a = b the ellipse becomes a circle and $\sigma_{11} = 3\sigma$, and when $a \gg b$ the ellipse develops into a crack and σ_{11} tends to infinity.

Inglis also showed that the stress σ_{11} could be calculated from the equation;

$$\sigma_{11} = \sigma \left[1 + 2\left(\frac{a}{p}\right)\right]^{\frac{1}{2}} \qquad (7)$$

where p is the radius of curvature of the elliptical notch. Neuber (1938) adopted similar analytical methods to calculate the stress distribution around internal and external notches in semi-infinite bodies. The results were expressed in terms of a stress concentration factor K_t, where $K_t = \frac{\sigma_{11}}{\sigma}$. Neuber's solutions are incorporated in several engineering design handbooks (eg. Peterson, 1953; 1975). The calculation of stress concentrations in biaxial stress fields and in semi-infinite plates has also been considered by other analysts (Durelli and Murray, 1943; Mindlin, 1948).

The classical theories of Inglis and Kolosoff from the early part of this century are clearly not capable of describing the stress distribution ahead of a notch in a three dimensional body of finite size. Some progress was made in the subsequent years by the development of more thorough analytical solutions. The breakthrough came however, with the development of the numerical finite difference and finite element methods of stress analysis.

The stress distribution ahead of a notch in a circumferentially notched bar subjected to axial loading is shown in Figure 6. The states of stress existing in a notched bar can be described as either being in plane strain or plane stress.

By definition,

the state of plane strain exists when one of the principle strains is zero,

the state of plane stress exists when one of the principal stresses is zero.

The state of stress in a thick specimen away from the notch root can vary from plane strain at the mid-thickness, to plane stress at the free surfaces. The state of plane stress also exists at the root of a notch

where, due to the absence of surface traction, the principle stress σ_{22} is zero (Figure 6).

Several workers (Voorhees and Freeman, 1960; Voorhees, Freeman and Herzog, 1962) recognised that the introduction of a stress concentration does not change any fundamental material properties. However, they realised that the behaviour of a notched creep rupture specimen would be influenced by the state of stress ahead of the notch, the initial level of the elastic stresses and their rate of relaxation. The redistribution of stresses ahead of a stress concentration in a creep rupture specimen has been analysed by Taira, Ohtani and Ito (1971), and Taira and Ohtani (1973). By using finite element methods and Norton's Power Law for secondary creep, they showed that following the initial loading the stresses were re-distributed to a steady state level. The rate of stress relaxation was approximately independent of notch acuity, decreased with decreasing initial stress and was slower for more highly constrained specimens. They also found that the position of the peak axial stress (σ_{11}) was a function of specimen geometry. The Von Mises equivalent stress was a maximum at the notch root whereas the hydrostatic stress always maximised ahead of the notch.

2.5.2 Notch Sensitivity

Before the advent of fracture mechanics, many workers attempted to characterise the response of a material to a stress concentration by simply comparing the rupture lives of notched and plain specimens. The term notch strength ratio (N.S.R.) was used to describe the materials behaviour,

$$\text{where N.S.R.} = \frac{\text{rupture life of notched specimen}}{\text{rupture life of plain specimen}}$$

both specimens having the same net section stress. Materials with a N.S.R. greater than 1 were classified as notch strengthening, while materials with a N.S.R. less than 1 were notch weakening. The results of this work have been extensively reviewed by Sachs and Brown, (1953); Sachs, Sessler and Brown, (1959); Smith and Murray, (1963). These authors have shown that

there is no simple explanation of the response of a notched material to changes in test parameters.

2.5.2.1 Effect of Notch and Specimen Geometry

Sachs, Sessler and Brown (1959) reported than an increase in notch acuity and notch depth could have a pronounced effect on the notch strength ratio of ferrous and non-ferrous materials. Davies and Manjoine (1953) observed that the notch strength ratio of a 12Cr3W steel increased and then gradually decreased as the notch acuity was increased. Similar observations were made by Seigfried (1945; 1953) for a Sn Cd alloy, Voorhees and Freeman (1960), and Voorhees, Freeman and Herzog (1962) for several high temperature alloys, and Goldhoff and Brothers (1968) for a CrMoV forging steel. Contradictory observations were made however, by Manjoine (1962) and Hanink and Voorhees (1962), whilst the work of Manjoine (1963) was inconclusive. Very little information is available on the relationship between notch depth and notch strength ratio. Goldhoff and Brothers (1968) have reported that for a low ductility steel the notch strength ratio can decrease and then increase as the notch depth increases.

Sachs, Sessler and Brown (1959) reported that the effect of specimen geometry on notch rupture strength was inconclusive, but commented that only a limited number of geometries had been examined. Subsequent work by Goldhoff (1963) showed that the notch strength ratio decreased as the specimen size was increased. Similar observations were made by Manjoine (1962) and Manjoine (1963). A recent publication by Schmeider (1976), also shows that notch rupture strength generally decreases with increasing section size in both notch strengthening and notch weakening materials.

2.5.2.2 Effect of Metallurgical Structure

The ductility of a notched stress rupture specimen is considered to be related to the ability of the microstructure to accommodate creep strain. Goldhoff and Brothers (1968) have shown that the notch strength of a wrought CrMoV steel varies according to the character of the heat treatment transformation products. They observed that a ferritic steel was

notch strengthening and a bainitic steel was notch weakening. In the ferritic steel, crack initiation occurred early in the life of the tests and was accompanied by extensive notch root deformation. In the bainitic steel, crack initiation occurred comparatively later and the initiation sites were at or just ahead of the notch root. The rupture life of the notch weakened bainitic steel was essentially controlled by the crack initiation time, while the crack propagation stage controlled the life of the notch strengthening ferritic steel.

Davies and Manjoine (1953) reported that notch strength ratio was dependent on grain size. Notch strengthening was observed in a fine grained structure and notch weakening in a coarse grained structure with a similar smooth bar ductility. Notch weakening was also connected with grain boundary precipitates (Brown, Jones and Newman, 1952).

There have also been several attempts to relate the notch sensitivity of a material to its smooth bar ductility (Brown and Sachs, 1951; Brown, Jones and Newman, 1952; Davies and Manjoine, 1953; Sachs, Sessler and Brown, 1959; Garofalo, 1959). These authors found that notch weakening was invariably associated with low smooth bar ductility. Notch strengthening was frequently observed in materials with a smooth bar ductility exceeding 10%. Voorhees, Freeman and Herzog (1962) however, found no relationship.

It is well known that the creep ductility of smooth bar specimens is strongly influenced by the temperature and duration of testing. Sachs, Sessler and Brown (1959) have shown that these parameters can affect the ductility of notched creep rupture specimens. Some materials initially notch strengthen and then notch weaken with increasing time, and then notch strengthen again. The notch weakening mode of behaviour is favoured by high temperature.

2.5.2.3 Effect of Stress State Ahead of The Notch

The time to rupture of a notched creep rupture test includes the initiation and propagation stages of crack development. Several workers have attempted to separate these two stages in the analysis of their

experimental data. Siegfried (1953) performed a series of interrupted tests on several steels. He observed that crack initiation at the root of a notch was the result of local ductility exhaustion, while internal cracks initiated under triaxial stress conditions. He also demonstrated that in the absence of intergranular failure crack growth would be slow and the material would be notch strengthening. Alternatively, notch weakening occurs when the material is susceptible to intergramular failure. Manjoine (1962) came to essentially the same conclusion on notch strengthening.

An alternative theory of notch sensitivity proposed by Garofalo (1959), suggests that notch strengthening occurs when the initiation of cracks is delayed following the relaxation of the notch root stresses. He observed that in general cracks initiated at the position of maximum tensile stress. Similar observations were made by Davies and Manjoine (1953), Manjoine (1963), and Voorhees and Freeman (1960).

More recent work by Ohtani et al. (1973) and Taira and Ohtani (1973), has indicated that notch strengthening may be the result of the maximum equivalent stress being less than in a smooth bar specimen subjected to the same nominal stress. This is a consequence of support from the extra material above and below the notch. Under these conditions, the low level of notch root strain leads to slow nucleation and propagation of cracks. For a notch weakening material, they showed that stress relaxation at the notch root was not as pronounced as in notch strengthening materials and as a result, crack initiation occurred more rapidly.

2.6 Stress Distribution Ahead Of A Sharp Crack

A natural extension to the study of crack initiation and growth in notched creep rupture specimens, was the study of the same phenomenon in precracked specimens. The work of Griffith (1920) showed that the failure of very brittle materials could be explained by a thermodynamic fracture criterion. In subsequent years, theories based loosely on

Griffith's work were developed to explain the fracture of ductile materials containing cracks.

2.6.1 Linear Elastic Fracture Mechanics

The system of stresses near the tip of a crack was considered by Westergaard (1939). He showed that for a crack of length 2a in an infinite body under an applied uniform biaxial tension (Figure 7), the angular dependencies of the normal and shear stresses can be expressed as:-

$$\sigma_{11}=\sigma\left(\frac{a}{2r}\right)^{\frac{1}{2}} \cos\frac{\theta}{2}\left(1+\sin\frac{\theta}{2}\sin\frac{3\theta}{2}\right)-\ldots \quad (8)$$

$$\sigma_{22}=\sigma\left(\frac{a}{2r}\right)^{\frac{1}{2}} \cos\frac{\theta}{2}\left(1-\sin\frac{\theta}{2}\sin\frac{3\theta}{2}\right)-\ldots \quad (9)$$

$$\sigma_{12}=\sigma\left(\frac{a}{2r}\right)^{\frac{1}{2}} \sin\frac{\theta}{2}\cos\frac{\theta}{2}\cos\frac{3\theta}{2}+\ldots \quad (10)$$

Irwin (1957) developed Westegaard's Theory by considering the near tip energy change when a crack propagates by an amount δa. He showed that the strain energy release rate (G) per unit crack extension could be expressed by

$$G = \frac{\sigma^2 \pi a}{E} \quad (11)$$

where E is Young's Modulus and σ is the remotely applied stress.

When θ in the Westergaard equations is zero and $r \ll a$, then:

$$\sigma_{ijk} = \frac{K}{(2\pi r)^{\frac{1}{2}}} \quad (12)$$

where $$K = \sigma(\pi a)^{\frac{1}{2}} \quad (13)$$

By combining equations (11) and (13), Irwin showed that

$$G = \frac{K^2}{E} \quad \text{for plane stress.} \quad (14)$$

For plane strain he obtained:

$$G = \frac{K^2}{E(1-\nu^2)} \quad (15)$$

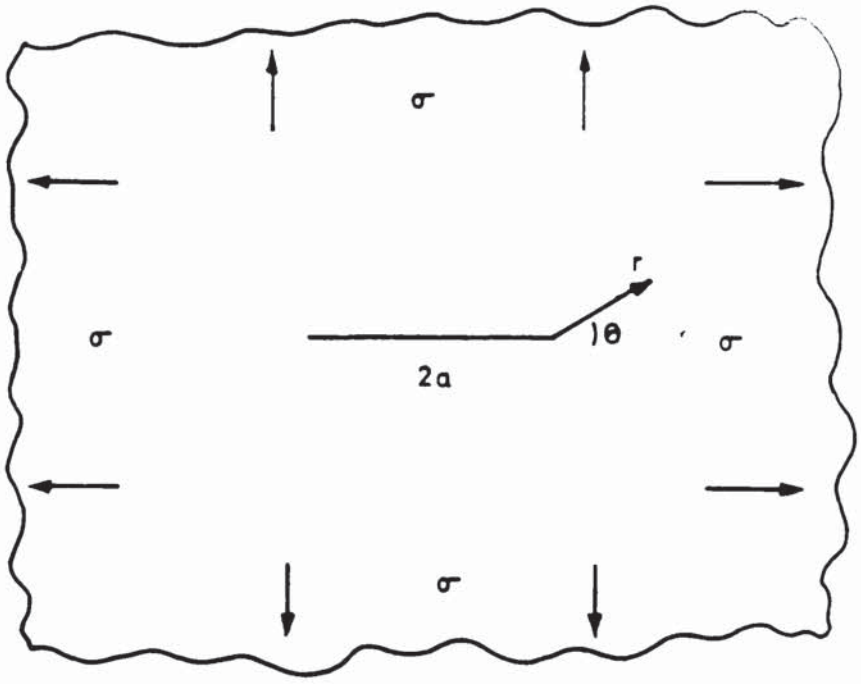

FIG 7 WESTERGAARD'S MODEL.

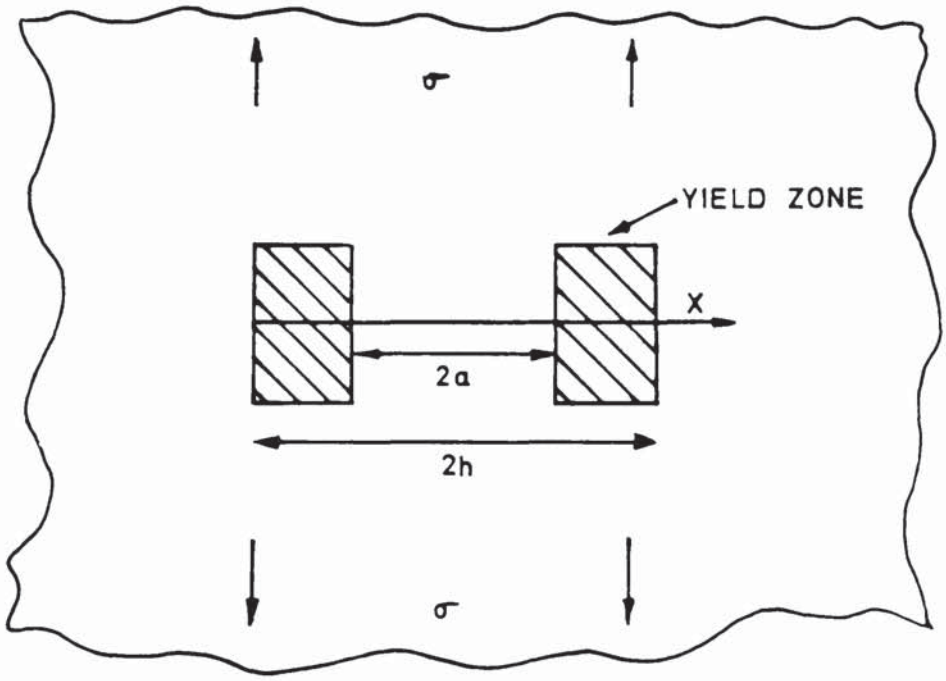

FIG 8 DUGDALE'S MODEL

The parameter K is the stress intensity factor which describes the stress and strain distribution immediately ahead of a crack tip in an elastic body. At fracture, the stress intensity factor reaches a critical value K_{IC}. When a load is applied remotely to a cracked body there can be three distinct modes of crack tip separation and hence three forms for K:-

Mode I (K_I) Crack tip separation normal to the crack plane. The operative stress is a tensile stress.

Mode II (K_{II}) Crack tip separation in the plane of the sheet. The operative stress is a shear stress.

Mode III (K_{III}) Crack tip separation out of the plane of the sheet. The operative stress is a shear stress.

These infinite plate solutions are not suitable for calculating the crack tip stress intensity factor in finite bodies. Appropriate correction factors accounting for changes in geometry and applied stress, are published in many standard fracture handbooks.

From the expression

$$\sigma_{11} = \frac{K}{\sqrt{(2\pi r)}} \tag{16}$$

it is clear that as the crack tip is approached ($r \rightarrow o$), the stress σ_{11} approaches infinity. In practice, the magnitude of σ_{11} is limited by the material near the crack tip yielding. For the case of a non-work hardening material, the plastic zone extends a distance d_y.

Where,

$$d_y \simeq 2r_y = \frac{K^2}{\pi \sigma_y^2} \quad \text{plane stress} \tag{17}$$

and

$$d_y \simeq 2r_y = \frac{K^2}{3\pi \sigma_y^2} \quad \text{plane strain.} \tag{18}$$

Where r_y is the distance at which σ_{11} calculated from equation (16) equals the yield stress, σ_y. The extent of the plastic zone (d_y) is greater than r_y because the system stresses and strains must be compatible and in equilibrium.

When small scale yielding occurs, Irwin (1964) has suggested that a more accurate estimate of the stress intensity factor would be obtained by using a notional crack length $(a + r_y)$. This value of crack length can then be incorporated into equation (13) to give:

$$K = \sigma \left[\pi (a + r_y)\right]^{\frac{1}{2}} \tag{19}$$

2.6.2 Post Yield Fracture Mechanics

A more accurate estimate of the extent of crack tip yielding was derived by Dugdale (1960). He considered a crack of length 2a subjected to a tensile stress σ (Figure 8). Plastic zones were assumed to develop and to spread out from the crack tips to a distance (h-a). Inside the plastic zones the stress σ_y was assumed to be constant and of yield point magnitude. By equating the stress intensity factor due to yield loads across the plastic zone with the stress intensity factor for an elastic crack of length 2h thus restricting the stress at (x=h) to a finite size, he showed that the plastic zone size could be determined from the relation:

$$\frac{a}{h} = \text{Cos}\left(\frac{\sigma\pi}{2\sigma_y}\right) \tag{20}$$

At low values of $\left(\frac{\sigma}{\sigma_y}\right)$

$$d_y = \frac{K^2\pi}{8\sigma_y^2} \tag{21}$$

which predicts a 23% larger plane stress plastic zone than equation (17).

An alternative method of calculating plastic zone sizes and crack opening displacements was developed by Bilby, Cottrell and Swinden (1963). The Bilby, Cottrell and Swinden (B-C-S) model had a distinct advantage over the Dugdale model in that it enabled displacements as well as stresses to be calculated. The crack and plastic zone were modelled as arrays of screw dislocations (Mode III deformation). By re-structuring the B.C.S. Model so that Mode I crack tip deformation occurs, and by substituting an elastic tensile modulus (E) for a shear modulus (G), it

can be shown that:

$$\delta = \frac{8\sigma_y}{E\pi} a \ln \left[\sec. \frac{\pi}{2\sigma_y} \right] \qquad (22)$$

δ is the crack opening displacement. Also, when the stress is very low equation (22) can be simplified to:

$$\delta = \frac{\sigma^2 \pi a}{\sigma_y E} = \frac{K^2}{\sigma_y E} \quad \text{for plane stress} \qquad (23)$$

Or, from $G = \frac{K^2}{E}$ (Irwin, 1957):

$$G = \sigma_y \delta \qquad (24)$$

Goodier and Field (1963) obtained equation (22) using continuum mechanics.

Heald, Spink and Worthington (1972) have proposed that K_{IC} can be used as a fracture criterion well into the post yield regime. By substituting for δ in equation (22), using equation (23), they have shown that K_{IC} can control the fracture behaviour.

They derived the equation

$$K_A = 2 \sigma_u \left(\frac{C}{\pi}\right)^{\frac{1}{2}} \cos^{-1} \left[\exp - \left(\frac{\pi K_{IC}^2}{8\sigma_u^2 C} \right) \right] \qquad (25)$$

which shows that the apparent stress intensity factor (K_A) associated with the fracture of a crack (C) under the action of a stress (σ_u), is related to the valid plane strain fracture toughness (K_{IC}).

2.6.3. General Yielding Fracture Mechanics

2.6.3.1 Crack Opening Displacement

Section 2.6.2 has shown that the crack opening displacement characterises the crack tip fracture events under small scale yielding. Cottrell (1961), and Wells (1961) have also suggested that the crack opening displacement fracture criterion could be used when general yield across the net section preceeds crack extension.

2.6.3.2 The J-Contour Integral

Rice (1968) introduced the concept of the J-contour integral to assess the toughness of a body undergoing non-linear elastic

deformation. By considering the change in potential energy ($-\Delta U$) when a hole in a body increases in size by a volume increase ΔV, equivalent to a surface increase ΔS, Rice showed that:

$$-(\Delta U) = J = \int_{\Gamma} \left[W dx_1 - T\left(\frac{\partial}{\partial x}\right) dS \right] \qquad (26)$$

The contour Γ surrounding the crack tip is traversed in the anti-clockwise direction, S is the arc length and T is the traction vector on Γ. When Γ is identical to the crack tip radius, the traction vector is zero and:

$$J = G \qquad (27)$$

Rice also showed that the difference in J for two curves with different path lengths, is zero. Thus, the J integral is path independent. However, the applicability of this approach to general yield when the contour must pass through the plastic zone remains a matter for conjecture.

2.7 Creep Crack Initiation and Growth Studies

At the beginning of this decade, Siverns and Price (1970) published a paper on the application of linear elastic fracture mechanics to creep crack growth. Since then, there have been a considerable number of papers published attempting to explain the creep behaviour of cracked bodies in terms of fracture mechanics. Some of these papers have been reviewed by McEvily and Wells (1973), Neate and Siverns (1973), James (1976) and Ellison and Harper (1978). Several workers have also developed theoretical models of creep crack growth.

2.7.1 Experimental Creep Crack Initiation and Growth

Siverns and Price (1970) examined a wrought 2¼Cr1Mo steampipe steel that had been quenched from 1350°C to simulate a weld heat affected zone. They showed that for tests on side edge notched tension specimens at 565°C, with the initial K varying from 10 to 40MNm$^{-3/2}$, the creep crack growth rate could be expressed by:

$$\frac{da}{dt} = A K^n \quad \text{with } n \simeq 5.5 \qquad (28)$$

All the data fell within a scatter band of approximately one order of magnitude in growth rate.

Robson (1972) showed that creep crack growth data from two 0.24%C steels tested at 450°C could also be fitted to a growth law incorporating K. The value of the K exponent for the two steels was 14 and 20. Test temperatures (T) were also varied to ascertain the activation energy (Q) for creep crack growth. Robson proposed that growth rates in the two carbon steels could be expressed by:

$$\frac{da}{dt} = C\, K^n\, e^{-\frac{Q}{RT}} \qquad (29)$$

Kenyon (1973) proposed a similar law for creep crack growth in an RR58 aluminium alloy.

An apparent correlation between creep crack growth rate and K was also observed by Thornton (1972) for wrought and cast CrMoV steels when tested at 550°C, and by James (1972) for Type 316 stainless steel. Both authors however, only tested a limited range of specimen geometries and crack sizes. Kaufman (1976), in analysing the data from a series of tests on an aluminium alloy 2219-T851, observed that the creep crack growth rate could be correlated with K. Unlike the previous authors however, he expressed his results in a semi-log form of

$$\log \frac{da}{dt} = BK - C \qquad (30)$$

where B and C are constants. Kaufman also proposed the existence of a threshold K for creep crack growth. This proposal was based on observations of prolonged crack incubation periods in low K tests.

Ellison and Walton (1973), in their work on creep and cyclic creep in a wrought 1CrMoV steel at 565°C, showed that the growth rate data from side edge notched tensile specimens could be correlated with either K or the net stress. Crack length/time plots showed that creep crack growth was preceeded by an incubation period. Ellison and Walton incorporated this incubation period into their empirical growth laws and showed that data

correlation was improved when the law

$$\frac{da}{dt} = A K^n t_p^x \qquad (31)$$

(where t_p is the crack propagation time) was used.

Other workers have also attempted to take account of the incubation stage prior to creep crack growth in the analysis of their data, and to consider using an alternative stress function to the stress intensity factor. Harrison and Sandor (1971) correlated the crack growth rate data from two centre-cracked panel 1CrlMo¼V steel specimens at 538°C, with K and the net stress. They showed that the most acceptable correlation was achieved with the net stress. Similar conclusions were reached by Taira and Ohtani (1973) from tests on double edge notched 1CrlMo¼V steel specimens, and by Nicholson and Formby (1975) from their work on side edge notched centre-hole solution treated Type 316 specimens. Reports supporting K rather than the net stress however, have been published by Holdsworth (1974; 1977) for CrMoV turbine steels, Koterazawa (1975) for Type 304 stainless steel, Batte (1975) for a 1CrMoV rotor steel, Floreen (1975) for six wrought Ni-base alloys, and Sadananda and Shahinian (1978) for Udimet 700.

A recent investigation into creep fracture of AISI 304 steel in the form of centre notched round bars and double edge notched tension specimens by Kawasaki and Horiguchi (1977), has shown that the creep crack velocity can be correlated for the indiviudal geometries with either K or net stress. Consistent correlation for the two geometries was however, only obtained with K. However, the effect of notch strengthening in the round bars was not considered and such consideration may have altered the conclusions.

The studies of creep crack growth in low alloy ferritic steels by Neate and Siverns (1973), Neate (1974), Neate (1976), and in Type 316 weld metal by Haigh and Laidler (1975; 1978), Laidler and Haigh (1976), have shown that the choice of stress parameter is dependent upon specimen

geometry, crack length, and the macroscopic and microscopic metallurgical structure. The work of these authors has shown that in general, a growth law incorporating K is appropriate when the creep ductility is low and when the specimen constraints are high. Alternatively, a law incorporating an 'average section stress' (net stress, reference stress) will be more appropriate when creep ductility is high and the constraints are low.

McEvily and Wells (1973), in their review on the application of fracture mechanics to elevated temperature problems, commented that the crack tip strain intensity could be a useful correlating parameter. They argued that the strain intensity reflects the crack opening displacement more accurately than the stress intensity factor and thus, should enable fracture mechanics to be extended into the creep range. Wells and McBride (1967) showed that the crack opening displacement (C.O.D.) adequately described the initiation and growth of creep cracks in semi-killed mild steel (BS15) tested at 350°C. A similar interpretation of test data was adopted by Pilkington et al. (1974), Soo (1974), Soo (1975), Haigh (1974), and Batte (1975). These authors argued that a linear elastic fracture mechanics assessment was invalid as significant amounts of time dependent crack tip plastic (creep) deformation was occurring both before and during the crack propagation stage. They proposed that a more suitable description of creep crack growth could be found in the expression;

$$\frac{da}{dt} \alpha \frac{d\delta}{dt} \tag{32}$$

where $\frac{d\delta}{dt}$ is the crack opening displacement rate.

Formby (1972), and Nicholson and Formby (1976), adopted a slightly different approach to the assessment of creep crack growth when the growth was accompanied by large amounts of creep deformation. They adopted the fracture angle criterion of McLintock (1968) and developed it into the model for creep fracture of the form:

$$a = \frac{1}{\omega} (\delta - \delta_i) \tag{33}$$

Here, a is the crack length, δ_i the initiation crack opening displacement, δ the creep crack opening displacement at the initiating position and ω is the included angle in radians. $\frac{1}{\omega}$ is termed the aspect ratio of the crack. The necessary condition for the application of this model is that the aspect ratio remains constant.

Although the crack opening displacement fracture criterion appears to correlate the creep behaviour of low creep strength laboratory specimens and is easily calculated in these geometries, analytical solutions for creep displacements in large and geometrically complicated components can be considerably more difficult. An alternative method of analysing data from low creep strength materials was proposed by Haigh (1974). He introduced the concept of an 'equivalent stress' to describe creep crack growth. This equivalent stress is based on a time independent fully plastic slip line field theory (Ewing and Richards, 1973; Haigh and Richards, 1974).

For typical laboratory specimens the equivalent stress σ_E can be calculated from

$$\sigma_E = \frac{P}{mBW} \tag{34}$$

where P is the load, B the thickness, W the width of the specimen, and

$$m = \frac{\text{load to yield the cracked specimen}}{\text{load to yield the uncracked specimen}} .$$

Haigh argues that because creep crack growth in low creep strength materials is deformation controlled and the deformation is determined by the equivalent stress, the latter is the appropriate controlling parameter.

Williams and Price (1975) attempted to rationalise the various approaches used to describe creep crack growth in steels by considering the relaxation of the elastic stresses ahead of the crack when the creep properties of the material were varied. They commented that any theory for general application must be able to account for time dependent creep cracking in ductile and brittle materials. By referring to continuum methods of analysing the relaxation of stresses in both a simple beam in pure bending and ahead of a hole in a plate, Williams and Price suggested

that the selection of the correct correlating stress parameter was dependent on the creep stress exponent.

By referring to Norton's Power Law

$$\dot{\varepsilon}_u = E\sigma^X \tag{35}$$

and the Time Hardening Law

$$\varepsilon = F\sigma^Y t^Z \tag{36}$$

the authors have suggested that when the stress exponent is greater than 5, the level of the elastic stresses ahead of the crack are markedly reduced and the reference stress (identical to Haigh's equivalent stress when the stress exponent tends to infinity) is the correlating parameter. Whereas, when the stress exponent is less than 5, K becomes the controlling parameter.

A model of creep fracture using the concept of the reference stress has been developed by Freeman (1977). By incorporating the expression for the equivalent stress from Haigh's work (equation 34), with the empirical creep rupture law;

$$\sigma^p t_f = \text{constant} \tag{37}$$

where σ is the applied stress and t_f the fracture time, Freeman has shown that the macroscopic creep crack velocity is of the form:

$$\frac{da}{dt} \alpha \sigma^{\frac{2p-1}{2}} \tag{38}$$

Good agreement between predicted and experimental crack velocities was obtained for a normalised and tempered ½Cr½Mo¼V steel.

In a recent review of creep crack growth (Ellison and Neate 1976), it was proposed that the J-contour integral would be an appropriate parameter to use on intermediate ductility materials. Webster (1975), Nikbin et al. (1976), and Landes and Begley (1976), have also considered the application of J to creep crack growth. They proposed a new parameter $\dot{J}$ (or C*) based on the J-contour integral. Here, $\dot{J}$ is an energy rate line integral which characterises the crack tip stress and strain rate field in a material deforming according to Norton's Power Law. These workers

argued that if the crack tip stress and strain rates determined crack propagation, then $\dot{J}$ would correlate the growth rate. Webster (1975) plotted $\dot{J}$ and K against the crack growth rates in a bainitic ¼CrMoV steel and found that only $\dot{J}$ consistently correlated the data. Similar observations were made by Nikbin et al. (1976) for RR58 aluminium alloy, and by Landes and Begley (1976) for a discalloy superalloy.

More recently, Harper and Ellison (1977) have shown that $\dot{J}$ is a good correlation parameter providing creep fracture proceeds slowly by a localised rupture process. Tests were conducted on a 1CrMoV steel in fatigue precracked compact tension and side edge notched bend specimens. A good $\dot{J}$ correlation was obtained once the effects of stress redistribution had become negligible.

2.7.2 Theoretical Models

2.7.2.1 Continuum Models

The theoretical treatment of macroscopic creep cracking using continuum mechanics falls into two distinct categories.

(a) The presence of a crack or notch is always recognised through well defined transient and steady state elastic stress profiles along the cracking plane.

(b) The transient and steady state elastic stress profile is fixed and is independent of the form of the stress concentrator.

Within the first category lies the work of Barnby and co-workers who treated creeping materials in a generally realistic manner. Barnby's early papers (1974, 1975) considered macroscopic creep crack growth for the case of steady state stress conditions. He assumed that the initial elastic stress field could be described by K and that the fracture criterion was a critical crack opening displacement. By using an elastic analogue for creep deformation to solve non-linear viscoelastic creep, Barnby showed that the nominal elastic stress distribution ahead of the crack tip relaxed to a steady state level. The final level and distribution of the stress was shown to be a function of the secondary creep rate stress exponent in

Norton's power law. When the stress exponent had the value 1, the stress distribution was shown to be analogous to linear elastic behaviour. Under these conditions, a K correlation of crack growth rate was predicted. At higher values of the stress exponent, the crack tip stresses were shown to fall more rapidly and approach the level of the net section stress, thereby favouring the net stress as the correlation parameter. A development of this model by Barnby and Nicholson (1977) has shown that the steady state stress (σ_{ss}) ahead of a crack varies according to the expression

$$\sigma_{ss} \alpha x^{-\left(\frac{1}{m+1}\right)} \qquad (39)$$

where x is the distance ahead of the crack tip and m is the creep power law stress exponent. Good agreement between theoretical predictions and experimental observations of steady state strain rates was obtained from creep tests on 0.75 mm thick double edge notched AISI 316 steel specimens.

As it stands at the moment, Barnby's theory cannot account for material behaviour under all multiaxial loading conditions and a wide range of applied loads, since only plane stress deformation has been considered and the restrictive Norton's law used to describe creep deformation. In addition, the work does not consider in sufficient detail the operative fracture stress local to the crack tip. However, as the theory always recognises the existence of the original stress concentrator and its effect on the transient and steady state stress distribution, the consequential accumulation of creep strain which leads to creep rupture will always be realistic.

An alternative approach to the creep response of cracked structures which falls within the first category, is that developed by Goodall and Chubb (1976). They adopted a model similar to that considered by Kachanov (1958), which considers a creep damage front spreading ahead of a physically identifiable crack. In a development of the basic Kachanov model, Goodall and Chubb considered an initial elastic stress distribution described by the

Bowie formula (see Paris and Sih, 1964) and a relaxed stress distribution which displayed a cube root dependence with distance ahead of the crack tip. Under the action of this stress field the material accumulated creep strain again according to Norton's law,with rupture at each discrete point ahead of the original crack governed by a life fraction rule. Unfortunately, no direct description of crack growth arises from the theory and only by drawing on analogy between the spread of the creep damage zone and macroscopic crack growth, were the authors able to explain a very selective set of experimental results on ductile CrMoV steel. In order to gain general acceptance, a theory on macroscopic creep crack growth must be versatile enough to cover a wide range of materials and be readily identifiable with classic theory on the mechanistics of creep fracture. In neither case does the theory of Goodall and Chubb comply.

Fracture theories classified according to category two include those of To (1975), Heaton and Chan (1976), Vitek (1976) and Ewing (1977). All these theories are based on the prime assumption that the stress field associated with a notch or crack can always be described by the Dugdale-BCS model. As a result, they are limited to analysing the situation of plane stress deformation in an infinite plate. In addition, they are effectively saying that the stress profile ahead of a crack is independent of the inherent creep strength of the material under investigation, this is clearly a matter for conjecture. To (1975) in common with Goodhall and Chubb (1976),adopted the Kachanov cumulative creep damage concept to describe the deterioration of a materials integrity under stress. To proposed that the creep crack advanced by the successive rupturing of 'creep process zones' ahead of the crack tip and by using a curtailed description of the crack tip zone stress profile, predicted a straight line in a double log plot of crack growth rate and K, and that the slope of this plot was always greater than 2.

In an attempt to generalise To's work, Heaton and Chan (1976) incorporated in their analyses a supposedly full description of the stress gradient ahead of the stress concentration, and also perpetuated the realistic concept of a critical strain fracture criterion. Under these conditions and using Norton's law, they predicted that the crack velocity in a material which had undergone a history of varying stresses would be proportional to $K^{2(n-1)}$. A modicum of success has been obtained between theoretical predictions and experimental results for cast CrMoV alloy steels (Chan, 1978).

As part of a natural development of the Dugdale-BCS model, Vitek (1976) considered the crack initiation aspects of creep fracture. He assumed quite reasonably, that in regions of non-uniform stress the material could be divided into elements which deform according to the creep law

$$\dot{\varepsilon} = \dot{\varepsilon}(\sigma) \tag{40}$$

σ being the local uniaxial stress. A computational technique was then used to simulate the accumulation of creep damage ahead of the crack tip to calculate dislocation densities and crack opening displacements as a function of total or incremental time. This model proved to be more versatile than its predecessors as it was capable of predicting with reasonable accuracy the creep fracture behaviour of both ductile and brittle CrMoV steels. Unfortunately Vitek's theory inherited all of the aforementioned approximations on material behaviour and as a consequence, had very limited practical application. The work of Ewing (1977) can be criticised in a like manner. He attempted to provide an overall picture of creep fracture by combining the work of Heaton and Chan (1976) on crack growth, and of Vitek (1976) on initiation, by using a creep deformation law that incorporated both primary and secondary creep effects. Ewing predicted in a somewhat nebulous way that initiation and fracture times would be K controlled at moderately high applied stresses and net stress controlled at low applied stresses.

The concept of creep cracks growing by the rupture of discrete elements lying ahead of the advancing crack tip has also been adopted by Purushothaman and Tien (1976). Using the Orowan-Irwin description of the stress field near a crack tip and assuming that for every element (dx) there would be a corresponding rupture life $t_r(x)$, they considered that the growth rate $\frac{da}{dt}$ would be equal to $\frac{dx}{dt_r}$. By obtaining the rupture life from the empirical law

$$t_r = \text{Constant } (\dot{\varepsilon})^{-\alpha} \tag{41}$$

and the creep rate ($\dot{\varepsilon}$) from the relevant Norton's power law, the authors showed that the creep crack growth rate of a crack possessing a constant tip radius and lying in a body of finite size would be proportional to K. In this theory, the authors have considered to their credit, the very important aspect of creep crack growth in finite bodies. At present, only one other theory, that of Barnby's, has this desirable quality.

2.7.2.2 Diffusion Models

Dimelfi and Nix (1977) considered the growth of a creep crack by the diffusional growth and linkage of cavities on grain boundaries. The stress field ahead of the crack was assumed to be described by linear elasticity whilst the effect of cavities on this stress distribution was ignored. A further assumption was that the deviatoric parts of the stress and strain rate tensor controlled the growth of cavities. Cavity growth was calculated from a model due to Hellan (1975), where a cavity surrounded by a material deforming according to Norton's power law grows by diffusion under the action of a remotely applied radial tensile stress. Although the model by its basic assumptions predicted a K correlation, the authors argued that with large cavity spacings (low creep damage) their model could predict very low crack velocities. Under these conditions, they proposed a net section stress dependence.

The growth of a crack by vacancy condensation has also been considered by Van Leeuwen (1977). Using stress modified diffusion equations to calculate the steady state concentration distribution of vacancies around an embedded penny shaped crack in an infinite body, Van Leeuwen was able to account for the primary and tertiary stages of creep crack growth behaviour.

Vitek (1978) has also considered the growth of creep cracks by a diffusion mechanism. The mechanism consisted of the removal of atoms from the crack tip by stress induced grain boundary diffusion and their deposition at the grain boundary. Diffusion rates were modified to account for stress relaxation ahead of the crack tip which arose from the non-uniform deposition of material onto grain boundaries. Vitek found that the rate of crack growth was determined by the nominal stress intensity factor. A minimum stress intensity was predicted below which no crack growth would take place, and above which crack growth would be proportional to the fourth

power of the nominal stress intensity factor. The theory however, was only applicable to brittle materials in which the plastic deformation at the crack tip was negligible. The development and growth of cavities and microcracks ahead of the main crack and their eventual linking up with it, was also ignored.

2.8 Multiaxial Creep Rupture

During the course of this Thesis, use is made of the Von Mises equivalent stress to calculate the magnitude of creep strain in a multiaxial stress system ahead of a sharp notch. The concept of equivalent stress or some similar 'effective stress' has been used by several other workers to calculate multiaxial creep rupture in un-notched specimens. These are reviewed below.

The provision of a rational basis for the design of undefective components required to operate under creep conditions and under any stress system was first attempted by Bailey (1935). Having considered the stress distribution in creep in tubes, cylinders, rotating discs and rotors, Bailey calculated that creep deformation would in the presence of the three principal stresses (σ_{11}, σ_{22}, σ_{33}), develop according to the equation;

$$\dot{\varepsilon}_{11} = \frac{A}{2}\left[\frac{1}{2}\left(\sigma_{11}-\sigma_{22}\right)^2 + \frac{1}{2}\left(\sigma_{33}-\sigma_{11}\right)^2 + \frac{1}{2}\left(\sigma_{22}-\sigma_{33}\right)^2\right]^m \times\left[\left(\sigma_{11}-\sigma_{22}\right)^{n-2m} - \left(\sigma_{33}-\sigma_{11}\right)^{n-2m}\right] \quad (42)$$

where $\dot{\varepsilon}_{11}$ is the tensile creep rate in the <11> direction and n, m and A are constants. For simple tension, Equation (42) reduces to the uniaxial case of:

$$\dot{\varepsilon}_{11} = A\,\sigma_{11}^{\,n} \quad (43)$$

Support for a Von Mises type of flow law (Equation 42) has come from Simonen (1973), who suggested that the effective creep stress (σ_e) could be obtained from the expression:

$$\sigma_e = \left(\sigma_{11}^{\,2} - \sigma_{11}\,\sigma_{22} + \sigma_{22}^{\,2}\right)^{\frac{1}{2}} \quad (44)$$

Several workers have attempted with varying degrees of success, to use a Von-Mises type flow law to explain the multiaxial creep rupture of thick tubes in both ferrous and non-ferrous alloys. Kooistra, Tucker and Coulter (1960) used an empirical effective stress with some success, whilst Davies (1960) found that an effective shear stress at mid-thickness gave a good correlation. Alternatively, Chitty and Duval (1963), and Taira and Ohtani (1968) found that a mean diameter normal stress formula gave excellent predictions of creep rupture life. Johnson, Henderson and Khan (1962) however, have found that the creep rupture of thin walled Mo steel tubes subjected to tension/torsion testing, was best described by the maximum principal stress. Support for a maximum principal stress rupture criterion has also been provided by Manjoine (1963), following his work on 'T' head models of blade retaining grooves of steam turbines.

Henderson and Ferguson (1977), following the work of Johnson et al. (1962), Johnson and Khan (1965) and Henderson and Snedden (1972), have proposed that under homogeneous stress conditions, two rupture criteria would dominate. For metals which develop random and continuous cracking during creep, the maximum principal stress criterion determines the rupture time. For metals showing virtually no cracking during creep, the criterion is the octahedral shear stress or the Von-Mises equivalent stress. The level of creep ductility was not however, found to be uniquely related to one or other criterion. Henderson and Ferguson (1977) developed a model for creep rupture based on the comparative predictions of rupture life from the two criteria. The authors considered that according to the octahedral shear stress and maximum principal stress criteria, the representative tensile stress for the general case would be the Von Mises equivalent stress ($\bar{\sigma}$) and the normal stress σ_{11} ($\sigma_{11}>\sigma_{22}>\sigma_{33}$) respectively. Applying these principles to rupture testing under pure shear for a material whose rupture life (t_f) could be expressed by the relationship;

$$t_f = A\,\sigma^{-V} \qquad (45)$$

Henderson and Ferguson showed that the ratio of the fracture time according to the two rupture criteria varied as:

$$\frac{t_f\ (\bar{\sigma})}{t_f\ (\sigma_{11})} = \left(\frac{\sqrt{3}}{1}\right)^{-V} \qquad (46)$$

A comparison of predicted and experimental rupture lives for a normalised and tempered ½CrMoV steel showed conclusively that the octahedral shear stress failure criterion was far superior to the maximum principal stress criterion. This observation is pertinent to the present investigation. Further torsion tests by the authors have also confirmed that the failure criterion established from short term tests is also valid for very long term tests.

CHAPTER 3

Experimental Methods

3.1 Material Selection

Two cast steels were selected for examination, these were the ½Cr½Mo¼V and the 1Cr1Mo¼V alloys. The ½Cr½Mo¼V alloy originated from a bolt hole trepan in the flange of a steam turbine high pressure outer casing. This casing was designed and manufactured by the General Electric Company. The 1Cr1Mo¼V alloy originated from cast blocks manufactured by F. H. Lloyds Limited.

The chemical composition of both alloys is given in Table 1.

Table 1. Chemical Composition % By Weight

Alloy	C	Mn	S	P	Si	Ni	Cr	Mo	V	Cu
½Cr½Mo¼V	.12	.70	.015	.015	.28	.21	.36	.52	.35	.11
1Cr1Mo¼V	.098	.56	.05	.01	.40	.05	1.11	.92	.35	-

The basic heat treatment given to each alloy followed normal practice and was designed to produce stable microstructures possessing adequate creep strength and high ductility (Section 2.1). In the case of the ½Cr½Mo¼V alloy an extra temper had been applied because the material had been part of a casing which had had to be repaired.

Samples of the 1Cr1Mo¼V alloy were also heat treated to produce a metastable microstructure possessing a relatively high creep strength but low ductility. These properties are often observed in thin sections of casings manufactured from this alloy and also, but less frequently, in weld repaired casings.

The heat treatments were as follows:-

½Cr½Mo¼V (normalised and tempered)

Homogenise 950°C 10 hour soak, furnace cool.

Normalise 950°C " " " air cool.

Temper 690°C " " " furnace cool.

Re-Temper 675°C 12 hour soak, furnace cool.

The microstructure consisted of equiaxed ferrite grains and pearlite (Figure 9a). The ferrite grain size as measured by the linear intercept method was 26μm. The pearlite content was estimated by the point counting method to be 2%.

1Cr1Mo¼V (normalised and tempered)

Homogenise 1010°C 9 hour soak, furnace cool.

Normalise 1000°C 3 hour soak, fast cooled to simulate a thin section.

Temper 700°C 12 hour soak, furnace cool.

The microstructure consisted of equiaxed ferrite grains with a grain size of 31μm (Figure 9b).

1Cr1Mo¼V (quenched and tempered)

Austenitise 975°C 8 hour soak, oil quench (heating rate 30°C/hour).

Temper 690°C 12 hour soak, furnace cool.

The microstructure consisted of tempered bainite (Figure 9c).

3.2 Design and Construction of Creep Facilities and Experimental Apparatus

The construction of a new Departmental Building in 1974 included a purpose-built creep laboratory, consisting of a control room and two test rooms. Six 50KN Denison creep machines, together with all the necessary services and ancillary equipment were installed in each test room (Figure 10). All temperature controllers, power packs and test monitoring equipment were located in the control room (Figure 11). The air temperature in all three rooms was maintained at 25 ± 5°C.

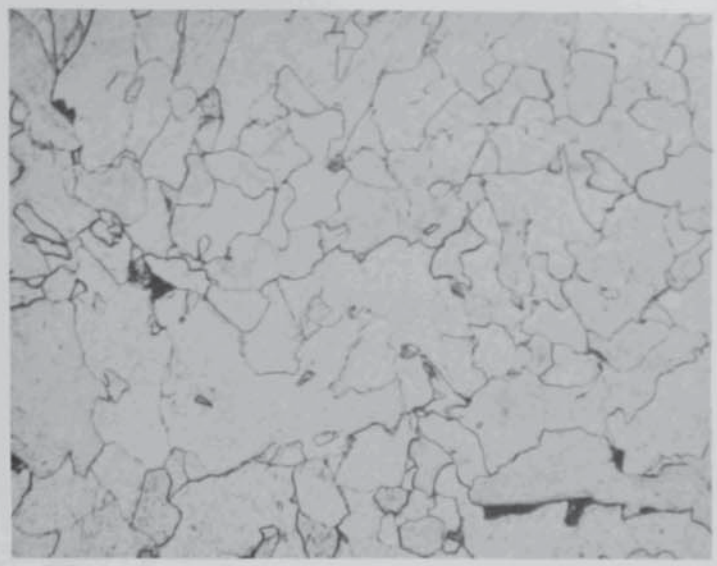

x 200

FIG. 9a $\frac{1}{2}$ Cr $\frac{1}{2}$ Mo $\frac{1}{4}$V NORMALISED & TEMPERED

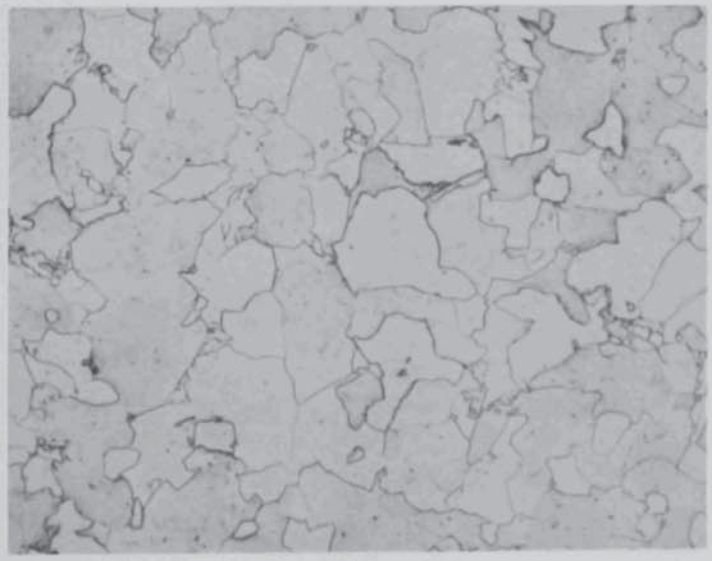

x 200

FIG. 9b 1Cr 1 Mo $\frac{1}{4}$V NORMALISED & TEMPERED

x 400

FIG. 9c 1Cr 1Mo $\frac{1}{4}$V QUENCHED & TEMPERED

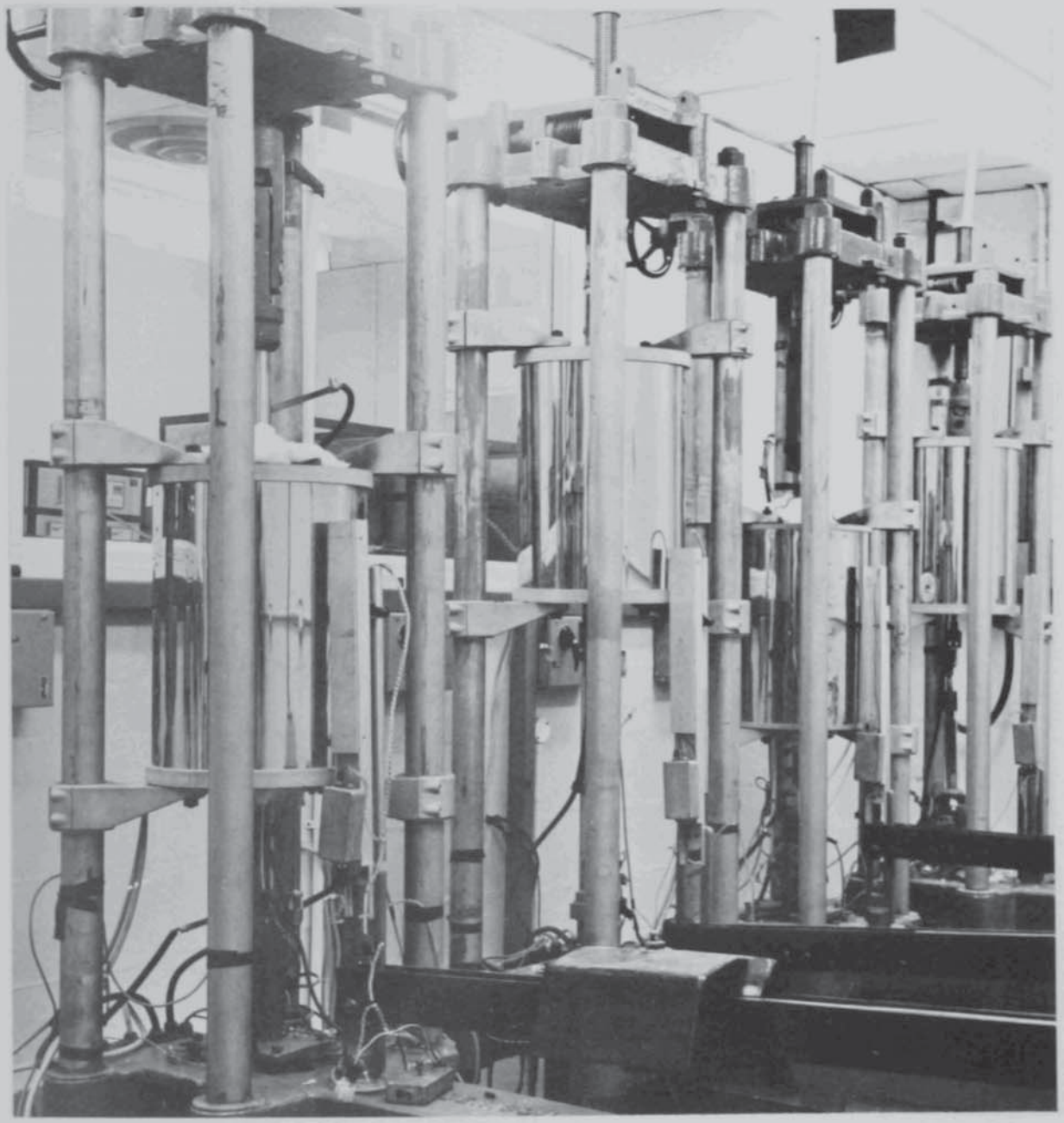

FIG. 10 TEST ROOM

FIG. 11 CONTROL ROOM

The loading system on each creep machine was calibrated with a proving ring to B.S.1610:1964 Grade A.

The majority of creep machines were equipped with large bore three-zone wire wound electrical resistance furnaces. These furnaces were designed to accept the standard 50mm thick compact tension fracture toughness specimen. The furnace temperature was controlled by either a three zone Eurotherm thyristor driven controller working from a Pt/Pt.Rh thermocouple attached to the specimen, or by a Mayes phase angle firing controller working from a platinum resistance thermometer (P.R.T.) located near the furnace windings. In either case, the specimen temperature was maintained within $\pm 1^{o}C$ of the required test temperature.

The specimen temperature was measured continuously by a Pt/Pt.Rh thermocouple attached to the specimen near the crack tip. The axial temperature gradient in all furnaces over a distance of 50mm either side of the cracking plane in a compact tension or centre-cracked panel specimen was $1^{o}C$ or better. Radial temperature gradients around the cracking plane were of the same order. Signals from the thermocouples and P.R.T's to the temperature controllers and recorders were carried through appropriate compensating cables.

Direct current for the potential drop crack monitoring technique (Section 3.5) was supplied to each machine by its own 50 ampere constant current power pack. The current was carried from the power pack to a junction box located on the creep machine frame, by a 100 ampere multi-strand cable. Copper strip was then employed to carry the current to the specimen (Section 3.5).

High temperature leads, consisting of an iron wire core surrounded by silica insulation and braided stainless steel screening, were connected to screened copper leads and used to transfer the potential signals from the specimens to the monitoring equipment. A disadvantage in using copper leads was that thermal electro-motive-forces (e.m.f.) could be generated at

the Fe/Cu junction. This effect was minimised by constructing two Fe/Cu junctions, one in the test room and the other in the control room, and immersing the junctions in separate 'constant temperature baths'. Thermal e.m.f's generated at probe/specimen junctions were considered to be negligible.

The potential signals were monitored by two data transfer units, modified to work together so that one digital volt meter and one output typewriter could be used (Figure 12). The signals were recorded at two hourly intervals during the initial stages of creep crack development and more frequently as the crack velocity increased.

All screened cables, electrical apparatus and creep machine frames were connected to mains earth to improve signal stability. Interference from alternating current (a.c.) circuits was minimised by careful routing of the direct current (d.c.) supplies between the control and test rooms. In order to improve the sensitivity of the potential drop crack monitoring technique, the bottom half of the specimen loading train was electrically insulated from the creep machine frame. This was achieved by inserting tufnol washers between the main loading bar and the knife-edge assembly located at the base of the creep machine.

The creep machine loading train was made from various Nimonic alloys. The choice of alloy was determined by the magnitude of the operating stress in the individual parts of the loading train. Thus, Nimonic 80 was used for the loading bars, Nimonic 90 for the clevices and Nimonic 105 for the clevice loading pins.

A schematic wiring diagram of the a.c. and d.c. circuits in the control and test rooms is shown in Figure 13.

3.3 Design of Tests

Two standard fracture toughness specimen geometries were chosen for the study of creep ductility. These were the compact tension (C.T.) geometry and the centre-cracked panel (C.C.P.) geometry (Figure 14). The C.T.

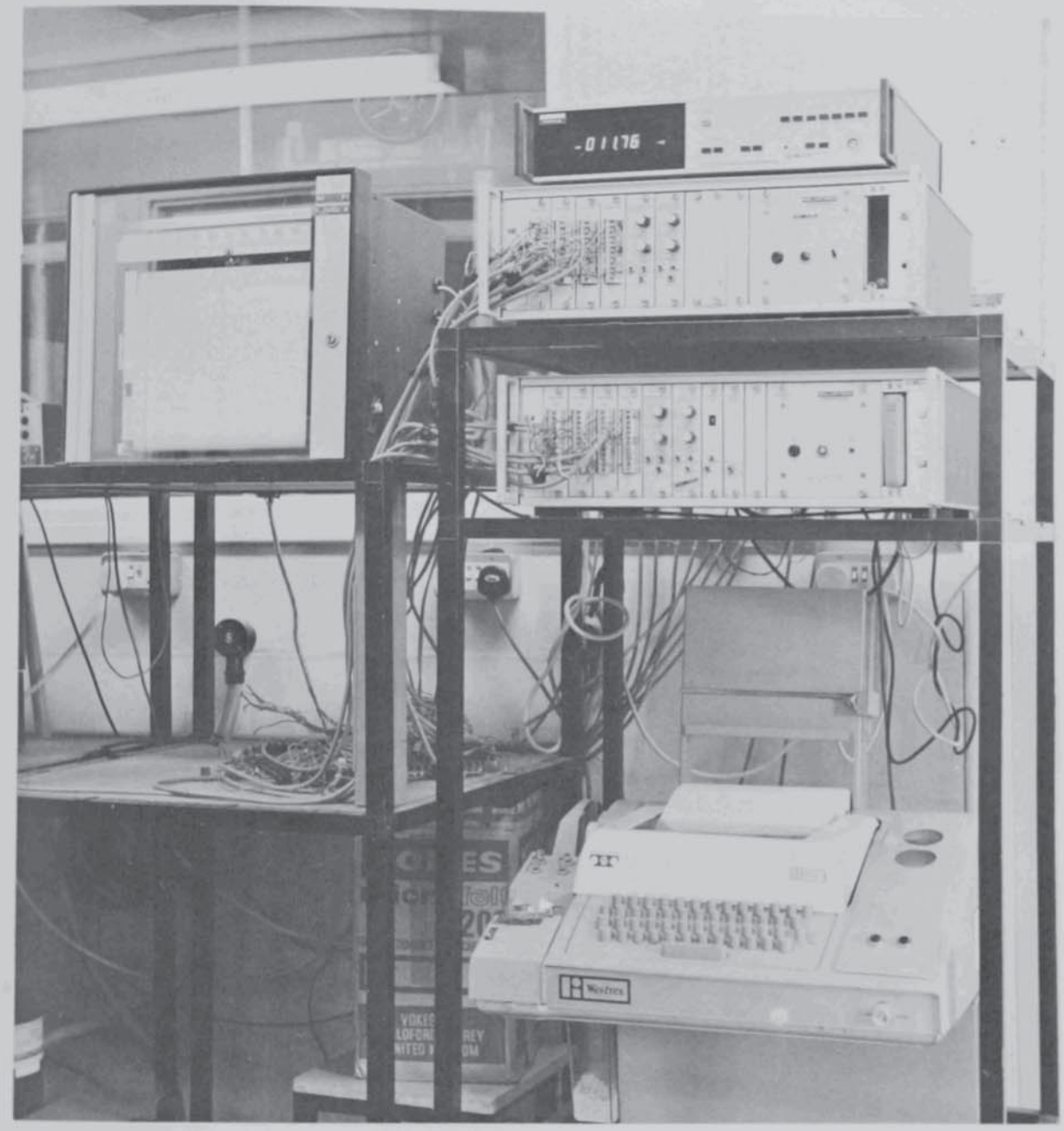

FIG. 12 DATA LOGGING SYSTEM

FIG 13 SCHEMATIC WIRING DIAGRAM

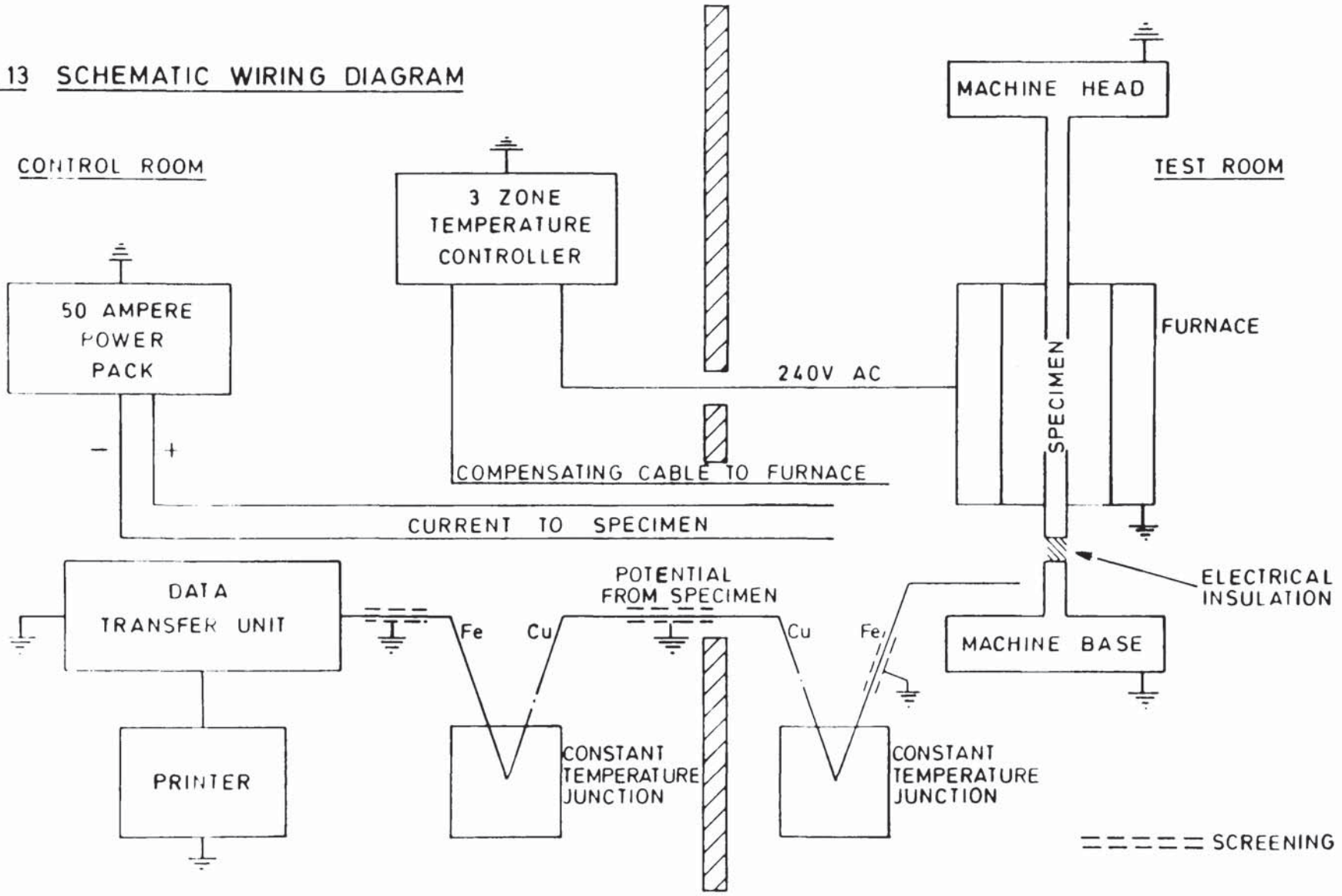

RC/SSR/A4/592

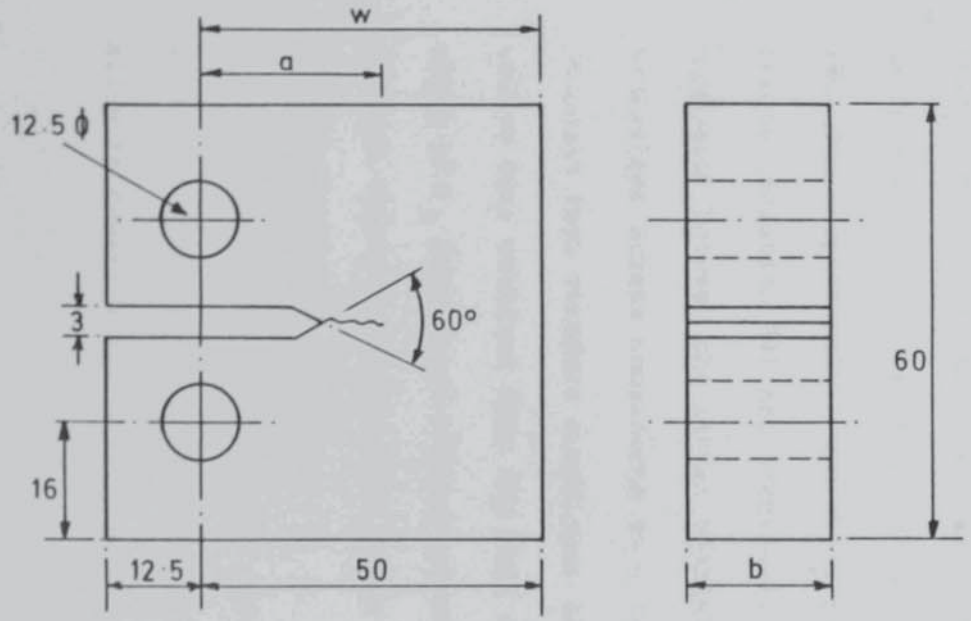

a = CRACK LENGTH (MACHINED + FATIGUE + (CREEP))

b = THICKNESS

ALL DIMENSIONS IN mm

(a) COMPACT TENSION GEOMETRY

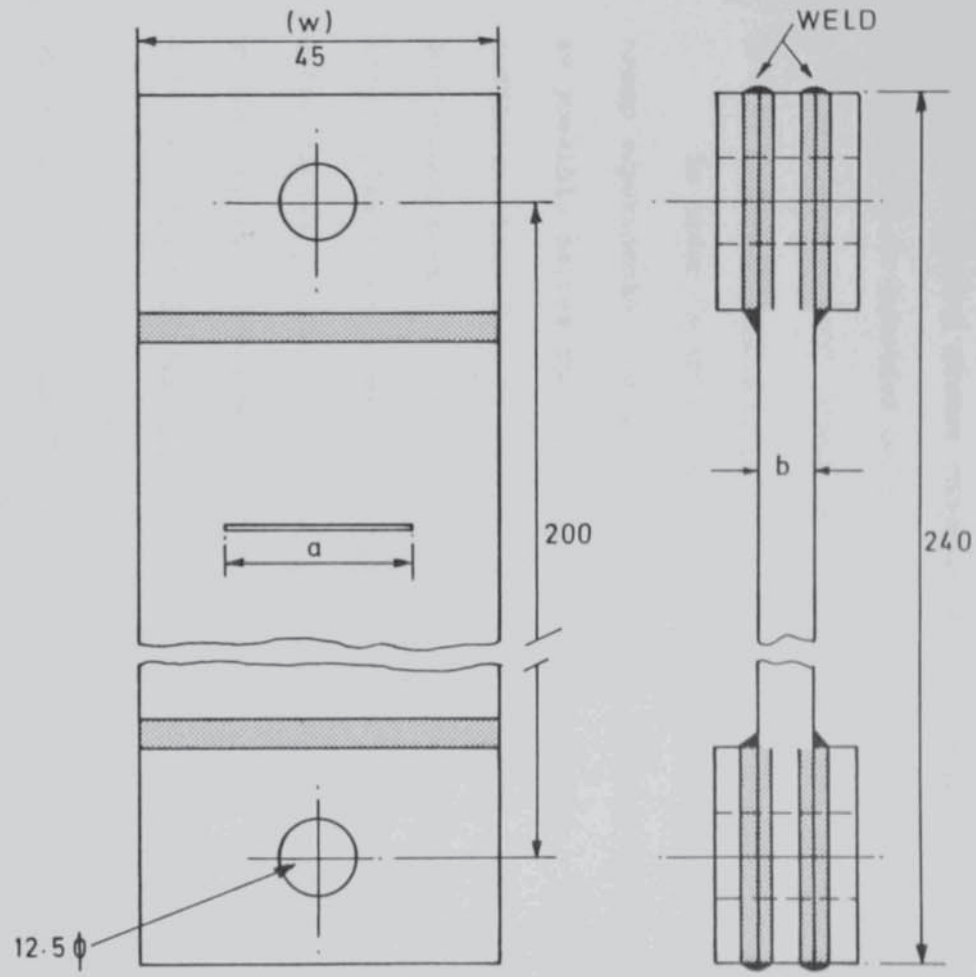

(b) CENTRE-CRACKED PANEL GEOMETRY

FIG. 14 SPECIMEN DIMENSIONS

specimen represented a surface defect lying in a stress field containing direct and bending stress components whereas the C.C.P. specimen represented an embedded defect under direct stress only.

All creep crack growth tests were performed at 550°C in air (Section 1).

3.3.1 Determination of Appropriate Test Conditions

In order to obtain realistic material responses from laboratory creep experiments, tests were designed to give as much creep crack growth as possible before the advent of plastic collapse. This would provide sufficient test data to enable any perturbations in growth rate due to un-characteristic local fracture events to be detected. Terminating tests before plastic collapse would enable tested specimens containing growing intergranular cracks to be sectioned and studied. Accordingly, the test parameters were designed as shown below.

3.3.1.1 Choice of Applied Stress

Figure 15 shows the fixed load relationship between the elastic stress intensity factor (K) and the reference stress (σ_R) for various initial values of relative crack length $\left(\frac{a}{W}\right)$ in a C.T. and C.C.P. specimen. In this instance, the width (W) of the C.T. and C.C.P. specimen was 50mm and 45mm respectively. The above reference stress and Haigh's Equivalent Stress (equation 34) are identical. Re-naming was done in order to avoid confusion between the latter equivalent stress and the Von-Mises Equivalent Stress considered in a later chapter. The values of K were obtained from standard compliance tables (Section 3.4.1), while the σ_R values were obtained from the work of Haigh and Richards (1974). As the value of σ_R depends on whether plane stress or plane strain deformation is assumed (Section 3.4.2), both modes of deformation have been considered initially in this Section.

By extracting the relevant initial σ_R value from Figure 15 and inserting it into the published plain-specimen creep rupture curve of the alloy in question (in this case the 1Cr1Mo¼V alloy in the normalised and

tempered condition, Figure 16), an estimate of the rupture life of the test piece can be obtained. An example of estimated rupture lives for a C.T. specimen whose initial K values vary from 10 to 50 $MNm^{-3/2}$ on cracks of 0.4, 0.5 and 0.6 $\frac{a}{W}$, is shown in Table 2.

Table 2. Estimated Specimen Rupture Lives

$\frac{a}{W}$	K $MNm^{-3/2}$	σ_R MNn^{-2} Plane Stress	σ_R MNm^{-2} Plane Strain	Rupture Life h.	
				Plane Stress	Plane Strain
0.4	10	49	35	>>30000	>>30000
	20	98	70	>>30000	>>30000
	30	147	105	11900	>30000
	40	196	140	1100	16800
	50	245	175	100	3200
0.5	10	57	41	>>30000	>>30000
	20	114	82	>30000	>>30000
	30	171	123	4000	>30000
	40	228	164	200	5300
	50	284	205	<100	700
0.6	10	66	50	>>30000	>>30000
	20	133	99	25100	>>30000
	30	198	150	1000	10600
	40	264	198	<100	1000
	50	331	247	<100	<100

It is clear from Table 2 that a plane strain reference stress rupture criterion provides an upper estimate of rupture life. In practice however, a rupture criterion such as this may prove to be invalid particularly if a stress concentration still exists at the crack tip. In the extreme case where little or no crack tip stress relaxation occurs, a stress intensity rupture criterion may well be more appropriate. A more central position can be obtained however, by adopting the plane stress reference stress rupture criterion. Thus, in the absence of relevant crack tip stress relaxation data, plane stress σ_R values were used to estimate

specimen rupture lives.

3.3.1.2 Validity of Test

Under conditions of fixed load and increasing crack length, the net section stress will rise and eventually exceed the general yield stress and the ultimate tensile stress. This would be undesirable in a creep test designed to simulate a defect growing under high constraint in a body with a low net section stress. The initial σ_R in the creep test must therefore be well below yield to allow for an adequate amount of creep cracking before constraint is lost.

A measure of the yield stress (0.2% Proof Stress) and the ultimate tensile stress at 550°C can be obtained from Figures 17 and 18 for the material under investigation. This data was obtained from constant displacement rate tensile tests in air, on specimens with gauge lengths of 100mm and gauge length diameters of 10mm. The initial strain rates were varied from approximately 10^{-2} to 10^{-5} min.$^{-1}$

Taking the 1Cr1Mo¼V alloy in the normalised and tempered condition as the basis for the design of the creep experiments, Figures 17 and 18 indicate that a conservative value of the yield and ultimate tensile stress would be approximately 200 MNm^{-2}. Therefore, by fixing the starting stress level (σ_R) between 150 and 200 MNm^{-2}, sufficient creep cracking should be obtained before constraint is lost and before stable ductile tearing occurs. Table 2 indicates the range of tests that meet this acceptance criterion. They are listed in Table 3.

Table 3.

$\frac{a}{W}$	K MNm$^{-3/2}$	σ_R MNm^{-2} Plane Stress	Rupture Life h.
0.4	30	147	11900
	40	196	1100
0.5	30	171	4000
0.6	30	198	1000

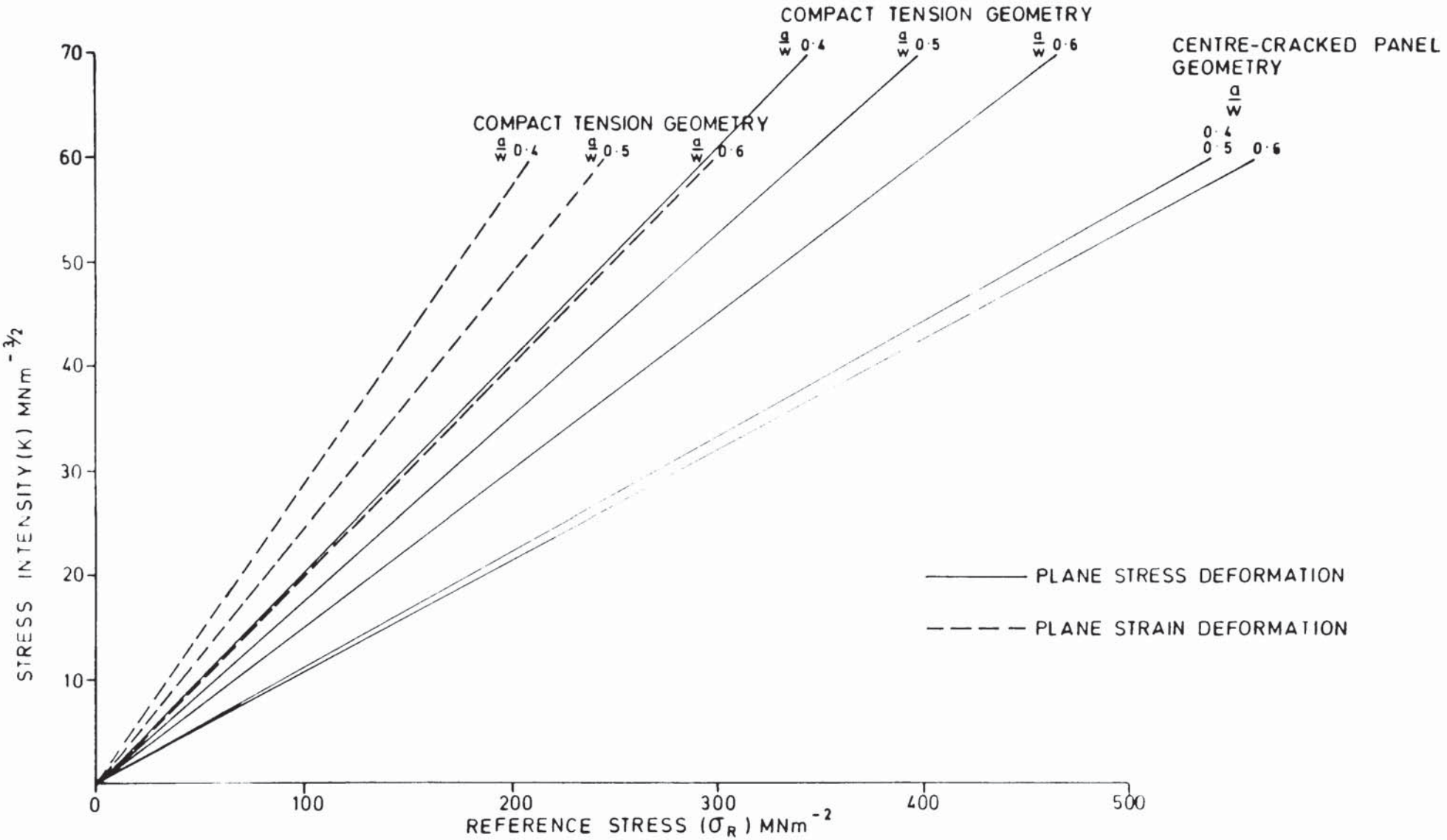

FIG 15 RELATIONSHIP BETWEEN STRESS INTENSITY AND REFERENCE STRESS

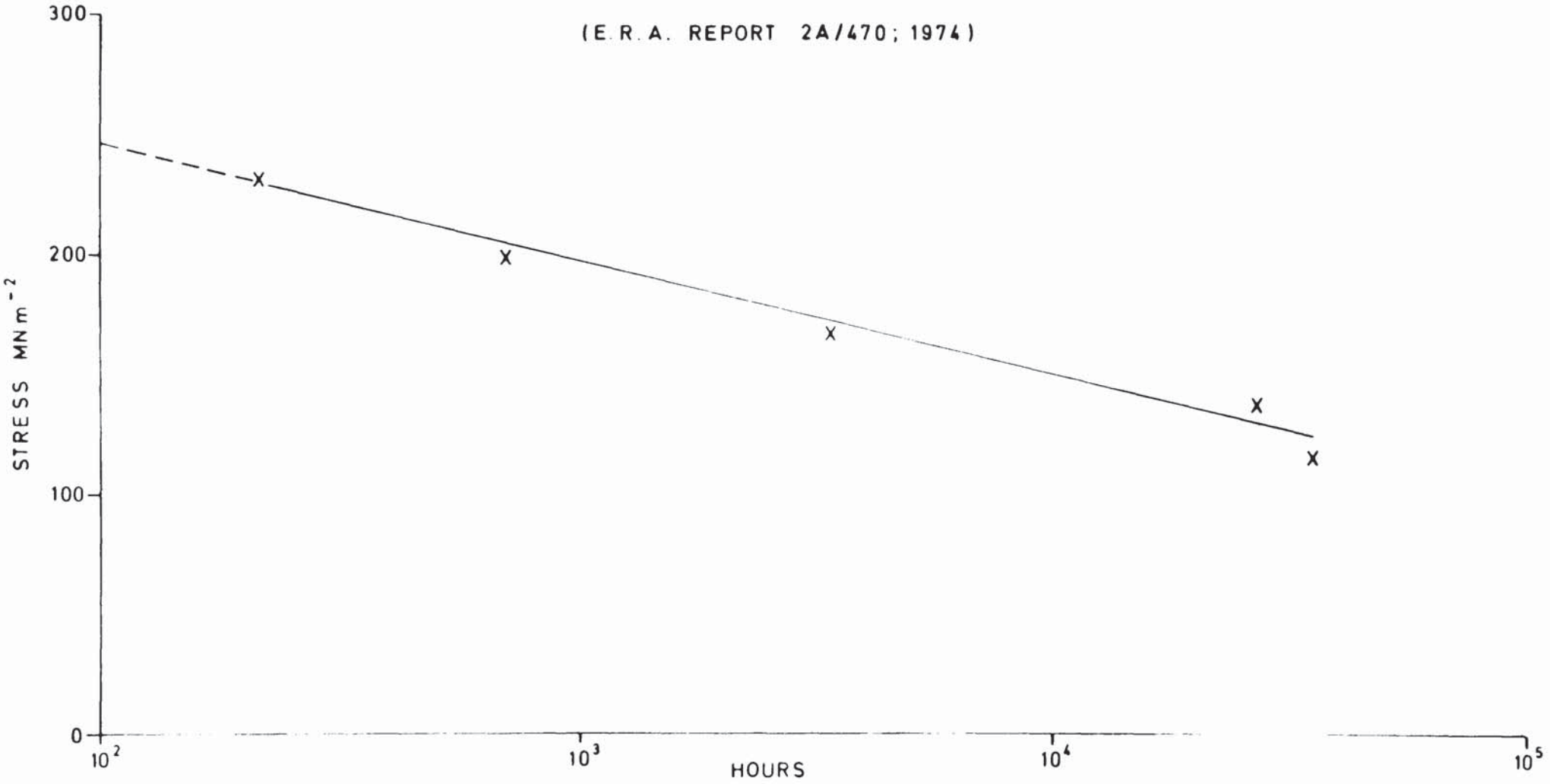

FIG 16. CREEP RUPTURE LINE FOR 1Cr 1Mo $^1/_4$V, NORMALISED AND TEMPERED, 550^{0}C.

RC/SSR/A4/595

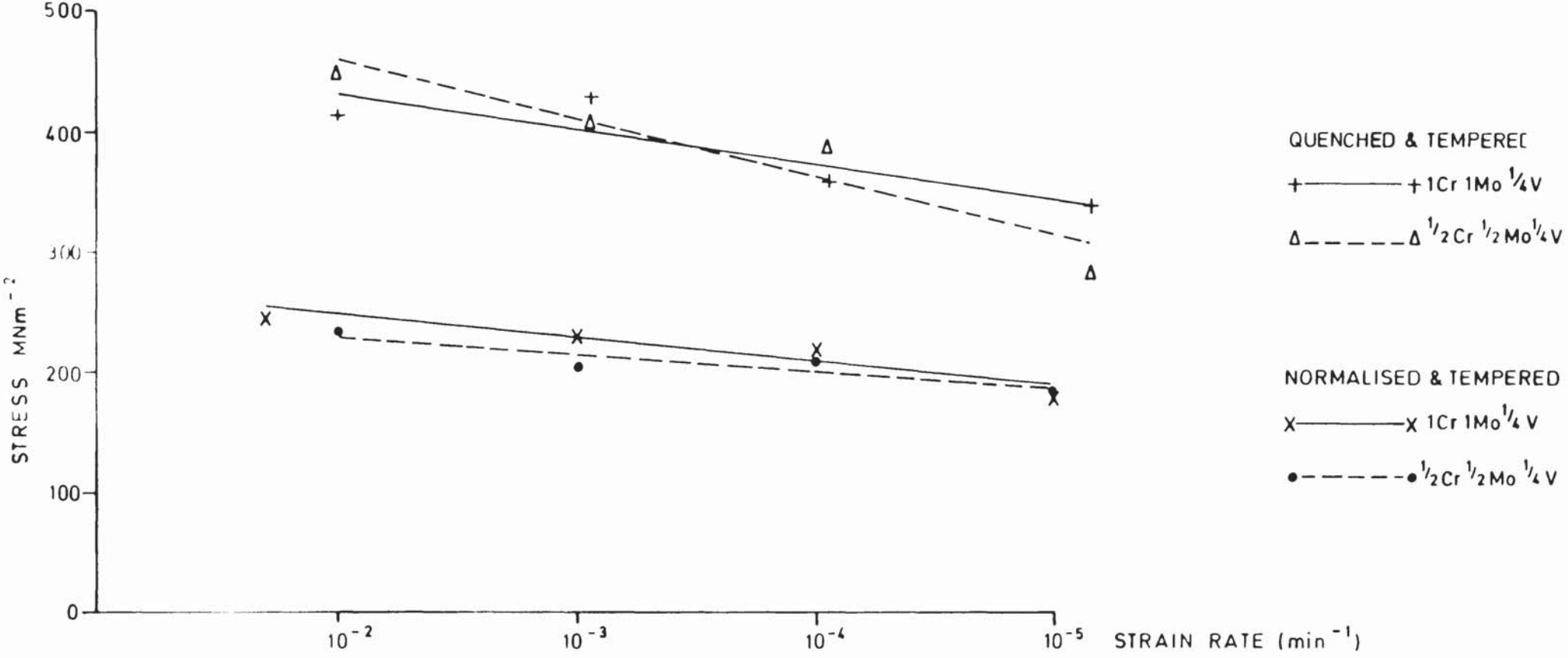

FIG. 17 VARIATION OF 0·2% PROOF STRESS WITH STRAIN RATE AT 550° C

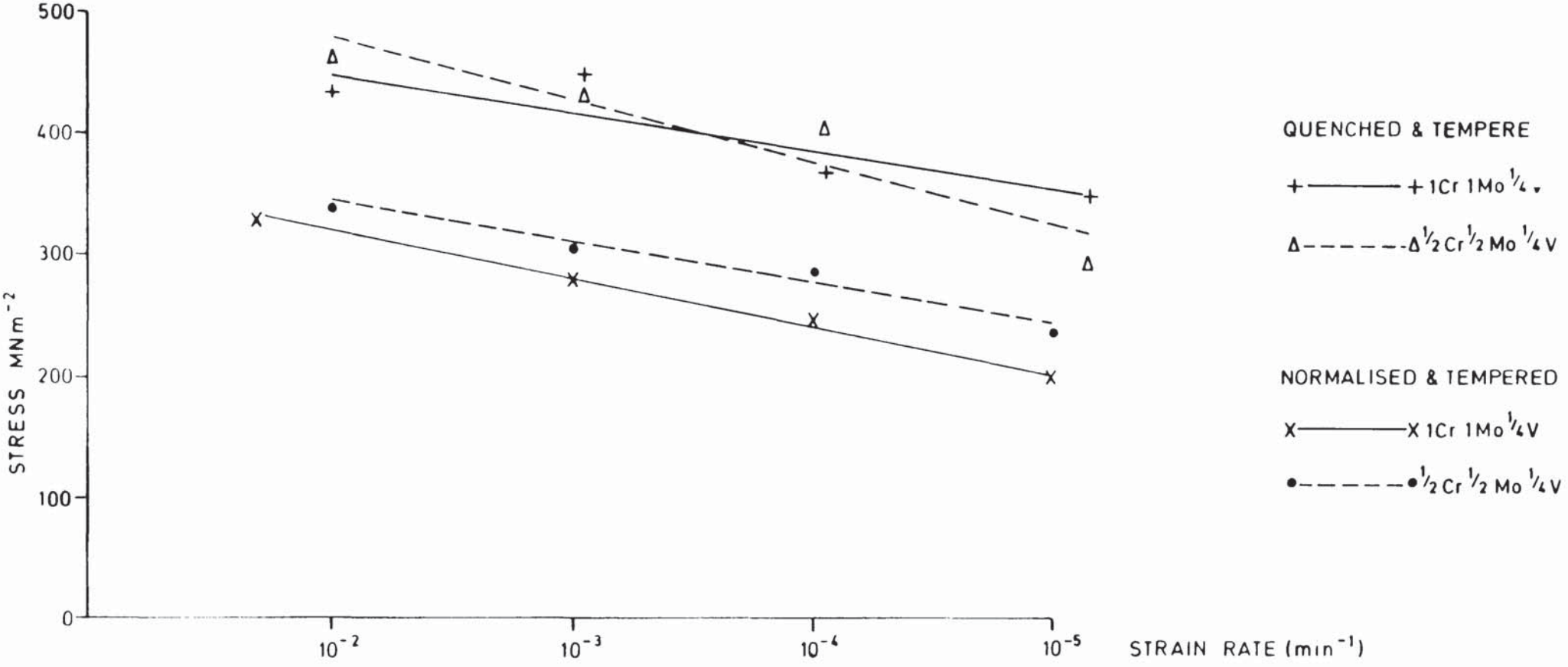

FIG. 18 VARIATION OF ULTIMATE TENSILE STRESS WITH STRAIN RATE AT 550°C

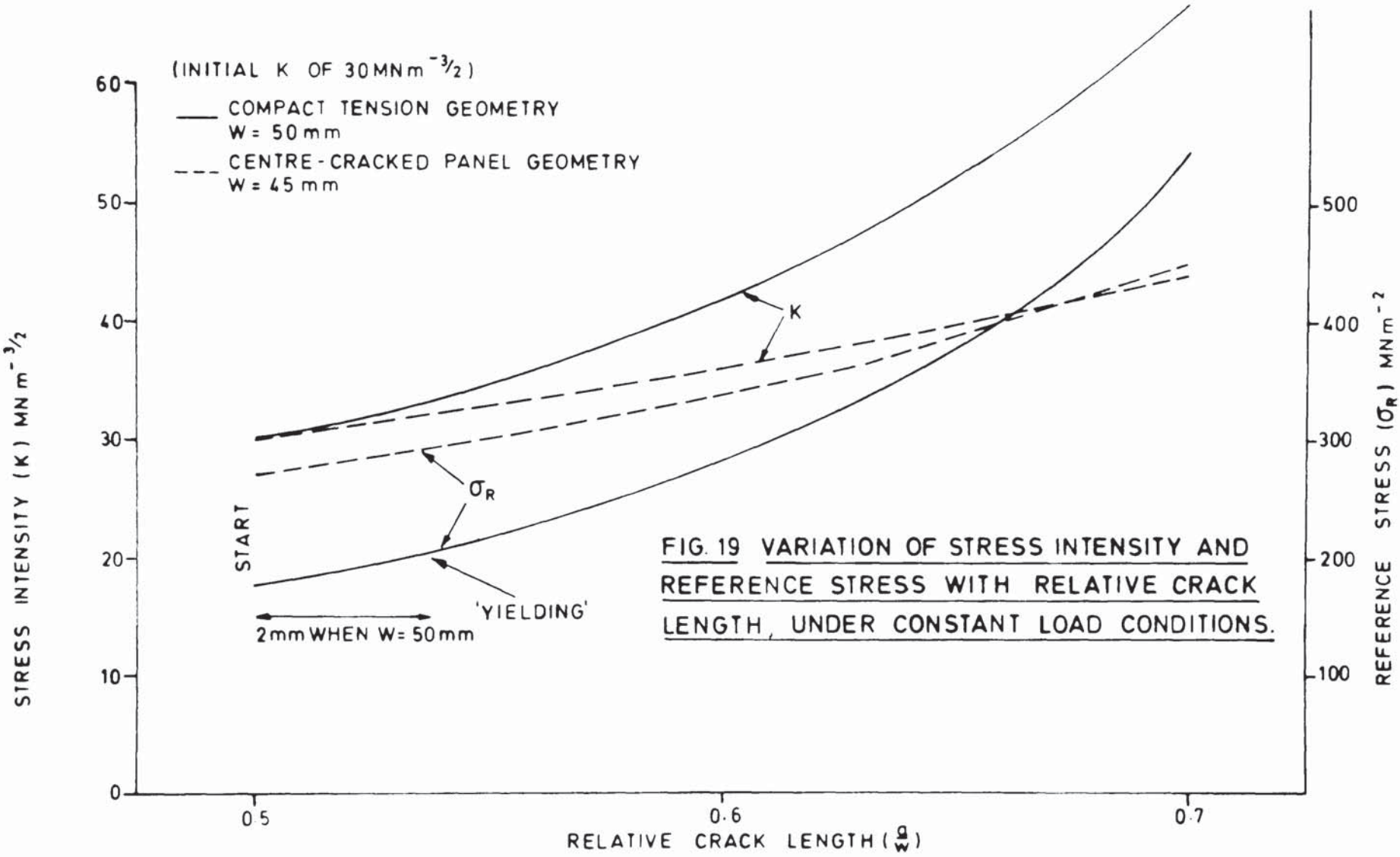

FIG. 19 VARIATION OF STRESS INTENSITY AND REFERENCE STRESS WITH RELATIVE CRACK LENGTH, UNDER CONSTANT LOAD CONDITIONS.

Stresses considerably lower than 150 MNm^{-2} would have resulted in extremely long rupture lives and were therefore considered unacceptable.

The specimen possessing an initial $\frac{a}{W}$ of 0.5 and K of 30 $MNm^{-3/2}$ was chosen as the basis for all creep crack growth tests. Figure 19 and Table 3 indicate that this particular specimen (C.T. geometry) should provide at least 2mm of creep crack growth in an acceptable time (< 4000 hours), before general yield or ductile tearing occurs.

It is evident from Figure 19 that the variation of K and σ_R with $\frac{a}{W}$ in the C.C.P. and C.T. geometries are different. For example, a C.C.P. 1Cr1Mo¼V alloy in the normalised and tempered condition when tested at an initial $\frac{a}{W}$ of 0.5 and K of 30 $MNm^{-3/2}$, will have an initial σ_R of 270 MNm^{-2} (see also Figure 15). This stress is above yield and possibly above the ultimate tensile stress. In order to avoid this situation, all comparative C.C.P./C.T. tests in the normalised and tempered material were based on the same initial σ_R of 170 MNm^{-2}.

Comparative tests in the quenched and tempered material could however, begin at a σ_R of 270 MNm^{-2} (K = 30 $MNm^{-3/2}$) as this is below the conservative value for the yield and ultimate tensile stress (Figures 17 and 18).

3.3.2 Precracking

All specimens were fatigue precracked to the desired value of $\frac{a}{W}$ before they were creep tested. The maximum stress intensity (K_m) in the fatigue cycle at the end of precracking was always less than the initial apparent stress intensity (K_A) in the subsequent creep test. The fatigue stress intensity range (ΔK) and K_m were invariably 20 $MNm^{-3/2}$ and 21 $MNm^{-3/2}$ respectively. When K_A was less than 21 $MNm^{-3/2}$, ΔK was reduced in steps as the desired $\frac{a}{W}$ was approached such that the final K_m was below K_A.

3.3.3 Short Term Tests

3.3.3.1 Effect of Initial Relative Crack Length

A series of 25mm thick C.T. specimens manufactured from the 1Cr1Mo¼V alloy in the normalised and tempered condition, were precracked to produce two sets of specimens with $\frac{a}{W}$ of 0.4, 0.5 and 0.6. One set was creep tested at an initial K_A of 30 $MNm^{-3/2}$ and the other set at an initial σ_R of 200 MNm^{-2}. A similar set of specimens was produced from the normalised and tempered ½Cr½Mo¼V alloy and creep tested under identical conditions to the 1Cr1Mo¼V alloy. Test details are displayed in Table 4.

3.3.3.2 Effect of Specimen Thickness

A set of nominally identical 20 or 25mm thick C.T. specimens was made from the normalised and tempered, and quenched and tempered 1Cr1Mo¼V alloy. Several of these specimens were then sliced by spark erosion to give pairs of specimens with thicknesses of 5,10 and 15 mm. Two 50 mm thick specimens were also produced from the normalised and tempered alloy. All specimens were precracked to 0.5 $\frac{a}{W}$ and then creep tested at a K_A of 30 $MNm^{-3/2}$. Test details are displayed in Table 4.

3.3.3.3 Effect of Specimen Geometry

Three normalised and tempered 1Cr1Mo¼V alloy, 8 mm thick C.C.P. specimens with relative crack lengths of 0.4, 0.5 and 0.6, were creep tested at an initial σ_R of 170 MNm^{-2}. The experimental results from these specimens were compared with those from the 'equivalent' C.T. tests (Section 3.3.3.1).

(An additional 1 mm thick C.C.P. specimen with an $\frac{a}{W}$ of 0.5 was tested at a σ_R of 170 MNm^{-2} in order to ascertain the effect of thickness).

A similar series of 8 mm (and one 1 mm) thick C.C.P. specimens were produced from the quenched and tempered 1Cr1Mo¼V alloy and creep tested at a K_A of 30 $MNm^{-3/2}$.

(An additional 8 mm thick C.C.P. specimen with an $\frac{a}{W}$ of 0.5 was tested at a K_A of 19 $MNm^{-3/2}$ and initial σ_R of 170 MNm^{-2}, in order to determine the effect of load).

Test details are displayed in Table 4.

3.3.4 Long Term Tests

All the tests in the previous sections have of necessity been short term with creep rupture lives of a few thousand hours. However, specimen rupture lives of this magnitude are considerably shorter than the 250,000 hour design life of many high temperature pressure vessels and, as a consequence, their creep fracture behaviour may be unrealistic. A good indication of long term (250,000 hour) creep behaviour can be obtained from laboratory tests lasting around 20,000 hours. Tests of this duration were carried out.

One 25 mm thick C.T. specimen from each of the alloys in the normalised and tempered condition and one from the 1Cr1Mo¼V alloy in the quenched and tempered condition, were precracked to 0.4 $\frac{a}{W}$ and creep tested at a K_A of 17 $MNm^{-3/2}$ and σ_R of 85 MNm^{-2} (Table 4). The creep rupture life of the normalised and tempered alloys was expected to be in excess of 30,000 hours (Figure 16), while a shorter life was expected from the quenched and tempered alloy.

3.3.5 Application of Creep Load

All specimens were soaked at 550°C for 24 hours prior to the start of the creep test. This procedure ensured thermal, mechanical and electrical stability of the specimen, loading train and test monitoring equipment. Load was then applied gradually to the specimen. The creep test was deemed to have started when the test load was attained. The time taken to reach the test load was between one and two minutes.

3.4 Analysis of Tests

Creep ductility was measured in terms of the macroscopic crack velocity, the initiating crack opening displacement and the crack aspect ratio. The crack velocity was correlated with the apparent elastic stress intensity factor and the reference stress.

Table 4. Test Parameters

N & T - Normalised and Tempered
Q & T - Quenched and Tempered

Section	Material	Specimen No.	b $\times 10^{-3}$ m	W $\times 10^{-3}$ m	$\frac{a}{W}$	K_A $MNm^{-3/2}$	σ_R MNm^{-2}
3.3.3.1	1Cr1Mo¼V	35, 75	25	50	0.4	30	148
	N & T	71	25	50	0.5	30	170
		34	25	50	0.6	30	200
		33	25	50	0.4	41	200
		62	25	50	0.5	35	200
		34	25	50	0.6	30	200
	½Cr½Mo¼V	82	25	50	0.5	30	170
	N & T	84	25	50	0.6	30	200
		83	25	50	0.4	41	200
		87	25	50	0.5	35	200
		84	25	50	0.6	30	200
3.3.3.2	1Cr1Mo¼V	55, 59	5	50	0.5	30	170
	N & T	53, 57	10	50	0.5	30	170
		54, 58	15	50	0.5	30	170
		71	25	50	0.5	30	170
		73, 74	50	50	0.5	30	170
	1Cr1Mo¼V	63, 72	5	50	0.5	30	170
	Q & T	56, 64	10	50	0.5	30	170
		65, 70	15	50	0.5	30	170
		80	20	50	0.5	30	170
3.3.3.3	1Cr1Mo¼V	86	1	45	0.5	19	170
	N & T	88	8	45	0.4	19	170
		89	8	45	0.5	19	170
		90	8	45	0.6	18	170
	1Cr1Mo¼V	76	1	45	0.5	30	270
	Q & T	81	8	45	0.4	30	270
		67	8	45	0.5	30	270
		85	8	45	0.6	30	280
		66	8	45	0.5	19	170
3.3.4	1Cr1Mo¼V N & T	25	25	50	0.4	17	85
	1Cr1Mo¼V Q & T	26	25	50	0.4	17	85
	½Cr½Mo¼V N & T	27	25	50	0.4	17	85

3.4.1 Elastic Stress Intensity Factor

The elastic stress intensity factor (K) associated with a crack in a C.T. and C.C.P. specimen can be calculated from the equation (Walker and May, 1967, following Brown and Srawley, 1966).

$$K = Y^1 \sigma a^{\frac{1}{2}} = \frac{PY}{BW^{\frac{1}{2}}} \qquad (47)$$

where Y and Y^1 are compliance functions, σ an applied stress, a the crack length, P the load, B and W the specimen thickness and width respectively (Figure 14).

This expression was used to calculate K in both specimen geometries. The relevant Y values were obtained from compliance tables published by Walker and May (1967).

3.4.2 Reference Stress

Haigh (1973), and Haigh and Richards (1974) showed that an equivalent uniaxial flow stress (σ_E) producing deformation of a C.T. or C.C.P. specimen could be calculated from equation (34). Values of m for plane stress and plane strain deformation in the relevant specimen geometries are given by these authors. The above equivalent stress has been re-named the reference stress σ_R (see Section 3.3.1.1).

3.4.3 Initiating Crack Opening Displacement

The initiating crack opening displacement was measured after the termination of each test. This involved sectioning the specimen along the mid-thickness plane using a continuous wire spark erosion technique, polishing the section with graded abrasive papers and diamond pads, and photographing part of the fatigue crack and all of the creep crack. The cracks were photographed at magnifications of x40 to x100 using a Reichert projection microscope and Polaroid Type 55 film.

A schematic representation of the area around the creep crack origin is shown in Figure 20.

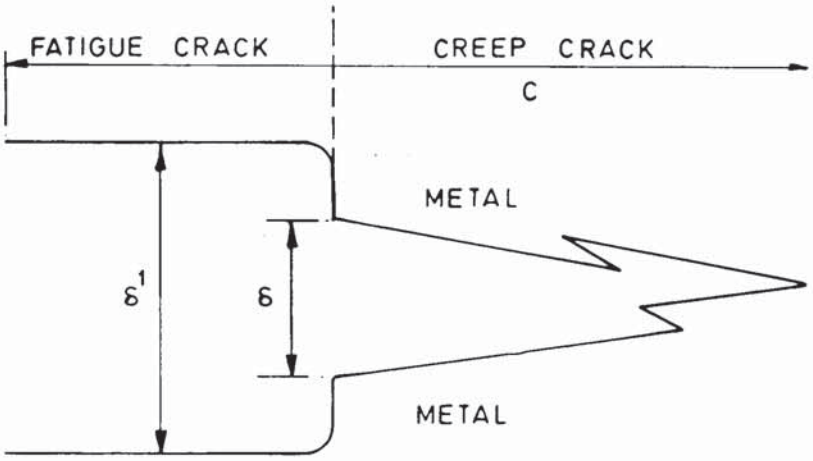

FIG. 20
MEASUREMENT OF THE INITIATING CRACK OPENING DISPLACEMENT

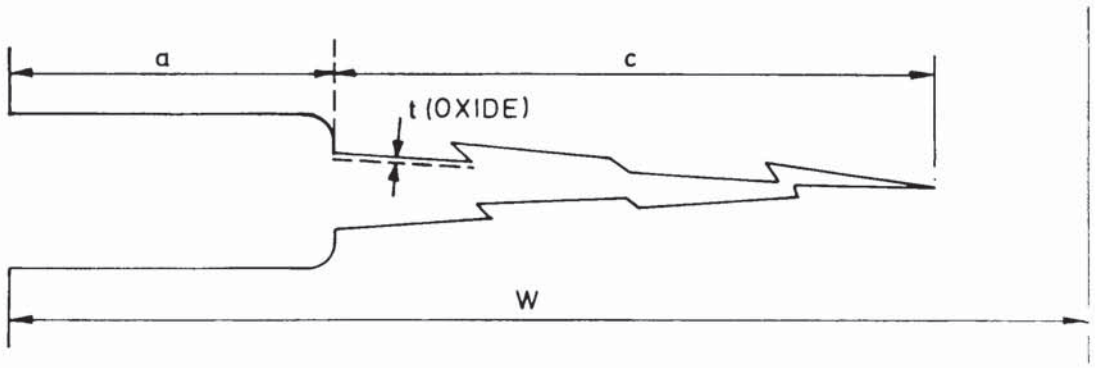

FIG. 21
MEASUREMENT OF CRACK ASPECT RATIO (METHOD A)

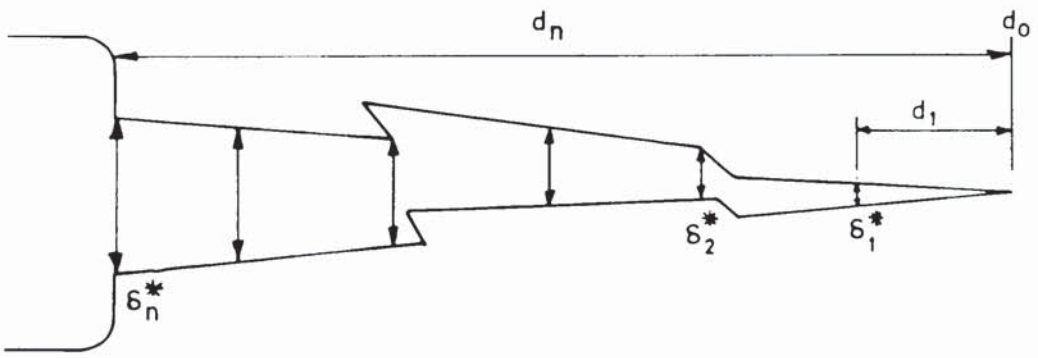

FIG. 22
MEASUREMENT OF CRACK ASPECT RATIO (METHOD B)

The initiating crack opening displacement (δ_i) was calculated from the expression:

$$\delta_i = (\delta^1 - \delta) \tag{48}$$

($\delta^1 - \delta$) is the double-step height at the origin of the creep crack (Figure 20).

3.4.4 Creep Crack Aspect Ratio

The creep crack aspect ratio was measured in two ways:-

A). Photographically, using the crack images from Section 3.4.3. The aspect ratio $\frac{l}{\omega}$ was defined as the ratio of the total length of creep crack at the mid-thickness plane (c) to the opening of the creep crack at its origin (δ). Hence:

$$\frac{l}{\omega} = \frac{c}{\delta} \tag{49}$$

. This expression was used to calculate the aspect ratio in the C.C.P. specimens.

The aspect ratio in the C.T. specimens was calculated from an expression derived by Nicholson and Formby (1976) that included a correction for bending. The expression used was;

$$\frac{\delta}{\omega} = 2\,(W-a)\quad \ln\left[\frac{(W-a)}{(W-a-c)}\right] \quad -c \tag{50}$$

where (W-a) is the initial ligament width (Figure 21).

The photographic method of calculating the aspect ratio was used for all specimens.

B). Photographically/Graphically, again using the crack images from Section 3.4.3. This time however, the distance between the creep crack faces (δ^*) was measured at regular intervals starting at the creep crack tip (Figure 22). δ^* was then plotted against distance (d) from the crack tip. The gradient of this plot, after applying appropriate bending corrections, was a measure of the aspect ratio.

Method B was only applied to specific C.T. tests where Method A had proved unuseable due to the occurrence of some stable tearing at the end of the test.

An oxidation correction factor was applied to the aspect ratios calculated by both methods. The method of correction consisted of measuring the crack surface oxide thickness (t; Figure 21) by optical microscopy and then calculating the oxidised metal thickness (t_m) by using a Pilling-Bedworth Ratio of 2.1 (value for magnetite in CrMoV steels at 550°C). Thus, the correct distance between the crack faces δ (or δ^*) is:

$$\delta \text{ (or } \delta^*) = \delta_{\text{Provisional}} - 2t_m \qquad (51)$$

3.5 Measurement of Crack Length by A Potential Drop Method

3.5.1 Experimental Technique

A constant 50 ampere direct current was delivered to the hot creep specimen by 10 x 2 mm copper leads. These leads were attached to the specimen by a low temperature brazing alloy. As a consequence, the heat affected zone was contained within an area that was remote from both the crack tip and the ligament ahead of the crack tip. The area of contact of the current leads on C.T. specimens greater than 10 mm thick and on all C.C.P. specimens, was 100 mm^2. The contact area on thinner specimens was proportionatly less. The current leads were located and positioned on the two specimen geometries as shown in Figures 23a and 23b.

Potential probes were spot welded to the specimen by an energy discharge welder. In the case of the C.T. specimen, two diagonally opposed pairs of probes were spot welded across the end of the machined notch (Figure 23a) and led out of the furnace through ceramic tubes. The individual probe pairs were twisted together and carefully routed away from the specimen and through the furnace in order to minimise electro-magnetic interference from the furnace windings.

Probe positioning on the C.C.P. specimen differed in that one half of the probe pair was located on the front face of the specimen and the other half on the back face (Figures 23b and 23c). The probes were also placed on the sides of the crack and not across the machined notch as in the C.T.

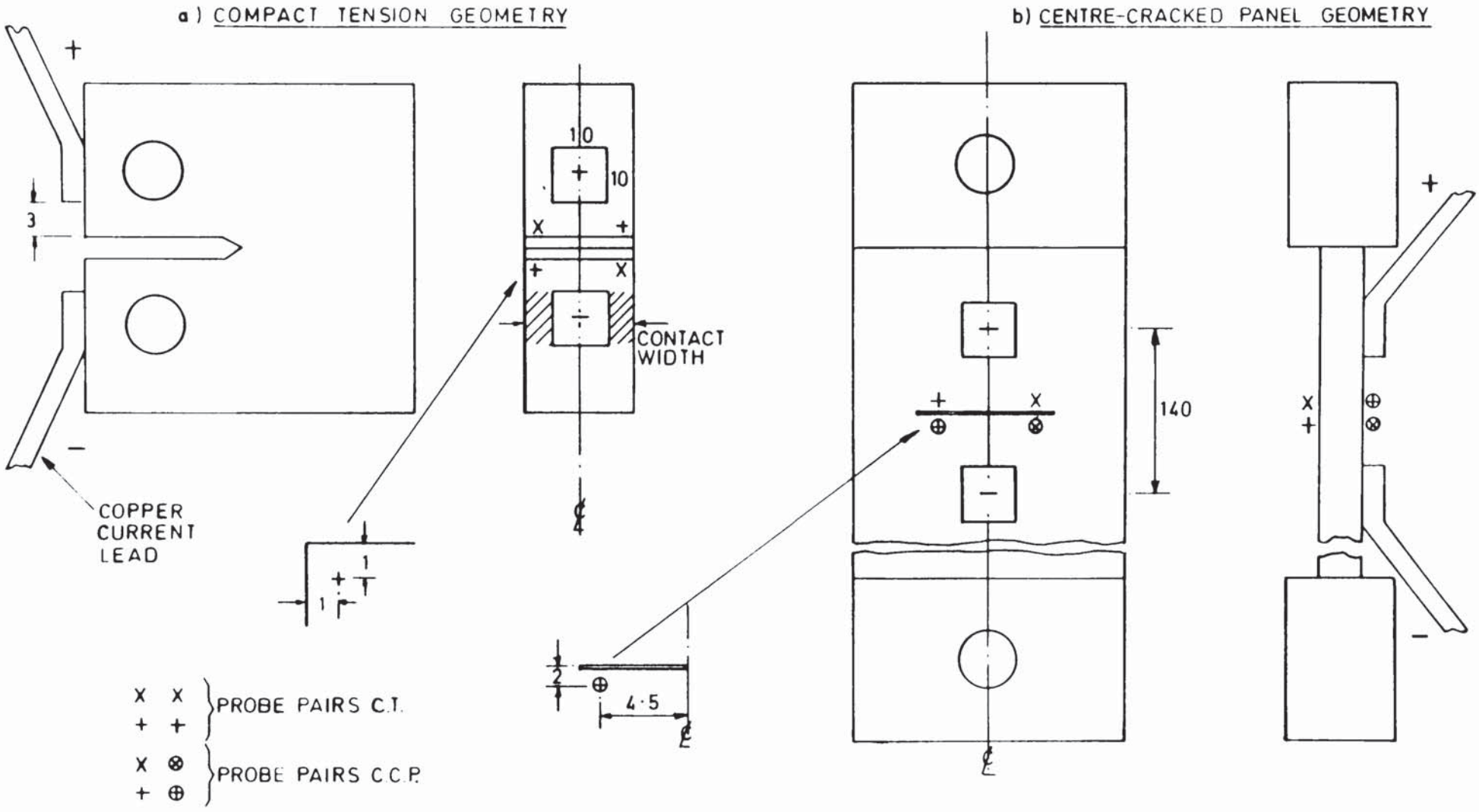

FIG. 23 POTENTIAL PROBE AND CURRENT LEAD POSITIONS

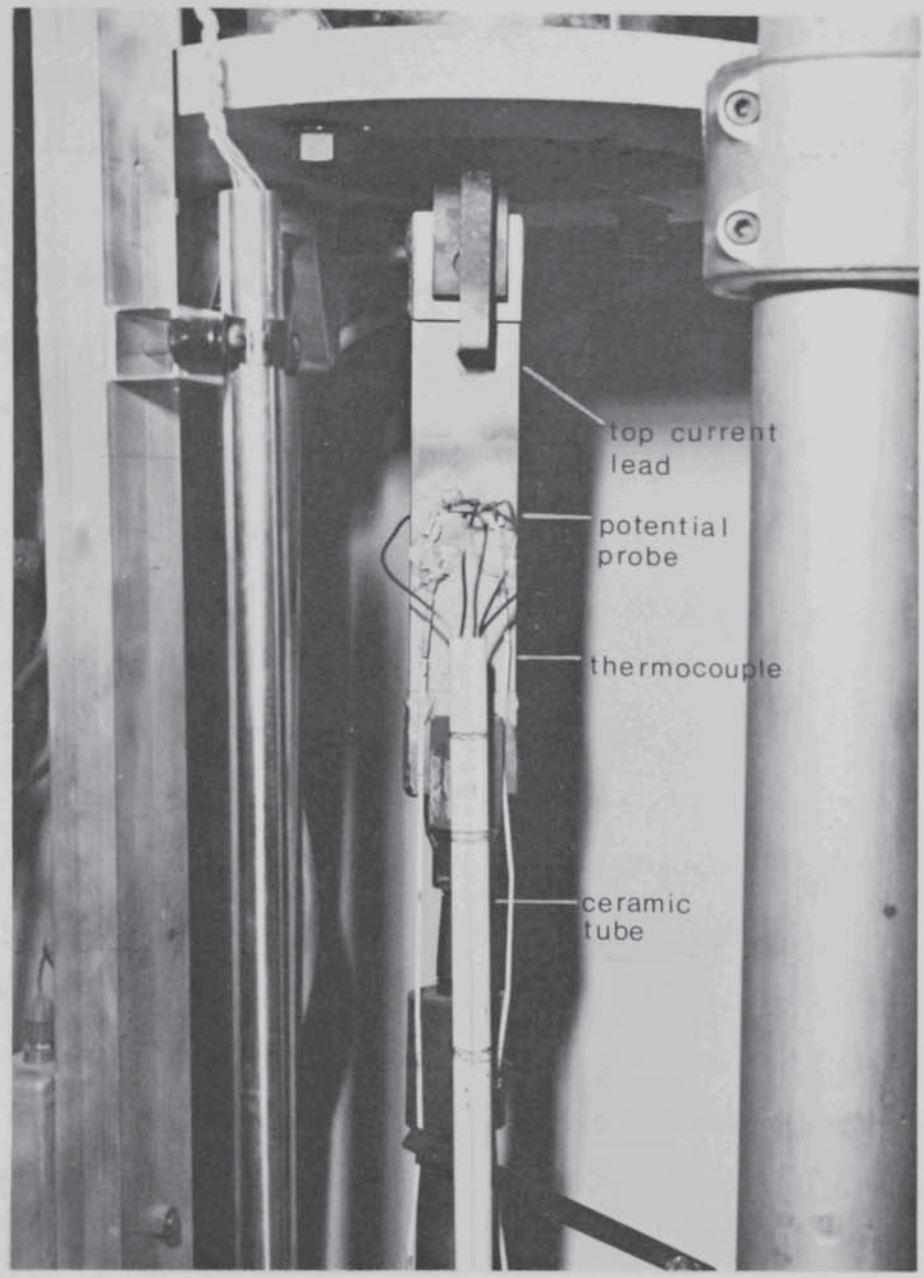

FIG. 23c

C. C. P. SPECIMEN PREPARED FOR CREEP TESTING

specimen. Electro-magnetic interference was again minimised by the aforementioned method.

Correct positioning of the probes on the specimen was important for accurate crack length measurements. This was accomplished by using a pen style welding probe and a thin copper rod electrode. The probe positions for both specimen geometries are shown in Figures 23a and 23b. The security of the spot welds was enhanced by the application of a high temperature ceramic cement. This cement also reduced the corrosion rate of the spot weld.

The potential drop across both pairs of probes was monitored continuously by the data transfer unit. The channel capacity of this unit enabled the potential outputs from all probes on several specimens to be assessed continuously.

3.5.2 Potential Drop/Crack Length Calibration Curves

A potential drop calibration curve produced by McIntyre and Priest (1970) was used to calculate the length of a creep crack in a C.T. specimen. The calibration curve (Figure 24) consists of a straight line plot of $\frac{Va}{Vo}$ against $\frac{a}{W}$, where Vo is the potential drop at the initial crack length and Va is the potential drop at any subsequent crack length.

Before commencing the C.T. creep crack growth programme, a check was made on the validity of this calibration curve. This was done in two ways:-

A). Artificial cracks with straight fronts were introduced into several C.T. specimens by a spark erosion technique. Their $\frac{a}{W}$ values varied from 0.4 to 0.7. A constant direct current was passed through the specimens and the potential drop measured across the crack in an identical manner to that used in the creep tests.

B). An electrolytic tank simulating the 1T C.T. specimen was made from perspex sheet to a scale of x5 (Figure 25). Cracks were represented by 1 mm thick perspex sheet cut to the required shape and $\frac{a}{W}$. Slots in the base of the tank and on the end of the simulated machine notch were used to support

and accurately position the artificial cracks relative to the current leads and potential probes. These leads and probes were positioned on the front face of the tank according to scale and normal experimental practice (Section 3.5.1). A potassium chloride solution was used as the electrolyte to simulate the steel specimen.

The electronic equipment used in conjunction with the electrolytic tank consisted of an oscillator, amplifier, oscilloscope and digital voltmeter. The oscillator produced a 10mA sinusoidal alternating current which, following amplification, was passed through the current electrodes into the potassium chloride electrolyte which possessed a resistance of 100 ohms. The digital voltmeter measured the potential drop across the probe electrodes.

The results from both calibration methods (Figure 24) confirmed that the McIntyre and Priest calibration curve was valid. Method B also revealed that a current lead contact width (Figure 23a) above 10 mm did not affect the potential drop calibration curve. For example, a 10 x 10 mm or 10 x 25 mm lead produced identical curves for a 25 mm thick C.T. specimen. Consequently, the dimensions of the current leads used in the creep tests were invariably 10 x 10 mm and not 10 mm x breadth of the specimen, as recommended by McIntyre and Priest (1970).

A p.d. calibration curve for the C.C.P. geometry was generated by adopting the electrolytic bath method as used for the C.T. geometry. The calibration technique was identical to the previous account except for replacing the C.T. model by a C.C.P. model and extending the artificial crack lengths down to an $\frac{a}{w}$ of 0.1. Current leads and potential probes were again positioned according to scale and normal practice (Section 3.5.1). The resultant potential drop calibration curve is shown in Figure 26.

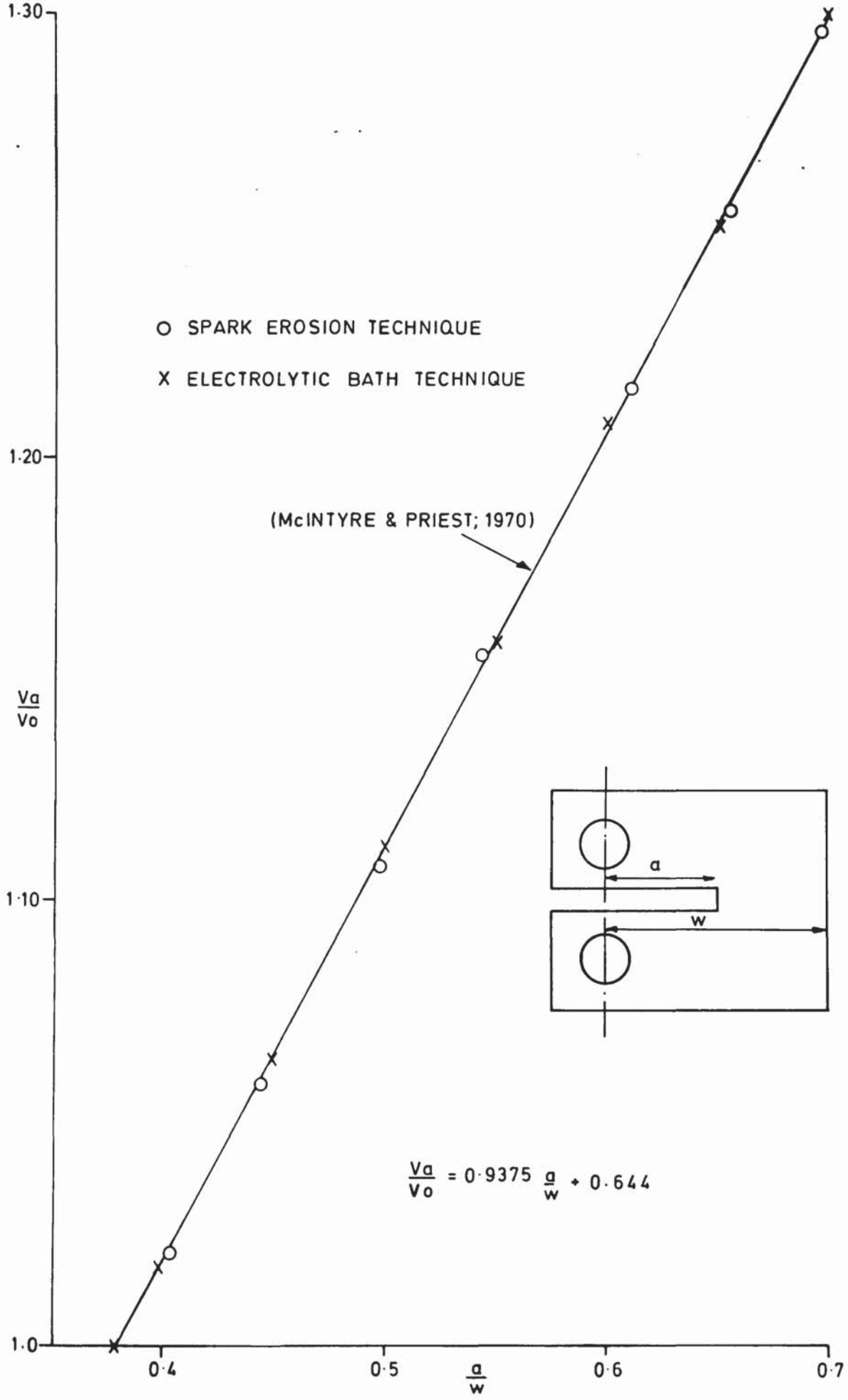

FIG. 24 COMPACT TENSION POTENTIAL DROP CALIBRATION CURVE

ALL DIMENSIONS IN MILLIMETERS

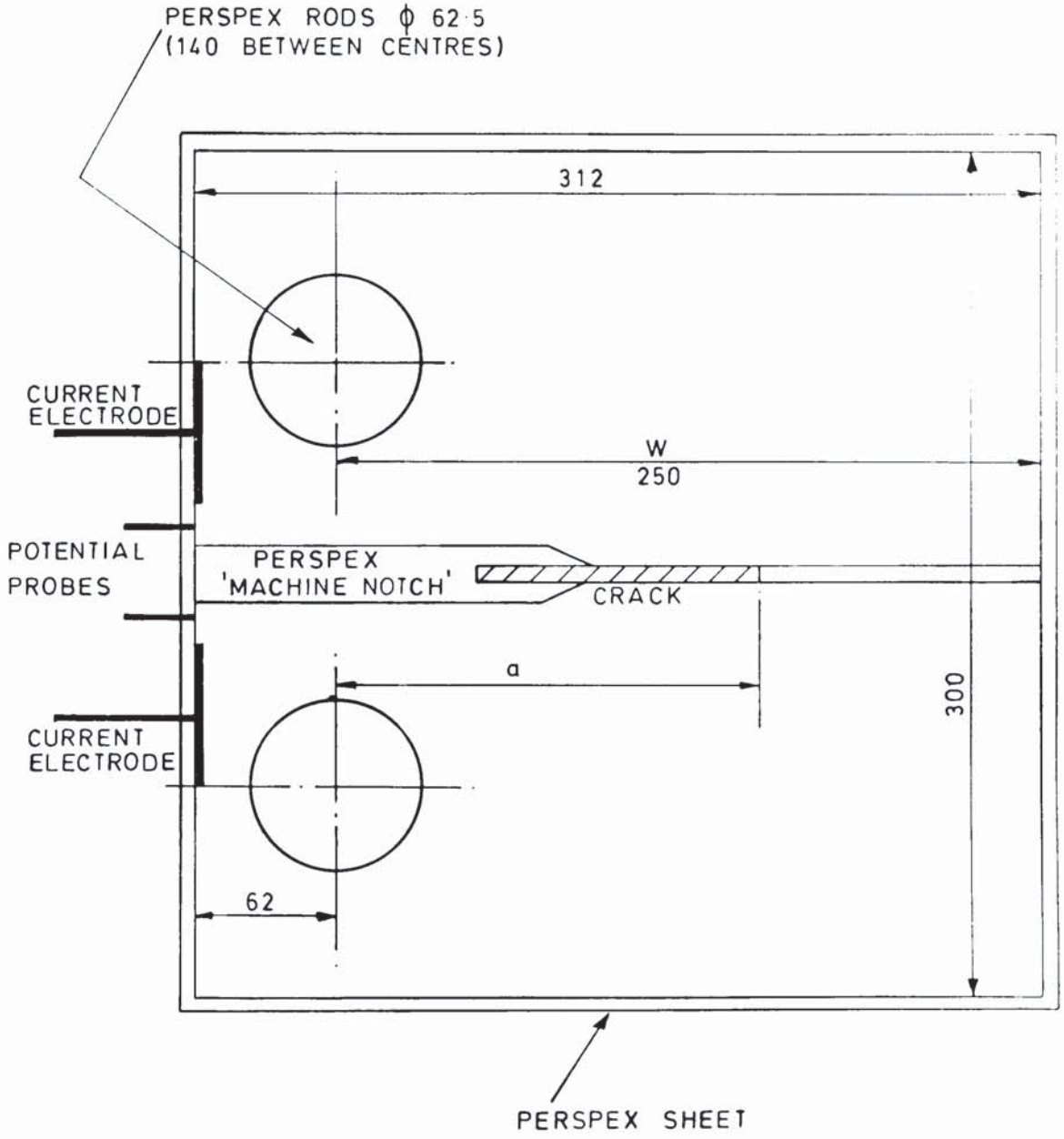

FIG. 25 PLAN VIEW OF COMPACT TENSION ELECTROLYTIC TANK MODEL

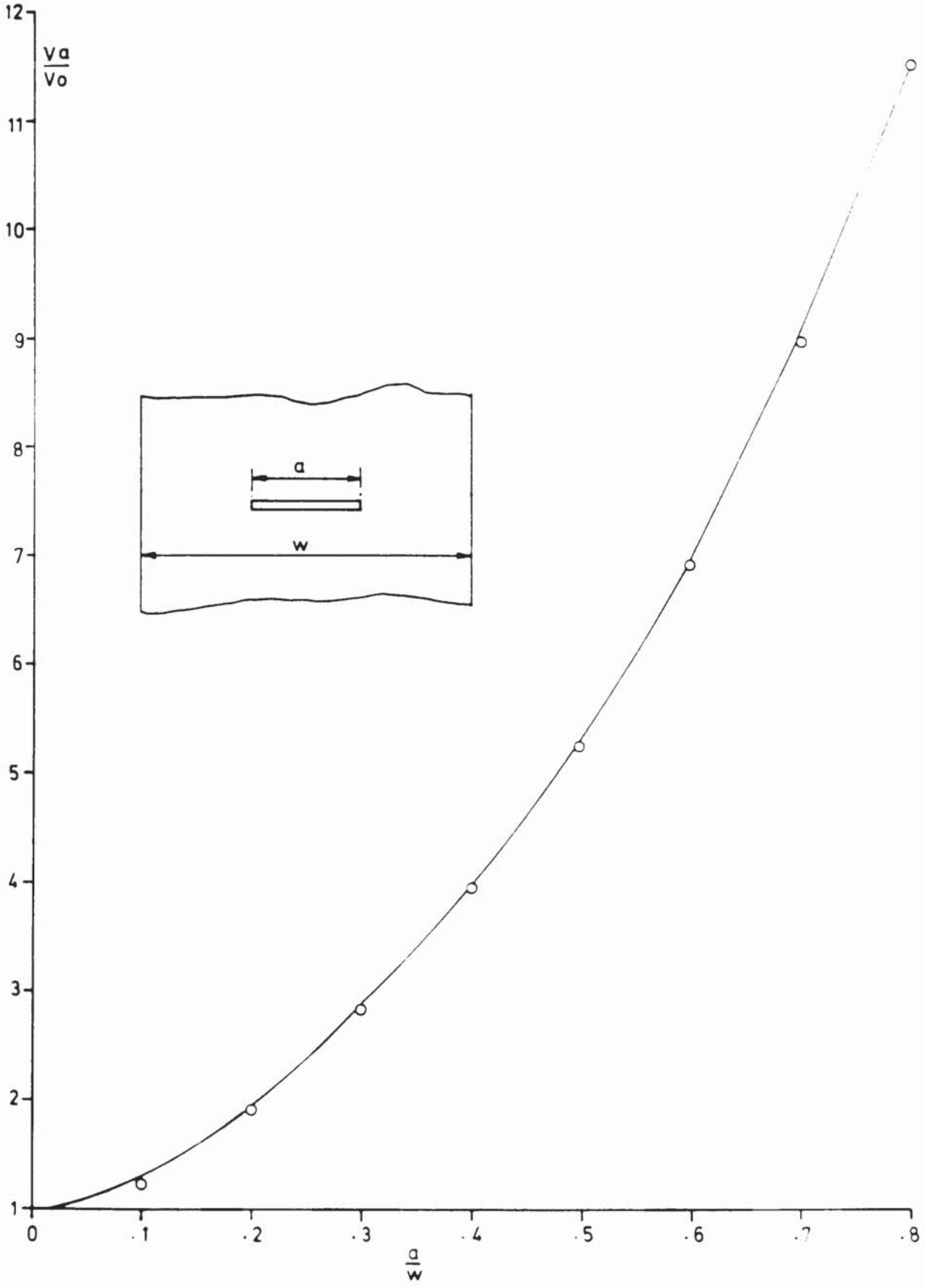

FIG. 26 CENTRE - CRACKED PANEL POTENTIAL DROP CALIBRATION CURVE.

3.6 Experimental Errors

The major sources of experimental error originated from instability of the 50 ampere power packs, the temperature controllers and the digital volt meter. Interference between the experimental a.c. and d.c. circuitry was negligible.

3.6.1 Power Packs

The power pack maintains the current at the desired level by sensing the potential drop across a high power resistor carrying the current, and adjusting the current accordingly. The variation in current about the nominal value of 50 ampere can be calculated from a knowledge of the temperature coefficient of the sensing resistors (50 ppm/^{o}C) and the power pack electronics, and a measure of the fluctuation in control room temperature. For a temperature change of $\pm 5^{o}$C, the output current of 50 ampere will vary by a maximum of ± 0.0625 amperes.

The output current can also vary due to fluctuations in the mains supply to the power pack. A variation of $\pm 10\%$ in this supply in combination with the above effects, will change the 50 ampere current by ± 0.0675 amperes. This variation in current will change the potential drop across a static crack by $\pm 0.135\%$.

3.6.2 Temperature Controllers

The change in resistivity of the ½Cr½Mo¼V and 1Cr1Mo¼V alloys between 500 and 600^{o}C is $1.4 \times 10^{-9}\ \Omega\ m/^{o}C$ (Smithells; 1955). As the temperature controllers maintain the specimen temperature within $\pm 1^{o}$C the resultant change in specimen resistivity will be $\pm\ 1.4 \times 10^{-9}\ \Omega\ m$. This change in resistivity plus the former variation in current (Section 3.6.1) will produce a maximum change in potential drop across a static crack of $\pm 0.33\%$ of the nominal output.

3.6.3 Digital Volt Meter

The accuracy of the potential drop measured by the digital volt meter was dependent on the voltage range selected, and the stability of the mains power supply. Variations in ambient temperature also affected

accuracy.

The voltage range selected for the creep tests was ± 20 mV; this had a last digit read out of 10μV. The potential drop resolution was therefore, limited to 10μV. To be added to this was the effect of a 10% variation in the mains supply and a ±5°C change in ambient temperature. An assessment of the compounded effects resulted in a maximum error of ±15μV in the potential drop read-out.

The initial potential drop across a creep crack in a C.T. or C.C.P. specimen at 550°C was typically 5mV. Consequently, the resolution of the potential drop crack monitoring system was better than $\left[15 + (5 \times 0.0033)\right]$ = 15.02 μV.

3.7 Post-Test Metallurgical Examination

Mid-thickness sections from all specimens were examined under the optical microscope. The surfaces were prepared by standard wet polishing techniques and then etched in 2% Nital.

A selection of specimens was examined under the scanning electron microscope. The surfaces were prepared by electropolishing and etching in a solution of acetic/perchloric acid. This solution contained 91% by volume of glacial acetic acid and 9% by volume of perchloric acid. The polishing and etching conditions were 5 volts for 60 seconds and 1 volt for 10 seconds respectively.

CHAPTER 4

Experimental Results

In Section 3.4 it was stated that creep ductility was measured in terms of macroscopic crack velocity, initiating crack opening displacement and crack aspect ratio. Experimental work has shown that the measurement of all three parameters was subject to error. These errors are quantified in the next section and then used in the subsequent sections to assess the significance of the experimental results.

4.1 Experimental Errors in the Measurement of Macroscopic Crack Velocity

Tunnelling of creep cracks was observed in all tests. Several workers have claimed that this phenomenon can be overcome by side grooving specimens according to the recommendations of Freed and Kraft (1966). In order to test this claim, a few specimens were side grooved and then creep tested. The results showed that side grooving did suppress crack tunnelling. Unfortunately, it also promoted excessive amounts of creep cracking at the specimen side faces resulting in a concave crack front. This effect was considered to be undesirable and as a consequence, side grooving was not adopted. The decision not to side groove test specimens however, meant that potential drop calibration curves based on planar crack fronts (Section 3.5.2) were possibly being used incorrectly. Further work was therefore necessary to establish the effect of crack bowing on these curves. This was accomplished by repeating the series of potential drop calibration tests in the electrolytic baths (Section 3.5.2) having first replaced the perspex models of straight edge cracks by models of bowed cracks whose final profile (ratio of maximum to minimum crack length, Figure 27) was typical of that observed in practice. This was typically 3:1. The result of the experiment was that the potential drop calibration technique measured the average crack length of the bowed cracks in both the C.T. and C.C.P. geometries.

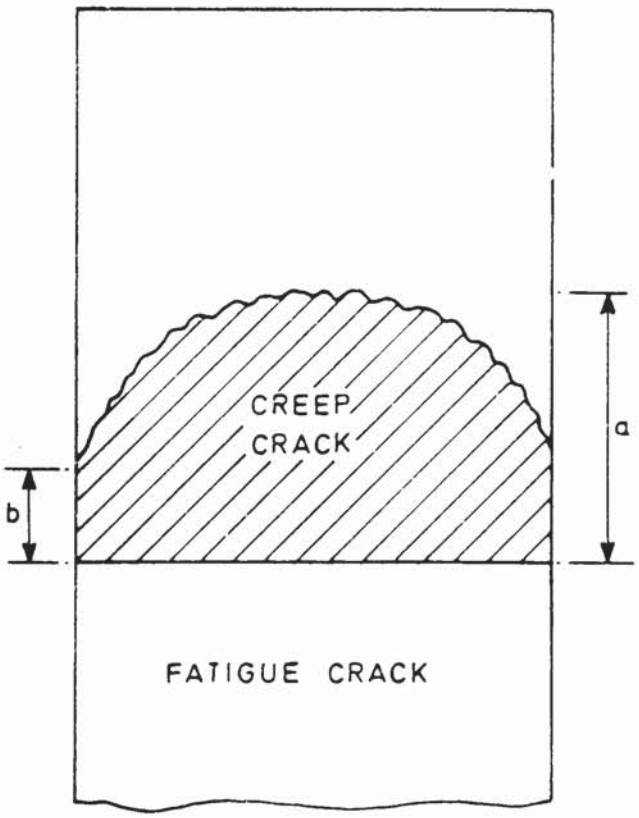

$$\text{CREEP CRACK PROFILE} = \frac{a}{b}$$

FIG. 27 DEFINITION OF CREEP CRACK PROFILE

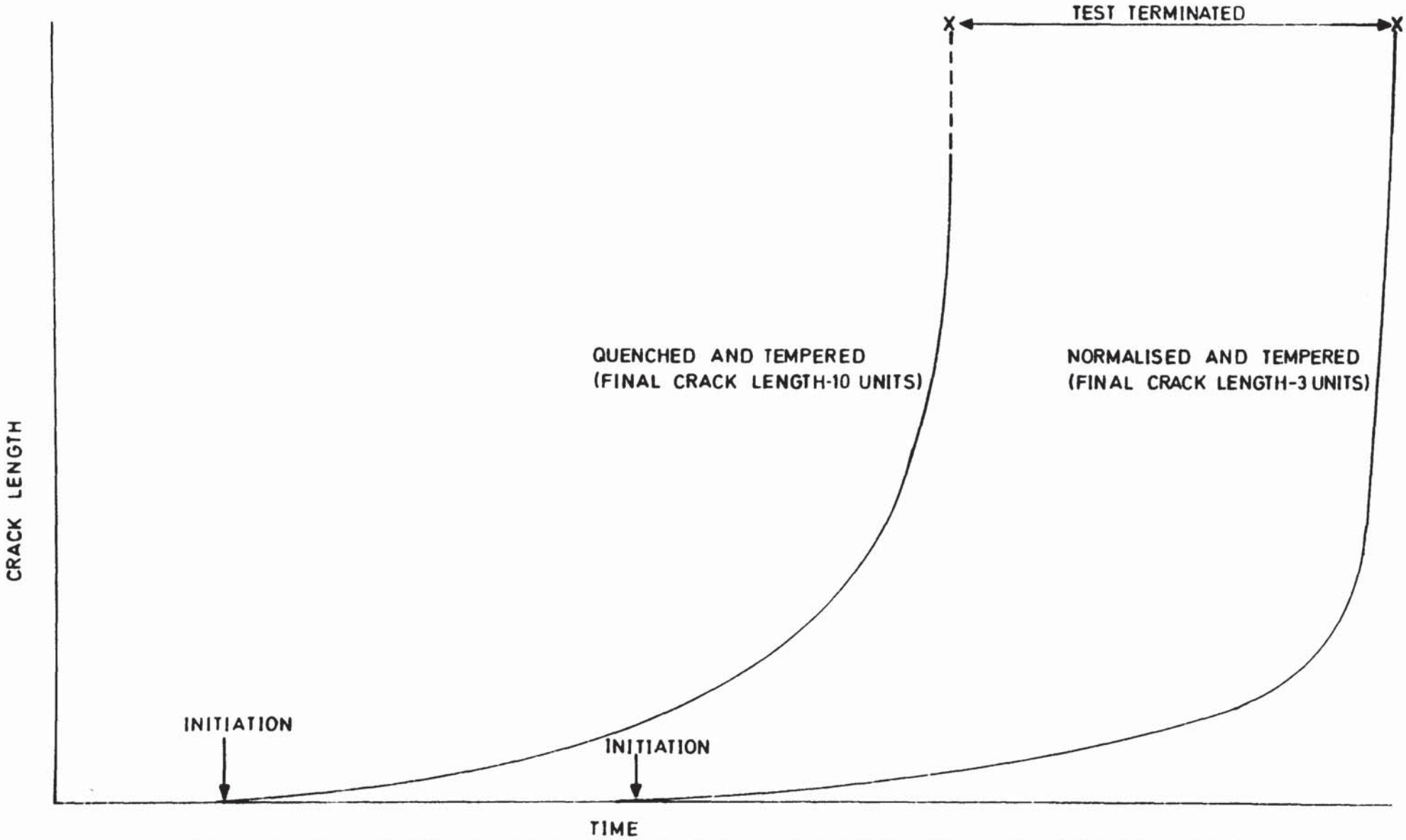

FIG 28 RELATIONSHIP BETWEEN CREEP CRACK LENGTH AND TEST TIME FOR TWO MATERIALS

Thus, the potential drop calibration curves shown in Figures 24 and 26 represent average relative crack lengths and as a consequence, will only provide average creep crack velocity measurements. In addition, they do not take account of the profile history of the growing crack.

A schematic representation of the average creep crack length versus time relationship observed in the ½Cr½Mo¼V and 1Cr1Mo¼V normalised and tempered, and 1Cr1Mo¼V quenched and tempered materials can be seen in Figure 28. When the geometry and test conditions were identical, the creep crack initiation time in the normalised and tempered material was always greater than that in the quenched and tempered material. The subsequent development of creep cracking in the normalised and tempered material was comparatively slower and the cracks never grew by the same amount as that observed in the quenched and tempered material prior to the advent of plastic collapse. This last observation was predicted in Section 3.3 and formed part of the design criteria for valid creep crack growth tests. Some encouragement can therefore be drawn from this and a greater degree of confidence placed in the philosophy behind the design of the overall creep programme.

In all cases the average final crack length measured by potential drop in the normalised and tempered specimens agreed with the post test optical measurement to within 0.1mm. The latter was obtained in the following manner:-

Having sectioned the test specimen (Section 3.4.3) and retained one half for microstructural examination, the other half was immersed in liquid nitrogen and then 'opened out' to leave a quasi-cleavage fracture ahead of the creep crack. The whole fracture face was then photographed at x10 magnification. This image was then traced onto graph paper from which the initial test crack length (fatigue crack) and the average creep crack length were measured. Crack lengths were measured at 50 equally spaced positions across the specimen and the average crack calculated.

In the quenched and tempered material the predicted average crack length was always less than the post test optical measurement. In some cases the crack length was underestimated by as much as 1mm. This underestimation of crack length was attributed to electrical short circuiting due to oxide and metal bridging between the crack faces. Oxide and metal bridging was also considered to have affected the intermediate measurements of creep crack length. This problem was overcome by applying initially a simple linear correction factor to the potential drop readings and then covering the eventuality of a non-linear factor by including error limits. The correction factor (C_L) was of the form

$$C_L = \beta \left[\frac{(t - t_i)}{(t_f - t_i)} \right] + 1 \qquad (52)$$

where t was any intermediate time, and t_i and t_f were the creep crack initiation time and final test time respectively. The initiation time defined as the time for the potential (Va) to rise 15.03μV above the base potential (Vo), was obtained from individual test records. The value $(\beta + 1)$ was obtained from a comparison between the actual and predicted final crack length, and was always greater than 1. Thus:

when $t = t_i$, $C_L = 1$

and when $t = t_f$, $C_L = (\beta + 1)$

An example of this correction factor is shown in graphical form in Figure 29.

A measure of the errors involved in using a linear correction factor for all quenched and tempered 1Cr1Mo¼V tests was obtained by performing a series of interrupted creep crack growth tests at a K_A of 30 $MNm^{-3/2}$ on 15mm thick, $0.5\frac{a}{w}$ quenched and tempered C.T. specimens. The tests were terminated after 250, 500 and 750 hours. A comparison between the predicted and actual average crack length for each test then enabled a plot to be made of intermediate correction factors against test life. The resultant line was found to be non-linear (Figure 29). The implication of this on the subsequent

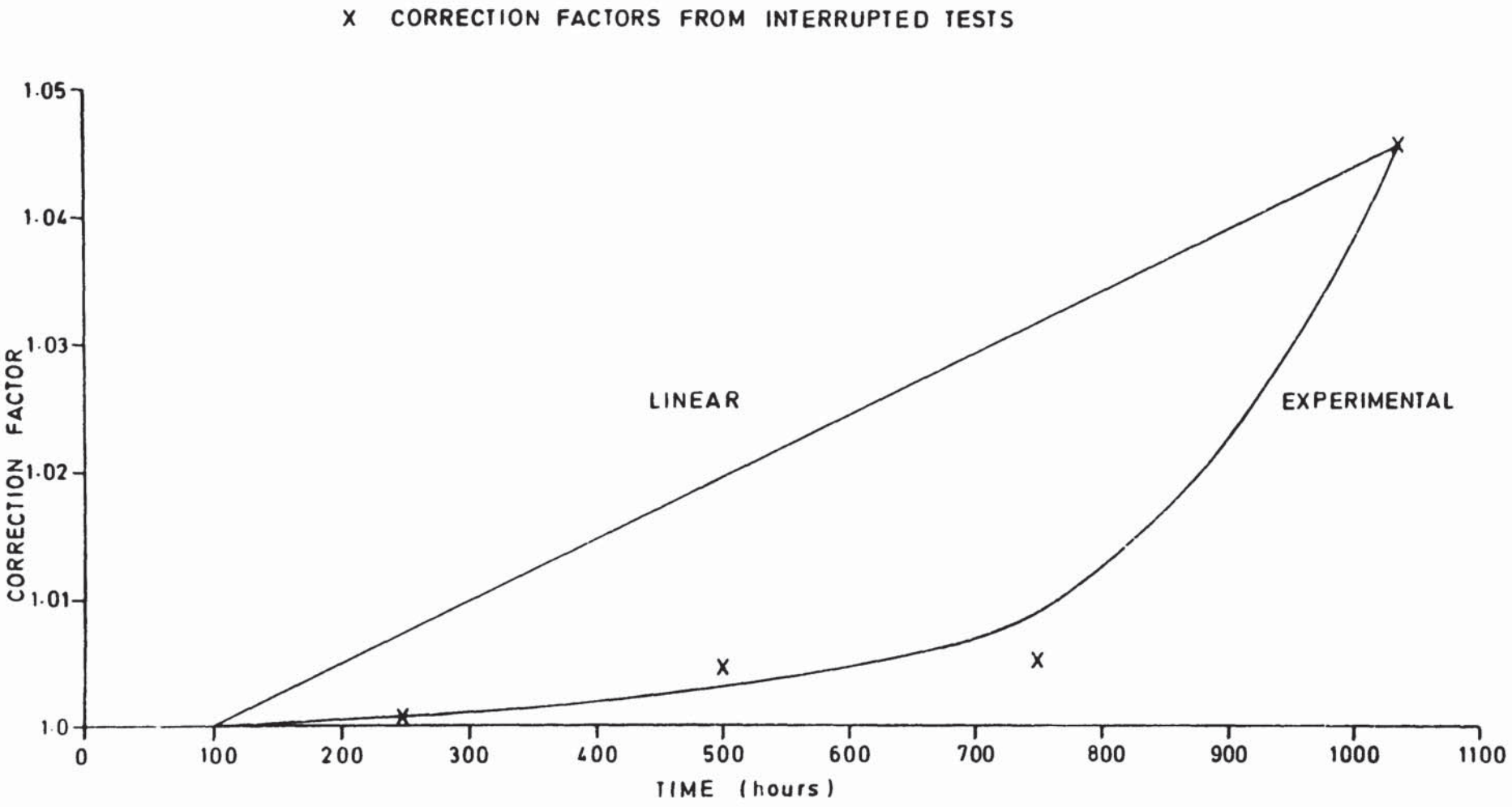

FIG. 29 POTENTIAL DROP CORRECTION FACTORS FOR THE QUENCHED & TEMPERED MATERIAL

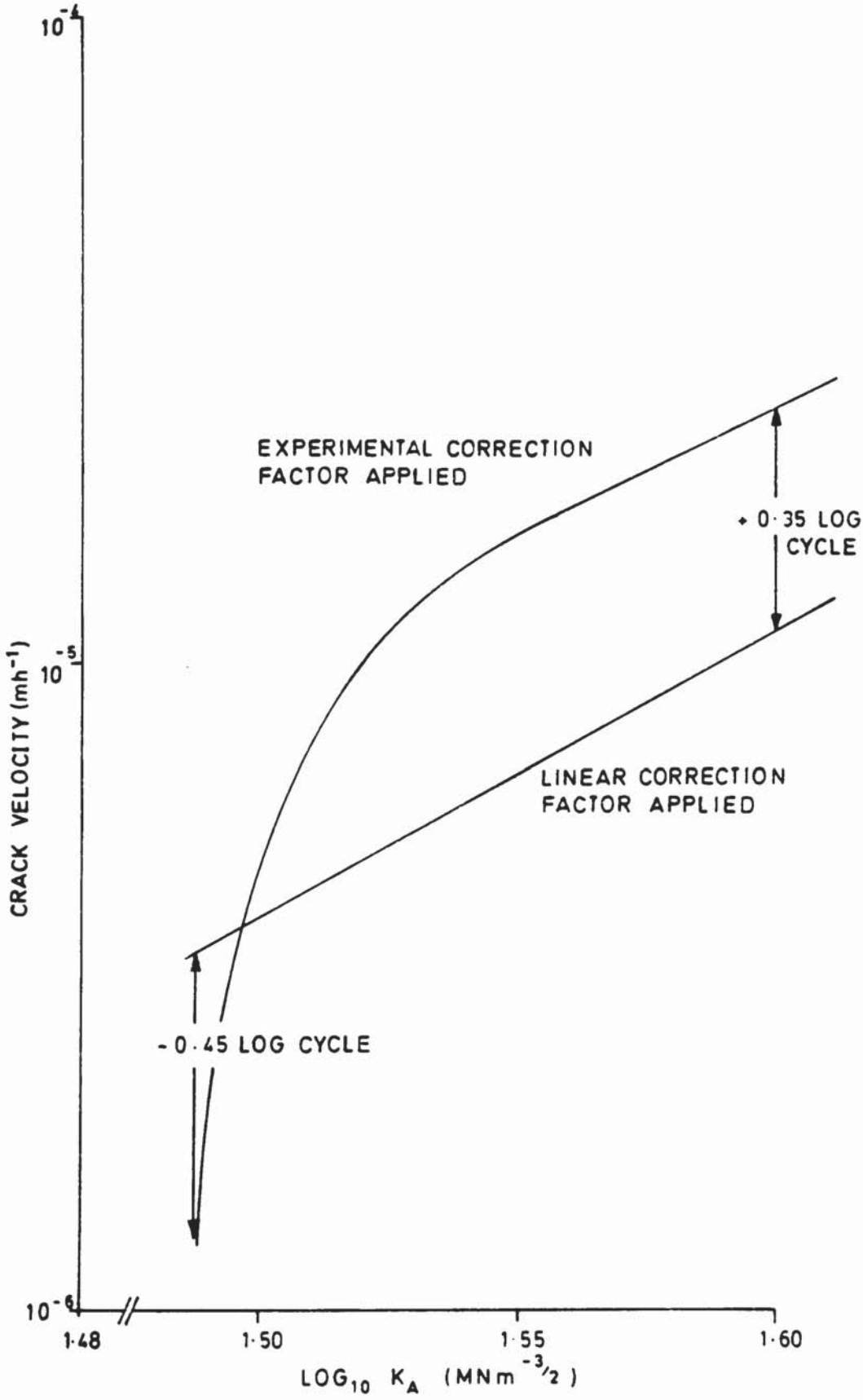

FIG. 30 EFFECT OF CORRECTION FACTOR ON CALCULATED CRACK VELOCITY IN A QUENCHED & TEMPERED MATERIAL

calculation of crack velocity in the above tests can be seen in Figure 30. The use of the experimental correction factor appears to change both the shape of the plot of crack velocity against K_A and its position on the velocity axis. The slope of the plot at high K_A values however, appears to be comparatively unaffected. Further work on experimental correction factors for all variations of test parameters was considered desirable but was not practicable. Consequently, the results and associated errors in the crack velocity measurements from the above experiment was assumed to be typical of all the quenched and tempered tests. Therefore, by using the linear correction factor, the errors in the crack velocity measurements could be of the order of -0.45 Log cycle shortly after crack initiation and +0.35 Log cycle at the end of a test (Figure 30).

Creep crack velocities in the normalised and tempered, and quenched and tempered materials were measured graphically by hand. The maximum error in calculating the velocity by this method was found to be within ± 0.10 Log cycle. The total error in the velocity measurements from the quenched and tempered material was therefore considered to be within +0.10, -0.55 Log cycle, and +0.45, -0.10 Log cycle immediately after crack initiation and at the end of a test respectively. The errors in velocity measurements in the normalised and tempered material where bridging effects were absent, was considered to be simply ± 0.10 Log cycle.

4.2 Experimental Errors in the Measurement of Crack Aspect Ratio and Initiating Crack Opening Displacement

As both the crack aspect ratio and initiating crack opening displacement were measured optically and photographically using a precision built projection microscope, the associated experimental errors were considered to be negligible.

4.3 Stability of Microsturucture

Microstructural stability in long and short term creep crack growth tests was considered to be an important indicator as to the validity of the test data. The microstructure of the two normalised and tempered materials was expected to remain stable over all test periods. However, some tempering of the quenched and tempered material was expected particularly in the long term test, with possible consequential effects on the creep ductility. Microstructural stability was assessed by measuring the surface hardness in the area around the crack tip before and after creep testing. The hardness was measured using a Vickers Hardness Testing Machine with a diamond indentor and a load of 30Kg. The results are shown in Table 5.

Table 5. Hardness Measurments

Alloy	Test Duration h	Hardness Before Testing. Hv30	Hardness After Testing. Hv30
1Cr1Mo¼V N & T	< 2,500	160 - 180	160 - 180
	∿ 20,000	160 - 165	163 - 165
½Cr½Mo¼V N & T	< 2,000	143 - 156	145 - 156
	∿ 9,000	135 - 138	135 - 139
1Cr1Mo¼V Q & T	< 2,000	240 - 250	235 - 245
	∿ 12,000	242 - 248	230 - 233

A change in hardness was only observed in the quenched and tempered material. This amounted to a 2% reduction in hardness in tests lasting less than 2,000 hours, and a 6% reduction in the test lasting approximately 12,000 hours. This reduction in hardness was so small that the accompanying change in creep ductility of the material was expected to be insignificant. Consequently, all creep ductility measurements in this material and also those in the normalised and tempered materials, were considered to be unaffected by microstructural changes during creep testing.

4.4 Effect of Initial Relative Crack Length

4.4.1 Significance of Scatter in Velocity Data

Evidence of the inherent scatter in the creep properties of the normalised and tempered 1Cr1Mo¼V material was obtained by comparing the creep crack growth results from duplicate tests on C.T. specimens possessing the same initial relative crack length. Figure 31 shows that the apparent variation in creep crack velocity at a given K_A ($0.5\frac{a}{w}$ test pair) can be accounted for by the inherent experimental errors in the measurement of velocity (Section 4.1). As a consequence, any crack velocity data lying outside the relevant error bars was considered to be a reflection of a real change in material behaviour.

4.4.2 Correlation Between Crack Velocity, K_A and σ_R

The creep crack velocity results from C.T. tests with initial relative crack lengths of 0.4 to $0.6\frac{a}{w}$ in the normalised and tempered 1Cr1Mo¼V material are shown in Figure 31. Error bars are shown on all the experimental points from a $0.4\frac{a}{w}$ test, and on the first and last point for the remaining tests. A close analysis of the experimental points from the above $0.4\frac{a}{w}$ test shows that they do not lie on a straight line. A more suitable description of the relationship between crack velocity and K_A on a double log plot is provided by either a curve whose tangential gradient decreases as the creep crack develops, or by two straight lines (Figure 31). In either case, there appears to be two distinct stages of crack development. In Stage I (Figure 31) crack tip acceleration is very high while in Stage II the acceleration is relatively lower and is either decreasing or remaining constant. All the tests appear to have behaved in the same general manner. A further analysis of Figure 31 reveals that an overall correlation of the crack velocity results using K_A is poor. The correlation is reasonably good shortly after crack initiation but thereafter the test data 'curves' diverge such that at a relatively high K_A the overall scatter in crack velocity is of the order of x6.3. This amount of scatter can not be accounted for by

experimental error or material variability. Consequently, the above observations are considered to reflect a fundamental difference in the behaviour of each test.

Similar observations can be made and conclusions drawn from Figure 32 which is a double log plot of creep crack velocity and σ_R for tests commencing at the same value of σ_R. It is noticeable however, that there is less overall scatter in the velocity results compared to that shown in Figure 31. In Stage II for example, the overall scatter is of the order of x1.7.

Figures 31 and 32 suggest that under restricted test conditions, creep crack velocity can be correlated with σ_R and to a lesser degree with K_A. For the general case however, Figures 33 and 34 which were obtained by re-analysing Figures 31 and 32 in terms of σ_R and K_A respectively, show that neither stress function correlates satisfactorily the velocity data. The scatter of data points in Stages I or II in Figure 34 for example, is between one and two orders of magnitude in crack velocity. This amount of scatter can not be accounted for by material variations or errors in experimental technique.

4.4.3 Correlation Between Relative Crack Length, Creep Crack Aspect Ratio and Crack Opening Displacement

The results of the measurement of creep ductility in terms of $\frac{1}{\omega}$ and δ_i in the two series of tests starting at a constant initial K_A and σ_R is shown in Figures 35 and 36. The reproducibility of ductility results in duplicate tests is very good when using $\frac{1}{\omega}$ (Figure 35) and only marginally worse for δ_i (Figure 36). This is considered to be a reflection of the averaging qualities of the $\frac{1}{\omega}$ ductility parameter. In contrast, δ_i is more susceptible to local pertubations in material behaviour. Figures 35 and 36 suggest that both $\frac{1}{\omega}$ and δ_i are invariant with relative crack length. Further, it appears that the creep ductility of the constant initial σ_R tests is higher than the corresponding constant initial K_A tests (higher δ_i, lower $\frac{1}{\omega}$).

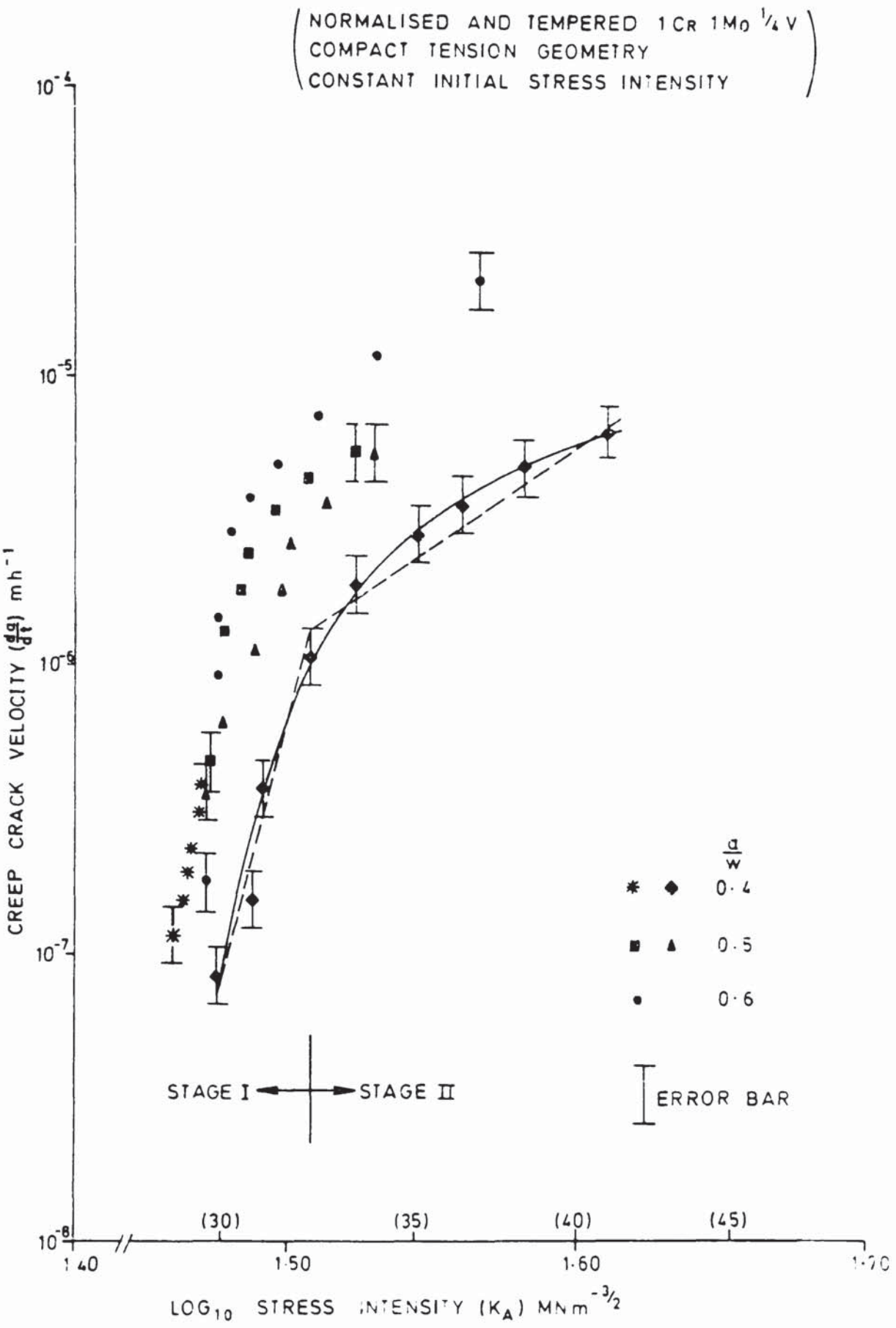

FIG 31 VARIATION OF CREEP CRACK VELOCITY WITH STRESS INTENSITY

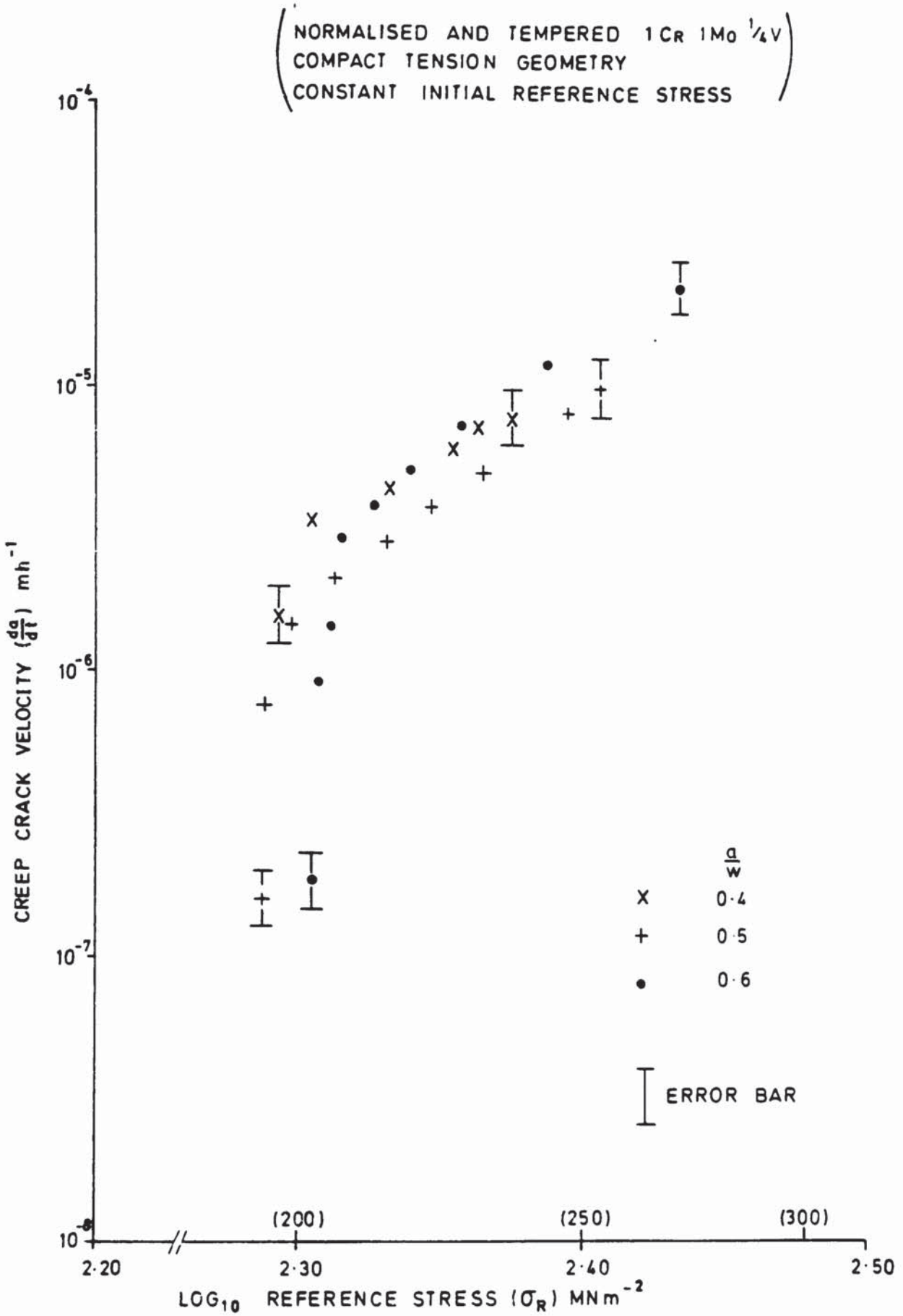

FIG. 32 VARIATION OF CREEP CRACK VELOCITY WITH REFERENCE STRESS

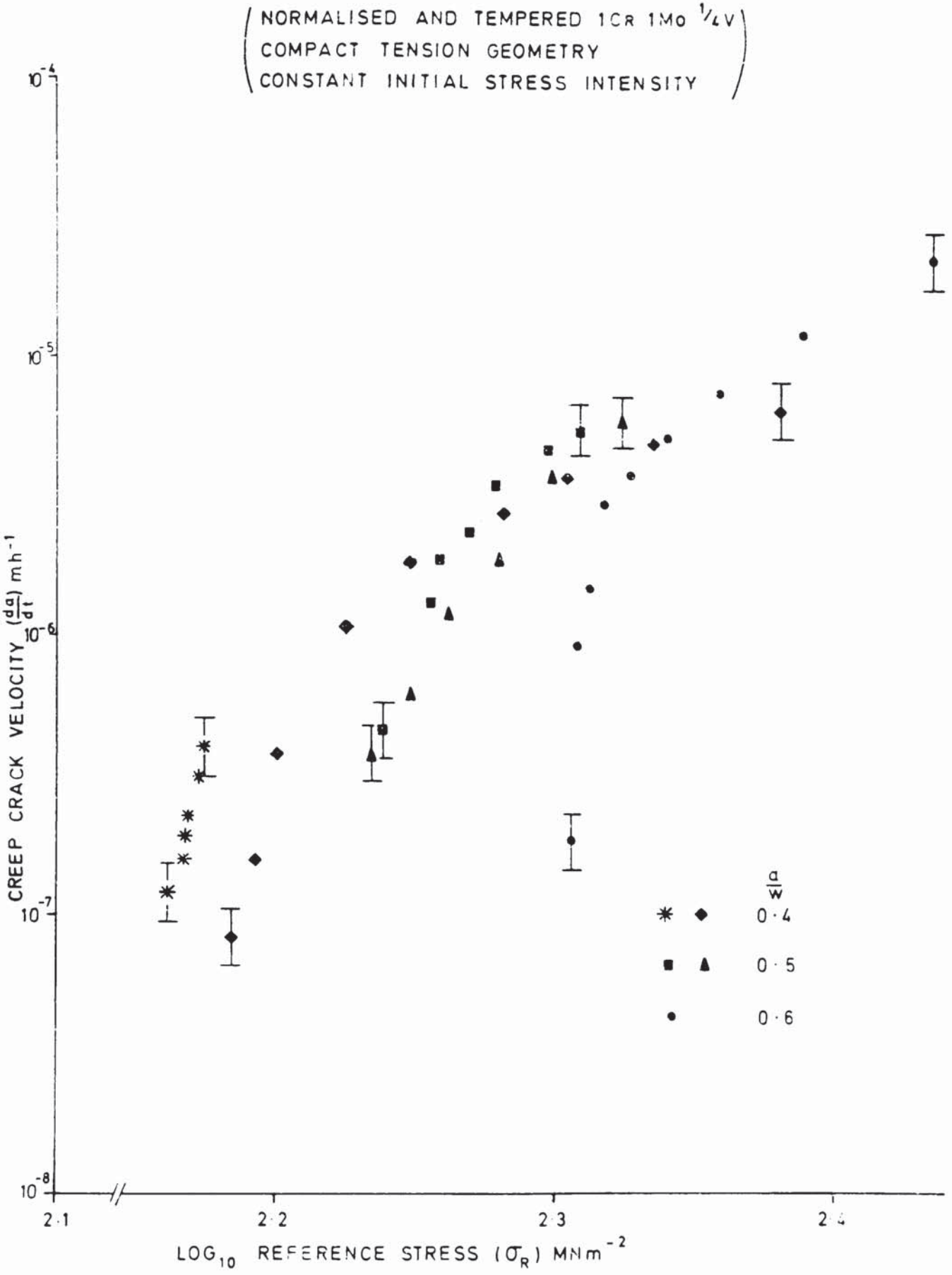

FIG. 33 VARIATION OF CREEP CRACK VELOCITY WITH REFERENCE STRESS

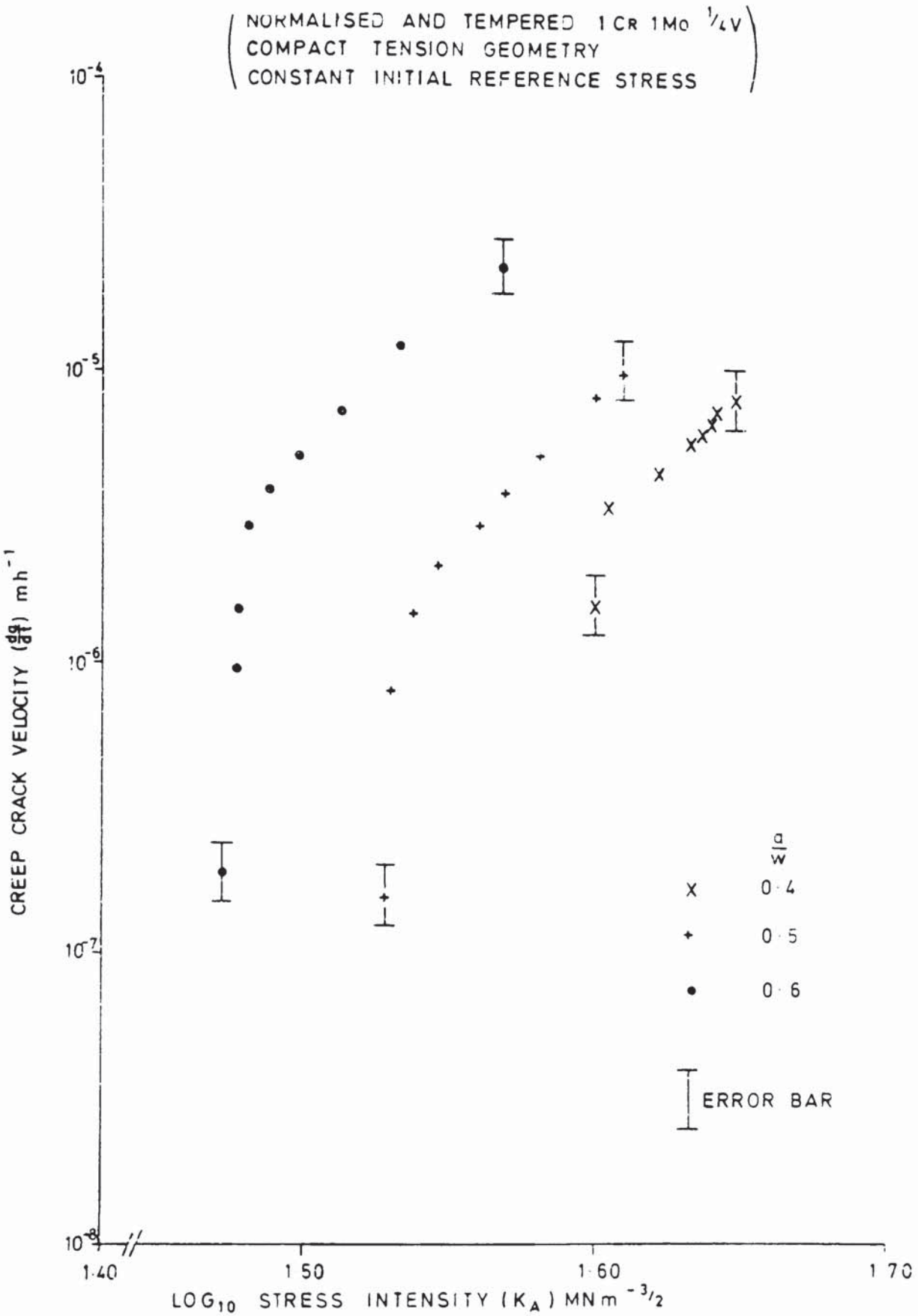

FIG. 34 VARIATION OF CREEP CRACK VELOCITY WITH STRESS INTENSITY

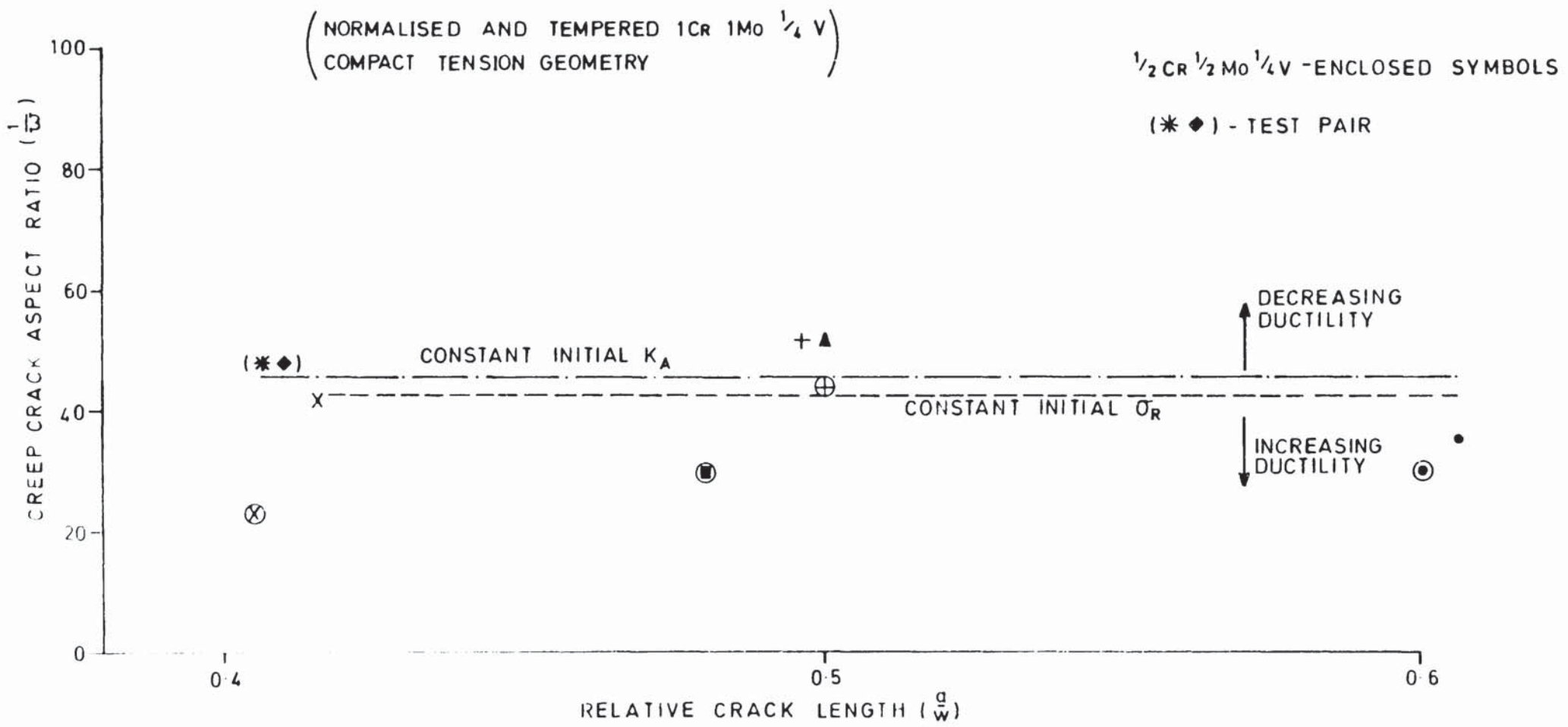

FIG. 35 VARIATION OF CREEP CRACK ASPECT RATIO WITH RELATIVE CRACK LENGTH

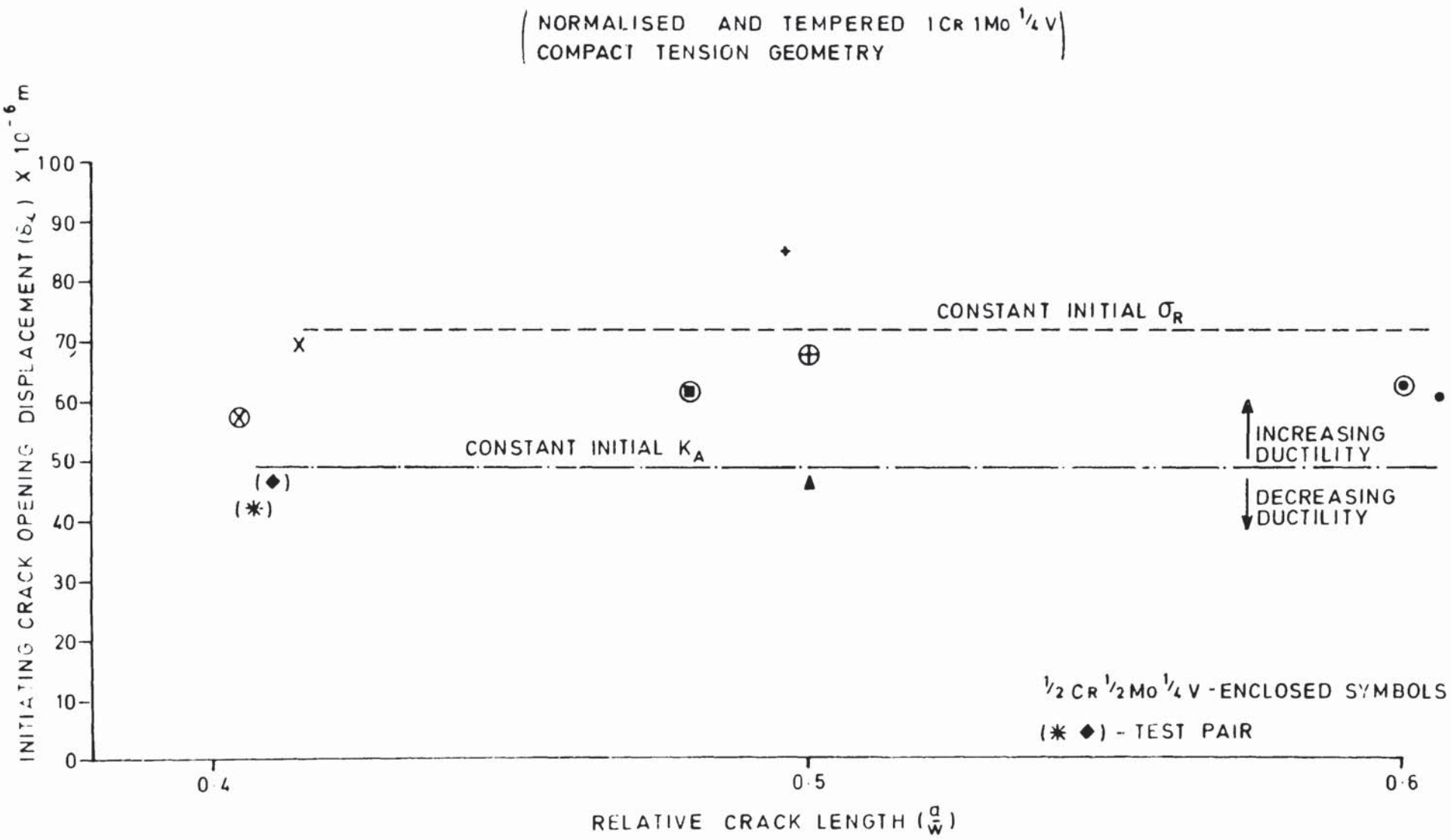

FIG. 36 VARIATION OF INITIATING CRACK OPENING DISPLACEMENT WITH RELATIVE CRACK LENGTH

4.5 Effect of Specimen Thickness

4.5.1 Normalised and Tempered 1Cr1Mo¼V

The variation of creep crack velocity with specimen thickness in the normalised and tempered 1Cr1Mo¼V materials is shown in Figure 37. There is no shift of data points to higher velocities with increasing thickness, although experimental scatter is appreciable.

A more positive indication of the effect of increasing specimen thickness on creep ductility can be observed in Figures 38 and 39. These show the variation of $\frac{1}{\omega}$ and δ_i with specimen thickness. Both figures indicate that creep ductility decreases with increasing thickness (higher $\frac{1}{\omega}$, lower δ_i). However, at thicknesses greater than approximately 20mm the ductility appears to reach a plateau. Further evidence of the increase in $\frac{1}{\omega}$ with increasing thickness can be seen in the macrophotographs of two typical creep cracks that were grown in a thin and thick specimen, Figures 40 and 41 respectively. A measure of the significance of these results can be obtained by comparing the variation of ductility in nominally identical tests with the change in ductility between the 5 mm and 50 mm thick specimens. Figures 38 and 39 show that the maximum variation in ductility for nominally identical tests is considerably smaller than the overall change in ductility. Thus, the observed change in ductility is considered to be significant. The comparative success of $\frac{1}{\omega}$ and δ_i in demonstrating a thickness effect is considered to be due to their insensitivity to specimen 'edge-effects'. The latter which is known to affect crack length measurements, does not have any influence on the optical measurement of $\frac{1}{\omega}$ or δ_i when these are measured at mid-thickness.

4.5.2 Quenched and Tempered 1Cr1Mo¼V

The variation of creep crack velocity with specimen thickness in the quenched and tempered 1Cr1Mo¼V material is shown in Figure42. It can be seen that this figure, unlike the corresponding one for normalised and

tempered material (Figure 37), shows a systematic increase in crack velocity with increasing specimen thickness. For example, at a K_A of 31.6 $MNm^{-3/2}$ (1.5 Log_{10}) the crack velocity of a 5, 10 and 15mm thick specimen is 1.5 x 10^{-6}, 2.5 x 10^{-6} and 4 x 10^{-6} mh^{-1} respectively. However, it is also apparent that the results from the 20mm thick specimen are at variance with this trend. The experimental errors are also significantly large. As a consequence, the initial observation on layering of velocity data may be fortuitous. A more positive thickness effect can be observed however, in Figures 43 and 44 which show respectively the variation in $\frac{1}{\omega}$ and δ_i with specimen thickness. It can be seen that the crack tip creep ductility decreases with increasing specimen thickness in a similar manner to that observed in the normalised and tempered material (Figures 38 and 39). This time however, the change in ductility between the 5mm and 20mm thick specimens is less marked than in the corresponding normalised and tempered specimens, but it is still significant. Further evidence of the effect of thickness on creep ductility can be seen in Figures 45 and 46 which show the image of a creep crack grown in a thin and thick specimen respectively.

4.6 Effect of Specimen Geometry

4.6.1 Normalised and Tempered 1Cr1Mo¼V

Previous sections have shown that either K_A or σ_R will under very limited test conditions, correlate creep crack velocity in C.T. specimens. This is also true for C.C.P. specimens manufactured from the normalised and tempered 1Cr1Mo¼V material (Figures 47 and 48). Both figures show that the scatter between each set of data points from specimens with initial relative crack lengths of 0.4, 0.5 and 0.6 $\frac{a}{w}$ is covered by the crack velocity error bars. This suggests that creep ductility in these tests is invariant with initial relative crack length. This conclusion is supported by the $\frac{1}{\omega}$ and δ_i results shown (connected by broken lines) in Figures 50 and 51.

Figures 47, 48, 50 and 51 also show the effect of specimen thickness on creep ductility in the C.C.P. geometry. A decrease in thickness from 8 to 1mm at constant initial relative crack length of 0.5 $\frac{a}{w}$ apparently did not affect the crack velocity (Figures 47 and 48) but did result in a marked change in $\frac{1}{\omega}$ and δ_i (Figures 50 and 51). These observations are in accord with those from corresponding C.T. tests (Section 4.5).

The effect of specimen geometry on creep crack velocity is illustrated in Figure 49. This figure shows that crack velocity in the C.T. and C.C.P. geometries is identical providing their thickness and initial relative crack lengths are the same. This point will be returned to in the Discussion. The relevant $\frac{1}{\omega}$ and δ_i results shown in Figures 50 and 51 also suggest that creep ductility is independent of specimen geometry.

4.6.2 Quenched and Tempered 1Cr1Mo¼V

Figures 52 to 56 inclusive show that this material responded to the test variables in an identical manner to that of the normalised and tempered material in the previous section. In particular, both K_A and σ_R correlated satisfactorily the crack velocity data from tests starting at the same initial K_A or σ_R (Figures 52 and 53). However, these figures also show that this correlation is destroyed when the low load data is included. In doing this, it can be seen that a back extrapolation of the high load data underestimates the low load data by approximately two orders of magnitude. A further effect of load on creep ductility is illustrated in Figures 55 and 56 where it can be seen that ductility is directly proportional to applied load. This 'load effect' has also been observed in the C.T. geometry (Section 4.8).

4.7 Effect of Alloy Composition

Comparisons between the creep crack velocity in the 1Cr1Mo¼V and the ½Cr½Mo¼V alloy using both K_A and σ_R as the correlating parameters have been made and are shown in Figures 57 and 58 respectively. Selecting initially the results from the ½Cr½Mo¼V material, Figure 57 shows that an apparent

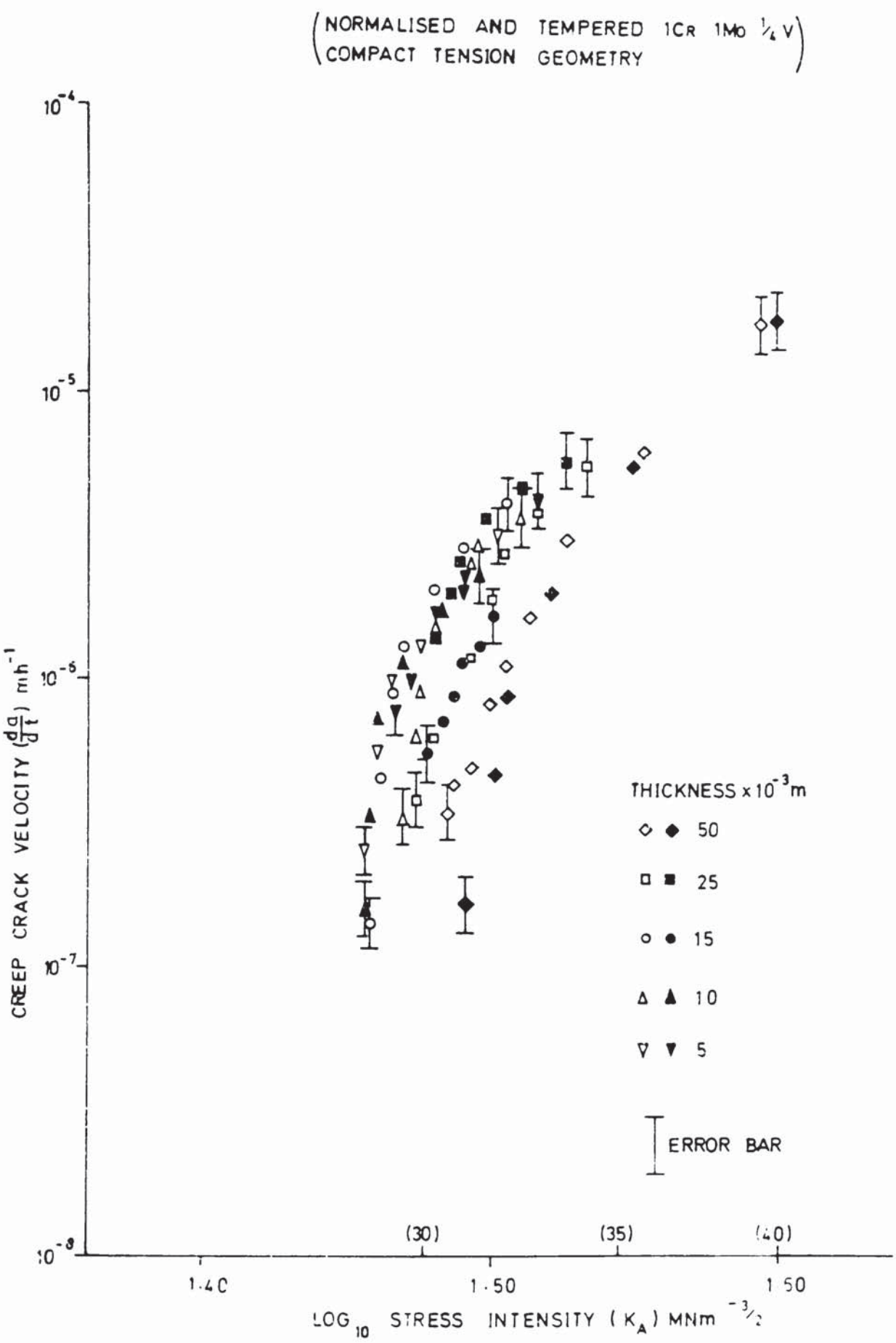

FIG 37 VARIATION OF CREEP CRACK VELOCITY WITH SPECIMEN THICKNESS

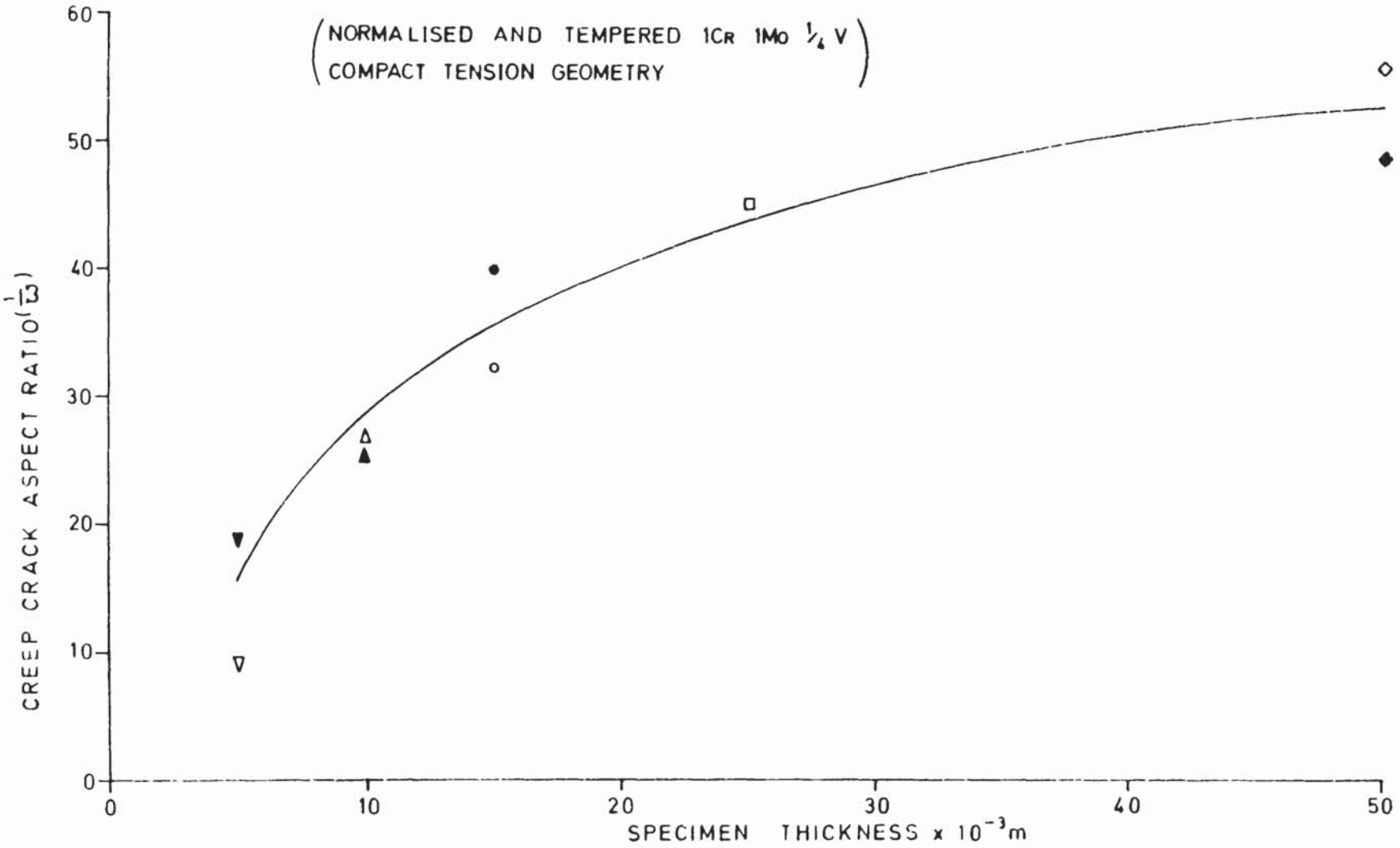

FIG 38 EFFECT OF SPECIMEN THICKNESS ON CREEP CRACK ASPECT RATIO

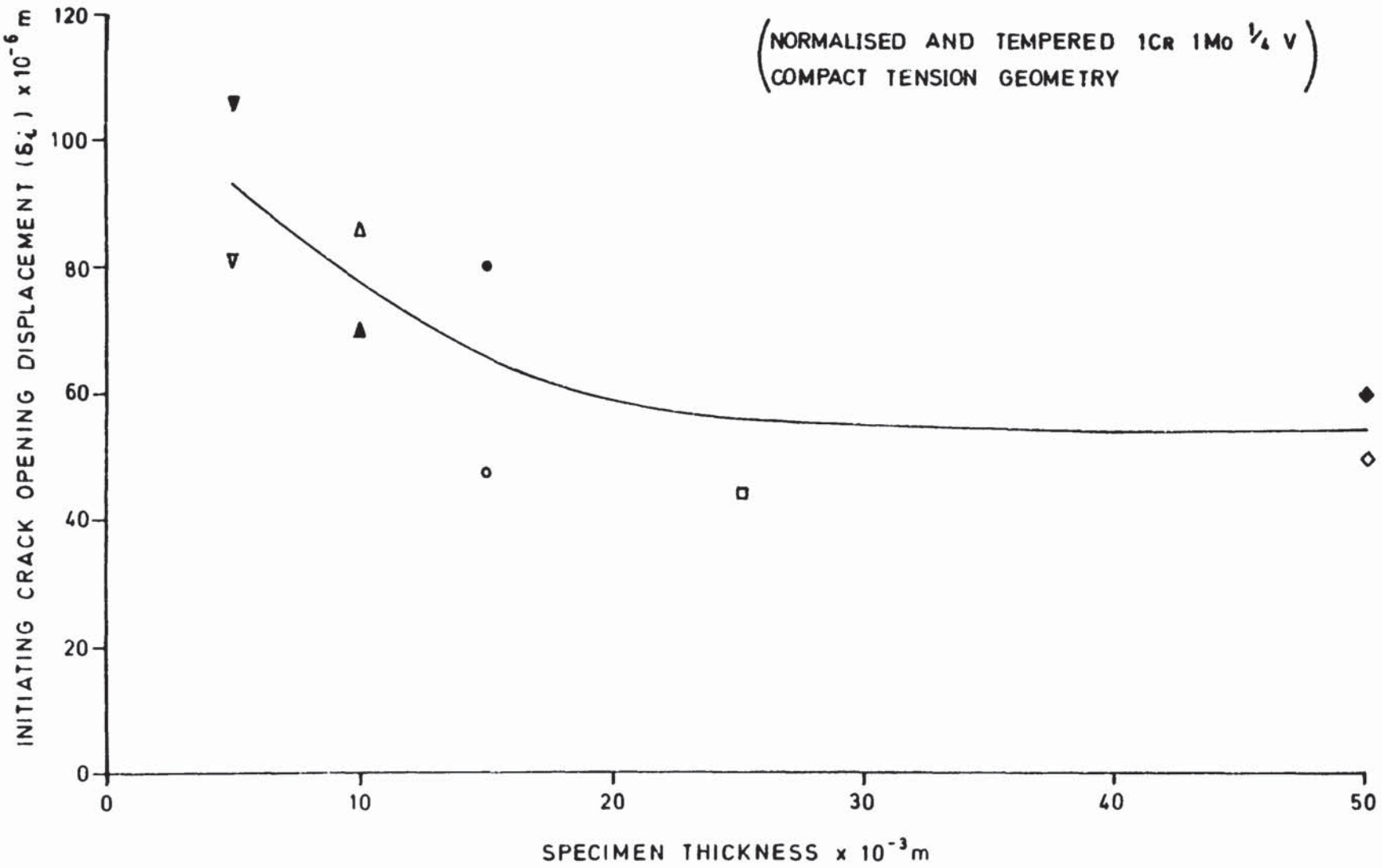

FIG. 39 EFFECT OF SPECIMEN THICKNESS ON INITIATING CRACK OPENING DISPLACEMENT

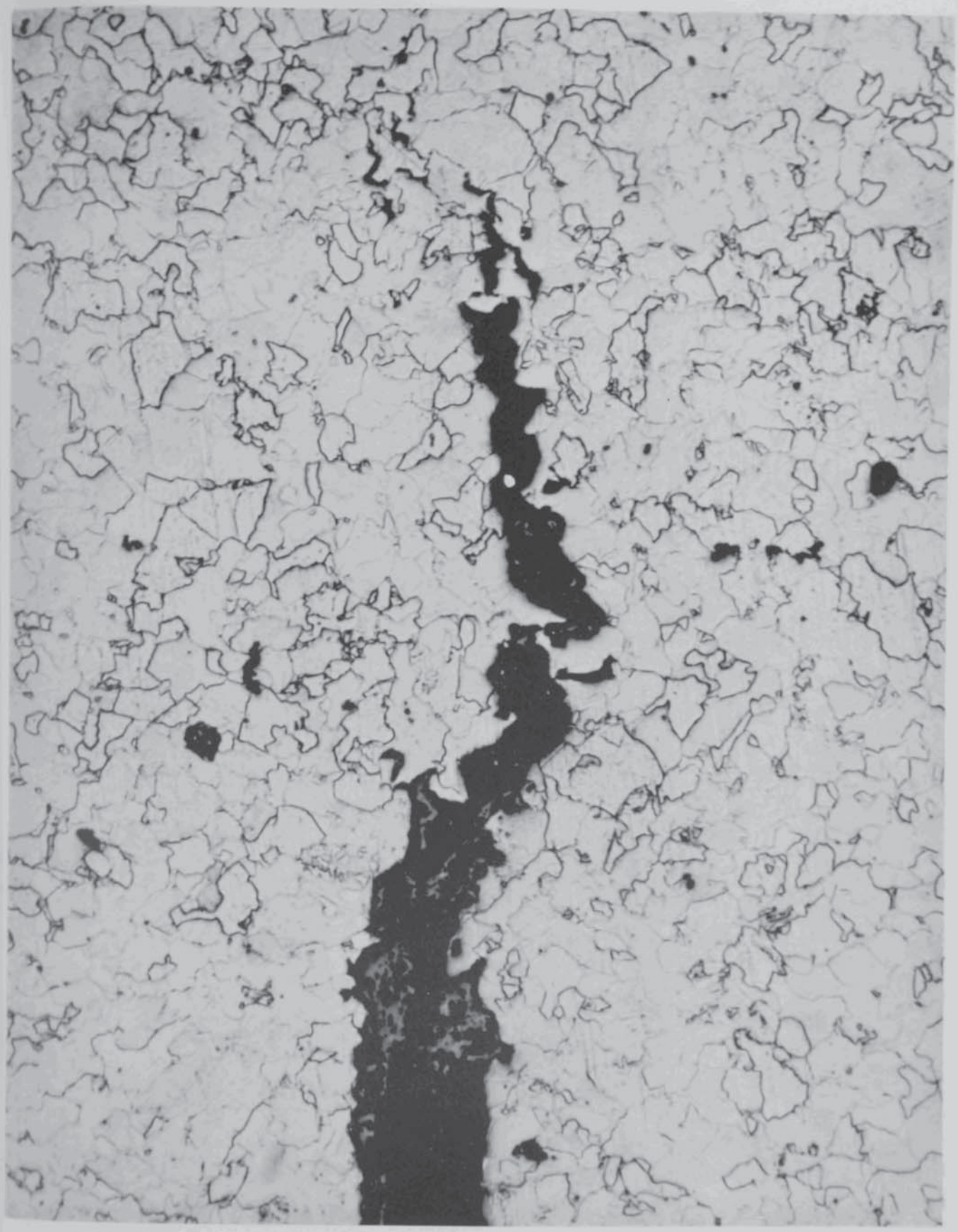

FIG. 40 CREEP CRACK IN A 5mm C.T. SPECIMEN
1 CR 1 MO ¼ V NORMALISED AND TEMPERED x 160

FIG. 41 CREEP CRACK IN A 25mm C.T. SPECIMEN
1 CR 1 MO ¼ V NORMALISED AND TEMPERED x 40

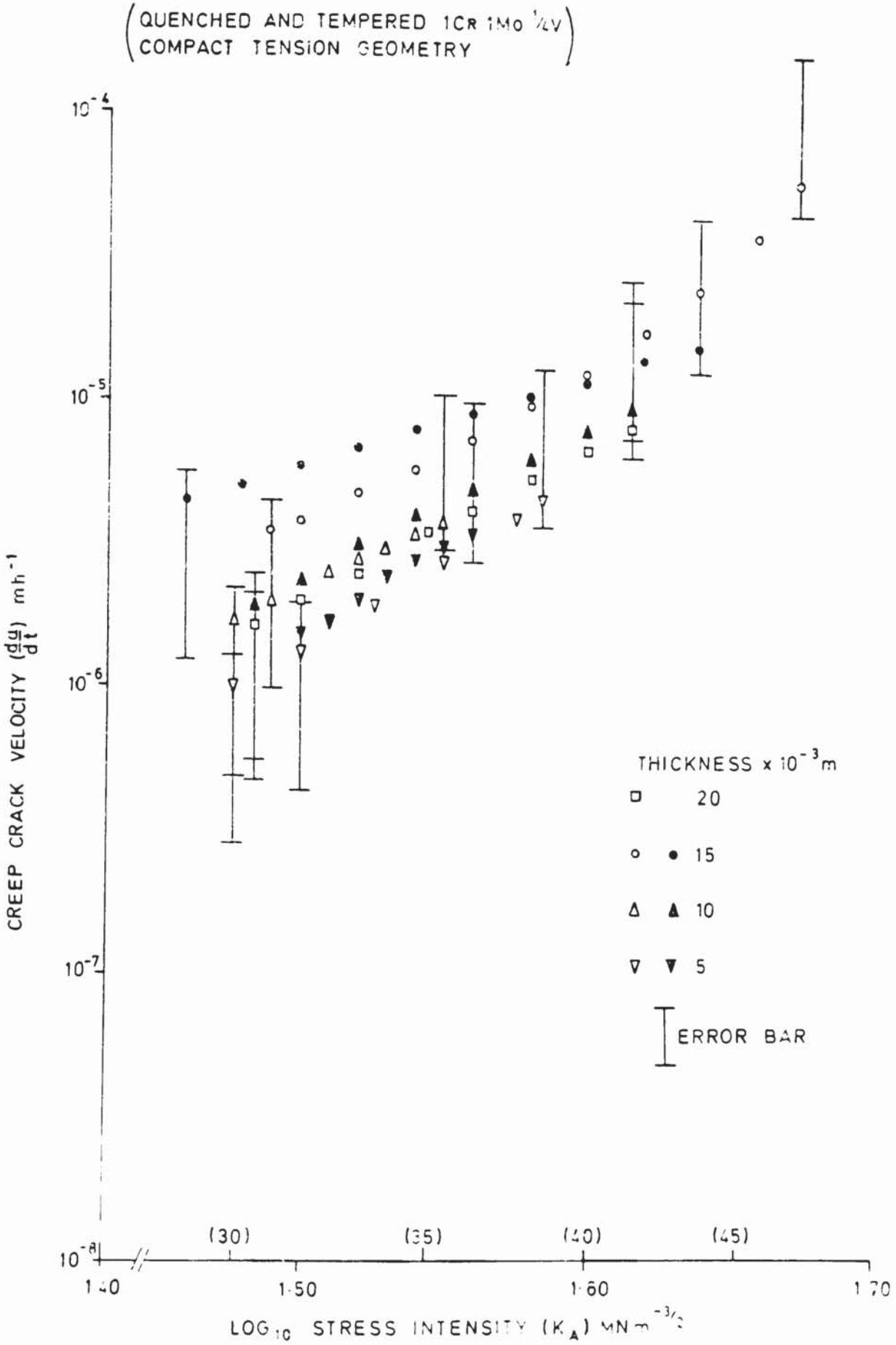

FIG 42 VARIATION OF CREEP CRACK VELOCITY WITH SPECIMEN THICKNESS

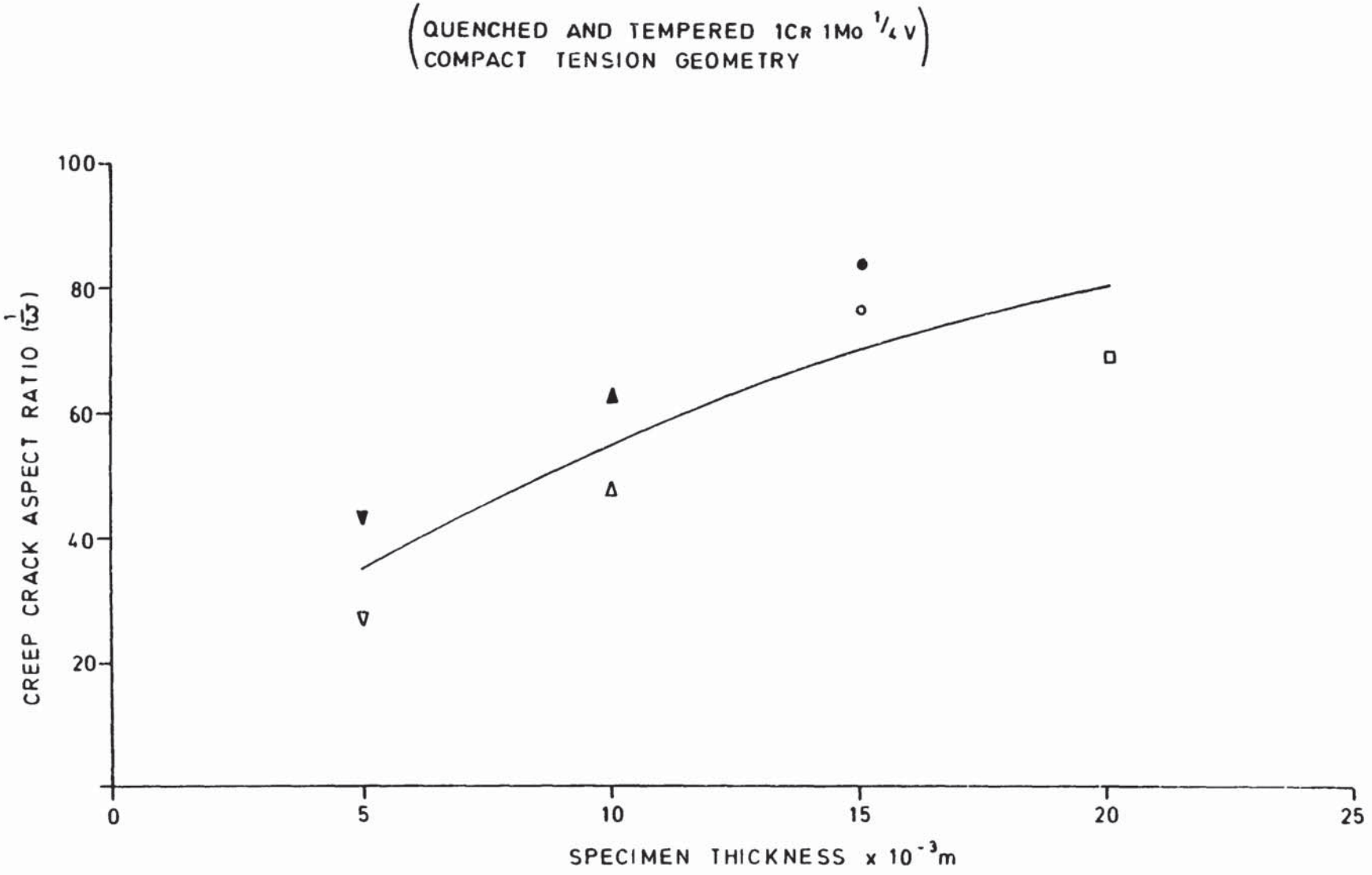

FIG. 43 EFFECT OF SPECIMEN THICKNESS ON CREEP CRACK ASPECT RATIO

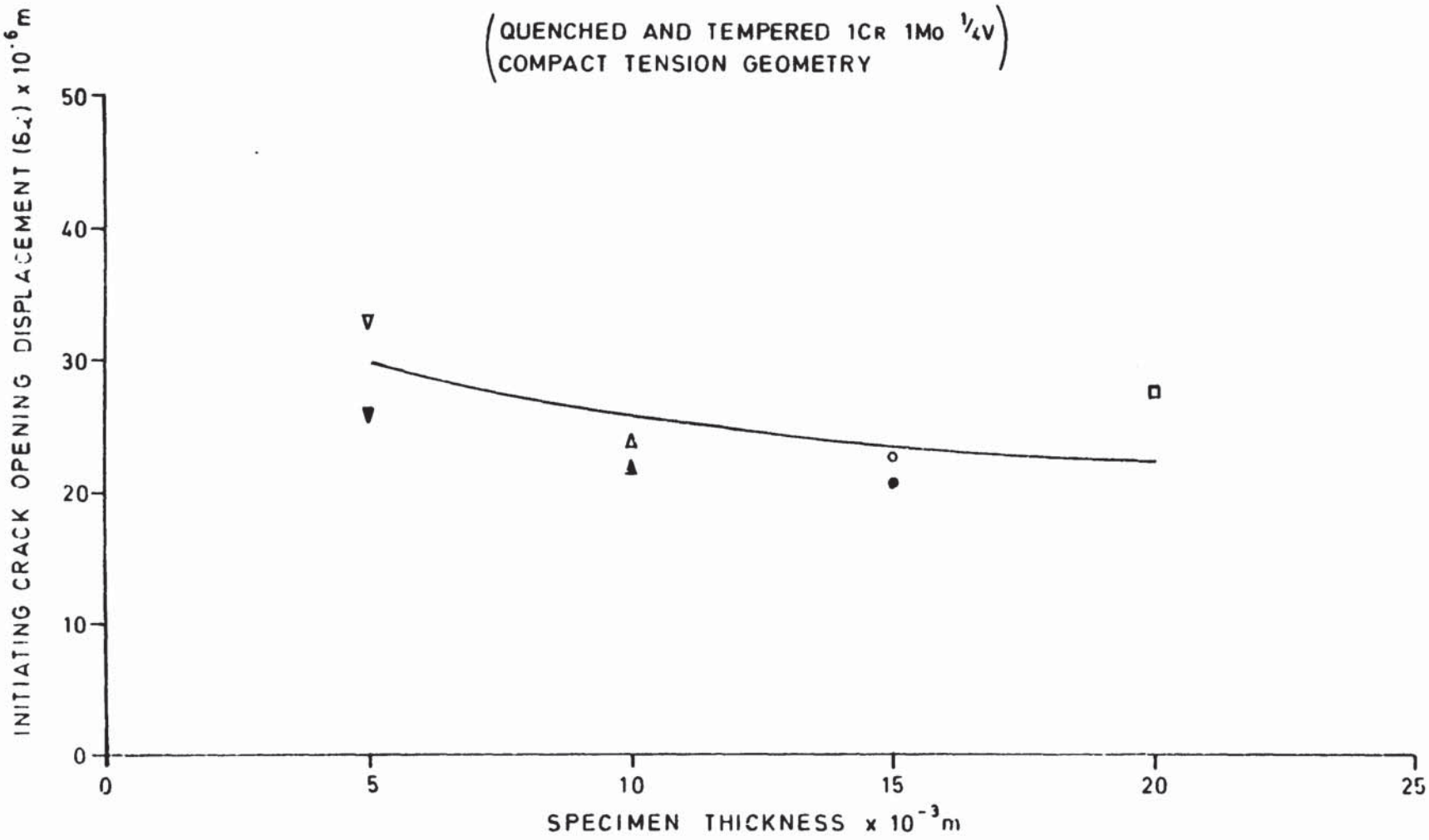

FIG. 44 EFFECT OF SPECIMEN THICKNESS ON INITIATING CRACK OPENING DISPLACEMENT

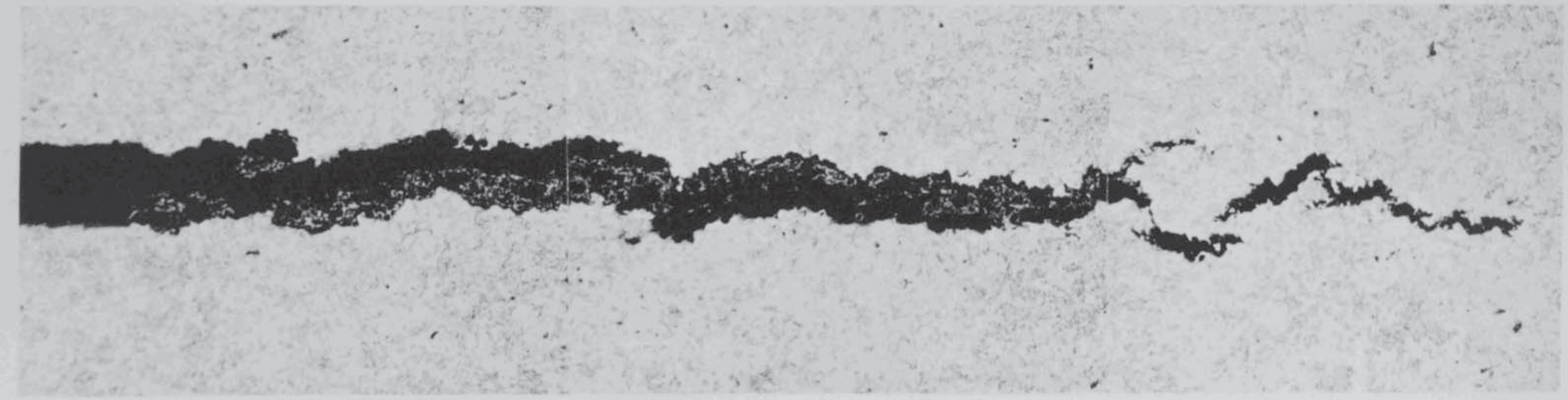

FIG. 45 CREEP CRACK IN A 5mm C.T. SPECIMEN
1 CR 1 MO ¼ V QUENCHED AND TEMPERED x 50

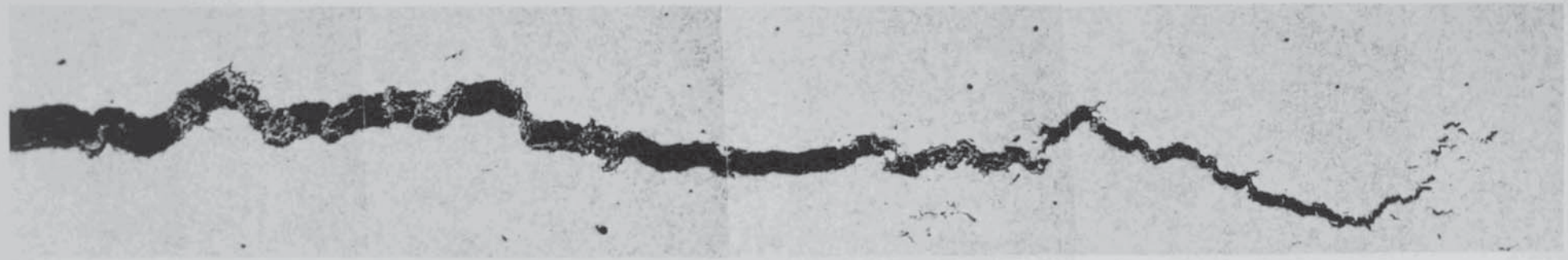

FIG. 46 CREEP CRACK IN A 20mm C.T. SPECIMEN
1 CR 1 MO ¼ V QUENCHED AND TEMPERED x 30

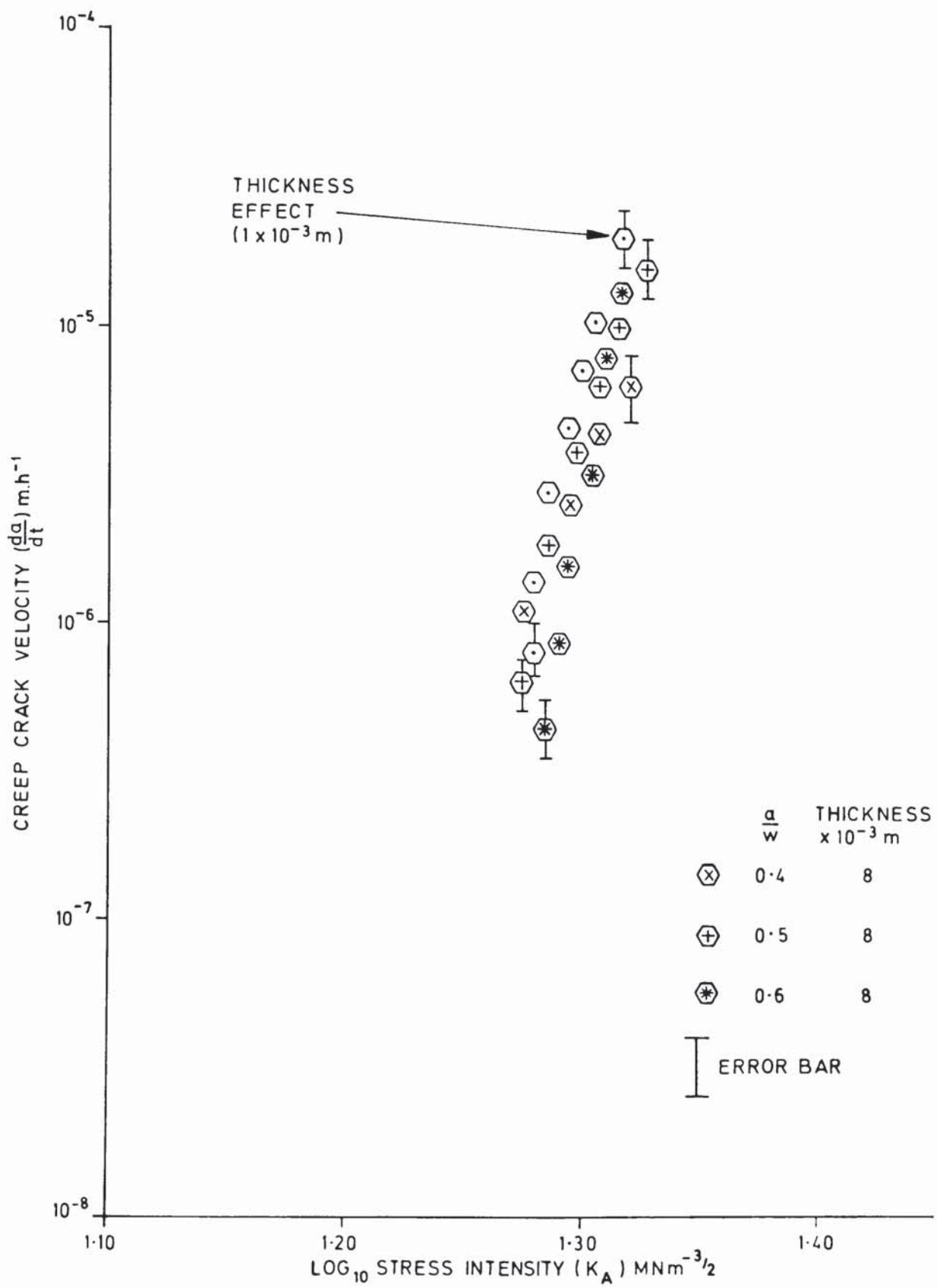

FIG. 47 VARIATION OF CREEP CRACK VELOCITY WITH STRESS INTENSITY

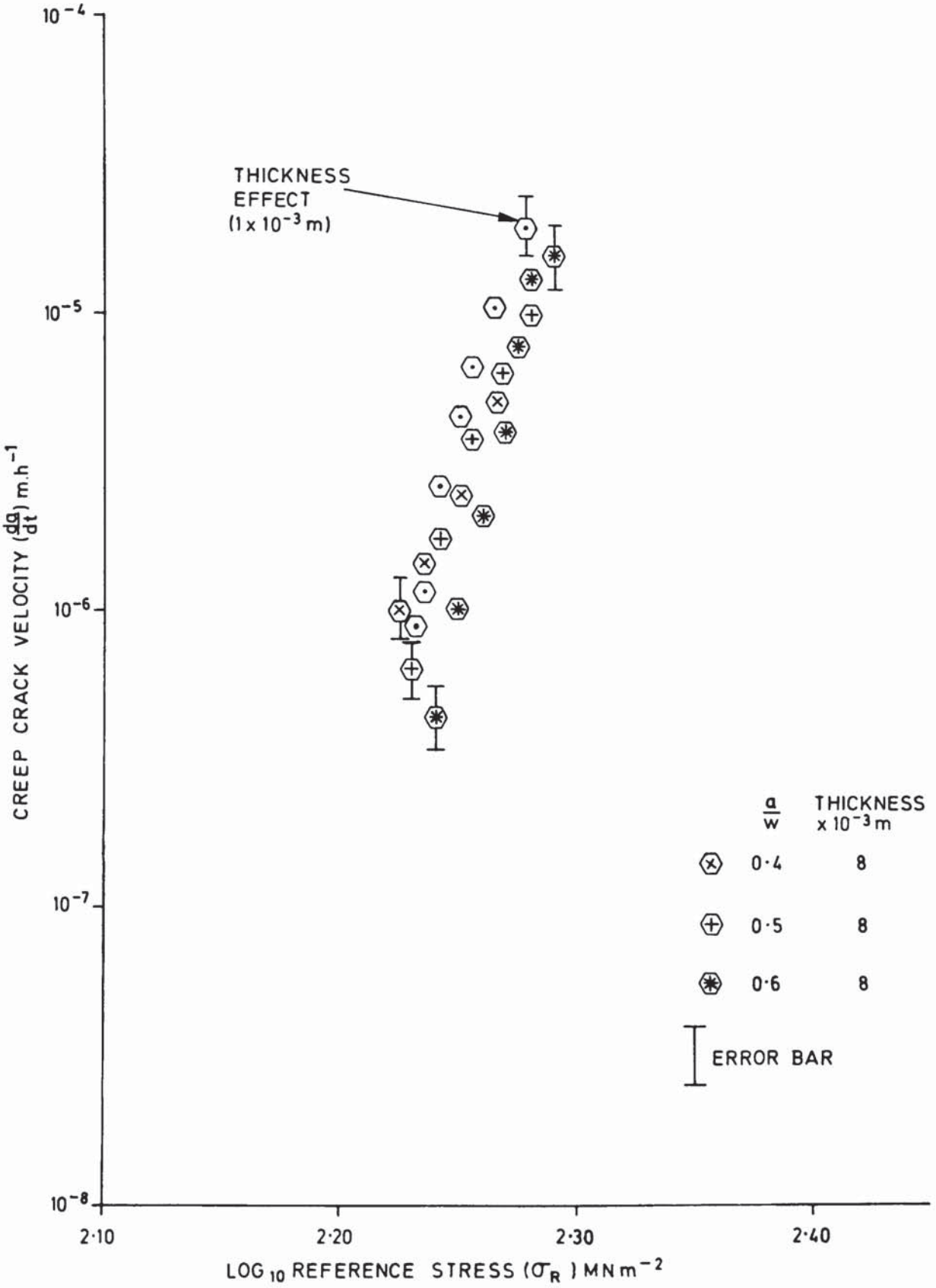

FIG. 48 VARIATION OF CREEP CRACK VELOCITY WITH REFERENCE STRESS.

(NORMALISED AND TEMPERED 1CR1MO 1/4 V)

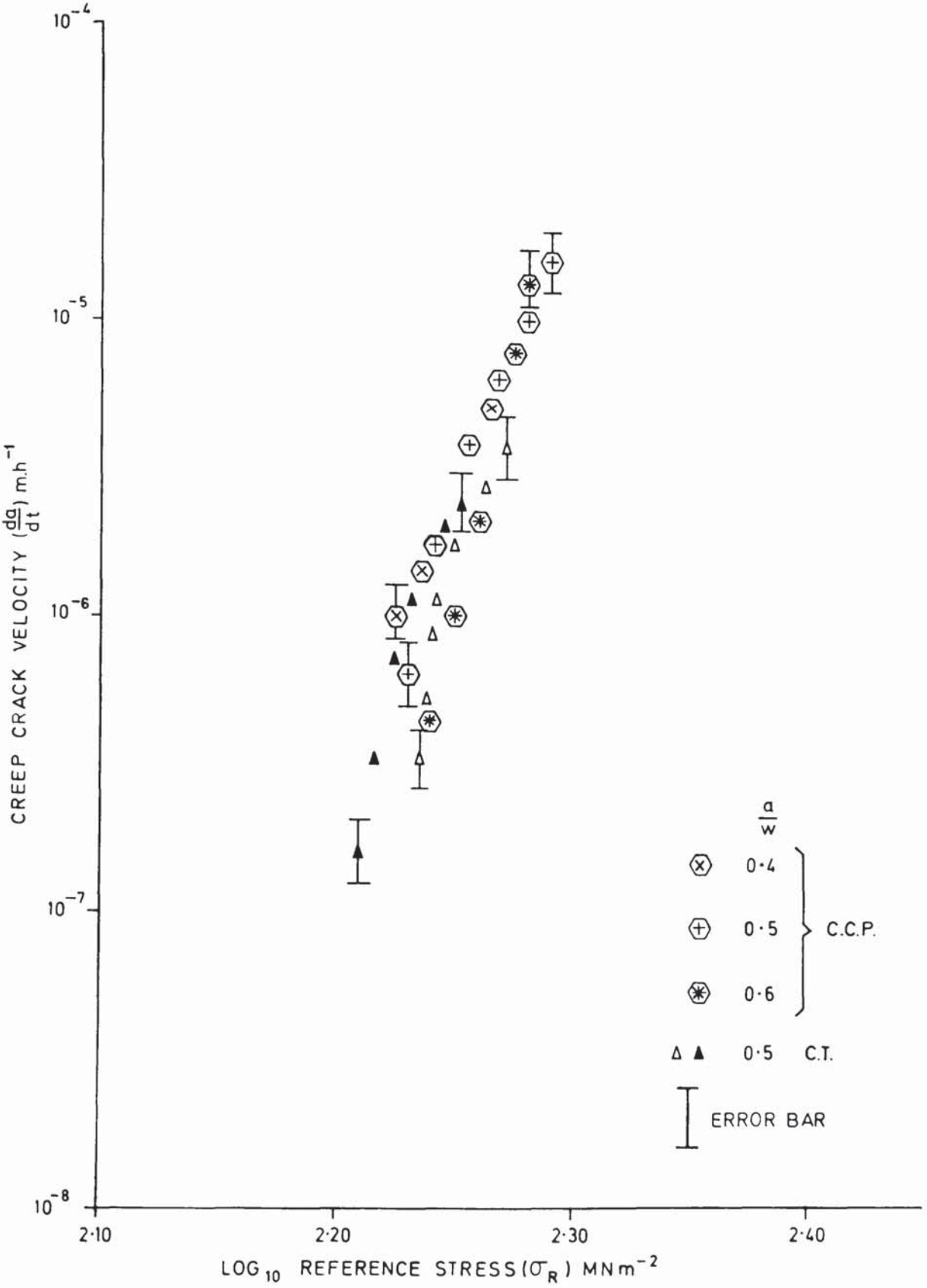

FIG. 49 EFFECT OF GEOMETRY ON CREEP CRACK VELOCITY

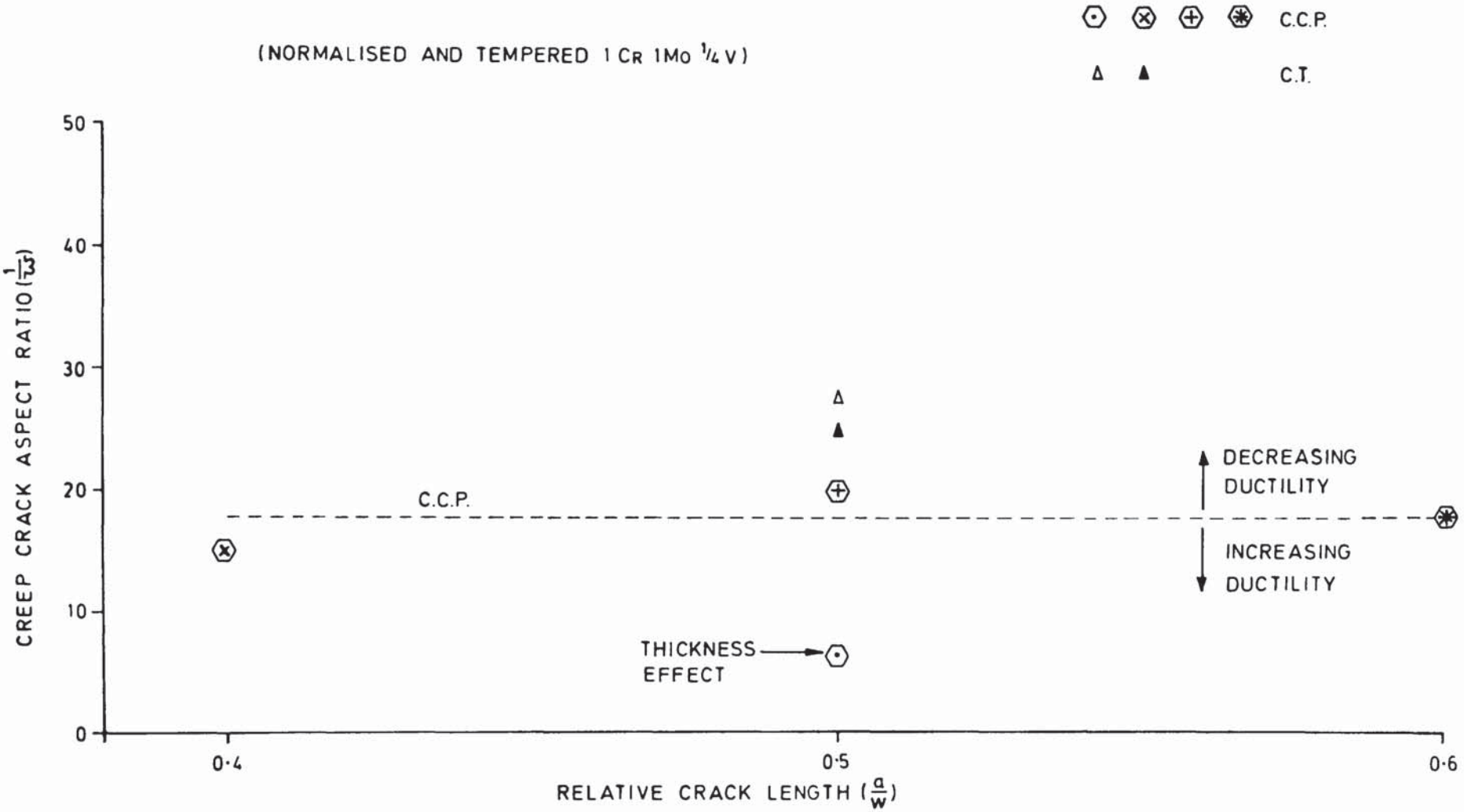

FIG. 50 VARIATION OF CREEP CRACK ASPECT RATIO WITH RELATIVE CRACK LENGTH

RC/SSR/A4/787

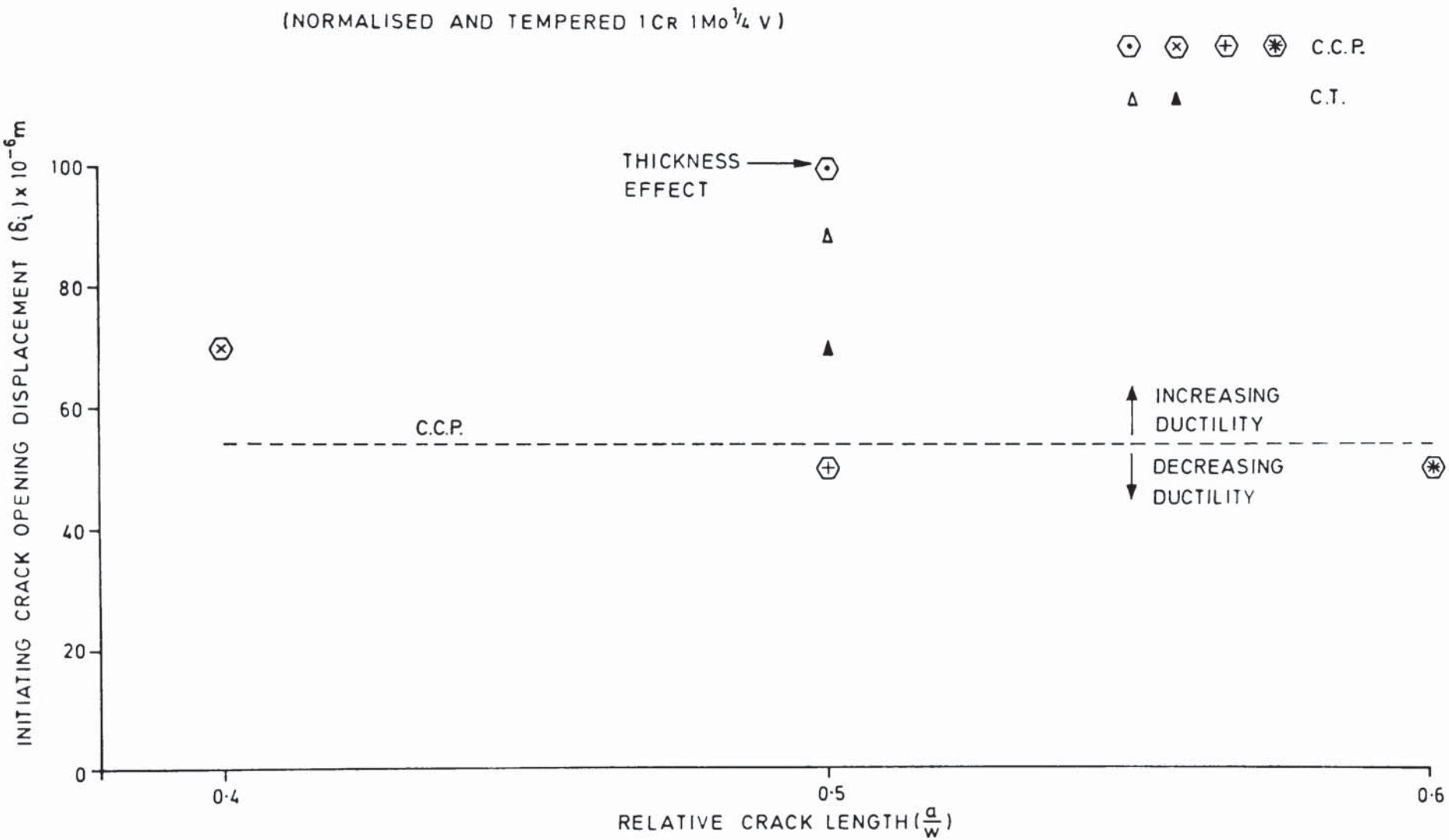

FIG. 51 VARIATION OF INITIATING CRACK OPENING DISPLACEMENT WITH RELATIVE CRACK LENGTH

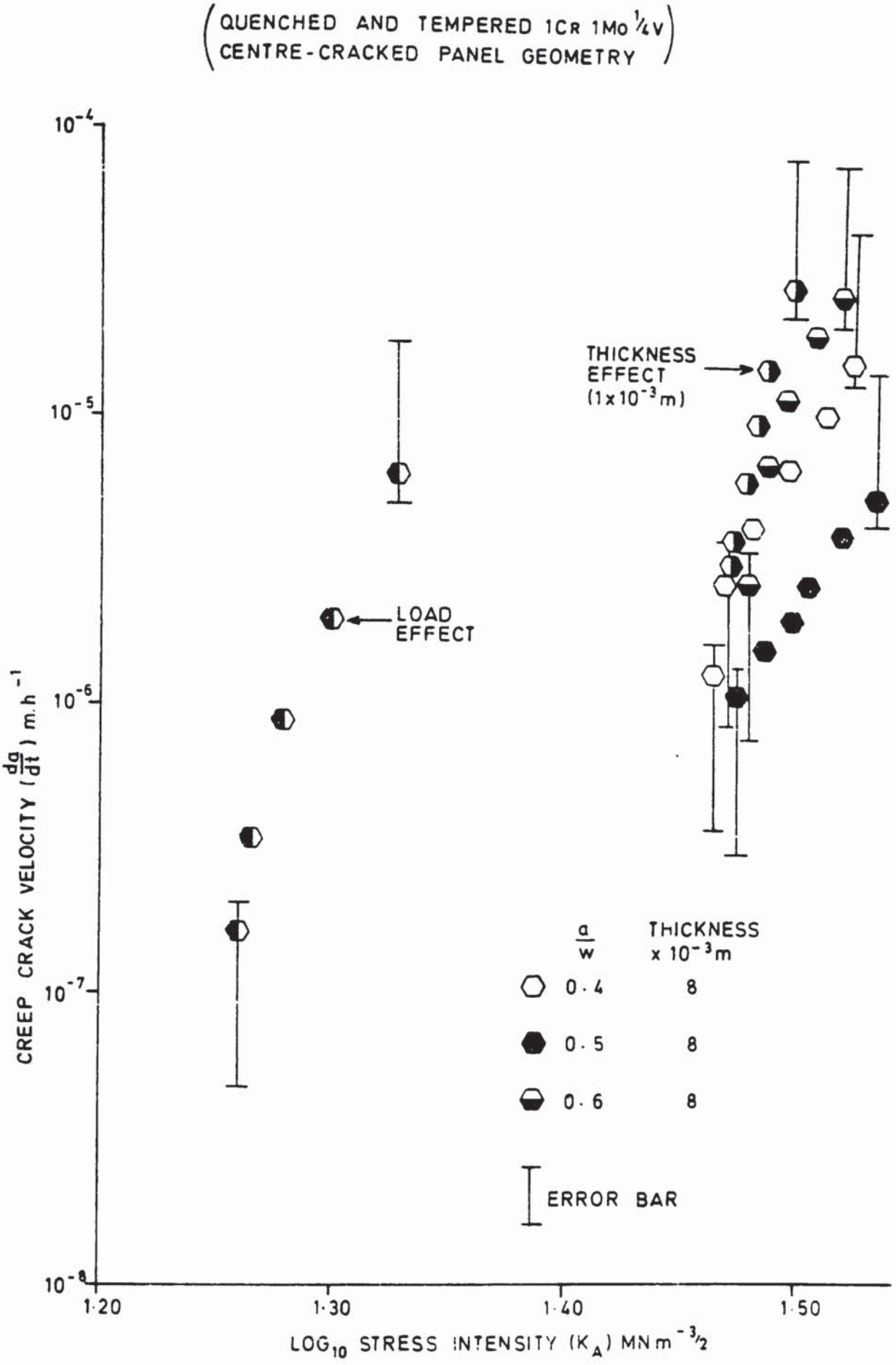

FIG. 52 VARIATION OF CREEP CRACK VELOCITY WITH STRESS INTENSITY

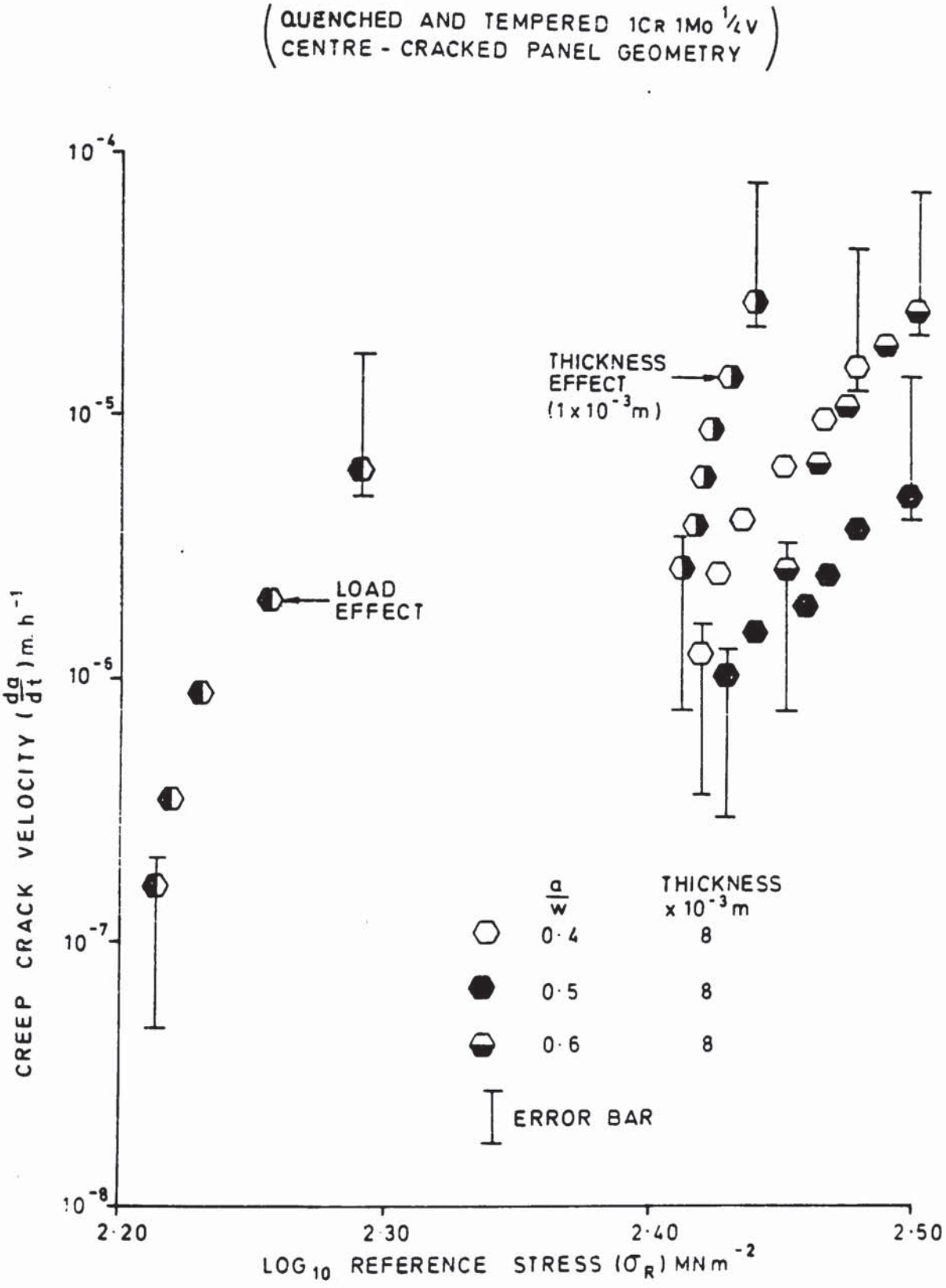

FIG. 53 VARIATION OF CREEP CRACK VELOCITY WITH REFERENCE STRESS

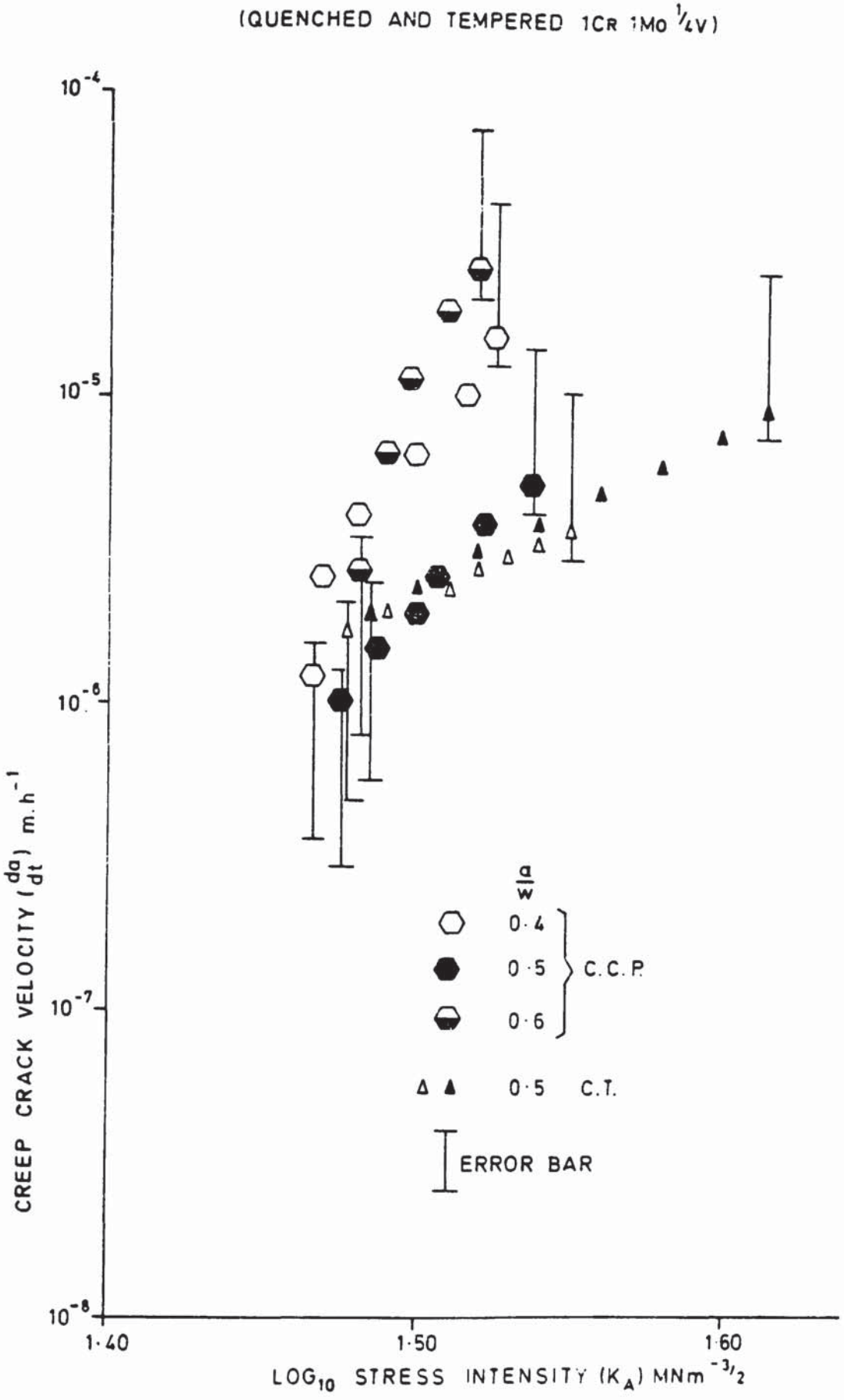

FIG. 54 EFFECT OF GEOMETRY ON CREEP CRACK VELOCITY

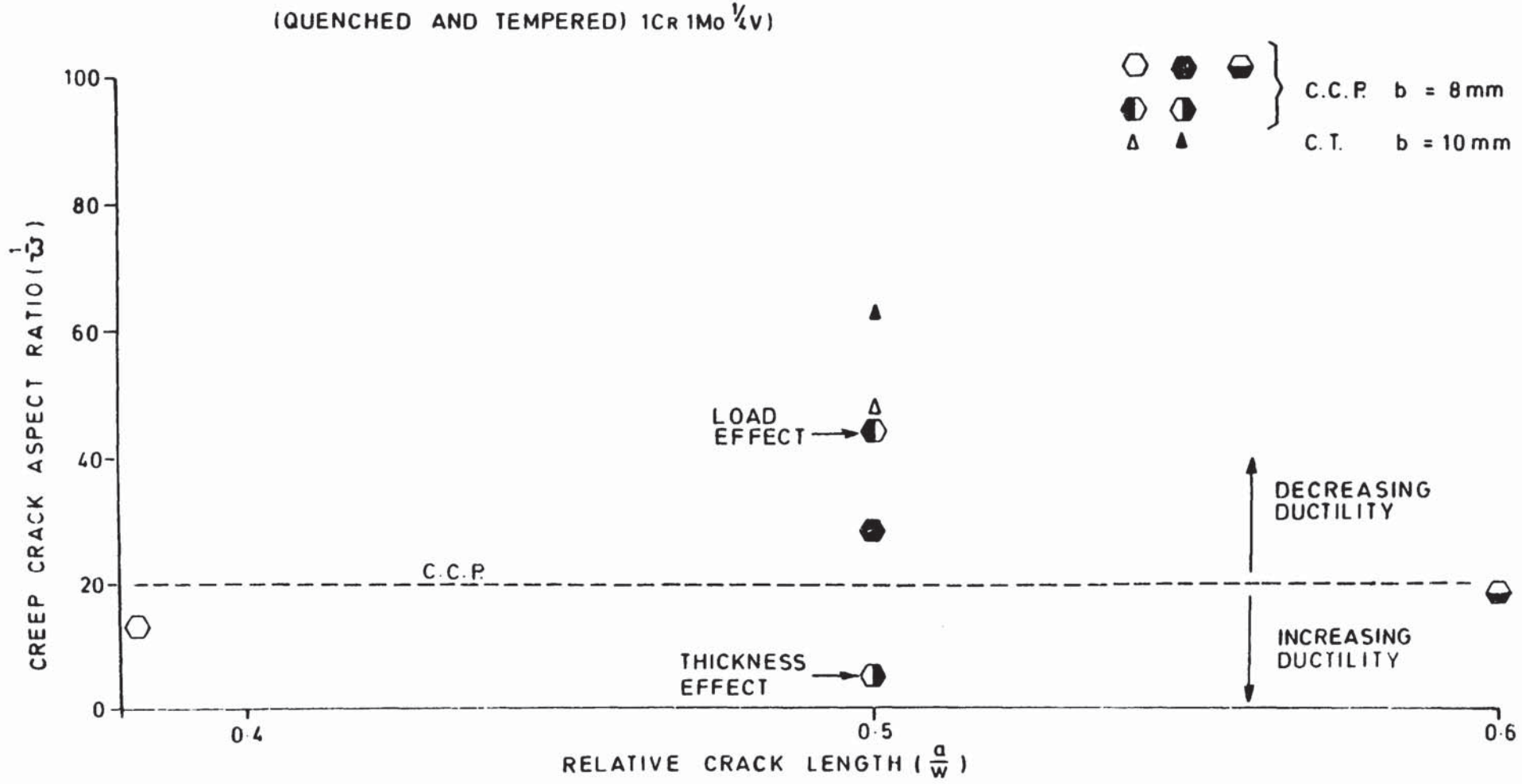

FIG. 55 VARIATION OF CREEP CRACK ASPECT RATIO WITH RELATIVE CRACK LENGTH

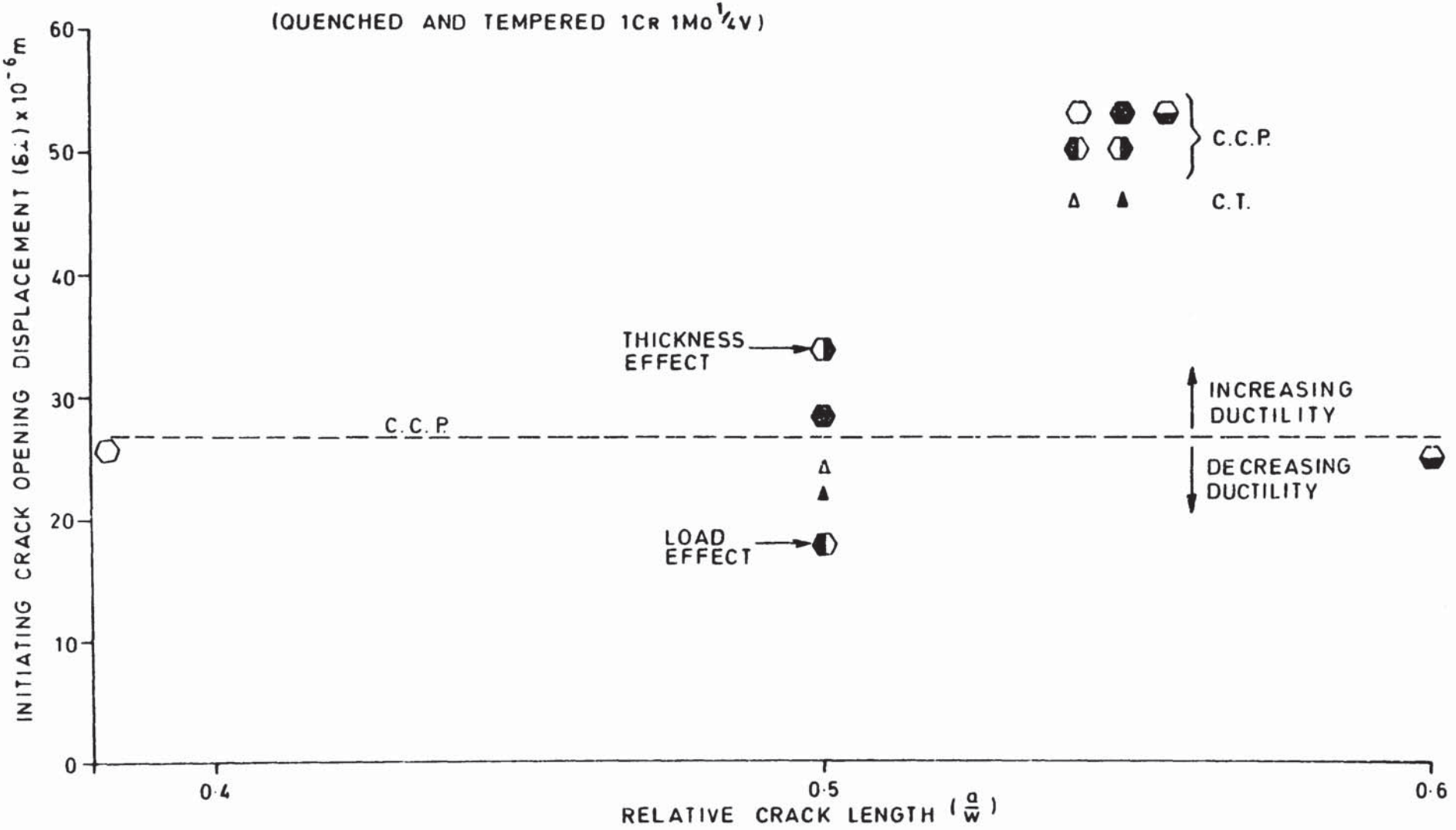

FIG. 56 VARIATION OF INITIATING CRACK OPENING DISPLACEMENT WITH RELATIVE CRACK LENGTH

(COMPACT TENSION GEOMETRY)

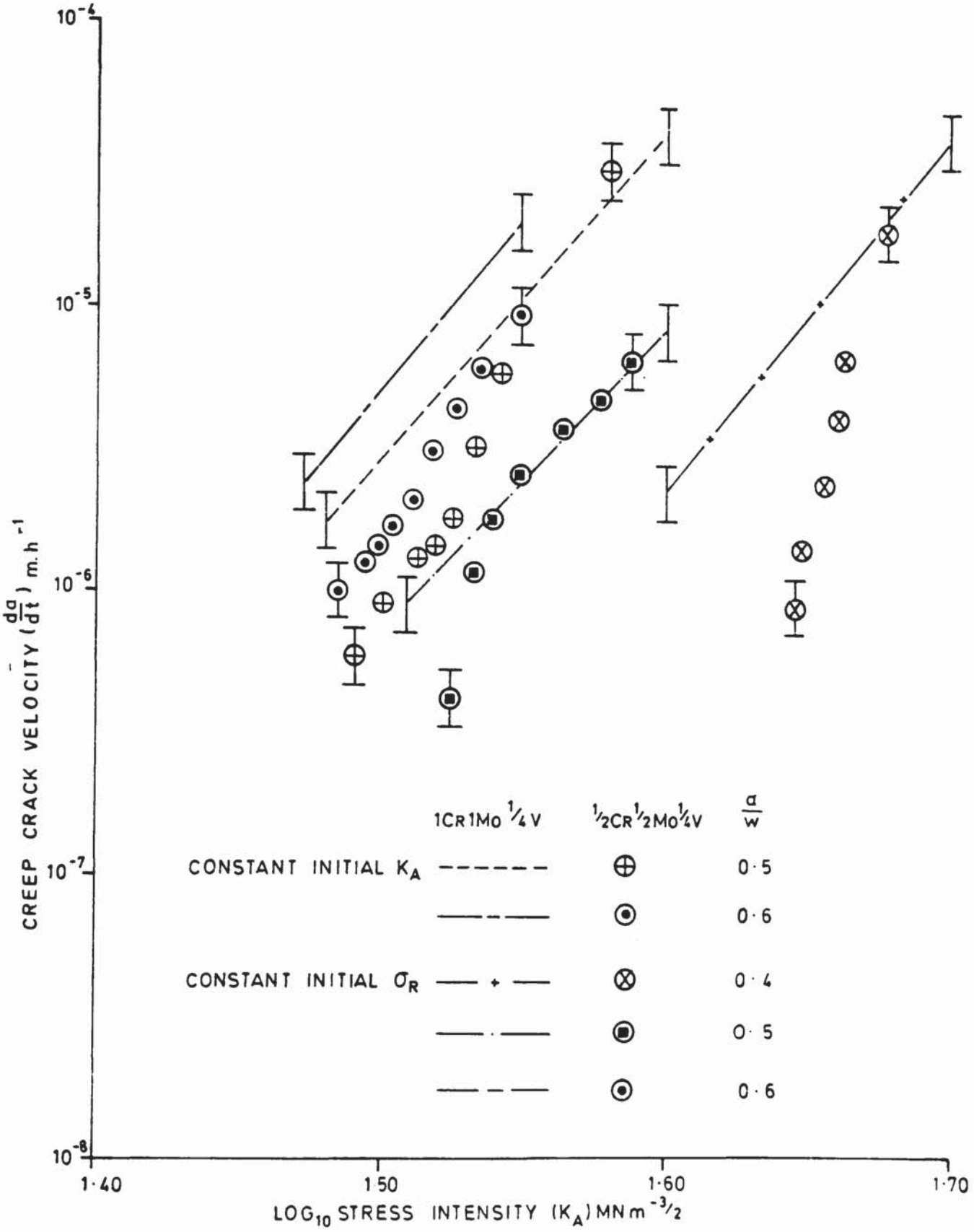

FIG. 57 COMPARISON OF CREEP CRACK VELOCITY IN THE NORMALISED AND TEMPERED 1CR 1MO 1/4 V AND 1/2 CR 1/2 MO 1/4V STEELS

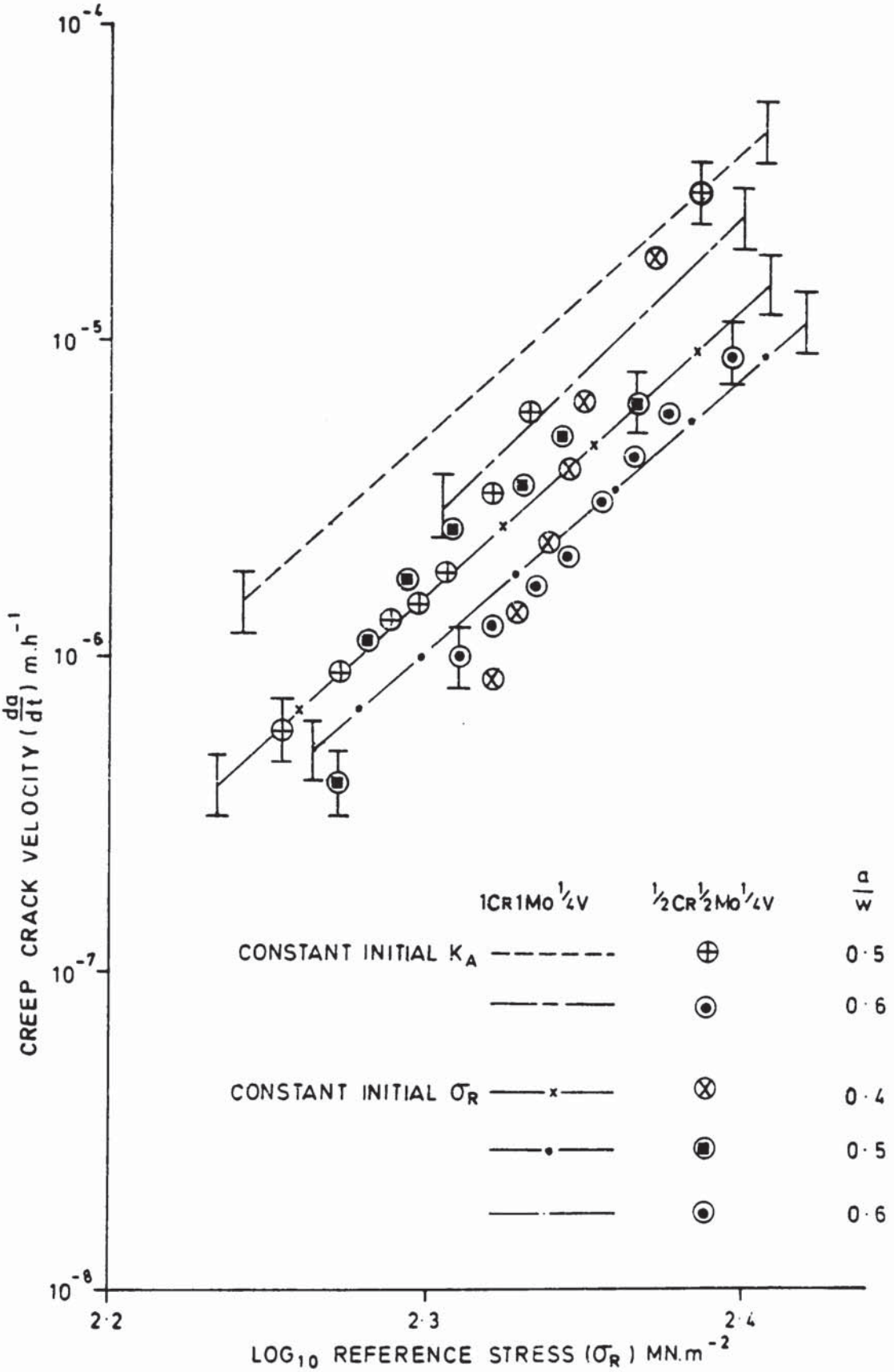

FIG. 58 COMPARISON OF CREEP CRACK VELOCITY IN THE NORMALISED AND TEMPERED 1CR 1MO ¼V AND ½CR ½MO ¼V STEELS.

correlation exists between those tests that started with identical values of initial K_A. However, this apparent K_A correlation breaks down when the constant initial σ_R test results are included. Overall correlation can be improved if the crack growth data from all of the above tests is plotted against σ_R (Figure 58). The scatter in crack velocity for a given σ_R in this case, is typically x4. This amount of scatter is comparable to the magnitude of the inherent experimental errors.

Figures 57 and 58 also compare the results from equivalent tests in both alloys. They show that the creep crack growth rates in the ½Cr½Mo¼V alloy are generally slower than in the 1Cr1Mo¼V alloy. These results indicate that the low Cr alloy is relatively more creep ductile. Further evidence of this is provided by the $\frac{1}{\omega}$ and δ_i results in Figures 35 and 36. Figure 35 shows that $\frac{1}{\omega}$ is consistently lower in the ½Cr½Mo¼V alloy for all values of initial relative crack length, while Figure 36 indicates a trend towards higher δ_i values in the same alloy.

4.8 Long Term Tests

A comparison, where appropriate, of creep crack velocities in long and short term tests is shown in Figure 59. Both sets of specimens were of similar thickness and had the same initial crack length. It can be seen that the correlation between the two sets of results is very poor for either the ½Cr½Mo¼V or the 1Cr1Mo¼V normalised and tempered material. No improvement in correlation occurs if K_A is replaced by σ_R. In contrast, the quenched and tempered material gave a good correlation.

The values of $\frac{1}{\omega}$ and δ_i from the above tests are shown in Table 6. The results indicate that the long term low load tests are less creep ductile than the corresponding short term high load tests.

Table 6.

$\frac{1}{\omega}$ and δ_i Results from Long and Short Term Tests

Alloy	Duration	Specimen Number	δ_i x10^{-6}m	$\frac{1}{\omega}$
1Cr1Mo¼V N & T	Long Term	25	22	56
	Short Term	33	70	42
		35	42.5	48
		75	47	48
1Cr1Mo¼V Q & T	Long Term	26	22	70
	Short Term	80	30	70
½Cr½Mo¼V N & T	Long Term	27	26	48
	Short Term	83	58	23

Confirmation of the above relationship between crack tip creep ductility and applied load is provided by Figures 60 and 61. These figures include the ductility results from Table 6 plus data from several other 25mm thick normalised and tempered 1Cr1Mo¼V compact tension tests. Both figures indicate a marked reduction in δ_i and increase in $\frac{1}{\omega}$ with decreasing initial applied K_A. These results are consistent with the load effect shown in Figures 55 & 56. This phenomenon is similar to the known relationship between applied load and strain to failure in smooth bar creep rupture tests.

4.9 Correlation of Creep Crack Velocity using K_A and σ_R

Previous sections have shown that in specific cases, a correlation of creep crack velocity can be achieved in cast ½Cr½Mo¼V and 1Cr1Mo¼V alloys using either K_A or σ_R. This is not true in the general case (Figures 62 and 63). In these figures the creep crack velocities from all of the 25mm thick C.T. specimens manufactured from the normalised and tempered 1Cr1Mo¼V material have been plotted against K_A and σ_R. The resultant scatter of data is much greater than can be accounted for by the inherent experimental errors.

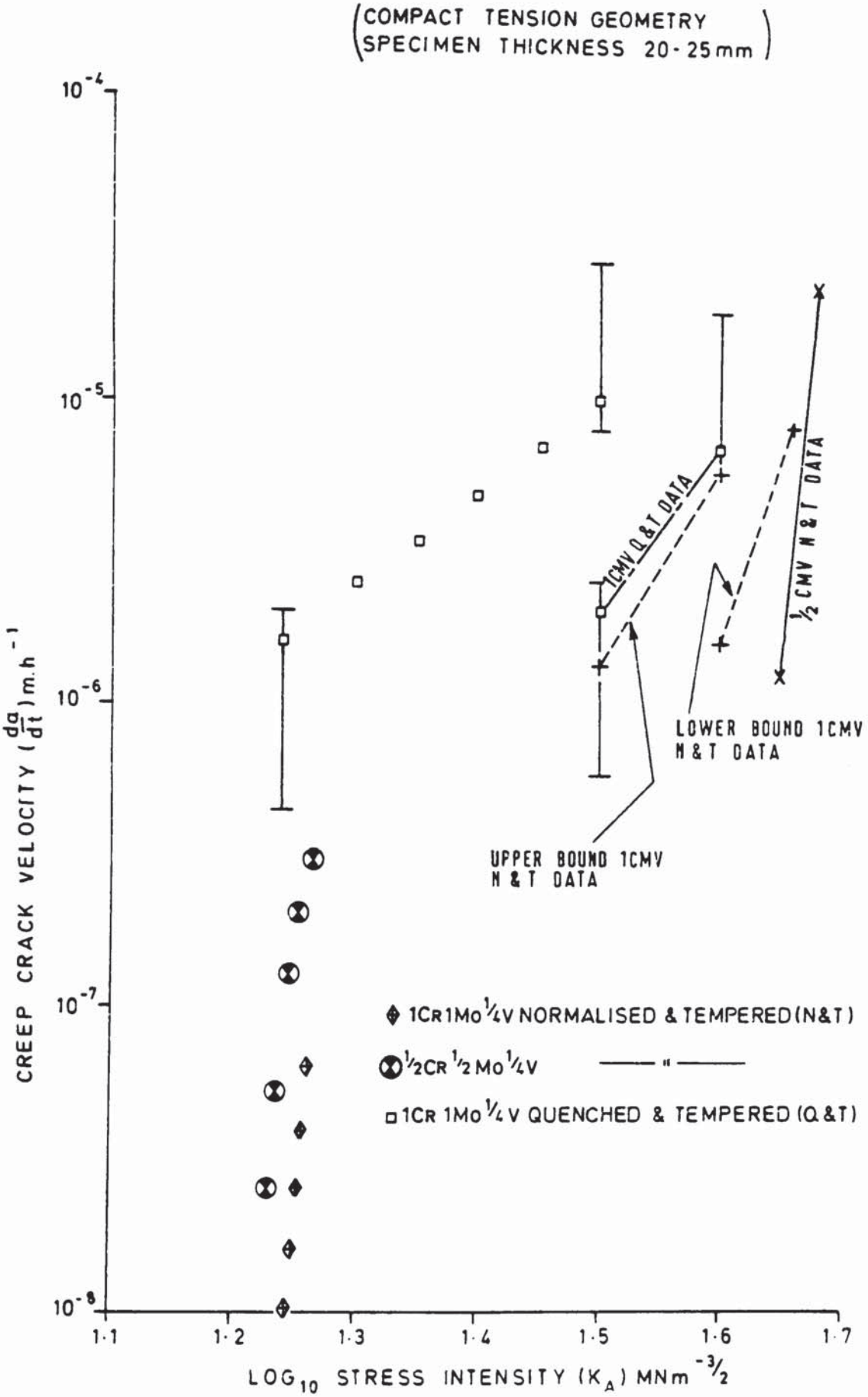

FIG. 59 COMPARISON OF LONG AND SHORT TERM TEST CREEP CRACK VELOCITY

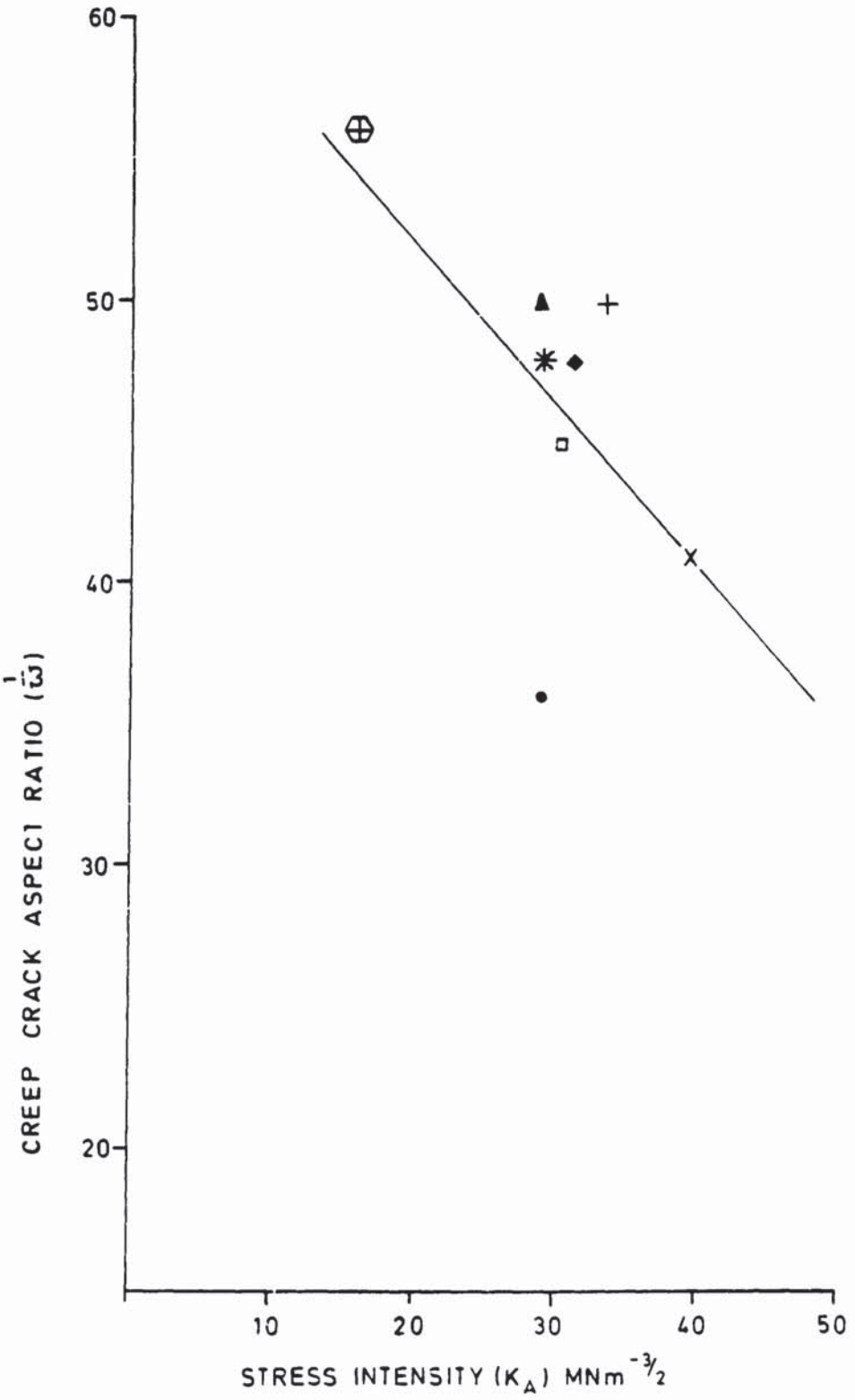

FIG. 60 VARIATION OF CREEP CRACK ASPECT RATIO WITH INITIAL STRESS INTENSITY

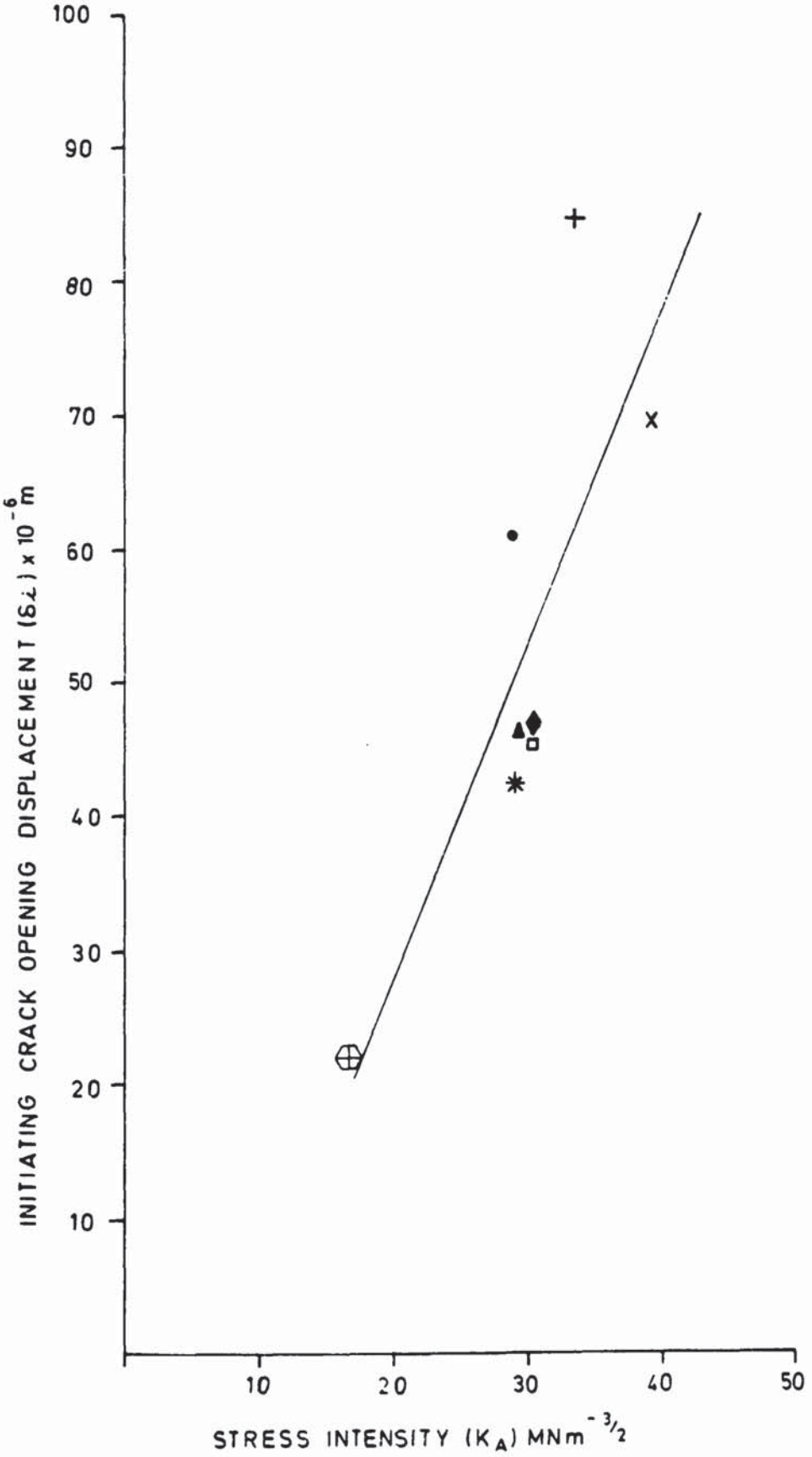

FIG. 61 VARIATION OF INITIATING CRACK OPENING DISPLACEMENT WITH INITIAL STRESS INTENSITY

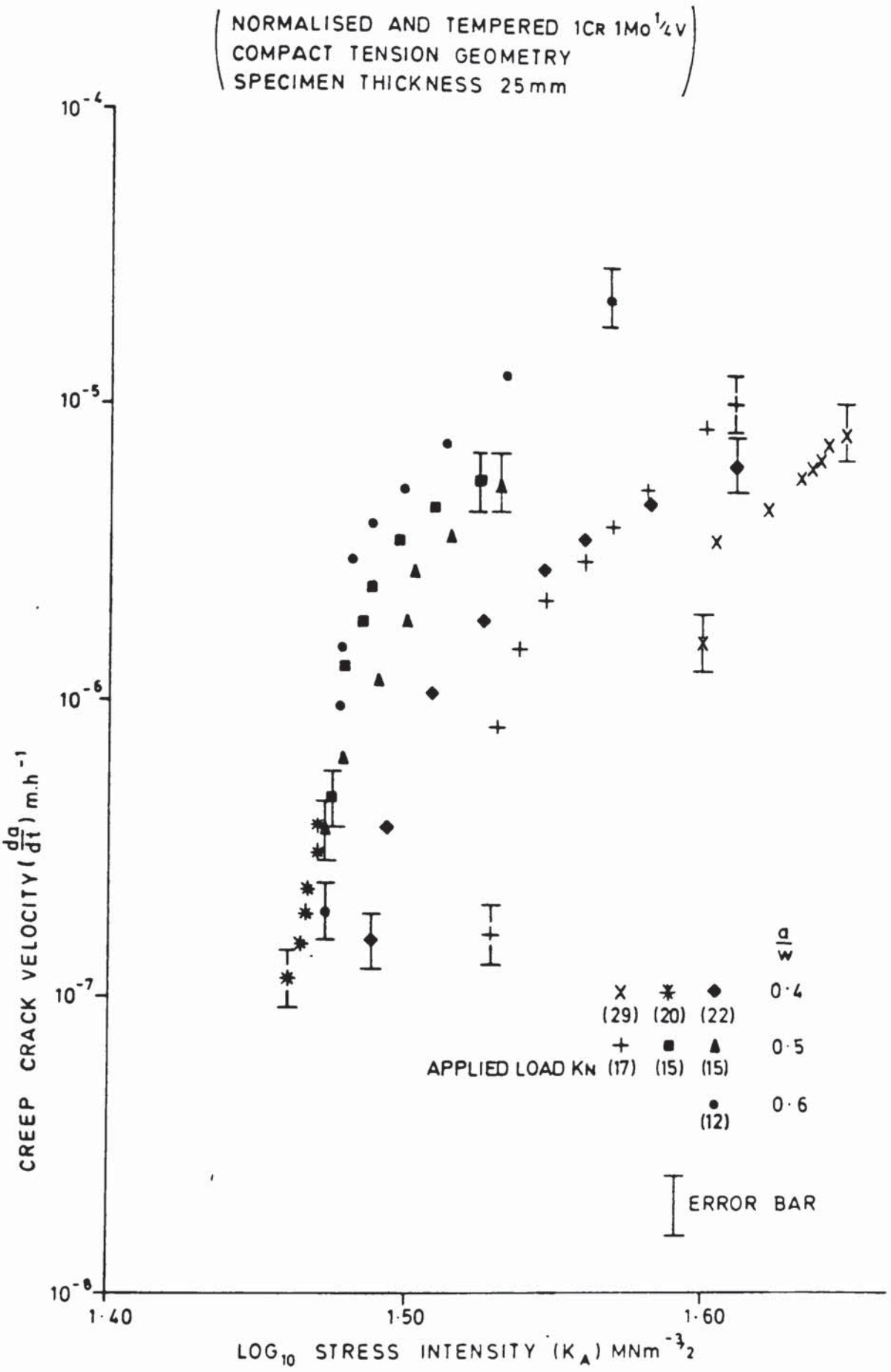

FIG. 62 VARIATION OF CREEP CRACK VELOCITY WITH STRESS INTENSITY

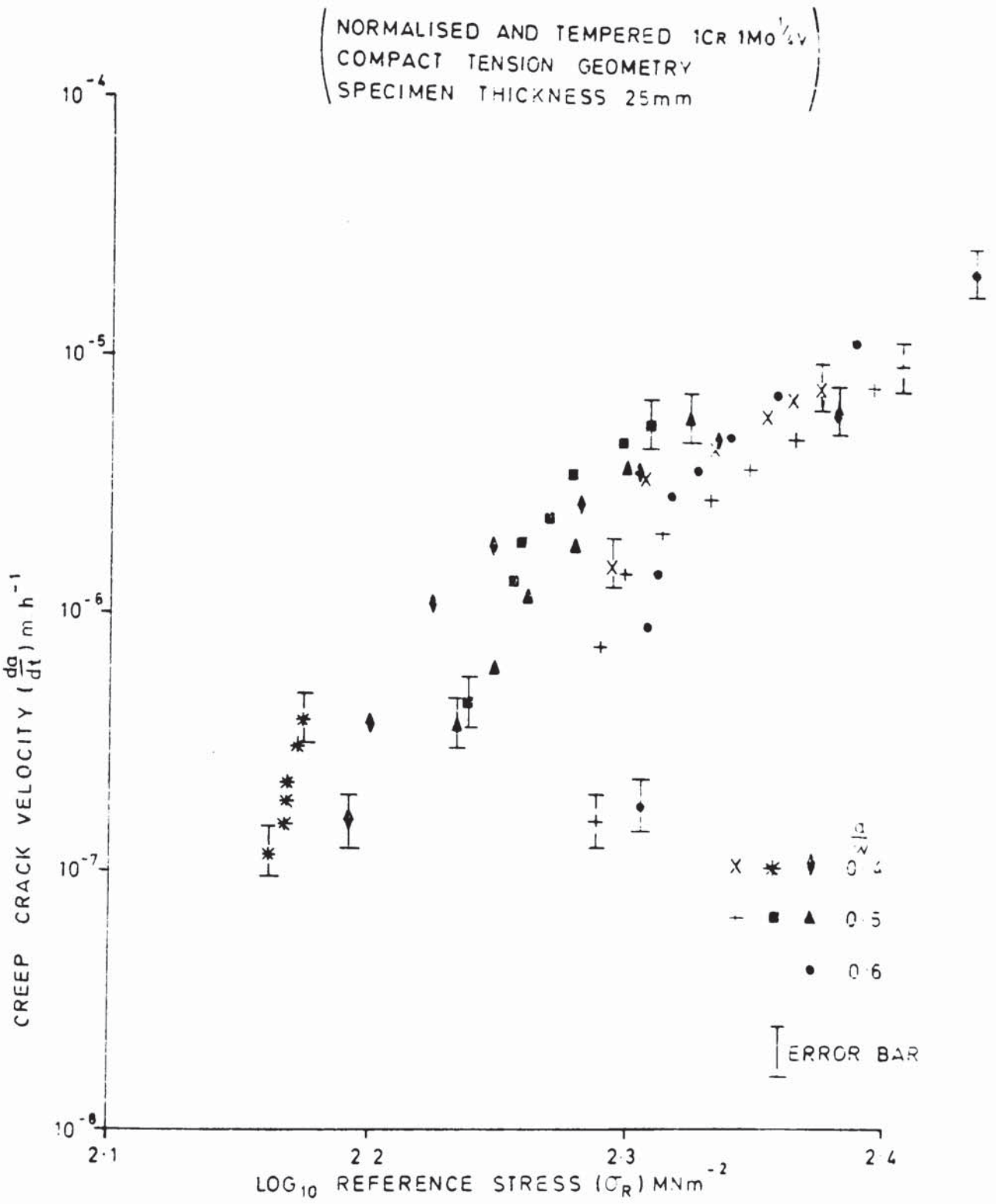

FIG. 53 VARIATION OF CREEP CRACK VELOCITY WITH REFERENCE STRESS

4.10 Creep Crack Initiation Time

Creep crack initiation time was defined as the time for the potential Va to rise 15.03μV above the base potential Vo. This figure was based on a marginal increase in potential above the maximum expected variation in signal due to experimental errors (Section 3.6). Initiation times were used to correct for oxide bridging between crack faces (Section 4.1) and to calculate equivalent crack tip fracture strains (Chapter 5). The initiation time (t_i) for C.T. tests at constant initial K_A and C.C.P. tests at constant initial σ_R or K_A (see Table 4), are shown in Table 7.

Table 7. Creep Crack Initiation Times

Material	Specimen No.	Geometry	t_i (hours)
1Cr1Mo¼V	34	C.T.	550
	35		450
N & T	71		650
	75		600
	54, 58	C.T.	530, 455
	53, 57		510, 520
	55, 59		480, 530
	73, 74		450, 550
	86	C.C.P.	450
	88		550
	89		450
	90		450
1Cr1Mo¼V	63, 72	C.T.	80, 90
	56, 64		100, 75
Q & T	65, 70		125, 110
	80		100
	76	C.C.P.	70
	67		150
	81		115
	85		125
½Cr½Mo¼V	82	C.T.	450
N & T	84		500

It can be seen that the initiation times for the normalised and tempered, and quenched and tempered materials were approximately 500 and 100 hours respectively. Also, these times were not affected significantly by either a change in specimen geometry or initial relative crack length.

4.11 Microstructural Creep Damage

4.11.1 Normalised and Tempered ½Cr½Mo¼V and 1Cr1Mo¼V

Creep cracking in these materials was intergranular and occurred along the ferrite grain boundaries (Figures 64A and 64B). Macrocracks formed by the nucleation and subsequent linkage of 'r' type cavities (Figures 65A and 65B). A few 'w' type cavities were also observed (Figure 65A). The latter could have formed either by the classical methods or by the linking of 'r' type cavities. No conclusive evidence was found to support either method. Creep damage extended typically to a distance of 0.3mm ahead of the main crack tip (Figure 66) in tests where crack tip constraint was maintained throughout the test. Extensive creep damage (several millimetres) was only observed in tests where plastic collapse was imminent.

4.11.2 Quenched and Tempered 1Cr1Mo¼V

Creep damage in this material extended typically to a distance of 0.04mm ahead of the main crack tip and was located predominently on the ferrite grain boundaries (Figure 67). Cavitation was also observed on either the bainite/ferrite or bainite/bainite boundaries (Figures 68A and 68B). A detailed examination of the microdamage ahead of the main crack tip revealed that the macroscopic crack advanced by the nucleation and growth of 'r' type cavities (Figure 68A). These cavities join together to form microcracks (Figure 68B) which in turn, link-up to produce a macrocrack (Figure 68C).

4.12 Summary of Observations

4.12.1 Creep crack tunnelling was observed in all tests. As a consequence, all crack velocities as calculated from the potential drop calibration curves were average values.

4.12.2 Under nominally identical testing conditions, creep crack initiation times in the quenched and tempered material were shorter than in the normalised and tempered material.

4.12.3 Hardness measurements of creep specimens before and after testing indicated that the change in microstructure was not appreciable for the normalised and tempered, and quenched and tempered materials.

4.12.4 A double log plot of creep crack velocity and K_A or σ_R for the materials under investigation was not a straight line. A better description was provided either by a curve whose tangential gradient decreased as the creep crack developed or alternatively, by two straight lines.

4.12.5 The development of creep cracks appeared to fall into two distinct stages. In Stage I, immediately after crack initiation, crack velocity was low but acceleration high. In Stage II, the crack velocity continued to increase whilst acceleration decreased.

4.12.6 In specific cases, either K_A or σ_R provided a satisfactory correlation of creep crack velocity in both alloys and specimen geometries. However, in the general case where relative crack lengths or applied loads were varied, neither stress function correlated the velocity data.

4.12.7 Creep crack ductility at constant initial K_A or σ_R and thickness, as measured by $\frac{1}{\omega}$ or δ_i, was invariant with relative crack length in all the materials and specimen geometries investigated.

4.12.8 Creep crack ductility at constant initial K_A or σ_R, as measured by $\frac{1}{\omega}$ or δ_i, decreased with increasing specimen thickness. The variation of creep crack velocity with specimen thickness was less conclusive.

4.12.9 The creep crack ductility in C.T. and C.C.P. specimens with identical thickness was comparable.

4.12.10 The creep crack ductility of the normalised and tempered ¼Cr½Mo¼V material was higher than the 1Cr1Mo¼V material.

4.12.11 Creep crack ductility in specimens with constant thickness and initial relative crack length was directly proportional to the applied load.

4.12.12 Creep cracking in both alloys was intergranular and occurred primarily along the ferrite grain boundaries. Macrocracks formed by the nucleation and linkage of'r' type cavities.

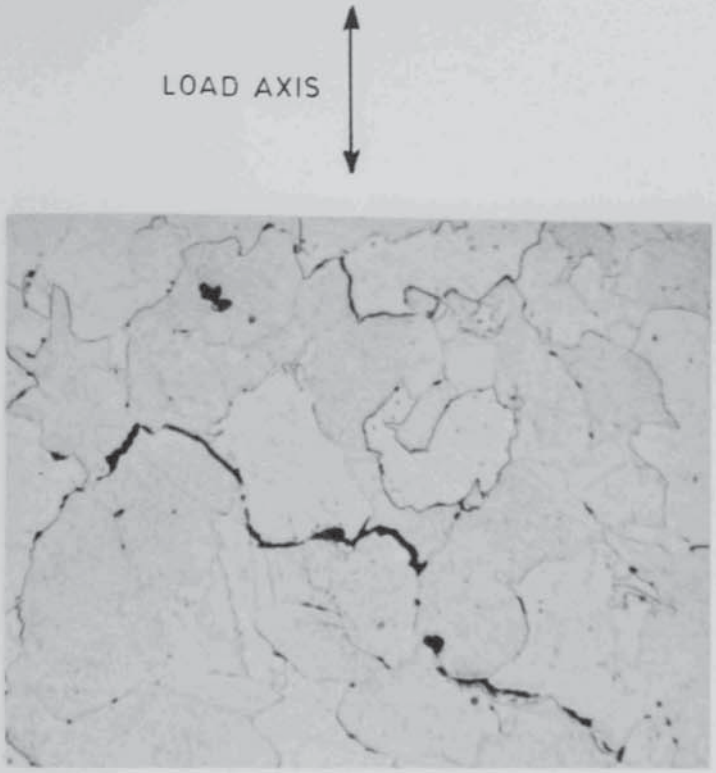

x400

FIG. 64A CREEP CRACKING IN NORMALISED AND TEMPERED ½ CR ½ MO ¼ V

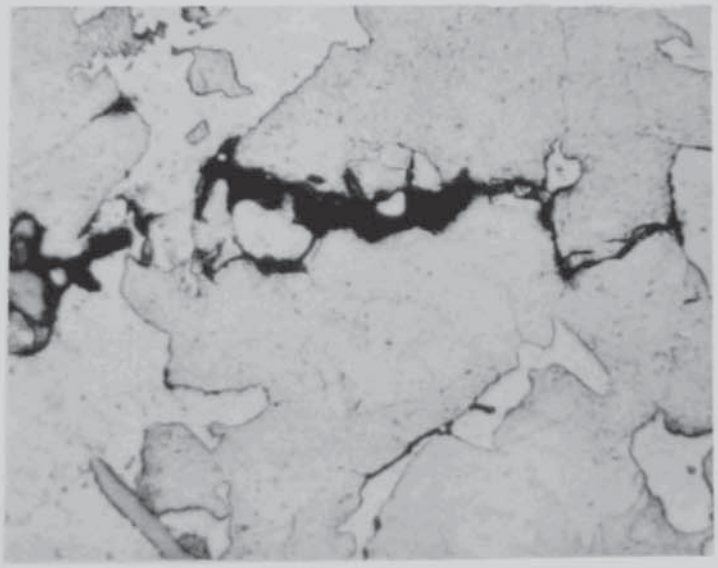

x400

FIG. 64B CREEP CRACKING IN NORMALISED AND TEMPERED 1CR 1MO ¼ V

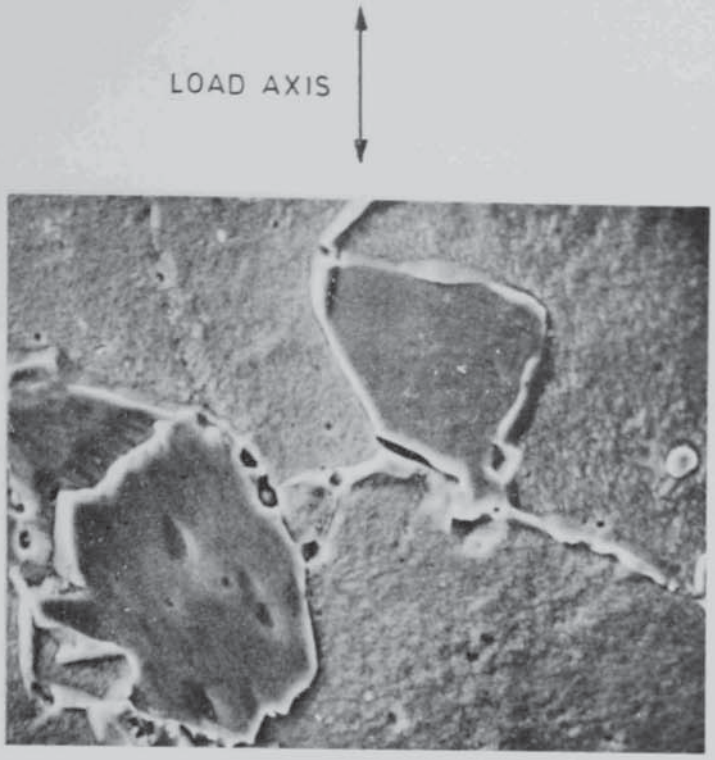

x1000

FIG. 65A

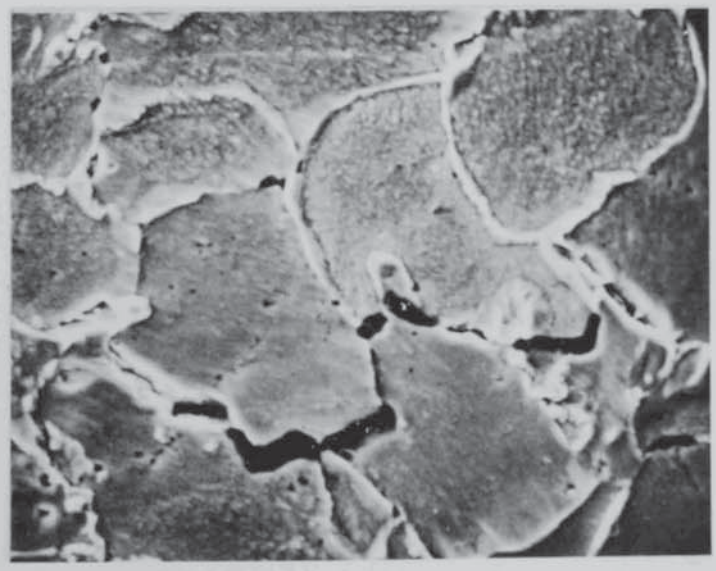

x1000

FIG. 65B

CREEP CAVITATION AHEAD OF MAIN CRACK TIP IN NORMALISED AND TEMPERED 1Cr 1Mo $\frac{1}{4}$V

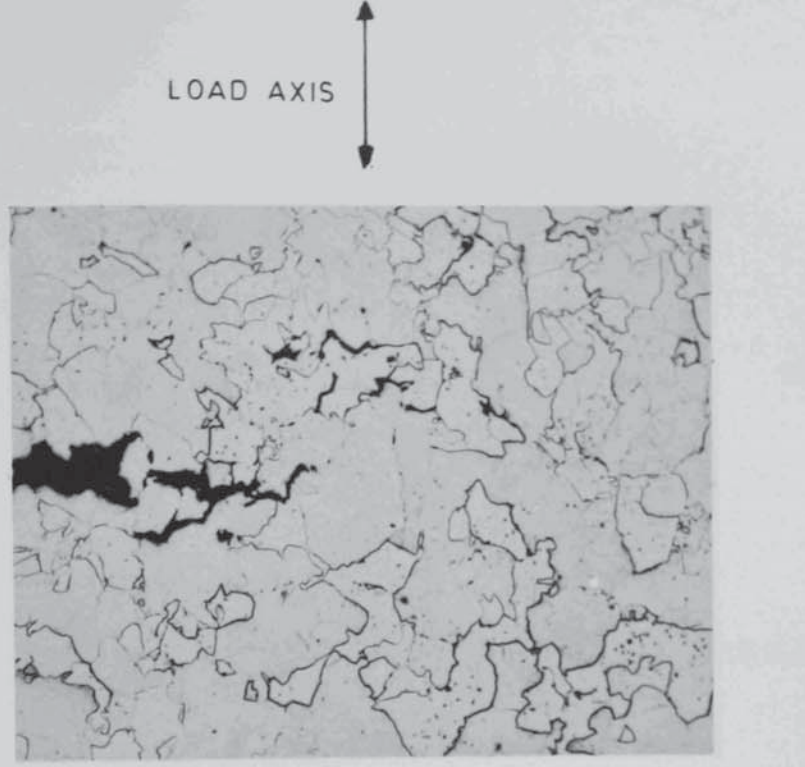

x 150

FIG. 66 CREEP CRACKING AHEAD OF MAIN CRACK TIP IN NORMALISED AND TEMPERED 1CR 1MO 1/4V

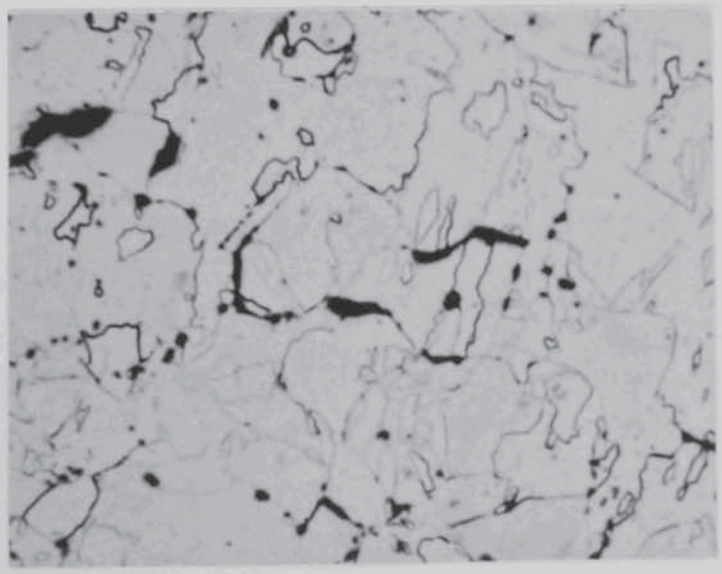

x 400

FIG. 67 CREEP CRACKING IN QUENCHED & TEMPERED 1CR 1MO 1/4V

FIG 68A

+0·04mm

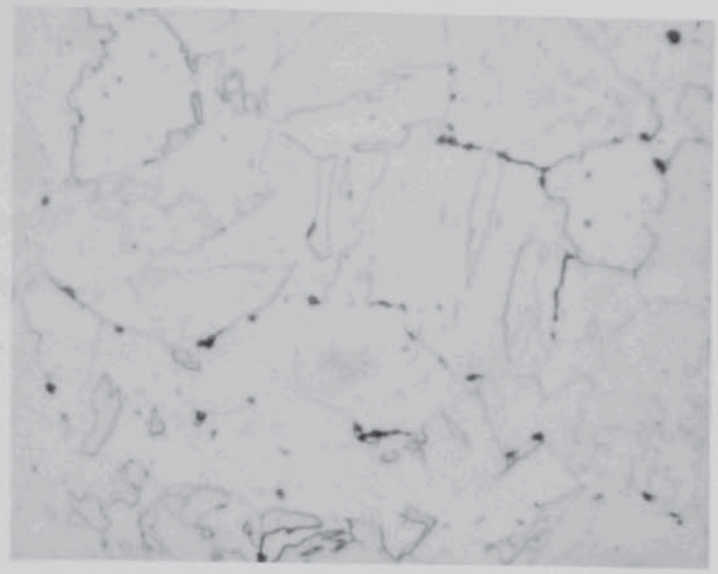

x700

LOAD AXIS

FIG. 68B

+0·02mm

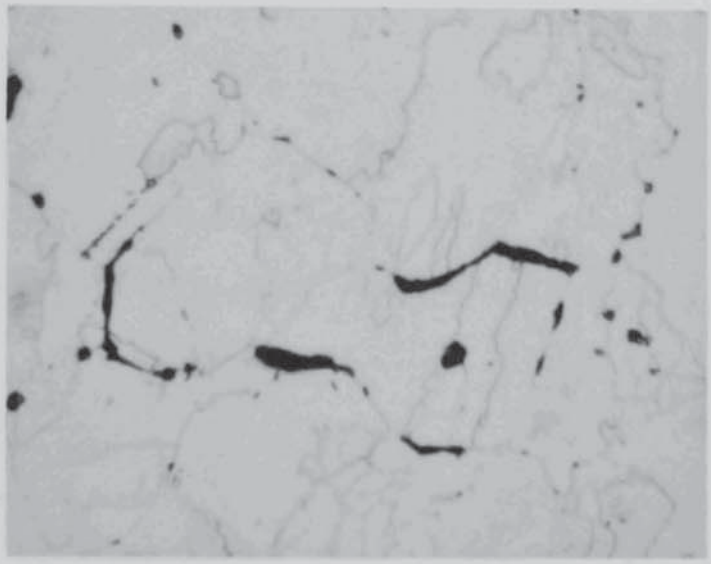

x700

FIG. 68C

MAIN CRACK

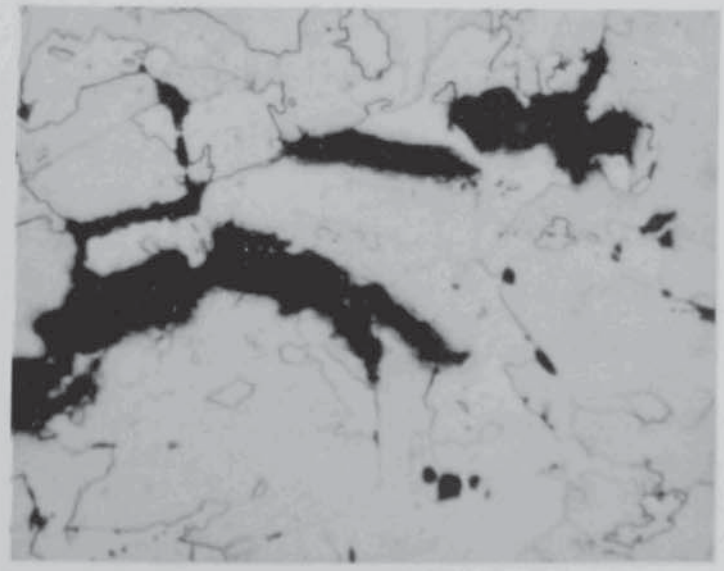

x700

CREEP CAVITATION AHEAD OF MAIN CRACK TIP IN QUENCHED AND TEMPERED 1CR 1MO 1/4V

Finite Element Stress Analysis

For an accurate analysis of creep stress relaxation and redistribution, it is necessary to follow the changes in stress and strain occuring in a test piece during the non-linear process. This has been accomplished by using a computer programme developed at the Berkeley Nuclear Laboratories of the Central Electricity Generating Board and known as BERSAFE. The BERSAFE finite element system has been used extensively in the study of bulk creep problems (Heaton, 1978) and localised creep events in cracked structures (Goodall and Chubb, 1974). In this Thesis, BERSAFE has been used to study creep stress relaxation and redistribution ahead of incubating creep cracks in structures undergoing plane stress and plane strain deformation. The results have then been developed by taking account of experimental observations to produce a model of macroscopic creep crack growth in cast CrMoV steels (Chapter 6).

5.1 Basic Theory

The assumptions made in the creep analysis are as follows.

5.1.1 The creep strain rate is a function of the stress deviator.

This has been observed for example, by Ratcliffe and Greenwood (1964) in magnesium laboratory specimens, and by Taira and Ohtani (1971) in 2¼ Cr 1Mo steel tubes.

5.1.2 Isotropic material.

5.1.3 Creep occurs at a constant volume.

This is a good approximation because the volume fraction of cavities at fracture is below 1% in materials where the elongation to fracture is less than 20% (McLean, Dyson and Taplin, 1977). Both cast CrMoV alloys have an elongation to fracture of this order.

5.1.4 Existence of a flow law.

The relationship between stress and the rate of creep deformation is based on classical theory of plastic flow.

5.1.5 Material properties are time independent.

Experimental work has shown that the creep properties of the two cast CrMoV alloys did not change significantly over periods of up to 20,000 hours (Section 4.3). This period is in excess of the simulated creep times considered in the numerical analysis.

In the general case, the increment in creep strain rate $\Delta \dot{\epsilon}_{ij}^{c}$ can be related to the deviatoric stress S_{ij} by

$$\Delta \dot{\epsilon}_{ij}^{c} = \Delta \lambda \, S_{ij} \tag{53}$$

where $\Delta\lambda$ is a proportionality factor so written to indicate that incremental creep rates are being related to finite stresses. From the Prandtl-Reuss Equation (Prandtl 1924; Reuss 1930)

$$\Delta\lambda = \frac{\Delta \dot{\epsilon}_{11}^{c}}{S_{11}} = \frac{\Delta \dot{\epsilon}_{22}^{c}}{S_{22}} = \frac{\Delta \dot{\epsilon}_{33}^{c}}{S_{33}} = \frac{\Delta \dot{\epsilon}_{12}^{c}}{\sigma_{12}} = \frac{\Delta \dot{\epsilon}_{23}^{c}}{\sigma_{23}} = \frac{\Delta \dot{\epsilon}_{13}^{c}}{\sigma_{13}} \tag{54}$$

where $S_{11} = \left(\sigma_{11} - \sigma_{H}\right)$ σ_{H} being the hydrostatic stress. $= \dfrac{\sigma_{11} + \sigma_{22} + \sigma_{33}}{3}$

Similar expressions exist for S_{22} and S_{33}. The stress components refer to Cartesian coordinates.

The amounts by which the creep rates are changing are controlled by the requirements of constant volume, thus;

$$\Delta \dot{\epsilon}_{11}^{c} + \Delta \dot{\epsilon}_{22}^{c} + \Delta \dot{\epsilon}_{33}^{c} = 0 \tag{55}$$

and by equilibrium, the flow criterion and the boundary conditions.

Combining equations 53, 54 and 55 results in

$$\Delta \dot{\epsilon}_{ij}^{c} = \frac{3}{2} \frac{\bar{\epsilon}^{c}}{\bar{\sigma}} S_{ij} \tag{56}$$

Equation 56 consists of three equations of the type:

$$\Delta \dot{\epsilon}_{11}^{c} = \frac{\Delta \bar{\epsilon}^{c}}{2\bar{\sigma}} \left[2\sigma_{11} - \sigma_{22} - \sigma_{33} \right] \tag{57}$$

and three of the type:

$$\Delta \dot{\epsilon}^{c}_{12} = \frac{3}{2} \frac{\Delta \bar{\epsilon}^{c}}{\bar{\sigma}} \sigma_{12} \tag{58}$$

$\bar{\sigma}$ is the equivalent stress and $\bar{\epsilon}^{c}$ is the equivalent creep strain. In a body undergoing plane stress deformation, the system stresses at all positions remote from traction free surfaces include:

$$\sigma_{11},\ \sigma_{22},\ \sigma_{12} \neq 0$$
$$\text{while} \quad \sigma_{33},\ \sigma_{13},\ \sigma_{23} = 0$$

In general, the equivalent stress is of the form:

$$\bar{\sigma}^2 = \frac{1}{2}\left[\left(\sigma_{11} - \sigma_{22}\right)^2 + \left(\sigma_{22} - \sigma_{33}\right)^2 + \left(\sigma_{33} - \sigma_{11}\right)^2 + 6\left(\sigma_{12}^2 + \sigma_{23}^2 + \sigma_{31}^2\right)\right]$$

If σ_{11}, σ_{22} and σ_{33} are principal stresses, then in plane stress this equation reduces to

$$\bar{\sigma}^2 = \frac{1}{2}\left[\left(\sigma_{11} - \sigma_{22}\right)^2 + \sigma_{22}^2 + \sigma_{11}^2\right] \tag{59}$$

For plane strain deformation:

$$\sigma_{11},\ \sigma_{22},\ \sigma_{33},\ \sigma_{12} \neq 0$$
$$\sigma_{13},\ \sigma_{23} = 0$$

Thus, in terms of principal stresses:

$$\bar{\sigma}^2 = \frac{1}{2}\left[\left(\sigma_{11} - \sigma_{22}\right)^2 + \left(\sigma_{22} - \sigma_{33}\right)^2 + \left(\sigma_{33} - \sigma_{11}\right)^2\right] \tag{60}$$

Equations 59 and 60 respectively define the equivalent stress in the near tip region in a body undergoing plane stress and plane strain deformation. It is these equivalent stresses which are plotted in the results section of this chapter, and incorporated into a model of creep fracture (Chapter 6).

The associated system creep strains along the principal axes for plane stress deformation are

$$\epsilon^{c}_{11},\ \epsilon^{c}_{22},\ \epsilon^{c}_{33} \neq 0$$

while for plane strain deformation

$$\epsilon^{c}_{11},\ \epsilon^{c}_{22} \neq 0$$
$$\epsilon^{T}_{33} = \left(\epsilon^{\text{elastic}} + \epsilon^{\text{creep}}\right)_{33} = 0$$

Thus, the equivalent creep strain which in general is of the form

$$\bar{\varepsilon}^{c\,2} = \left\{ \frac{2}{9} \left[\left(\varepsilon^c_{11} - \varepsilon^c_{22} \right)^2 + \left(\varepsilon^c_{22} - \varepsilon^c_{33} \right)^2 + \left(\varepsilon^c_{33} - \varepsilon^c_{11} \right)^2 \right] + \frac{1}{3} \left[\varepsilon^{c\,2}_{12} + \varepsilon^{c\,2}_{23} + \varepsilon^{c\,2}_{31} \right] \right\} \tag{61}$$

reduces to

$$\bar{\varepsilon}^{c\,2} = \left\{ \frac{2}{9} \left[\left(\epsilon^c_{11} - \epsilon^c_{22} \right)^2 + \left(\epsilon^c_{22} - \epsilon^c_{33} \right)^2 + \left(\epsilon^c_{33} - \epsilon^c_{11} \right)^2 \right] \right\} \tag{62}$$

along the principal axes for both plane stress and plane strain deformation, the relevant ε^c_{33} being defined above.

In the creep analysis, it is assumed that an increment of creep strain rate can be calculated from a time hardening creep law of the form

$$\Delta \bar{\varepsilon}^c = f\left(\sigma, t, \theta \right) \tag{63}$$

t being time and θ temperature.

As both equivalent stress and equivalent strain reduce to the axial normal component of stress and strain in a tensile creep test, Equation 63 can be derived from uniaxial creep data. In this case:

$$\bar{\sigma} = \sigma_{11}$$
$$\bar{\varepsilon}^c = \varepsilon^c_{11}$$

Thus, substituting in Equation 56, Equation 63

$$\Delta \dot{\varepsilon}^c_{ij} = \frac{3}{2} \frac{f^{I}_{\bar{\sigma}} \cdot f^{II}_{t} \cdot f^{III}_{\theta}}{\bar{\sigma}} \quad S_{ij} \tag{64}$$

which again gives three equations of the type

$$\Delta \dot{\varepsilon}^c_{11} = \frac{f^{I}_{\bar{\sigma}} \cdot f^{II}_{t} \cdot f^{III}_{\theta}}{2\bar{\sigma}} \left[2\sigma_{11} - \sigma_{22} - \sigma_{33} \right] \tag{65}$$

and three of the type

$$\Delta \dot{\varepsilon}^c_{12} = \frac{3}{2} \frac{f^{I}_{\bar{\sigma}} \cdot f^{II}_{t} \cdot f^{III}_{\theta}}{\bar{\sigma}} \quad \sigma_{12} \tag{66}$$

Equation 64 is used in the numerical analysis to calculate the increments of creep strain in a multiaxial stress system ahead of an incubating creep crack. This equation effectively says that at any point and moment, the creep rate increments in all directions are of such magnitude that their ratios are equal to the ratios of their corresponding deviatoric stresses.

5.2 Numerical Solution Technique

At any point in the non-linear process, the total strain vector $\{\varepsilon^T\}$ equals the elastic strain vector $\{\varepsilon^e\}$ plus the creep strain vector $\{\varepsilon^c\}$. Thermal and plastic strains are considered to be small. Thus, in incremental form:

$$\Delta\{\varepsilon^T\} = \Delta\{\varepsilon^e\} + \Delta\{\varepsilon^c\} \tag{67}$$

The total strain vector at any point in a finite element mesh is related to nodal displacements $\{\delta\}$ by:

$$\{\varepsilon^T\} = [B]\ \{\delta\} \tag{68}$$

Along the principal planes, strains are defined in terms of the displacements at each nodal point in the finite element mesh by:

$$\{\varepsilon\} = \begin{Bmatrix} \varepsilon_x \\ \varepsilon_y \\ \varepsilon_z \end{Bmatrix} = \begin{Bmatrix} \frac{\partial u}{\partial x} \\ \\ \frac{\partial v}{\partial y} \\ \\ \frac{\partial w}{\partial z} \end{Bmatrix}$$

As
$$\Delta\{\sigma\} = [D]\ \Delta\{\varepsilon^e\} \tag{69}$$

then by combining equations 67, 68 and 69 it can be shown that

$$\Delta\{\sigma\} = [D]\ [B]\ \Delta[\delta] - [D]\ \Delta\{\varepsilon^c\} \tag{70}$$

where $[D]$ is a vector relating stress and strain, and $[B]$ is a vector relating strain and displacement.

Using the principle of virtual work, it is possible to equate the applied loading with the element stresses (Lewis and Hellen, 1973) to give the equilibrium equation

$$\int_V [B]^T\ \Delta\{\sigma\}\ dV = \Delta\{R\} \tag{71}$$

where $\{R\}$ is a vector of structure nodal force.

Thus by substituting Equation 70 for $\Delta\{\sigma\}$ in Equation 71, the equilibrium equation becomes

$$\left[K^{o}\right] \Delta\{\delta\} = \Delta\{R\} + \int_{V} \left[B^{T}\right]\left[D\right] \Delta\{\varepsilon^{c}\} \, dV \qquad (72)$$

where $\left[K^{o}\right]$ is the initial elastic stiffness matrix.

A typical BERSAFE algorithm is as follows.

5.2.1 At time t = 0, the system stresses are calculated from the instantaneous constitutive relations between displacement, strain and stress, account being taken of boundary conditions, compatability and equilibrium between neighbouring elements. Knowing the system stresses, $\bar{\sigma}$ can be calculated (Equations 59 and 60)

5.2.2 For each element in the structure the creep strain increments are calculated from Equation 64. These are then substituted into the integral of Equation 72 to accumulate the creep strain vector $\{\varepsilon^{c}\}$. This equation is then solved to find a new set of displacements, which in turn gives a new strain vector. The new stress distribution is then calculated from this strain vector (Equations 67 to 70).

5.2.3 A new value of $\bar{\sigma}$ is calculated from the new system stresses. Stage 5.2.2 is then repeated for t > 0 using small time intervals dt.

5.3 General Technique

5.3.1 Material Creep Data

Material creep data may be input using either strain/time curves for various temperatures and stresses, or mathematical relationships based on these curves. The former approach was adopted in the numerical analysis. The creep data for the ½Cr½Mo¼V and 1Cr1Mo¼V alloys was generated by using high sensitivity creep machines with a load capacity of 20KN. Creep tests were performed at 550 $\pm$ 1°C on uniaxial specimens with gauge lengths of 25mm and gauge length diameters of 6.3mm. The resultant strain/time curves are shown in Figures 69 and 70. By introducing creep data in this form into

the computer programme, intermediate stress creep curves can be calculated accurately by the method of logarithmic interpolation.

An alternative method of calculating creep strains at intermediate stresses is by the use of parametric creep equations. This technique has been incorporated in a model of creep fracture (Chapter 6). The time hardening form of these equations for the CrMoV alloys are as follows.

Normalised and Tempered $\frac{1}{2}Cr\frac{1}{2}Mo\frac{1}{4}V$ and $1Cr1Mo\frac{1}{4}V$

$$\varepsilon^c = 6{\cdot}73 \times 10^{-17} \quad \sigma^{5{\cdot}8} \quad t^{0{\cdot}5} \tag{73}$$

over the initial test stress range of 100 to 175 MNm^{-2}.

Quenched and Tempered $\frac{1}{2}Cr\frac{1}{2}Mo\frac{1}{4}V$ and $1Cr1Mo\frac{1}{4}V$

$$\varepsilon^c = 1{\cdot}10 \times 10^{-13} \quad \sigma^{3{\cdot}7} \quad t^{0{\cdot}6} \tag{74}$$

over the initial test stress range of 150 to 300 MNm^{-2}.

5.3.2 Construction of Finite Element Mesh

A finite element mesh for both the C.T. and C.C.P. geometry was generated with the assistance of a mesh generation programme (Neale; 1972). Both meshes were based on specimen dimensions as shown in Figure 14. The resultant meshes are shown in Figures 71 and 72.

5.3.3 Analytical Route

Before commencing the creep analysis, the accuracy of both finite element meshes was assessed by performing a simple fixed load linear elastic stress analysis on the C.T. and C.C.P. geometry, each one containing a crack of size $0.5\frac{a}{w}$. In both cases the value of K as calculated by the method of virtual crack extension, was in good agreement with that given by equation 47. As a consequence, both meshes were considered to be sufficiently refined and hence suitable for the creep analysis.

The creep analysis was confined to examining the effect of the mode of deformation (plane stress, plane strain) and the material creep properties, on the relaxation and redistribution of stress, and the accumulation of creep strain ahead of an incubating creep crack. At zero time, the crack

FIG. 69. CREEP CURVES FOR NORMALISED AND TEMPERED MATERIALS AT 550° C.

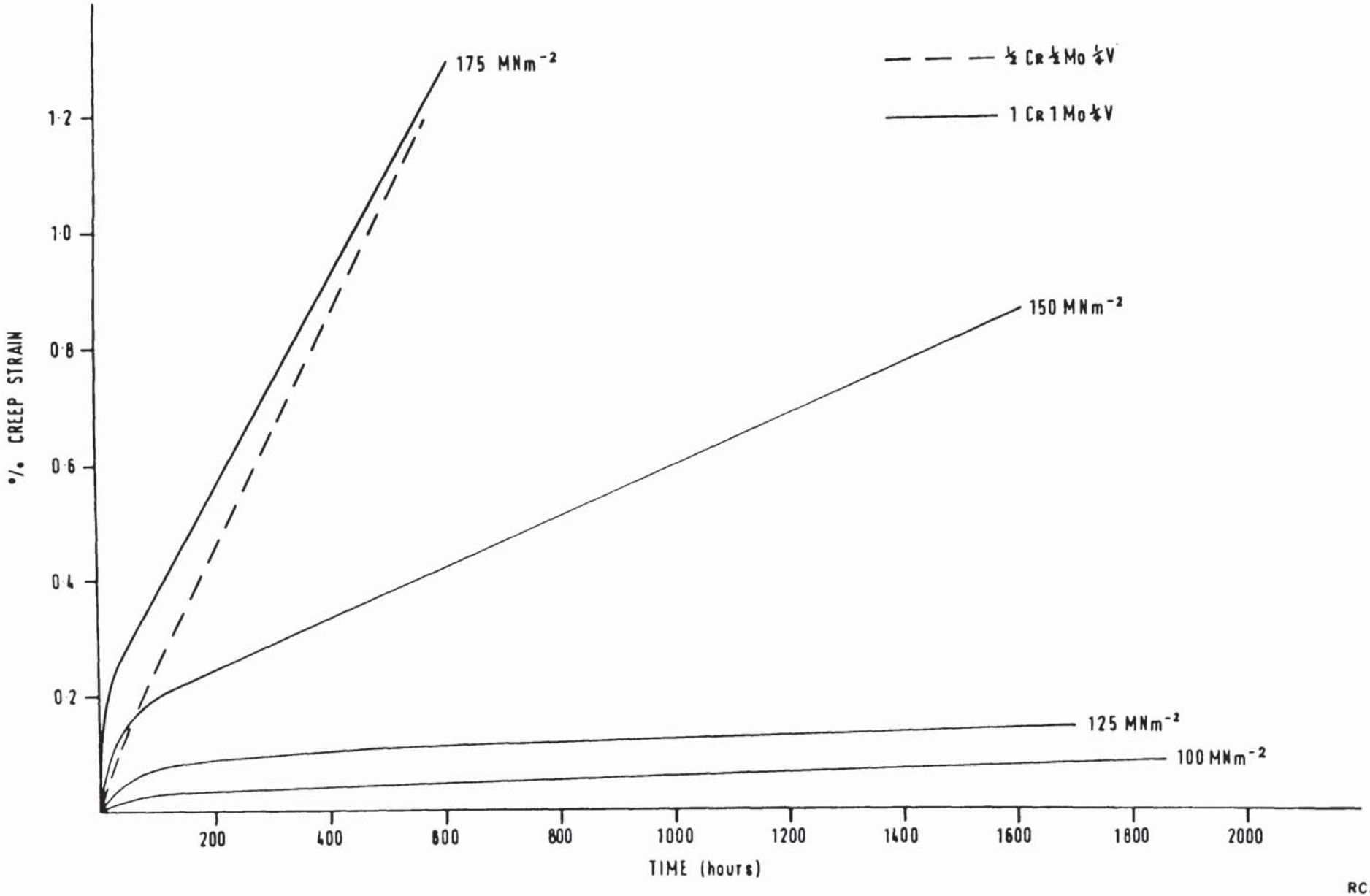

RC/SSR/A4/812

FIG. 70. CREEP CURVES FOR QUENCHED AND TEMPERED MATERIALS AT 550° C.

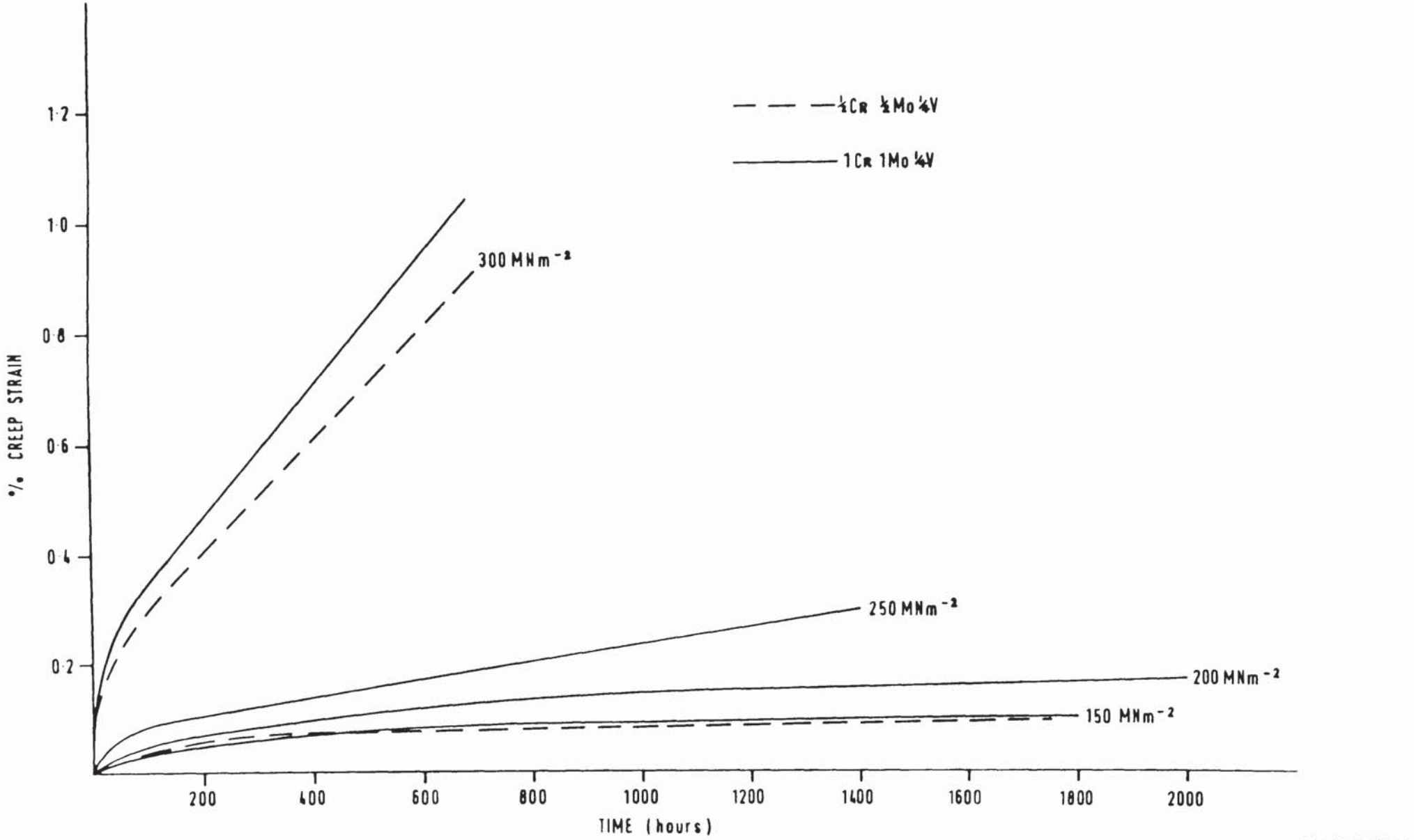

RC/SSR/A4/813

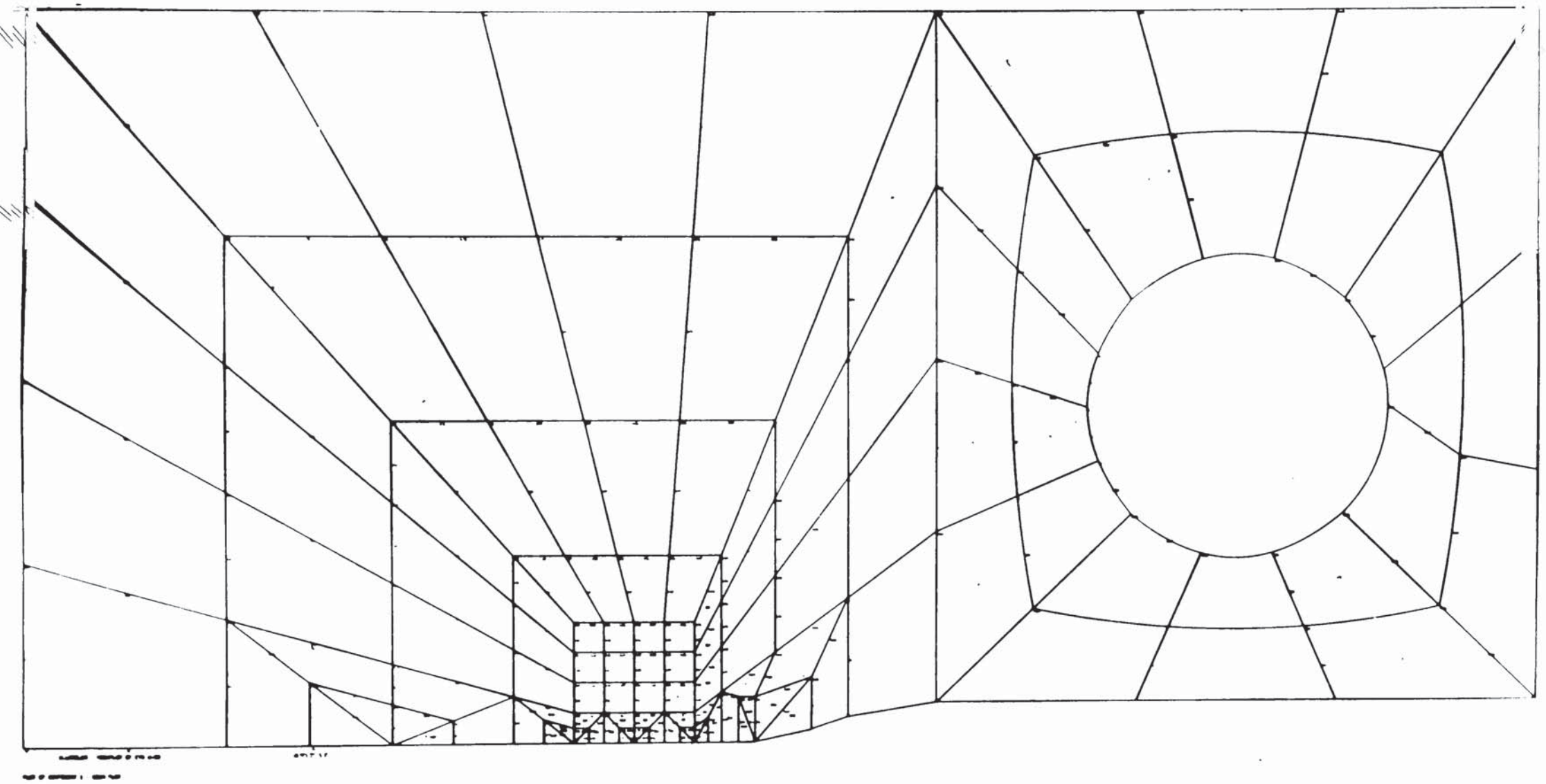

FIG. 71 C.T. FINITE ELEMENT MESH

JOB Y8SWL051.TAPE 63874S

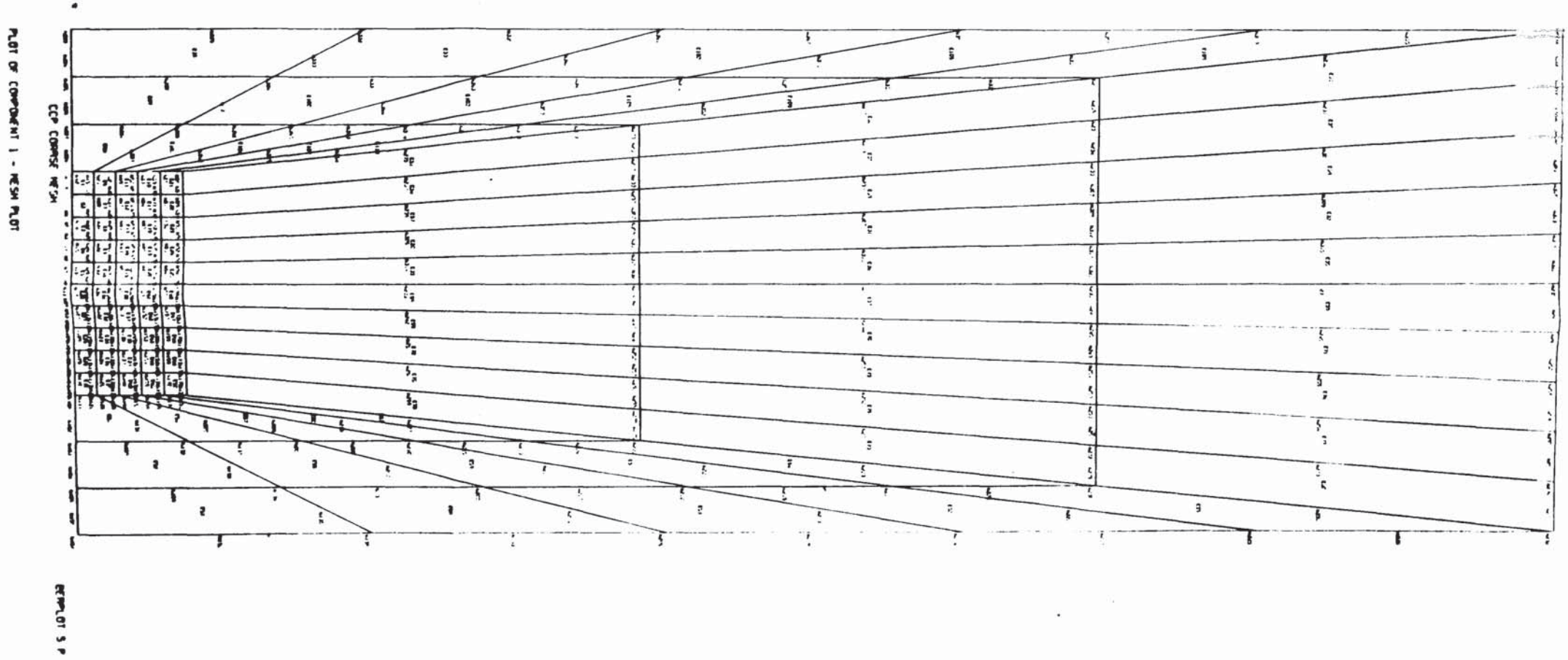

FIG. 72 C.C.P. FINITE ELEMENT MESH

FIG. 73. COMPARISON OF THEORETICAL AND EXPERIMENTAL EQUIVALENT ELASTIC STRESS DISTRIBUTION FOR PLANE STRESS DEFORMATION.

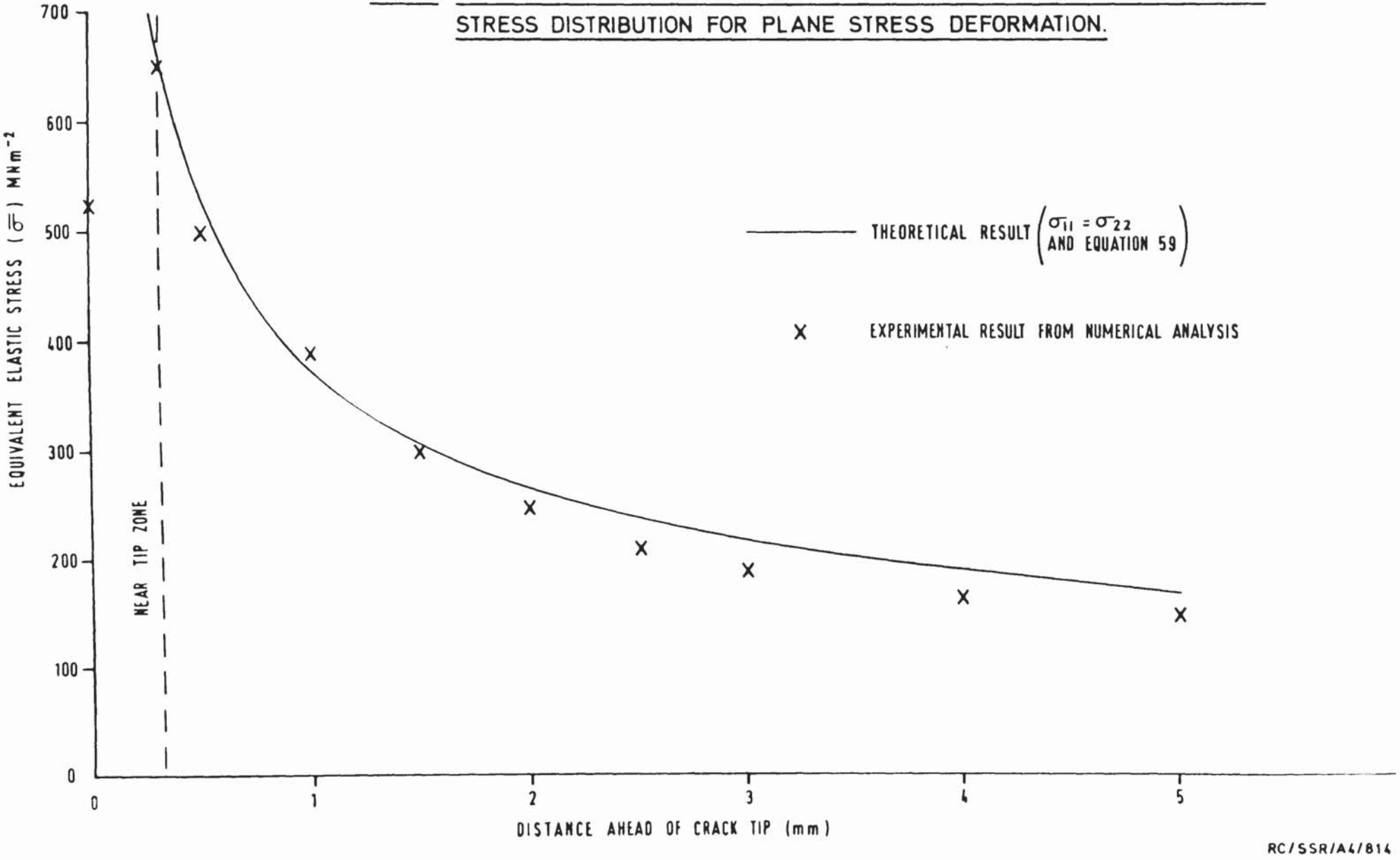

RC/SSR/A4/814

had a length of $0.5\frac{a}{w}$ and was assumed to have an infinitesimally small radius. Computation proceeded for 100 and 500 hours of simulated creep time in the quenched and tempered, and normalised and tempered materials respectively. These times corresponded with the experimentally observed creep crack incubation periods in the relevant tests.

5.4 Results

5.4.1 Accuracy of the Numerical Analysis

The numerical analysis has the ability to describe accurately the stress field ahead of a slit crack. In theory by using very refined meshes, the programme will calculate near crack tip elastic stresses which are compatible with the Westergaard Equations and in the limit, will show that σ_{11} tends towards infinity and σ_{22} is zero at the crack tip. In practice for reasons of economy, mesh refinement is optimised to achieve a good approximation to the 'true' near tip stress field (e.g. Figure 73).

5.4.2 Stress Relaxation

The relaxation of equivalent elastic stress ahead of an incubating creep crack in the C.T. geometry for the normalised and tempered, and quenched and tempered materials undergoing plane stress and plane strain deformation, is shown in Figures 74 and 75. It is clear from both figures that there is a significant amount of stress relaxation. Also, the change in the stress exponent from 5.8 for the normalised and tempered to 3.7 for the quenched and tempered material, does not affect significantly the rate of stress relaxation. The time taken to attain a steady state stress level also appears to be insensitive to the above changes in stress exponent.

The stress relaxation characteristics of the C.C.P. geometry are very similar to that predicted for the C.T. geometry. This is illustrated by Table 8 which compares the predicted steady state times for both geometries.

Table 8 Comparison of Steady State Stress Times

C.T. Geometry				C.C.P. Geometry			
N & T K_A=30		Q & T K_A=30		N & T K_A=19		Q & T K_A=30	
Plane Stress	Plane Strain	Plane Stress	Plane Strain	Plane Stress	Plane Strain	Plane Stress	Plane Strain
25h	80h	50h	150h	50h	170h	40h	140h

h - hours

K_A in units of $MNm^{-3/2}$

5.4.3 Steady State Stress Levels

At zero time, before creep deformation commences, the equivalent elastic stress distribution near the crack tip is as shown in Figures 76 and 77. Subsequent creep deformation then results in a reduction in stress level in the near tip zone and an increase in stress level in the far field. The former observation is of great significance as it suggests that the stress distribution near the crack tip cannot be described by the initial linear elastic stress intensity factor in the materials and specimen geometries under investigation. The significance of this observation and how it affects the present understanding of the mechanics of macroscopic creep fracture is discussed in Chapter 6.

5.4.4 Distribution of Equivalent Creep Strain

The distribution of equivalent creep strain ahead of a creep crack at the instant of its initiation is shown in Figures 78 and 79. All the curves possess three distinctive features. Firstly, the strain always peaks at the crack tip. Secondly, the strain gradient near the crack tip is markedly higher than that in the remainder of the section. Finally, the accumulated creep strain in the normalised and tempered material is greater than that in the quenched and tempered material. The information provided by these figures is used in the following chapter to develop a

model of macroscopic creep crack growth. In particular, they provide the model with information on the critical strain for crack initiation (critical fracture strain) and the accompanying strain profile.

FIG. 74

RELAXATION OF EQUIVALENT STRESS AT A POINT 0·3mm AHEAD OF THE CRACK TIP IN NORMALISED AND TEMPERED 1 CR 1 Mo ¼ V, AT 550°C.

(K_A 30MNm$^{-3/2}$, 0·5 $\frac{a}{w}$, COMPACT TENSION GEOMETRY)

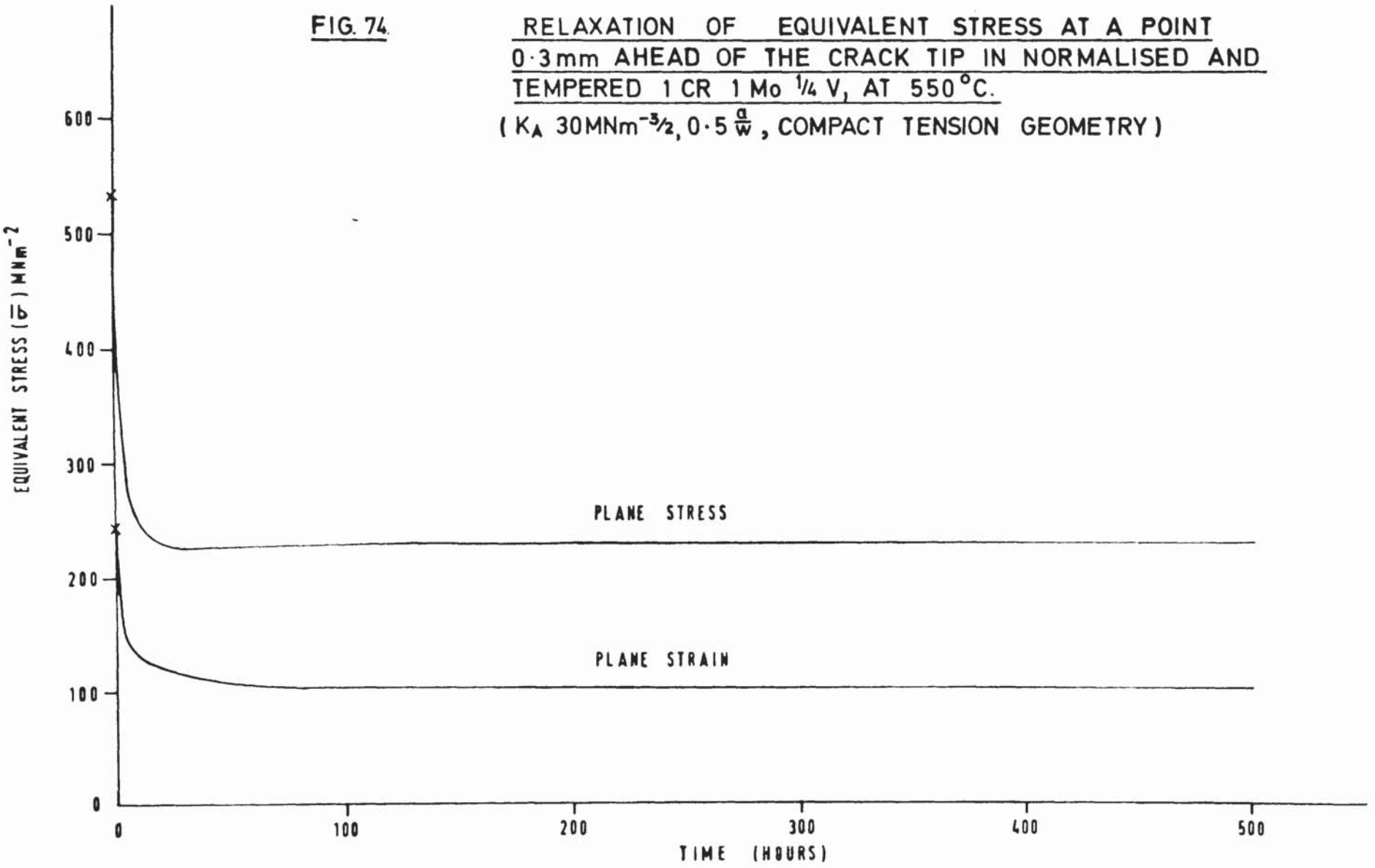

FIG. 75. RELAXATION OF EQUIVALENT STRESS AT A POINT 0·3mm AHEAD OF THE CRACK TIP IN QUENCHED AND TEMPERED 1 CR 1 Mo ¼ V, AT 550 °C.
(K_A 30 $MNm^{-3/2}$, 0·5 W, COMPACT TENSION GEOMETRY)

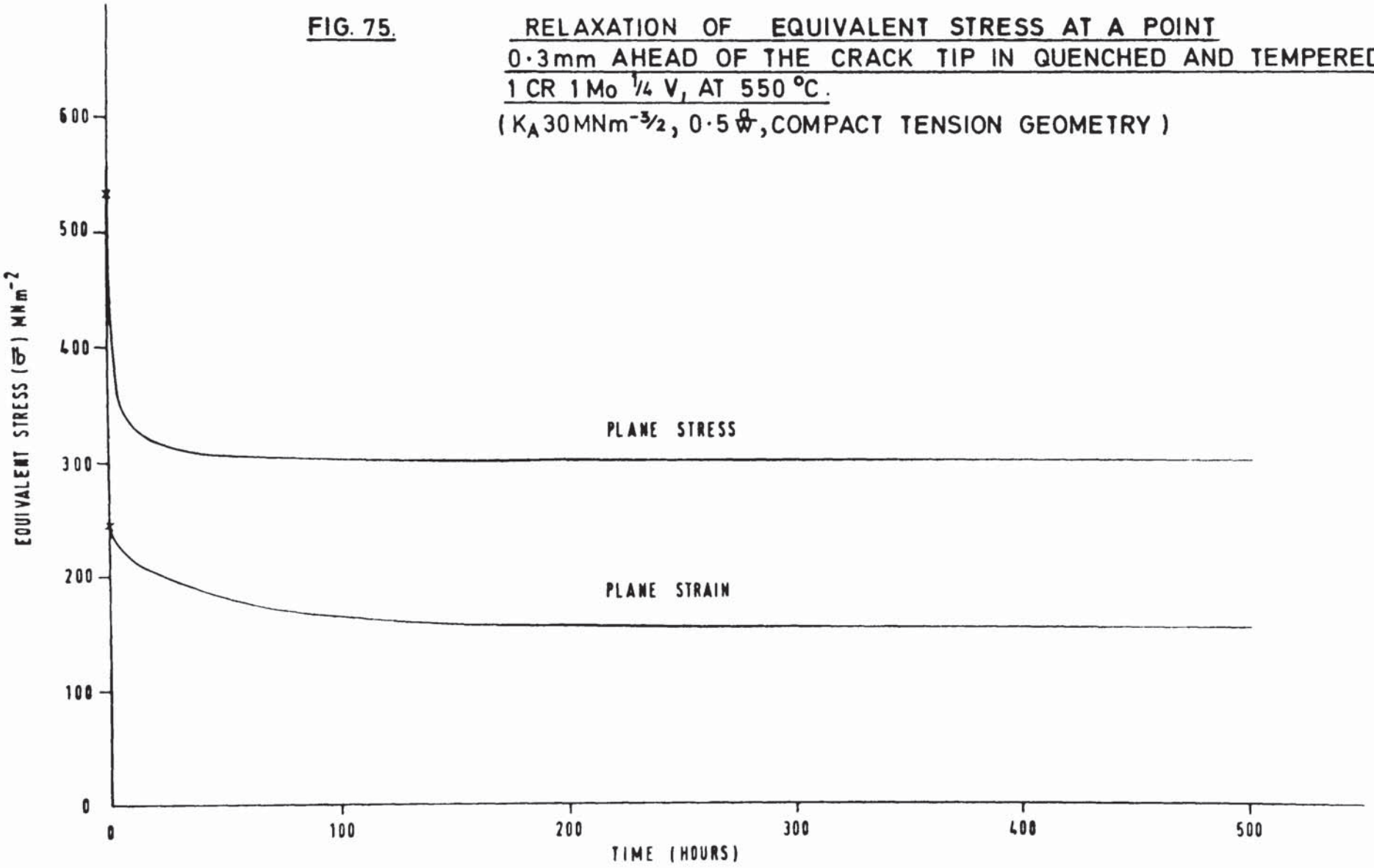

RC/SSR/A4/36

FIG. 76. COMPARISON OF THE INITIAL AND STEADY STATE EQUIVALENT ELASTIC STRESS DISTRIBUTION AHEAD OF THE CRACK TIP IN 1 Cr 1 Mo ¼V, AT 550° C.

(PLANE STRESS DEFORMATION, K_A 30MNm$^{-3/2}$, 0·5$\frac{a}{W}$, θ =0°, EQUATIONS 8 TO 10.)

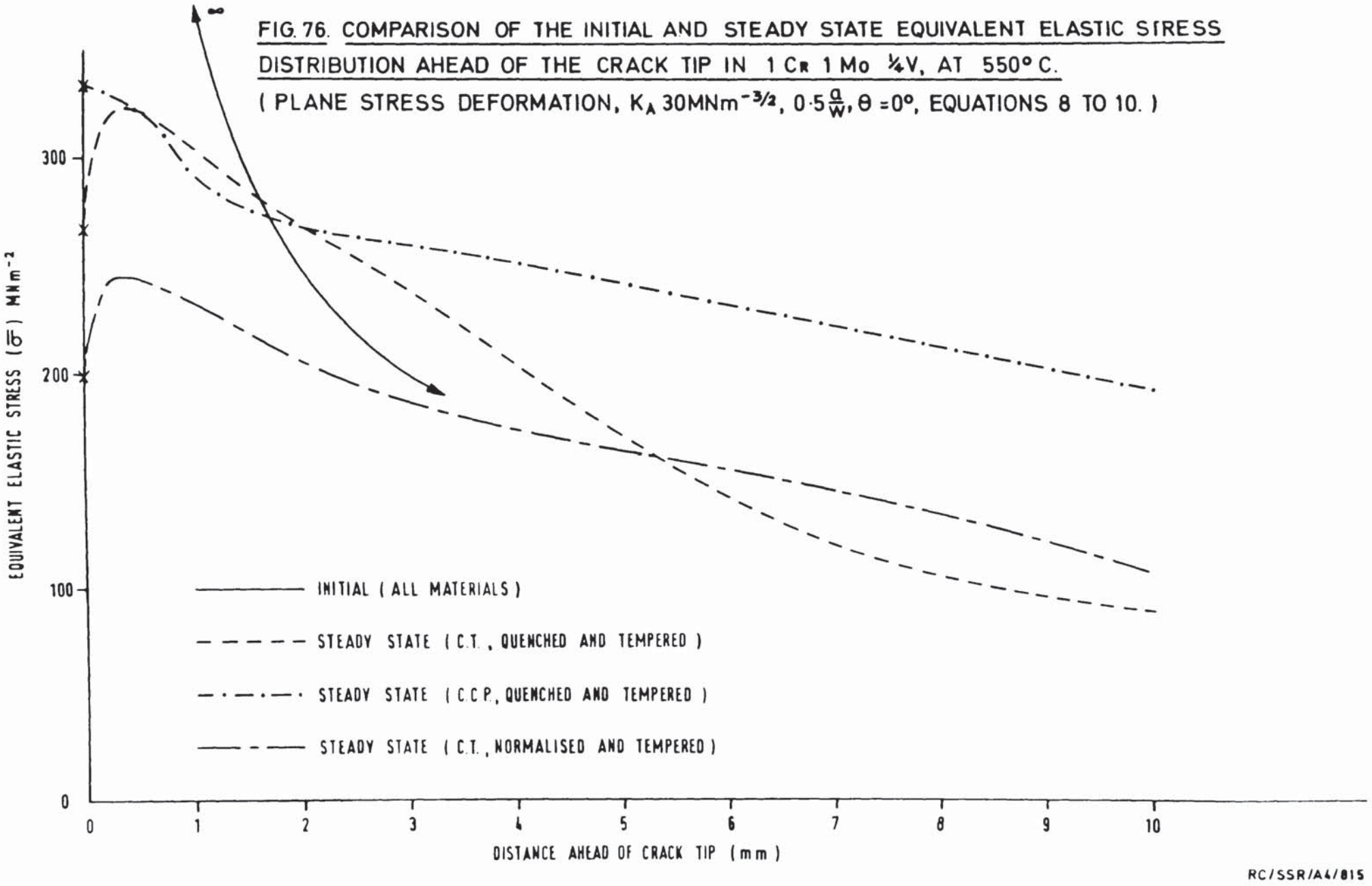

RC/SSR/A4/815

FIG. 77. COMPARISON OF THE INITIAL AND STEADY STATE EQUIVALENT ELASTIC STRESS DISTRIBUTION AHEAD OF THE CRACK TIP IN 1 Cr 1 Mo ¼V, AT 550° C.
(PLANE STRAIN DEFORMATION, K_A 30 $MNm^{-3/2}$, $0{\cdot}5\frac{a}{W}$, $\theta = 0°$, EQUATIONS 8 TO 10.)

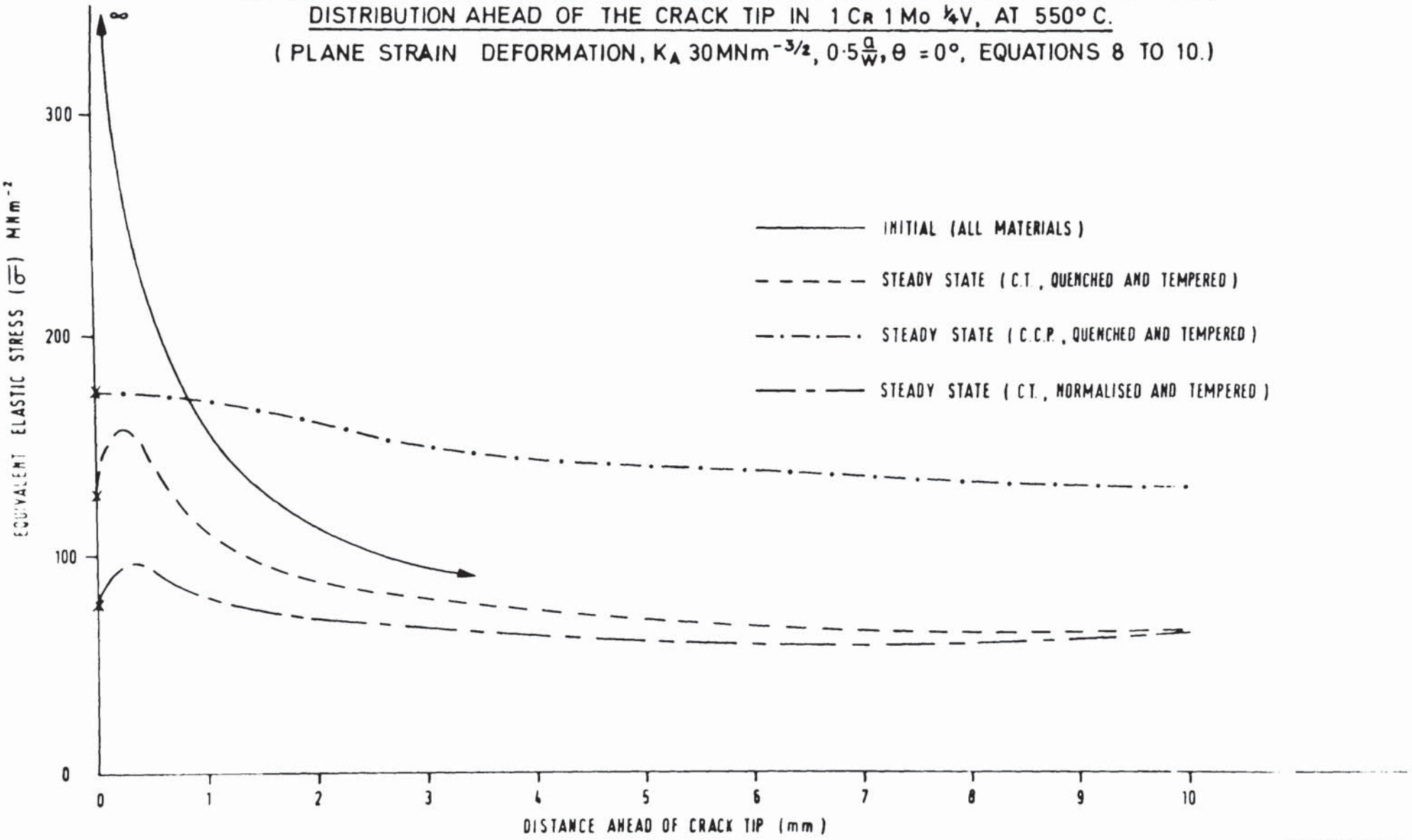

RC/SSR/A4/816

FIG. 77. COMPARISON OF THE INITIAL AND STEADY STATE EQUIVALENT ELASTIC STRESS DISTRIBUTION AHEAD OF THE CRACK TIP IN 1 Cr 1 Mo ¼V, AT 550° C.
(PLANE STRAIN DEFORMATION, K_A 30 $MNm^{-3/2}$, $0{\cdot}5\frac{a}{W}$, $\theta = 0°$, EQUATIONS 8 TO 10.)

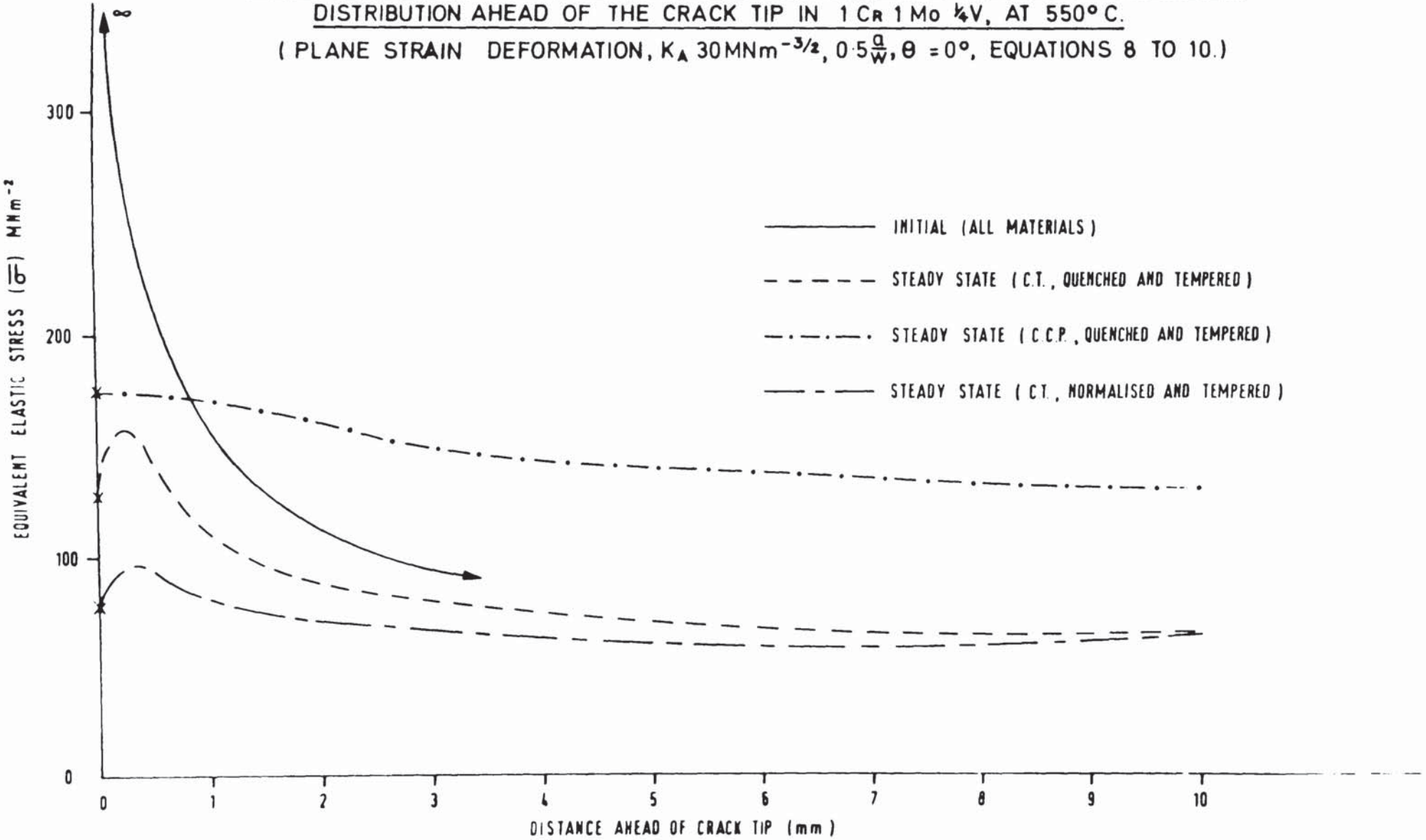

RC/SSR/A4/816

FIG. 78. EQUIVALENT CREEP STRAIN DISTRIBUTION AHEAD OF A CREEP CRACK AT THE INSTANT OF INITIATION.

(PLANE STRESS DEFORMATION, C.T. AND C.C.P. GEOMETRY)

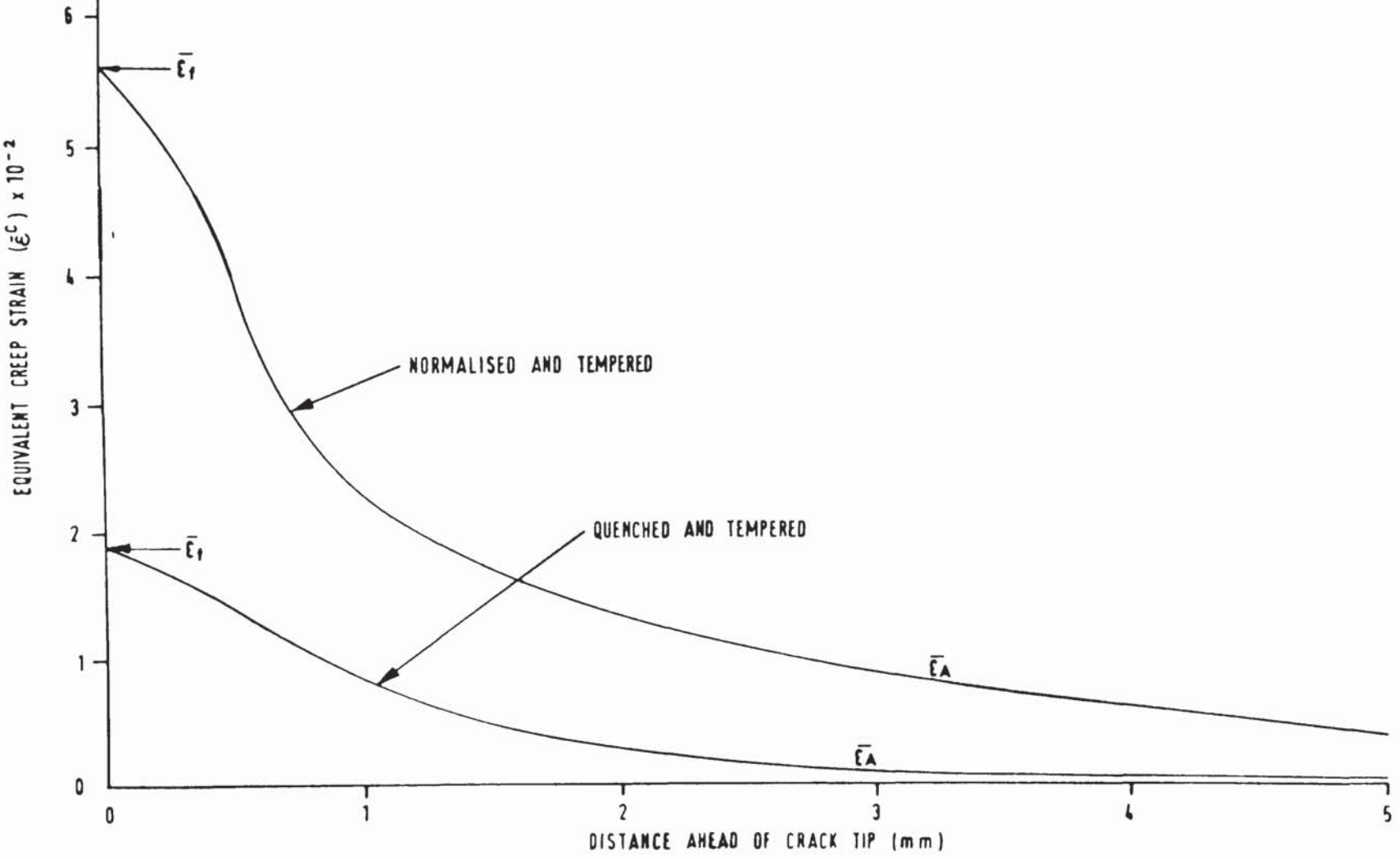

RC/SSR/A4/817

FIG. 79. EQUIVALENT CREEP STRAIN DISTRIBUTION AHEAD OF A CREEP CRACK AT THE INSTANT OF INITIATION.

(PLANE STRAIN DEFORMATION, C.T. AND C.C.P. GEOMETRY.)

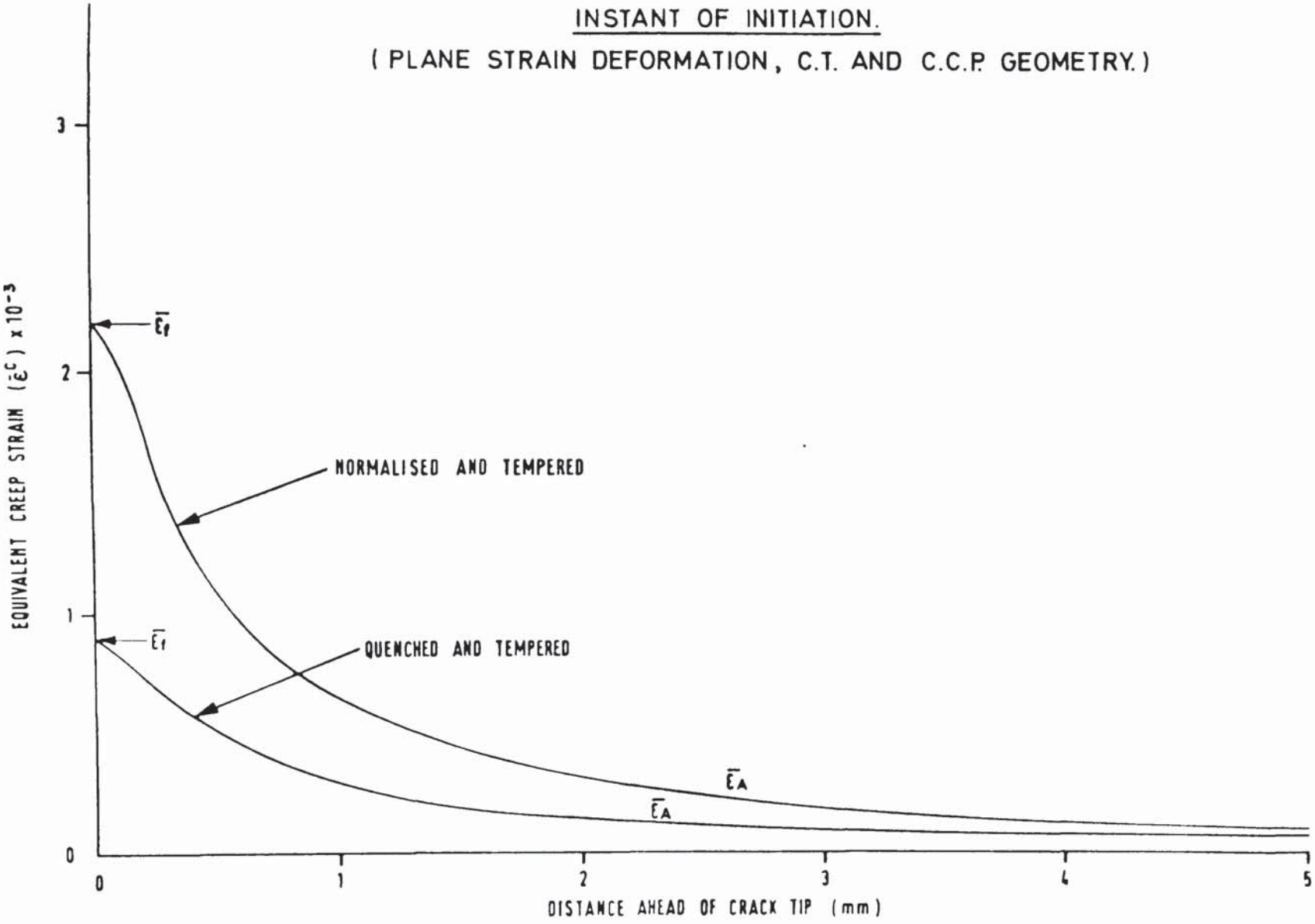

RC/SSR/A4/818

CHAPTER 6

DISCUSSION

It has been shown in Chapter 4 that neither K_A, nor σ_R which is based on Haigh's 'equivalent stress' (Equation 34), correlates satisfactorily the creep crack growth rate in the two CrMoV alloy steels under the test conditions. This observation is at variance with the results from several other investigations (Section 2.7.1) where it has been claimed that K_A and σ_R can correlate creep crack growth rates in quenched and tempered, and normalised and tempered CrMoV steels respectively. This claim has been justified on the grounds of comparability between the scatter in crack velocity results (claimed to be ± 1 log cycle) and cast to cast variation in the smooth bar uniaxial creep rupture life of the relevant steel. However, this argument cannot explain the scatter in crack velocity data observed in the present test programme. In this instance, specimens were selected carefully from only one cast of ½Cr½Mo¼V and 1Cr1Mo¼V steel and tested under precise laboratory conditions. In these circumstances, the crack velocity measurements had a scatter of only ± 0.1 to 0.2 log cycle and not ± 1 log cycle (Section 4.4.1).

K has been adopted by other workers on the premise that it describes approximately the elastic stress distribution in the near tip zone ahead of an advancing macroscopic creep crack. It has been argued that such a stress distribution would exist in a high creep strength steel where the stress exponent in the creep deformation law is less than approximately 4. Alternatively, σ_R applies when the steel has a relatively low creep strength and the stress exponent is much greater than 4. In this case the stress concentration at the macroscopic crack tip has relaxed out completely and the stress distribution takes the form of that for a material which has deformed under time independent plasticity. These two stress models form

the bounds of real material behaviour and it is to be expected that the true stress distribution will lie between these limits. The precise level and shape of the stress distribution will depend on the creep strength and ductility of the material, the specimen or component geometry and the degree of crack tip constraint.

A simple stress relaxation model used by Nicholson (1975) showed that the local crack tip stress in AISI Type 316 stainless steel at 750°C, relaxes to 1.5x the nominal applied net section stress in 60 seconds. This analysis was offered as an explanation as to why an excellent correlation was obtained between creep crack velocity and net section stress. Subsequent theoretical work by Barnby (1975) which was based on steady state creep and plane stress deformation, rationalised Nicholson's work very effectively. As part of a natural development of their work, this Thesis has considered the stress relaxation characteristics of materials deforming under conditions of plane stress and plane strain and in addition, has considered the geometrical effect. The numerical stress analysis results described in Section 5.4 show that the initial elastic stress distribution ahead of a pre-existing macroscopic crack relaxes very quickly to a steady state level, the amount of relaxation being a function of the material and the crack tip constraint. These results will now be considered in detail.

6.1 Crack Initiation Model

Consider first the numerical analysis results shown in Figures 76 and 77. These show that the steady state equivalent stress distribution in the near crack tip zone is significantly lower than the initial elastic stress distribution which over a limited distance ahead of the crack tip, can be described by K (Section 5). Further afield, the steady state stress levels are in excess of the initial elastic stress distribution. This occurs because the load bearing capability of the specimen must be maintained. Tables 7 and 8 show that these steady state stress distributions are effectively attained before creep crack initiation during either plane

stress or plane strain deformation. Thus, at the instant of initiation, creep cracks in either the normalised and tempered or the quenched and tempered materials see a relaxed stress and not the elastic stress. Consequently, it is wrong to use K to describe the initial stages of creep crack growth in these materials.

In general, the steady state stress distributions shown in Figures 76 and 77 can be regarded as being linear right across the uncracked ligament apart from a slight pertubation near the crack tip. The results from the C.T. geometry are particularly interesting as they are in good agreement with the work of Penny and Marriott (1971) on the creep of a simple beam in bending. In particular, the form of the steady state stress distribution from the cracked specimens is very similar to that in the beam for materials whose creep stress exponents are less than 5. Now as the long range stress distributions are determined by the applied moment and with a 'linear' assumption of these distributions, equations describing the stresses will be independent of whether deformation is elastic or plastic. Thus, by modelling the C.T. geometry as a beam which is subjected to a constant bending moment about its neutral axis (Figure 80a) and an axial load, it is possible to represent the steady state stresses ahead of the crack using the relationships familiar from elastic theory (e.g. Equation 76 below). The C.C.P. geometry is treated in a similar manner. The similarity between elastic and plastic stress distributions when both are linear has been used in other contexts (e.g. Highton, 1978). A description of the C.T. and C.C.P. models now follows.

6.1.1 Blunt Notch Models

Figure 80a shows the form of the blunt notched C.T. model. The symbols a, W and b represent the crack length, the specimen width and the specimen breadth respectively. The elastic stresses developed along the plane of symmetry in the 'uncracked ligament' due to the application of a load P, will contain direct and bending components. The plastic stresses will also be the same. The direct stress component σ_D is simply

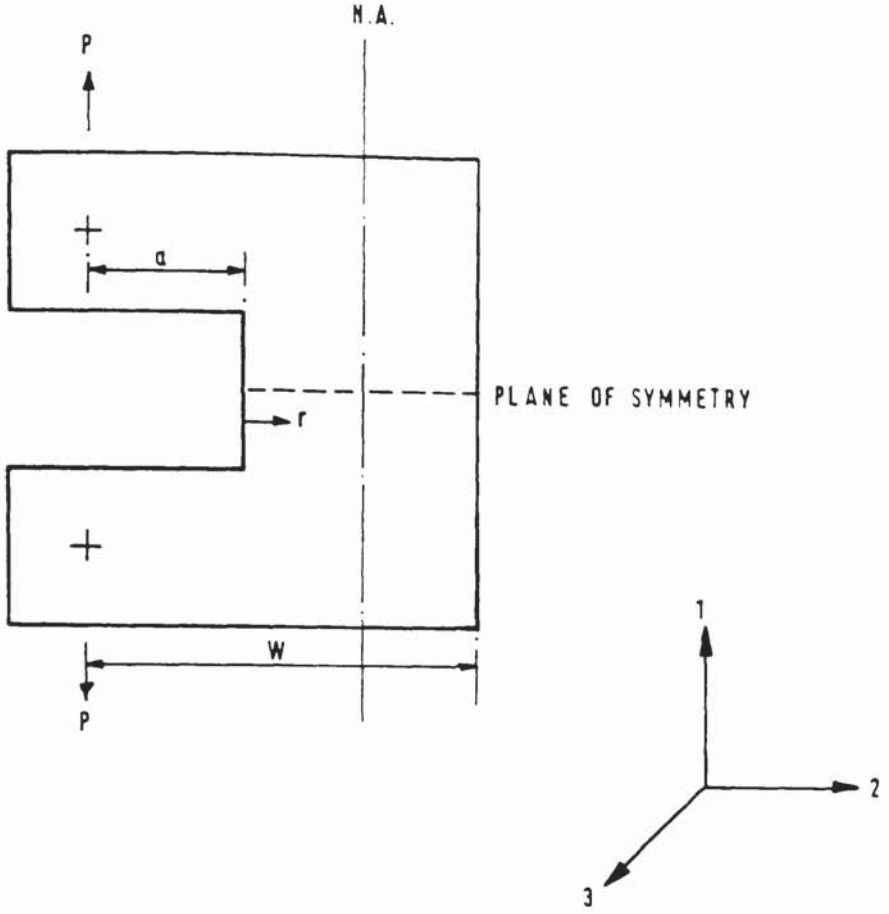

FIG 80a. NOTCHED COMPACT TENSION STRESS MODEL

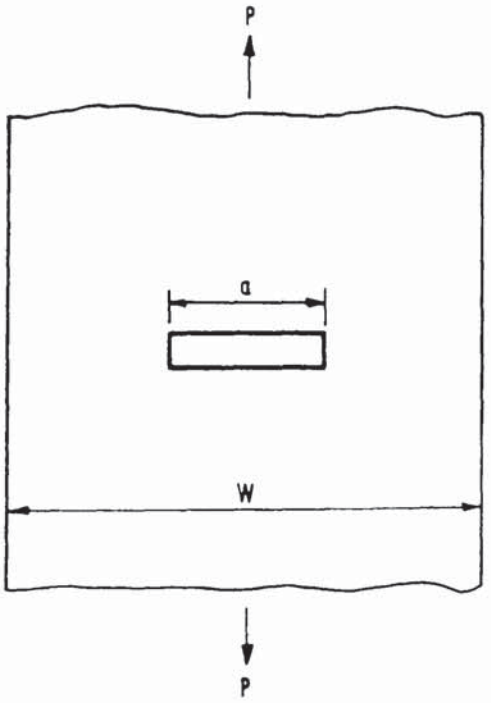

FIG. 80b. NOTCHED CENTRE-CRACKED PANEL STRESS MODEL

$$\sigma_D = \frac{P}{b\,(W-a)}$$

or in the general case where the dimension 'a' varies by δa:

$$\sigma_D = \frac{P}{b\left[W-\left(a+\delta a\right)\right]} = \frac{P}{Wb\left(1-x\right)} \qquad (75)$$

where

$$x = \frac{a+\delta a}{W}$$

The outer fibre bending stress σ_B can be calculated from the general expression

$$\sigma_B = \frac{M\,Y}{I} \qquad (76)$$

In this case the bending moment $M = P\left[\frac{W+(a+\delta a)}{2}\right]$ (77)

the distance from the neutral axis to the outer fibre $Y = \frac{W-(a+\delta a)}{2}$ (78)

and the second moment of inertia $I = \frac{b\left[W-(a+\delta a)\right]^3}{12}$ (79)

Substituting for M, Y and I in Equation 76, Equations77, 78 and 79,

$$\sigma_B = \frac{3P(1+x)}{Wb(1-x)^2} \qquad (80)$$

Similarly, the bending stress σ_B' at any position r along the plane of symmetry can be calculated from the expression:

$$\sigma_B' = \frac{3P(1+x)\,(1-x-\frac{2r}{W})}{Wb(1-x)^3} \qquad (81)$$

Thus, the total stress σ_T at any point along the plane of symmetry $= \sigma_D + \sigma_B'$

Therefore: $$\sigma_T = \frac{3P(1+x)(1-x-\frac{2r}{W}) + P(1-x^2)^2}{Wb(1-x)^3} \qquad (82)$$

In the centre-cracked panel model (Figure 80b) the application of a load P will result only in direct stresses in the 'uncracked ligament' providing the ligaments are large in the axial direction. These stresses can be calculated from Equation 75.

As σ_T in both models acts in a direction normal to the plane of

symmetry, it is equivalent to σ_{11}. This σ_{11} represents the stress ahead of a blunt notch lying in a body which is undergoing uniaxial deformation. In this instance as there are no shear stresses and as $\sigma_{22} = \sigma_{33} = 0$, $\sigma_{11} = \bar{\sigma}$ (Equation 59). A similar relationship between σ_{11} and $\bar{\sigma}$ for biaxial (plane stress) and triaxial (plane strain) deformation is not provided directly by the elastic models. However, a possible solution to this problem is to consider the effect of plastic constraint at notches in materials undergoing elastic-plastic deformation. Plastic constraint leads to stress intensification Q which by definition is the ratio of σ_{11} to the uniaxial yield stress. Alternatively, by substituting the deviatoric stress $\bar{\sigma}$ for the yield stress, Q can be defined as $\frac{\sigma_{11}}{\bar{\sigma}}$. In this form, Q can be used in combination with the uniaxial stress model to provide plane stress and plane strain 'elastic' equivalent stress ($\bar{\sigma}_E$) profiles. A direct comparison can then be made between the equivalent stress distribution in Figures 76 and 77 and those in the elastic models. In the limit, Q is 1 for plane stress deformation and 2·6 for plane strain deformation - (Griffiths and Owen, 1971). Thus, from equations 75 and 82,for the C.T. geometry

Plane Stress
$$\bar{\sigma}_E = \sigma_T \left(\text{from Eq. 82}\right) \tag{83}$$

Plane Strain
$$\bar{\sigma}_E = \frac{1}{2{\cdot}6}\left\{\sigma_T\left(\text{from Eq. 82}\right)\right\} \tag{84}$$

and for the C.C.P. geometry

Plane Stress,
$$\bar{\sigma}_E = \sigma_D\left(\text{from Eq. 75}\right) \tag{85}$$

Plane Strain,
$$\bar{\sigma}_E = \frac{1}{2{\cdot}6}\left\{\sigma_D\left(\text{from Eq. 75}\right)\right\} \tag{86}$$

Equations 83 to 86 have been used to calculate the appropriate $\bar{\sigma}$ distributions inthe models which have then been compared with the steady state $\bar{\sigma}$ distributions (Figures 81 to 84). Where the near crack tip zone

FIG. 81

COMPARISON OF THE STEADY STATE EQUIVALENT STRESS DISTRIBUTION AHEAD OF THE CRACK TIP AT 550° C AND THE INITIAL EQUIVALENT STRESS DISTRIBUTION IN THE BLUNT NOTCH MODEL

(NORMALISED AND TEMPERED 1 CR 1 Mo 1/4 V, K_A 30MNm$^{-3/2}$ 0·5 $\frac{a}{w}$)
COMPACT TENSION GEOMETRY.

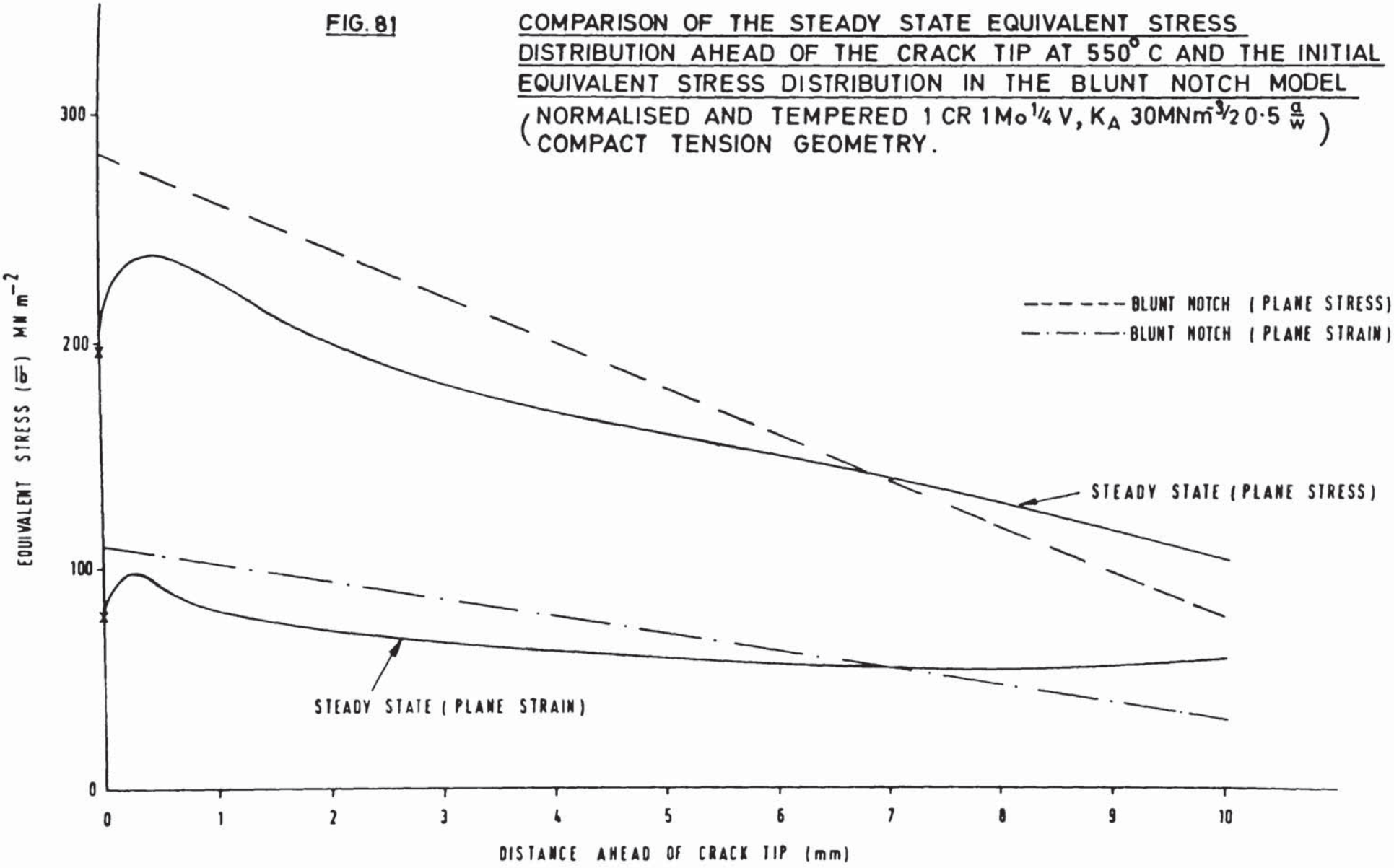

FIG. 82

COMPARISON OF THE STEADY STATE EQUIVALENT STRESS DISTRIBUTION AHEAD OF THE CRACK TIP AT 550°C AND THE INITIAL EQUIVALENT STRESS DISTRIBUTION FROM THE BLUNT NOTCH MODEL
(QUENCHED AND TEMPERED 1 CR 1 Mo ¼ V, K_A 30MNm$^{-3/2}$ 0·5 $\frac{a}{w}$ COMPACT TENSION GEOMETRY.)

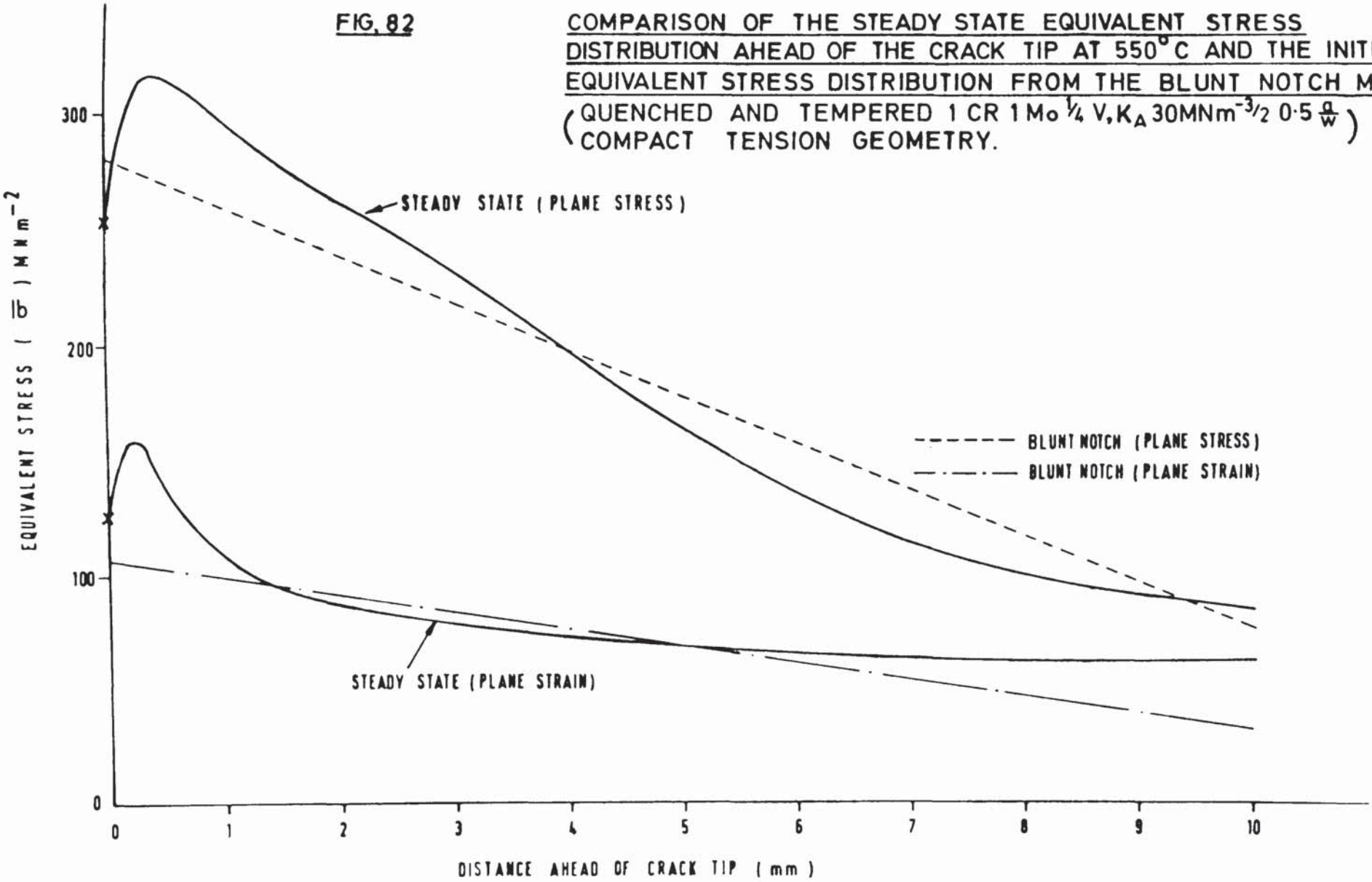

FIG. 83 COMPARISON OF THE STEADY STATE EQUIVALENT STRESS DISTRIBUTION AHEAD OF THE CRACK TIP AT 550°C AND THE INITIAL EQUIVALENT STRESS DISTRIBUTION FROM THE BLUNT NOTCH MODEL (NORMALISED & TEMPERED 1CR 1MO 1/4V, K_A 19MNm$^{-3/2}$, 0·5 $\frac{a}{w}$) CENTRE-CRACKED PANEL GEOMETRY

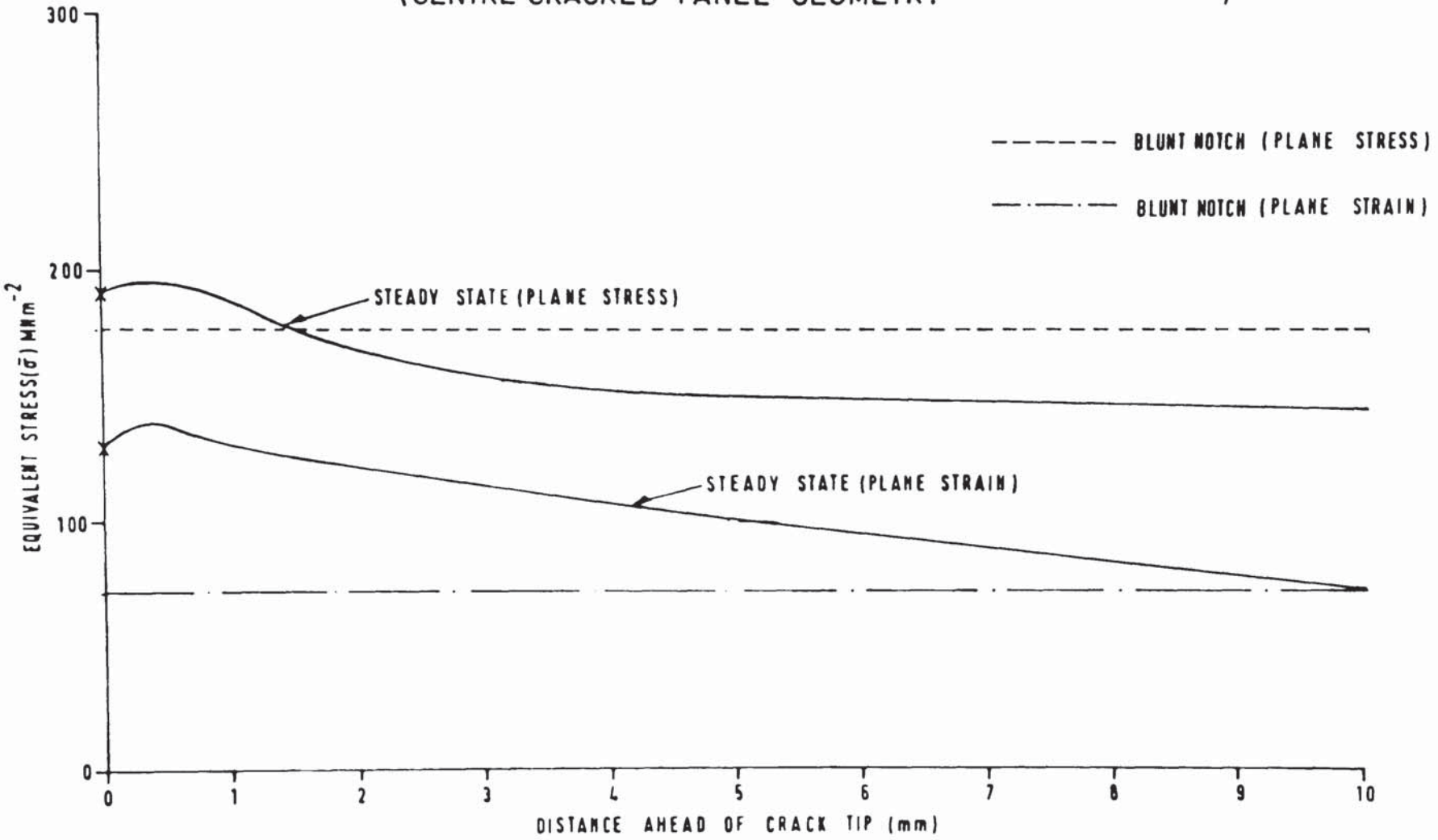

FIG. 84 COMPARISON OF THE STEADY STATE EQUIVALENT STRESS DISTRIBUTION AHEAD OF THE CRACK TIP AT 550°C AND THE INITIAL EQUIVALENT STRESS DISTRIBUTION FROM THE BLUNT NOTCH MODEL (QUENCHED & TEMPERED 1Cr 1Mo ¼V, K_A 30MNm$^{-3/2}$ 0·5 $\frac{a}{w}$ CENTRE-CRACKED PANEL GEOMETRY)

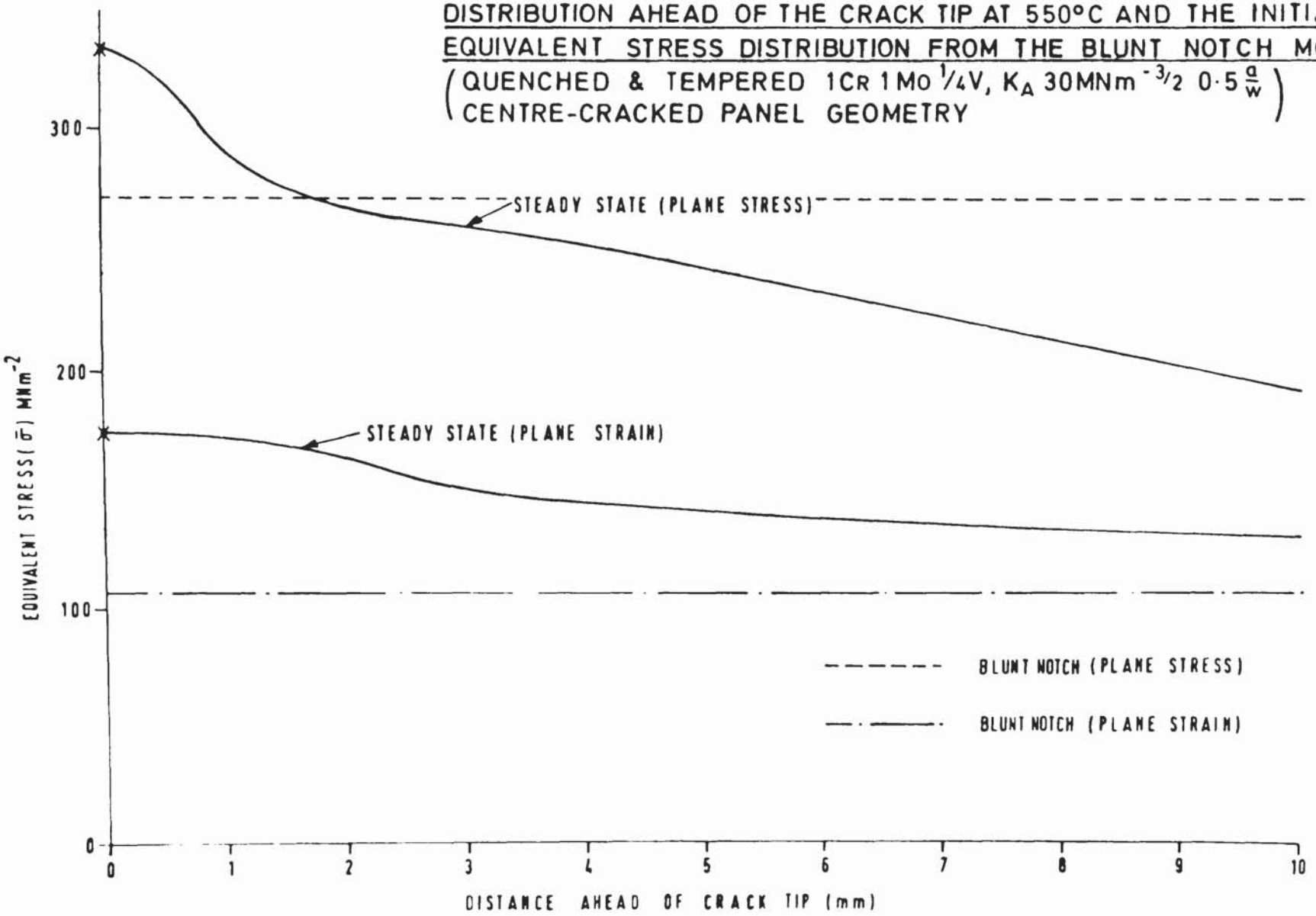

RC/SSR/A4/863

stresses are effectively the same in both solutions, it can be assumed that all notch effects have been removed by the creep deformation process. When Figures 81 to 84 are compared with Figures 76 and 77, it can be seen that significant amounts of stress relaxation has occurred in the near crack tip zone. This phenomenon is more apparent in the normalised and tempered material and follows from the creep laws assumed (Section 5). Thus K_A does not work as we have seen, but this type of behaviour does agree approximately with the first requirement for σ_R controlled creep cracking. This states that the original elastic stress concentration must be completely absent. However, a further requirement is that the relaxed stress distribution must take the form of that for a material whose creep stress exponent is effectively infinite. This stress distribution does not exist in the C.T. specimens.

6.1.2 General Comments

The accuracy of a non-linear finite element creep stress analysis rests on its ability to simulate accurately real material behaviour. In the present finite element stress analysis an attempt has been made to achieve this primarily by employing the concept of the Von Mises equivalent stress ($\bar{\sigma}$) and a time hardening creep law. The strength of the finite element stress analysis lies in the fact that through the use of $\bar{\sigma}$ it can calculate the magnitude of creep strain at any point in a body of abitrary shape containing multiaxial stresses. It also considers in detail the continuum mechanics of a body deforming by time dependent plasticity and as such, is far superior to all other existing models of creep stress relaxation. The results from a relatively sophisticated creep stress relaxation model are however, of little significance unless the material creep law used in the analysis is basically sound. In using a time hardening creep law, the finite element stress analysis achieves that extra degree of realism that is not provided by a law based purely on

secondary creep. In essence, a time hardening law covers the primary stage of creep where large strains can develop and creep damage can form (Greenwood, 1977). These facts will have an important effect on the stress relaxation characteristics of a material and on the development of a realistic macroscopic creep fracture model.

The ability of the BERSAFE analysis to simulate satisfactorily the real material behaviour is demonstrated in Figures 85 and 86. These figures compare predicted and experimentally observed initiating creep crack opening displacements in C.T. specimens manufactured from the 1CrlMo¼V alloy. The predicted displacements were obtained by stopping the appropriate stress analysis programmes at simulated creep times equal to the measured initiation times of 100 hours for the quenched and tempered material and 500 hours for the normalised and tempered material, and extracting the displacement readings from the data output sheets. Both figures show that the experimental results fall generally within the predicted values for plane stress and plane strain deformation. This is to be expected as the test pieces deformed neither in pure plane stress nor plane strain. However, the remarkably good correlation between predicted and observed values of δ_i in the thin test specimens together with the trend of δ_i in the thicker specimens towards the plane strain prediction, suggests that the BERSAFE analysis has simulated accurately real material behaviour. Further evidence of this is provided by Table 9 which compares predicted and observed values of δ_i in C.C.P. specimens. Table 9 also shows that the numerical analysis effectively predicts δ_i to be geometry independent. This phenomenon has been observed experimentally.

FIG. 85 COMPARISON OF PREDICTED & OBSERVED EFFECT OF CONSTRAINT ON INITIATING CRACK OPENING DISPLACEMENT

(NORMALISED & TEMPERED 1CR 1MO 1/4V COMPACT TENSION GEOMETRY, K_A 30MNm$^{-3/2}$)

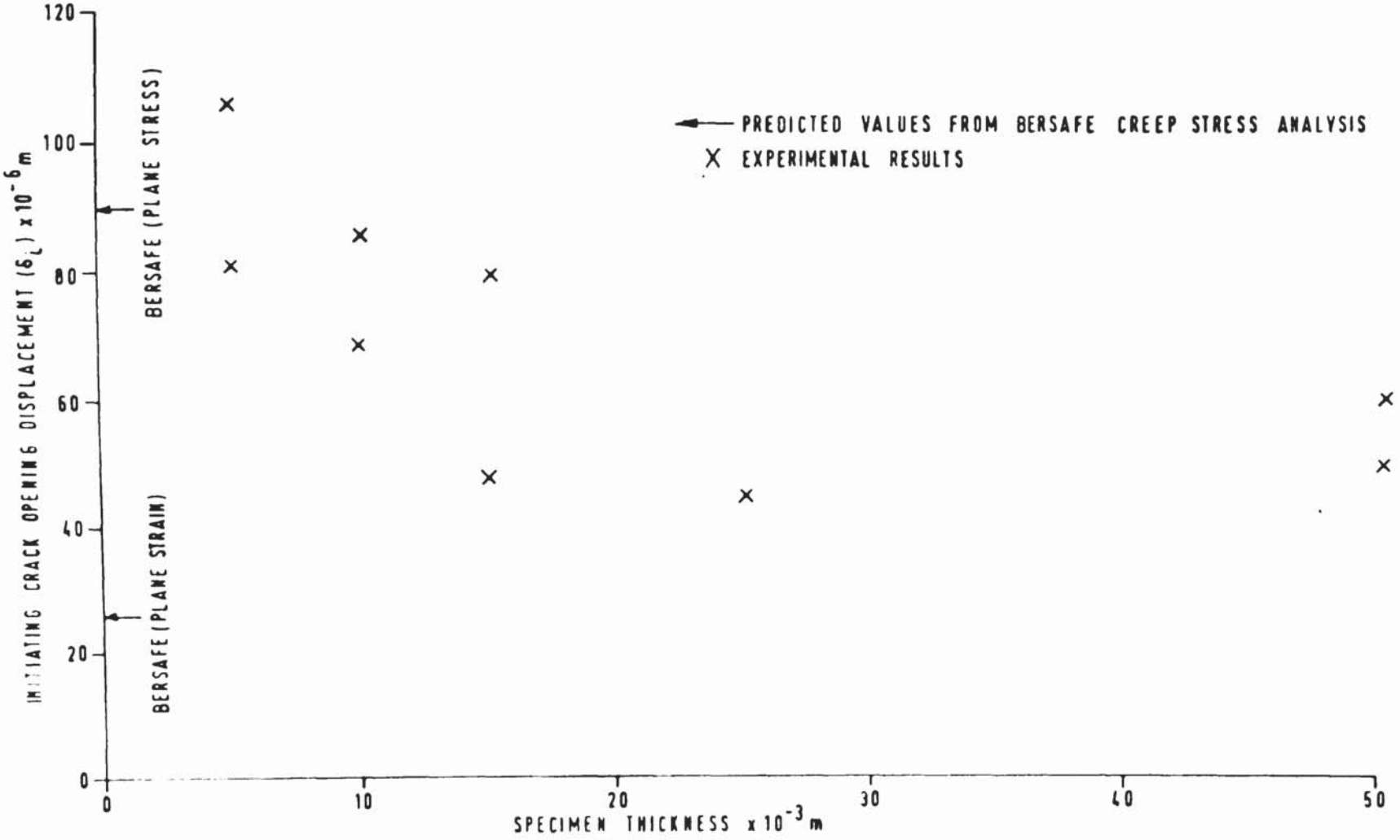

RC/SSR/A4/864

FIG. 86 COMPARISON OF PREDICTED & OBSERVED EFFECT OF CONSTRAINT ON INITIATING CRACK OPENING DISPLACEMENT
(QUENCHED & TEMPERED 1CR 1MO 1/4V
COMPACT TENSION GEOMETRY, K_A 30MNm$^{-3/2}$)

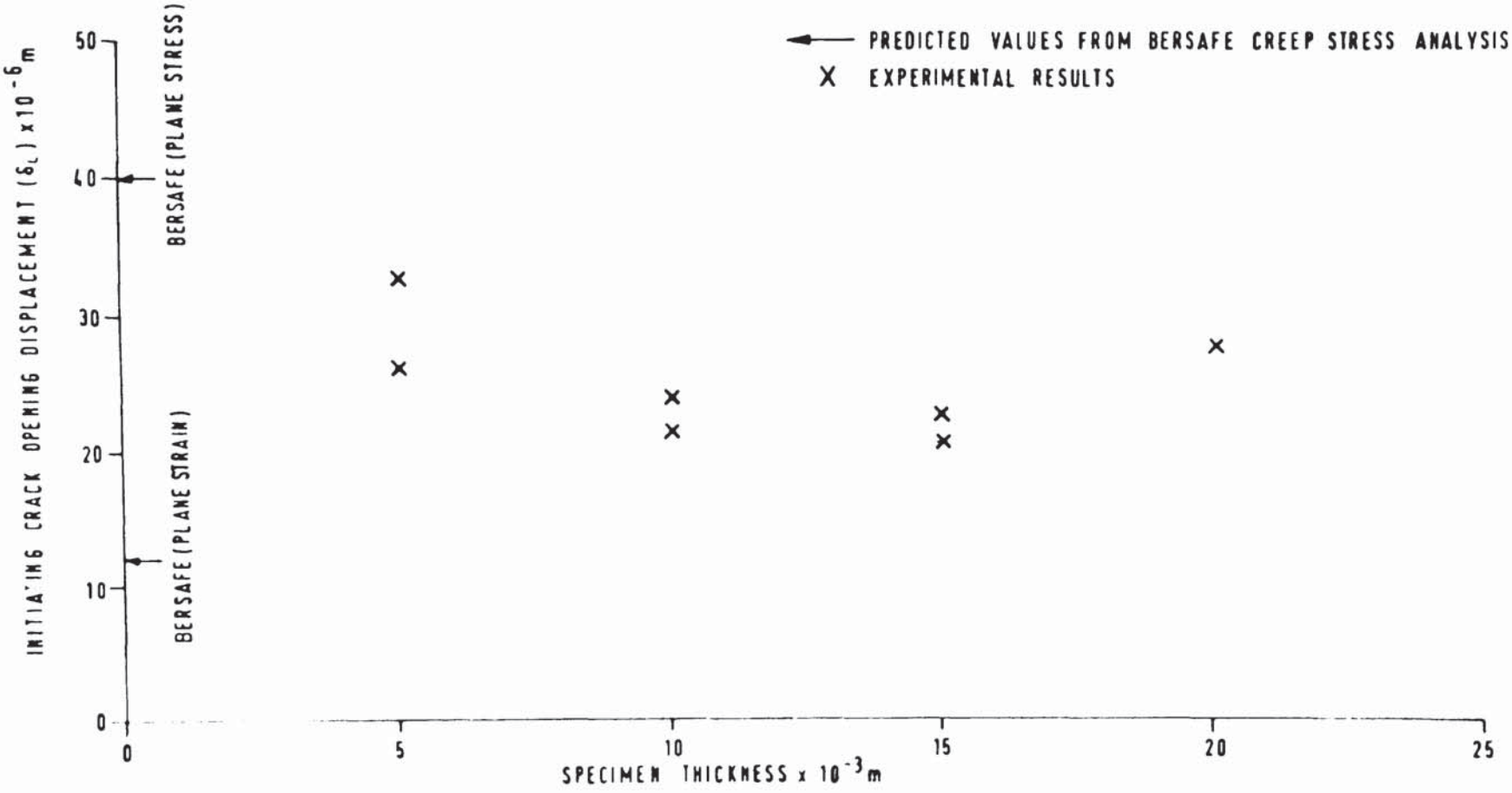

Table 9 Comparison of Predicted and Observed δ_i Values

Material	Geometry	Initiating Crack Opening Displacement (δ_i) x 10^{-6} m			
		Plane Stress		Plane Strain	
		Predicted	Observed	Predicted	Observed
1CrlMo¼V N & T	C.T. (K_A30)	90	81 - 106 (5mm)	26	50 - 62 (50mm)
	C.C.P. (K_A19)	104	100 (1mm)	45	50 (8mm)
1CrlMo¼V Q & T	C.T. (K_A30)	40	26 - 33 (5mm)	12	~22 (>10mm)
	C.C.P. (K_A30)	46	34 (1mm)	14	28 (8mm)

K_A units in $MNm^{-3/2}$

mm units refers to specimen thickness

The development of a creep fracture model which uses finite element stress anlysis has its attractions. Apart from being able to calculate local creep stress relaxation, this analytical technique can predict successfully bulk creep deformation in three dimensional components (Harper, 1968). However, the success of this technique relies heavily on the interpretive skill of the user, it can also be very time consuming. In contrast, existing models of creep fracture are easier to use and provide an immediate picture of the physical processes occuring in the deforming body. In view of these facts it would seem sensible to develop a model of macrosocpic creep fracture which has the desirable qualities of the numerical and analytical techniques. To this end, a model of macroscopic creep fracture in cast CrMoV steel has been developed. It is based on the simple model of stress distribution described in Section 6.1, utilises the time hardening law to calculate creep strain and recognises the influence of deviatoric and normal stress components on the mechanism of creep fracture.

6.2 Macroscopic Creep Crack Growth

In order to simplify the analysis of the experimental results it has been assumed that creep crack growth can be represented by a series of small steps, each element of material deforming according to the magnitude of the local stress. The crack is assumed to advance when the first element adjacent to its tip has accumulated a critical amount of strain. The magnitude of this strain and consequently the creep crack initiating time and velocity, will depend on the level of the local transient and steady state stress field, and the material properties.

6.2.1 Local Stress Field

It is generally accepted that primary, secondary and tertiary creep deformation in both ferrous and non-ferrous alloys can be expressed in terms of $\bar{\sigma}$, σ_{II}, or some combination of the stress components. For the case of CrMoV steels, there is strong evidence to show that the controlling stress at approximately 550°C is $\bar{\sigma}$ (Taira and Ohtani, 1971; Henderson and Ferguson, 1977; Cane, 1976). Thus, as far as the mechanics of creep deformation is concerned, estimates of transient and steady state stress fields ahead of a macrocrack can be made with relative ease. Relating the mechanisms of creep fracture to particular stress components however, is far more difficult. In order to do this, it is necessary to consider local stress fields comprising $\bar{\sigma}$ and $\frac{\sigma_{II}}{\bar{\sigma}}$ or $\frac{\sigma_H}{\bar{\sigma}}$ (McLean et al., 1977). Consider first the stress field acting on an element of material lying ahead of an incubating creep crack. Numerical analysis has shown that this element sees effectively only the relaxed steady state $\bar{\sigma}$ field (Figures 81 and 82 for example). Under the action of this stress field, cavities can nucleate on grain boundaries according to the classical theories of deformation creep and providing they are thermodynamically stable, can grow by either a deformation creep mechanism or a diffusion process. Whether or not a cavity can grow depends primarily on its surface energy and the magnitude of the local normal stress (Equation 4).

The higher the magnitude of this stress, the more thermodynamically stable are the cavities and the greater their chance of growing and linking with neighbouring cavities to form microcracks. Following the work of Cane, 1976 and 1978; Dyson and McLean, 1977; Dyson and Rogers, 1977, the significant stresses controlling nucleation and growth of cavities in cast CrMoV alloys under the prevailing test conditions are considered to be $\bar{\sigma}$ and $\frac{\sigma_{11}}{\bar{\sigma}}$. Viscous creep and hence the contribution of σ_H to the fracture process is assumed to be negligible. In the general case, this would not be a valid assumption as it is known that viscous hole growth can be important at high strain rates and low homologous temperatures (Dyson and Taplin, 1976). However, for the purposes of comparing the creep response of a material undergoing plane stress deformation with plane strain deformation, Figure 87 illustrates that it is unnecessary to have a precise knowledge of the active stress components. The figure shows that the most significant factor influencing the magnitude and profile of the steady state stress quotient is the mode of deformation and not the stress component chosen to characterise the situation.

In general, it is not intuitively obvious that an increase in crack tip constraint such as exists when traversing from the side face to the centre of a test specimen, will result in a more rapid development of creep cracks. With plane strain deformation we would expect crack opening displacement rates to be relatively low. Thus, as creep cracking occurs at a critical crack opening displacement (e.g. Figure 51) less creep cracks should develop with plane strain deformation. However, opposing this is the fact that increasing constraint can lead to a reduction in creep ducility (e.g. Figure 39). It is clear that the response of a creep crack to plane strain deformation will depend upon which of these two opposing processes is rate controlling. This may depend on the material being examined and the imposed test conditions. Nevertheless, from the above account on the character and significance of the local stress field ahead of an incubating

FIG. 87. COMPARISON OF STEADY STATE STRESS QUOTIENT AHEAD OF A STATIONARY CRACK TIP.

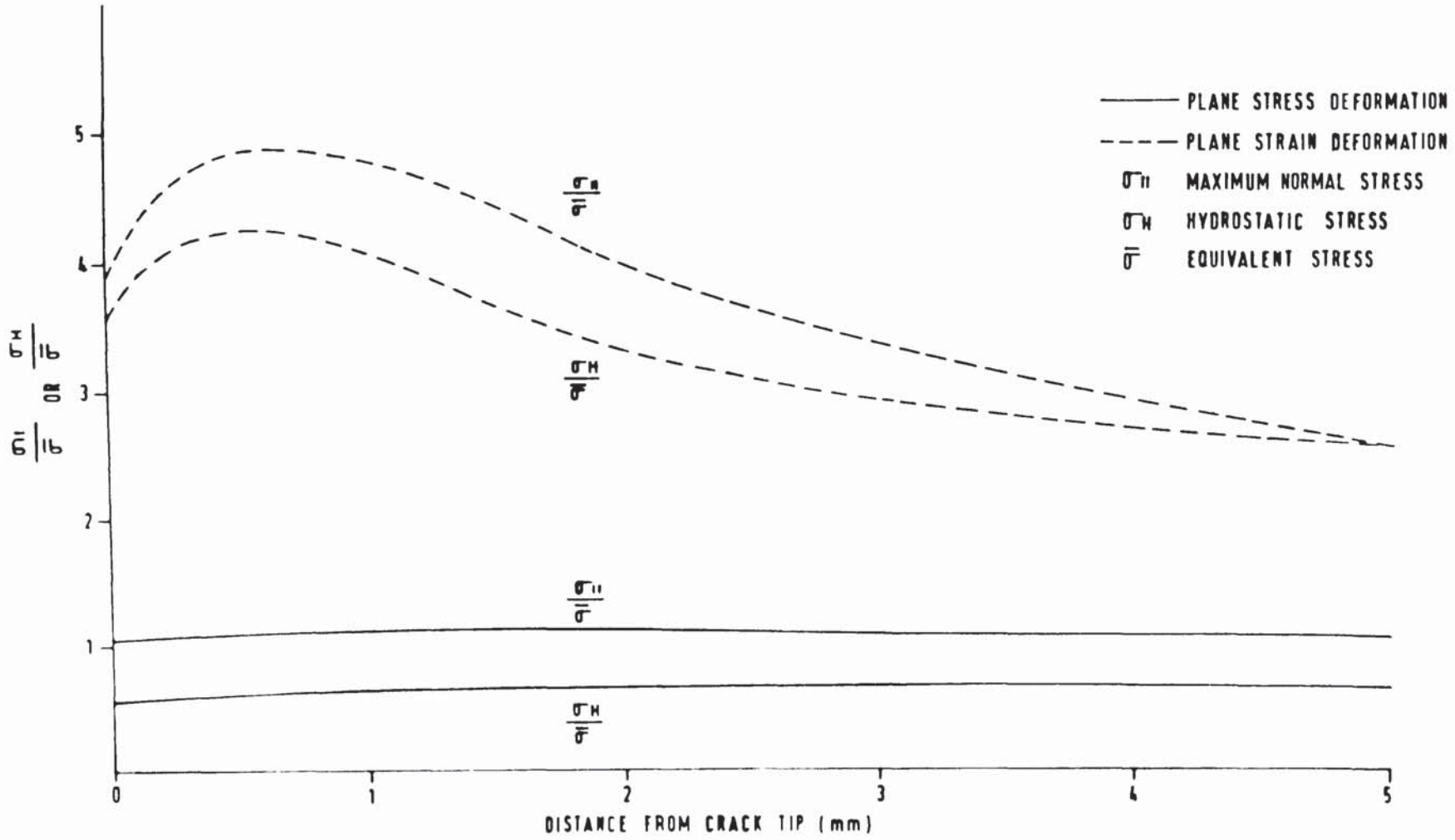

RC/SSR/A4/903

FIG. 88. EFFECT OF MODE OF DEFORMATION ON GRAIN BOUNDARY CAVITATION AHEAD OF CRACK TIP ALONG CRACKING PLANE.

(NORMALISED AND TEMPERED 1CR 1MO¼V COMPACT TENSION GEOMETRY, b = 10 mm)

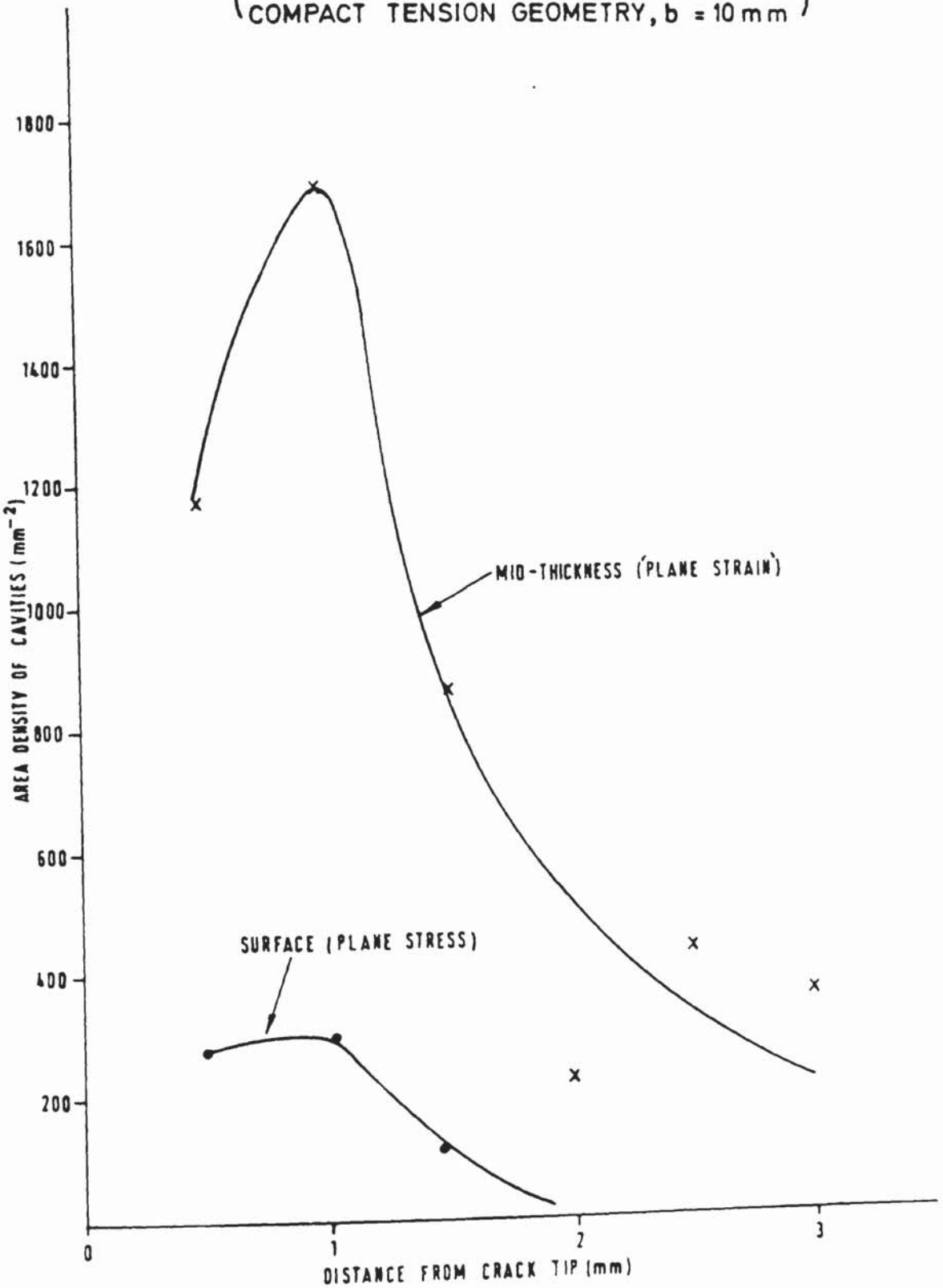

RC/SSR/A4/904

creep crack, it would appear that Figure 87 together with Figures 76 and 77 can be used to rationalise the creep behaviour of cast CrMoV materials when they are undergoing either plane stress or plane strain deformation. For the case of an element of material subjected to plane stress deformation, it can be reasoned that because the steady state equivalent stress ($\bar{\sigma}_{ss}$) is relatively high (Figure 76), nucleation of cavities by a deformation mechanism will occur readily. However, as the magnitude of the stress quotient is low (Figure 87), most of the cavities will be thermodynamically unstable. As a consequence, the density of cavities capable of growing and linking with their neighbours to form microcracks, will be low. Alternatively, when a ligament deforms under plane strain deformation, the relatively high stress quotient (Figure 76) would be expected to counteract the effect of a low $\bar{\sigma}_{ss}$ and increase the proportion of stable cavities. This has been observed experimentally (Figure 88) by methods described in Section 3.7. Thus, although fewer cavities would be nucleated, the majority of the cavities would be available to form microcracks and ultimately a macrocrack. In general, the rate at which microcracks form and develop into a macrocrack depends not only on the density of stable cavities but also on the uniformity of their distribution and their location on grain boundaries (Raj and Ashby, 1975). These last two factors will be particularly significant in highly anisotropic and inhomogenous materials. As this does not include the present materials, these two factors can be ignored.

If a fixed number of cavities are required to form grain boundary cracks and subsequently a macrocrack, it is reasonable to conclude that crack initiation will occur more readily in the centre of a test specimen, the result being crack bowing. This phenomenon has been observed experimentally in the cast CrMoV alloys. In addition, the associated low level of total strain accumulation (matrix plus grain boundary strain) resulting from the relatively low $\bar{\sigma}_{ss}$ in plane strain deformation, will effectively reduce the critical fracture strain for creep crack initiation.

This has also been observed experimentally in the measurements of δ_i and $\frac{1}{\omega}$ (eg Figures 85 and 86 for δ_i). Here, δ_i and $\frac{1}{\omega}$ can be replaced by strain by incorporating an appropriate gauge length.

The observed variations in macroscopic creep crack ductility on changing either the microstructure or alloy can also be explained in terms of the character of the local stress field and its effect on cavitation. For the case of a change in microstructure, it has been observed (Section 4.11) that more cavity nucleation sites exist in the quenched and tempered material compared to that in the normalised and tempered material. Thus, for a given mode of deformation, the total strain input required to develop the necessary population of cavities for crack formation will be lower in the quenched and tempered material. As a consequence, the fracture strain will be relatively lower in this material. A relatively higher matrix creep strength in the same material (Townsend, 1971) may also have the effect of raising the proportion of grain boundary strain per unit strain input, and thereby enhance cavitation and crack formation. Drawing together the above factors it is reasonable to conclude that for a given set of testing conditions, creep crack initiation times in the quenched and tempered material will be shorter than in the normalised and tempered material. This effect will be compounded by the fact that the steady state stress field components are significantly higher in the former material.

The experimental observation that creep crack ductility in the ¼Cr½Mo¼V alloy is higher than in the 1Cr1Mo¼V alloy can be explained in part, by the fact that the lower matrix strength of the low Cr alloy will in effect lower the grain boundary/matrix strain ratio. This will result in a reduction in the amount of grain boundary cavitation per unit strain input. As a consequence, more strain has to be introduced into the system in order to develop the necessary population of cavities for crack formation.

Creep ductility as measured by $\frac{1}{\omega}$ and δ_i has been observed to be invariant with crack length (Section 4.4.3). Therefore it would appear that

the criterion for creep crack initiation and growth is the attainment of a critical strain. In the present analysis of creep fracture under multiaxial stresses, this critical strain has been called the equivalent fracture strain $\bar{\varepsilon}_f$. Using this fracture criterion and the predicted stress and strain fields along the cracking plane, the growth of a crack can be modelled in the following manner.

During stress relaxation, creep strain will accumulate ahead of the incubating creep crack. Following the attainment of steady state, creep strain will continue to accumulate according to the magnitude of the stress field profiles shown in Figures 81 to 84. The crack incubation stage will be completed when the strain in the first element attains the level of $\bar{\varepsilon}_f$. According to the above figures, the preferred site for crack initiation is some distance ahead of the initial crack tip since the maximum stress occurs there. However, if the initial strain profile is taken into account (Figures 78 and 79) it can be argued that the first stage of crack growth will take place immediately ahead of the crack tip where the accumulated strain is a maximum. Following the rupture of the first element, the magnitude of the stress field in the remaining uncracked section of a specimen subjected to a constant applied load, will increase. During this event, the material response is considered to be completely elastic with the stresses rising according to the conditions of equilibrium and compatability for the particular mode of deformation. Assuming that proportional loading continues to hold during this growth stage, with the effect that the relative proportions of the stress field components remain unaltered, it is reasonable to conclude that the functional relationship between strain and distance, and stress and distance will be unchanged. Transient stress fields associated with an advancing crack tip can therefore be characterised by elevating the original steady state stress profiles using the analytical procedure described in Section 6.1.

Having established a foundation for a model of creep crack growth based on the successive rupture of elements it is now necessary to define their size. This has to be done with regard to the inherent structural character of the materials under investigation and to the limitations of the elastic-plastic stress analysis. From Figures 81 to 84, the peak stress occurs at approximately 0.25mm ($\frac{1}{200}$ th. of the specimen width) ahead of the crack tip suggesting that there may be advance nucleation occurring at this distance. The increment of crack growth chosen for repeat calculations was therefore 0.25mm.

In summary, the relevant parameters controlling the development of macroscopic creep cracks in cast CrMoV alloys are considered to be as follows.

(a) The creep deformation is controlled by the Von Mises equivalent stress $\bar{\sigma}$. In order to provide a realistic account of the development of creep strain in a deforming body, $\bar{\sigma}$ must be incorporated in a creep deformation law that covers all stages of cavity formation. The time hardening law is a suitable candidate.

(b) The mechanism of creep fracture in the macroscopic crack tip zone is controlled by the local stress field which requires a deviatoric stress component ($\bar{\sigma}$) and a dilatational or normal stress (σ_{11}) component in its description.

6.2.2 Crack Propagation Model

Under the action of $\bar{\sigma}$, creep strain will accumulate in the uncracked ligament. When the creep strain in the element of material immediately ahead of the crack tip attains the value $\bar{\varepsilon}_f$, the crack will advance. The stress producing this strain is called the equivalent fracture stress ($\bar{\sigma}_f$) and is considered to be the average stress acting on the element which in this case, is taken as the value of $\bar{\sigma}$ at a point 0·125mm (i.e. half of element width) ahead of the macroscopic crack tip. The initial value of this stress can be obtained from Figures 81 to 84. All subsequent values

of $\bar{\sigma}_f$ associated with the fracture of neighbouring elements must however, be calculated from a combined knowledge of the apparent and 'true' functional relationship between $\bar{\sigma}$ and distance. Although there is reasonable agreement between these two relationships, a small adjustment to the simple model is necessary such that it agrees with the numerical analysis results and the effect of constraint. In doing this, material behaviour will be predicted more accurately. This adjustment can be accomplished by first calculating the appropriate apparent stress ($\bar{\sigma}_E$) using Equations 83 to 86, and then factoring the results by $M = \frac{\bar{\sigma}}{\bar{\sigma}_E}$ to obtain the 'true' stress ($\bar{\sigma}$). The assumptions made in this analysis will result in M remaining unchanged as the macrocrack propagates through the section. As an example of M, the magnitude of $\bar{\sigma}$ and $\bar{\sigma}_E$ acting on the first element in the normalised and tempered material undergoing plane stress deformation (Figure 81) is 225 and 280 MNm^{-2} respectively. Thus, M = 0.80. Similarly, for the same material undergoing plane strain deformation M = 0.81. Values of M covering all the relevant test parameters are shown in Table 10. It can be seen that the correction factors are close to unity indicating that the simple model is satisfactory. These factors have been used to reanalyse the experimental crack velocity data in terms of $\bar{\sigma}_f$. This is valid providing the functional relationship between $\frac{\sigma_{II}}{\bar{\sigma}}$ or $\frac{\sigma_H}{\bar{\sigma}}$ and distance remains constant along the cracking plane.

Table 10 Equivalent Stress Quotient M

Heat Treatment	Specimen Geometry	M	
		Plane Stress	Plane Strain
N & T	C.T.	0.80	0.81
N & T	C.C.P.	1.06	1.89
Q & T	C.T.	1.0	1.40
Q & T	C.C.P.	1.22	1.67

It is clear from Figures 89 and 37, that $\bar{\sigma}_f$ improves the overall correlation of crack velocity data obtained from normalised and tempered C.T. specimens. The effect is most marked in the Stage II growth area (Section 4). Similarly, if Figures 33 and 34 are reanalysed (Figure 90), data correlation is again improved. In this case, the scatter in Stage II data has been reduced by such an extent that the residuals can be accounted for by the inherent experimental errors and material variability.

A numerical creep stress analysis of the C.T. and C.C.P. structures is expensive and insufficient funds were available for a complete analytical coverage of all the test variables considered in the experimental programme. In order to reanalyse experiments that were not modelled by the numerical analysis, it has been assumed that the observed invariance between the ductility parameters $\frac{1}{\omega}$ and δ_i, and crack length in all but the low load tests, is an indication of the existence of an identical local crack tip fracture stress field. Thus, $\bar{\sigma}_f$ in these tests can be calculated by using the appropriate value of M (Table 10). The results of using this method for reanalysing the remainder of the experimental creep crack velocity data are shown in Figures 91 to 94.

Figures 91, 92 and 93 demonstrate the good agreement between creep crack velocity and $\bar{\sigma}_f$ in the C.T. and C.C.P. geometries in both the normalised and tempered, and quenched and tempered materials. These results contrast with the generally poor correlation obtained when K_A or σ_R is used (Section 4). A comparison of Figures 94 and 57 also demonstrates how effective is $\bar{\sigma}_f$ in correlating crack velocity data in the ½Cr½Mo¼V alloy. In this instance, the scatter in crack velocity data is reduced from approximately two orders of magnitude using K_A as the correlating parameter, to less than one order of magnitude using $\bar{\sigma}_f$.

It is interesting to note that the results from the C.C.P. tests are in accord with the observations of Nicholson (1975) on the relationship between crack velocity and net section stress which in this geometry, is

equivalent to the reference stress (see Equation 34). This accordance can be explained by referring to Figure 83 which shows that a simple relationship exists between net section stress and the equivalent fracture stress $\bar{\sigma}_f$. Thus, although the net section stress may not in general be the correct stress component, it does reflect the level of $\bar{\sigma}_f$. A correlation between creep crack velocity and net section stress in the present cast CrMoV C.C.P. tests is therefore to be expected.

In the absence of a BERSAFE creep model of the long term tests, it has been assumed that the M values listed in Table 10 can be used to calculate the appropriate values of $\bar{\sigma}_f$ in these tests. Figures 90, 92 and 94 illustrate the excellent correlation obtainable between long and short term test data. These results contrast with the generally poor relationship obtained between long and short term tests when K_A or σ_R is used (see Section 4.8). However, the assumption is clearly questionable and further work is necessary in order to check the validity of these results.

The ability of $\bar{\sigma}_f$ to rationalise creep crack velocity data in CrMoV alloy steels from alternative sources of work (Holdsworth, 1974; Neate, 1977) is illustrated in Figures 95 and 96. Figure 95 shows the relationship between K_A and creep crack velocity in three specimen geometries where the section dimensions and the magnitude of the nominal direct and bending elastic stress components are either identical or very similar to those in the present C.T. and C.C.P. specimens. Assuming that the relaxed stress field in these specimen geometries is effectively the same, $\bar{\sigma}_f$ can be calculated from the appropriate value of $\bar{\sigma}_E$ (see Appendix) and from $\bar{\sigma}$ (Figures 81 to 84 inclusive). In doing this (Figure 96), the overall correlation of the velocity data is improved significantly. The results as plotted in Figure 96 are also consistent with those from the present work whose upper and lower bounds are also shown in Figure 96.

FIG. 89. VARIATION OF CREEP CRACK VELOCITY WITH EQUIVALENT FRACTURE STRESS, AT 550° C.

(NORMALISED AND TEMPERED 1CR 1MO ¼ V
FIG. 37. RE-ANALYSED)

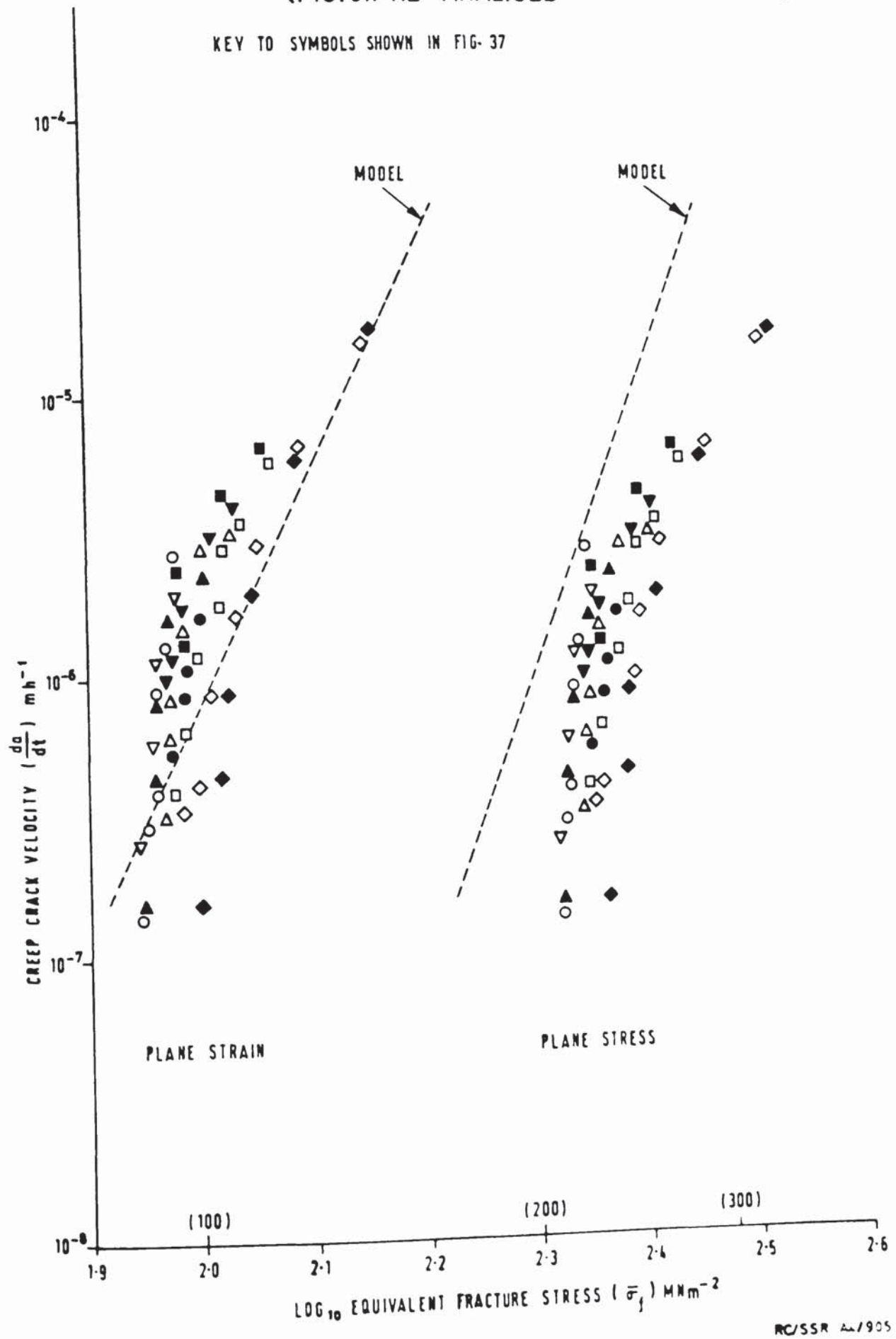

RC/SSR A1/905

FIG. 90. VARIATION OF CREEP CRACK VELOCITY WITH EQUIVALENT FRACTURE STRESS, AT 550° C.

(NORMALISED AND TEMPERED 1CR 1MO ¼ V
FIGS. 33 AND 34 RE-ANALYSED
PLUS FIG. 37.)

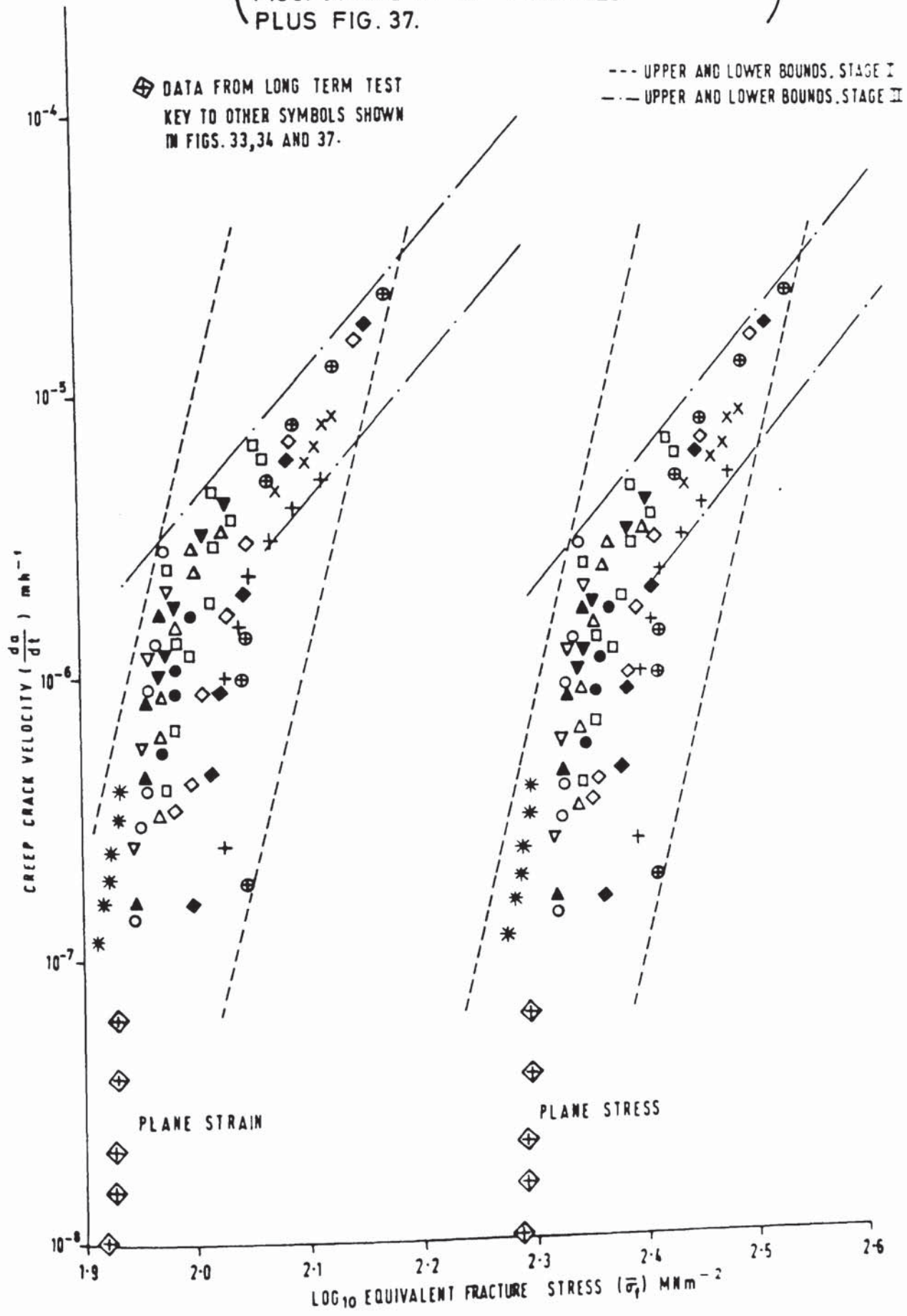

RC/SSR/A4/906

FIG. 91. VARIATION OF CREEP CRACK VELOCITY WITH EQUIVALENT FRACTURE STRESS, AT 550°C

(NORMALISED AND TEMPERED 1CR 1Mo 1/4 V
FIG. 49. RE-ANALISED)

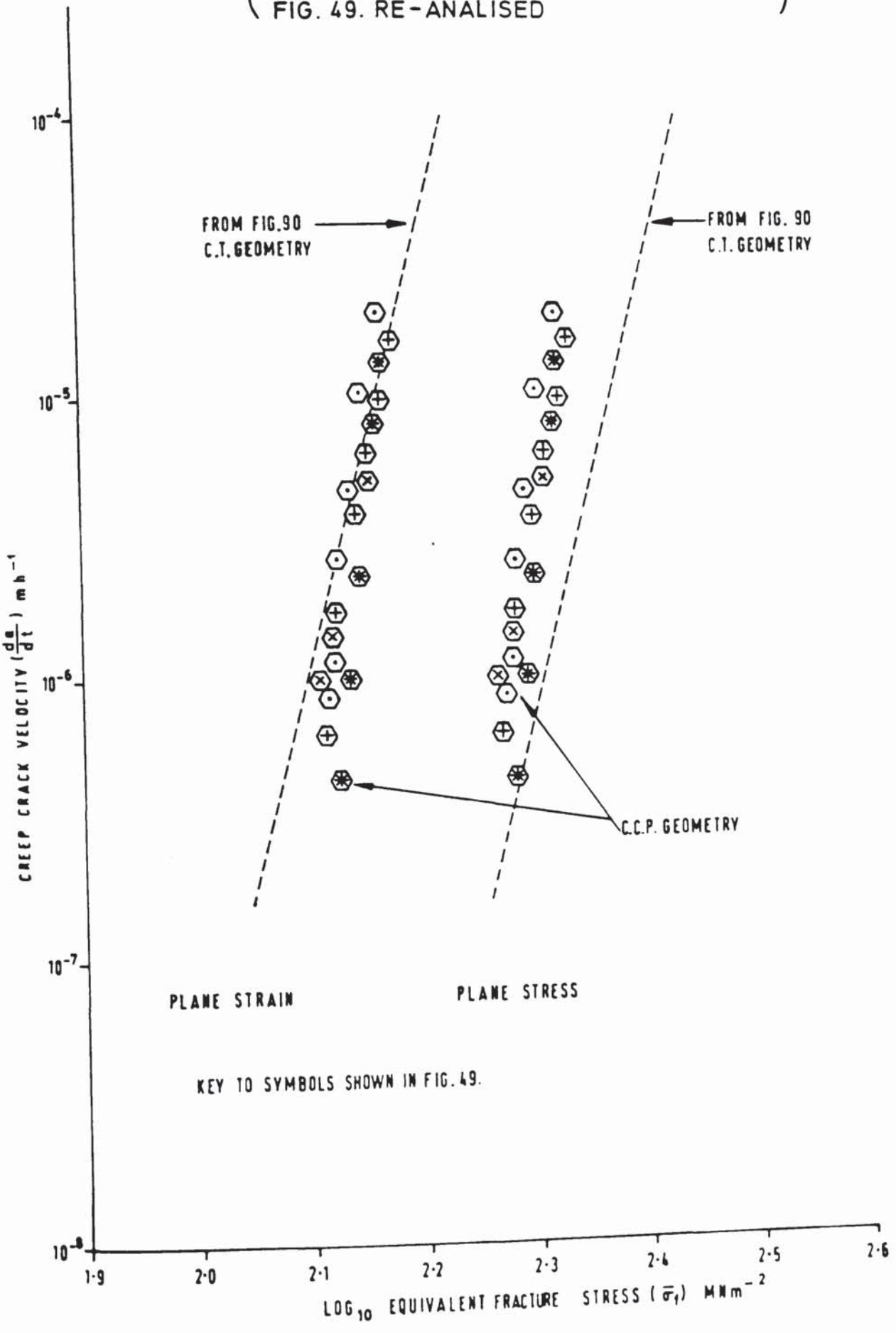

RC/SSR/A4/907

FIG. 92. VARIATION OF CREEP CRACK VELOCITY WITH EQUIVALENT FRACTURE STRESS, AT 550° C.

(QUENCHED AND TEMPERED 1 CR 1Mo ¼ V)
FIG. 42. RE-ANALYSED.

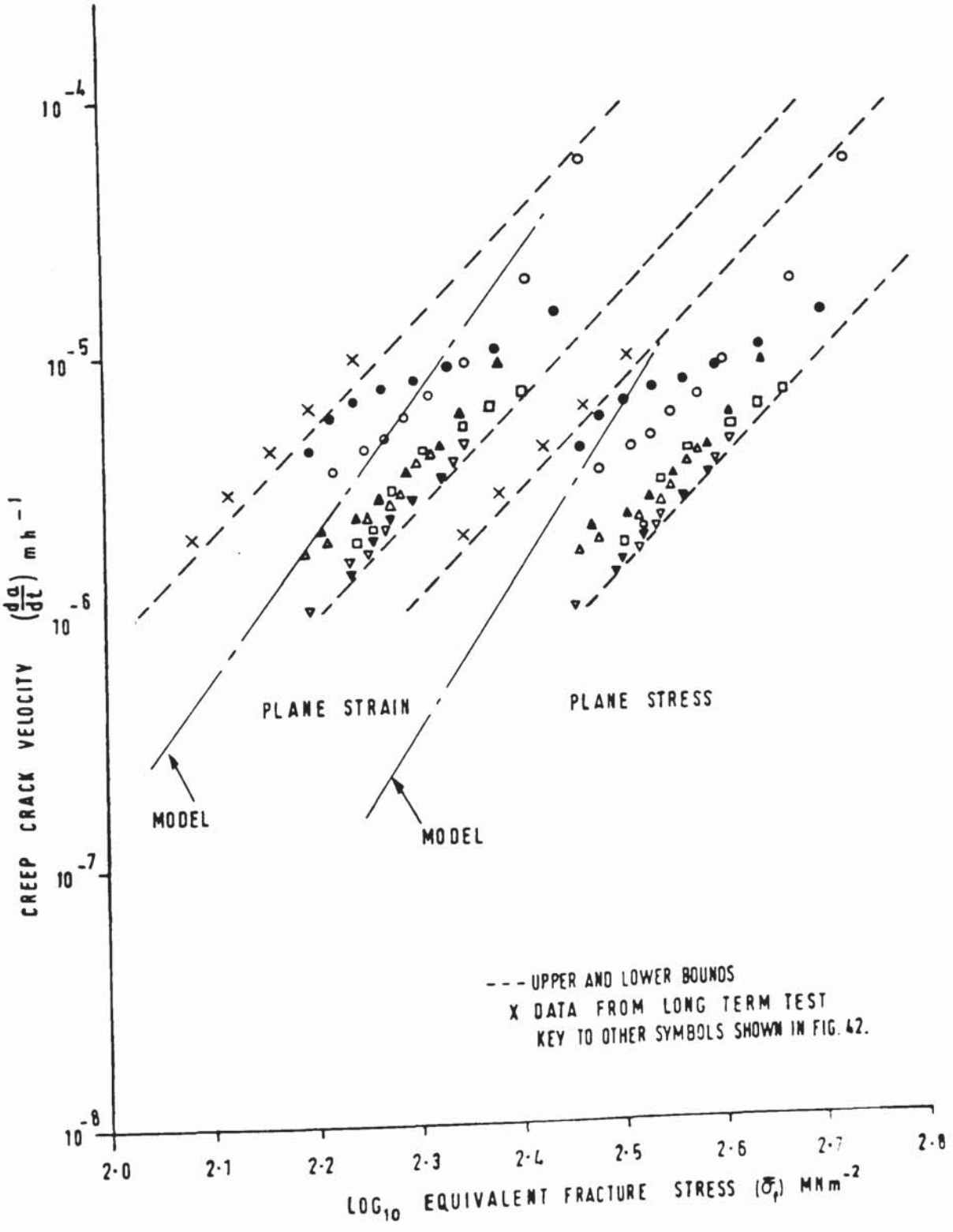

FIG. 93. VARIATION OF CREEP CRACK VELOCITY WITH EQUIVALENT FRACTURE STRESS, AT 550° C.
(QUENCHED AND TEMPERED 1 CR 1 MO ¼ V)
FIG. 54. RE-ANALYSED

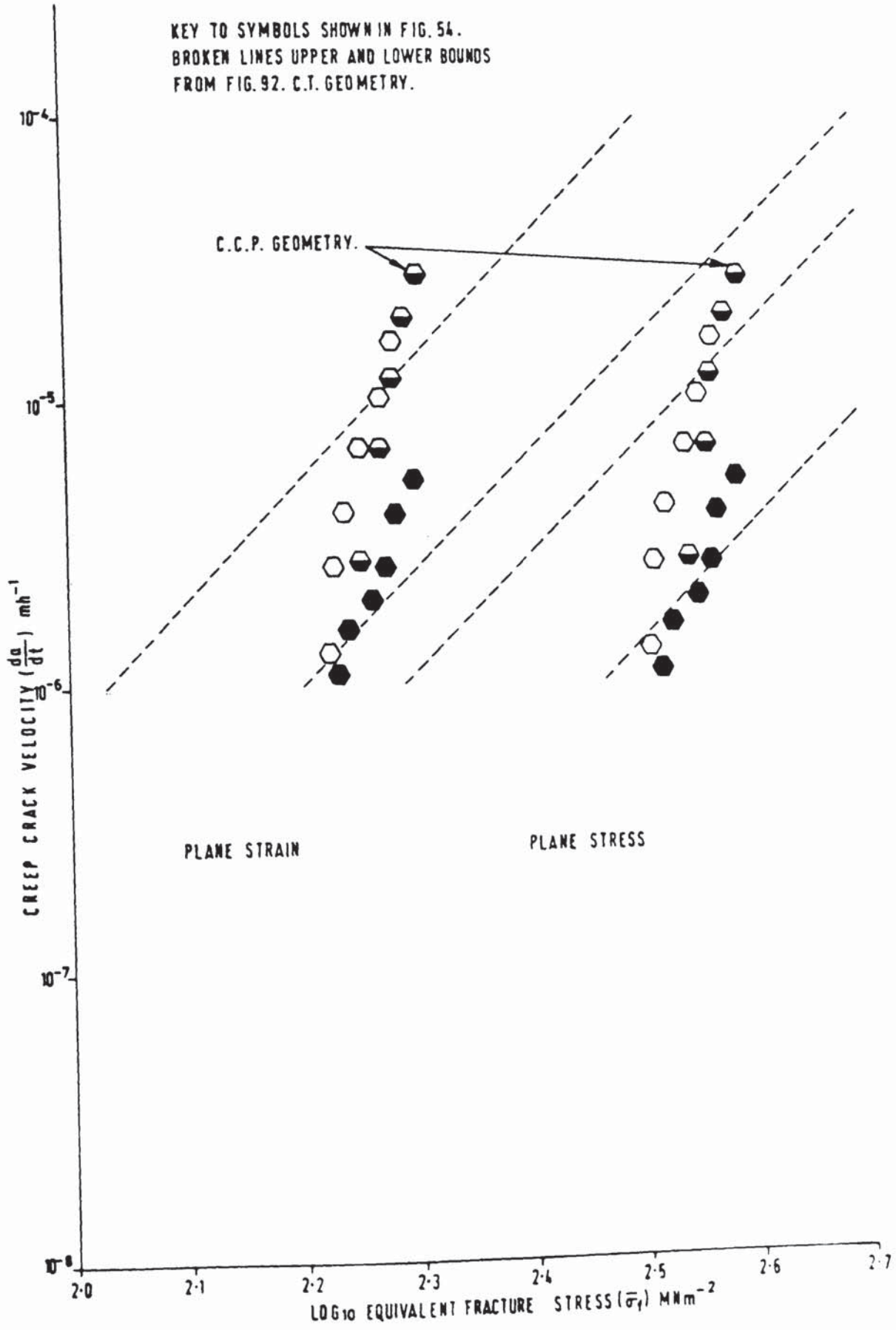

RC/SSR A4/909

FIG. 94. VARIATION OF CREEP CRACK VELOCITY WITH EQUIVALENT FRACTURE STRESS. AT 550°C

(NORMALISED AND TEMPERED ½ CR ½ Mo ¼ V
FIG. 57 RE-ANALYSED.)

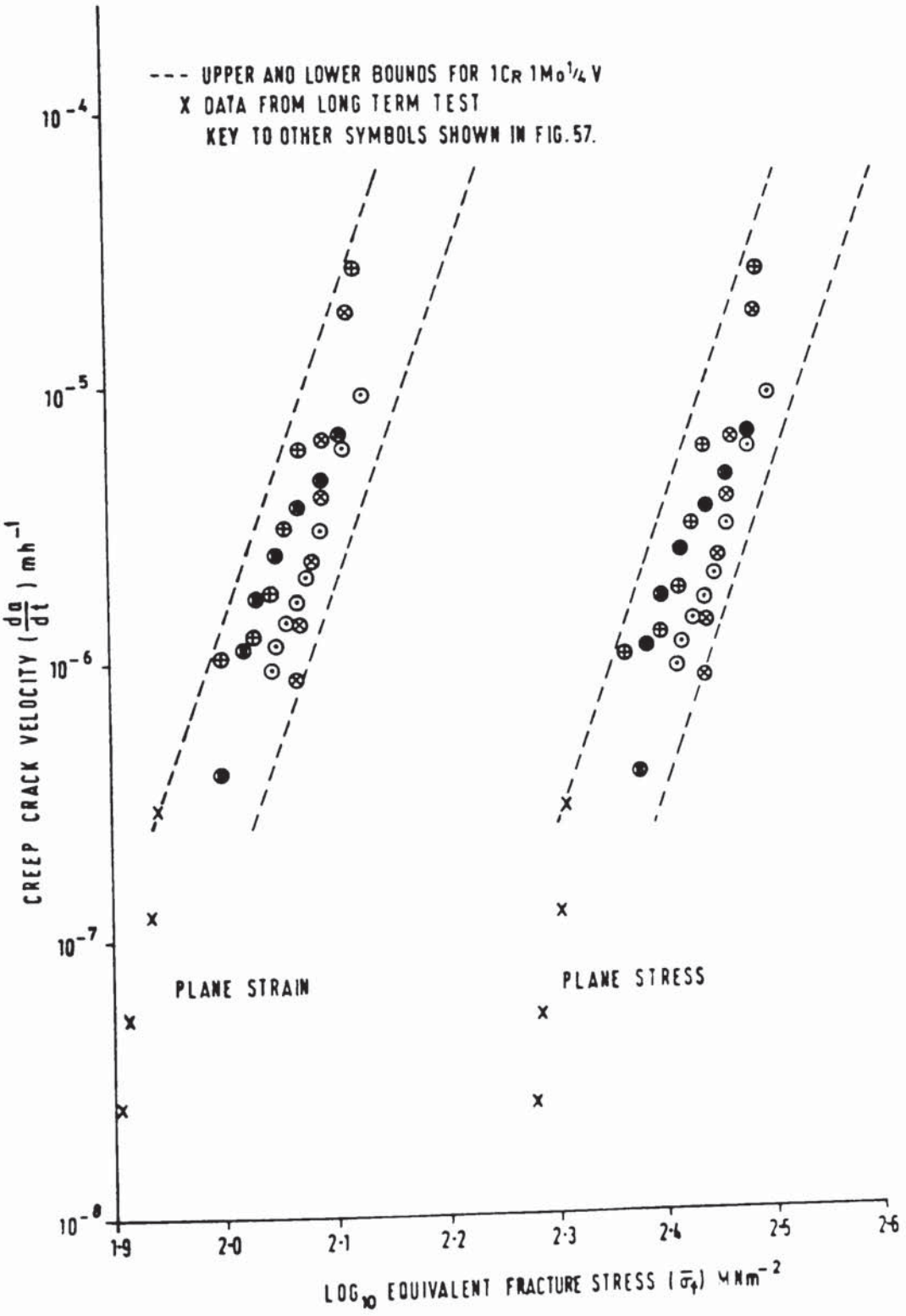

FIG. 95. VARIATION OF CREEP CRACK VELOCITY WITH STRESS INTENSITY, FROM PUBLISHED RESULTS.

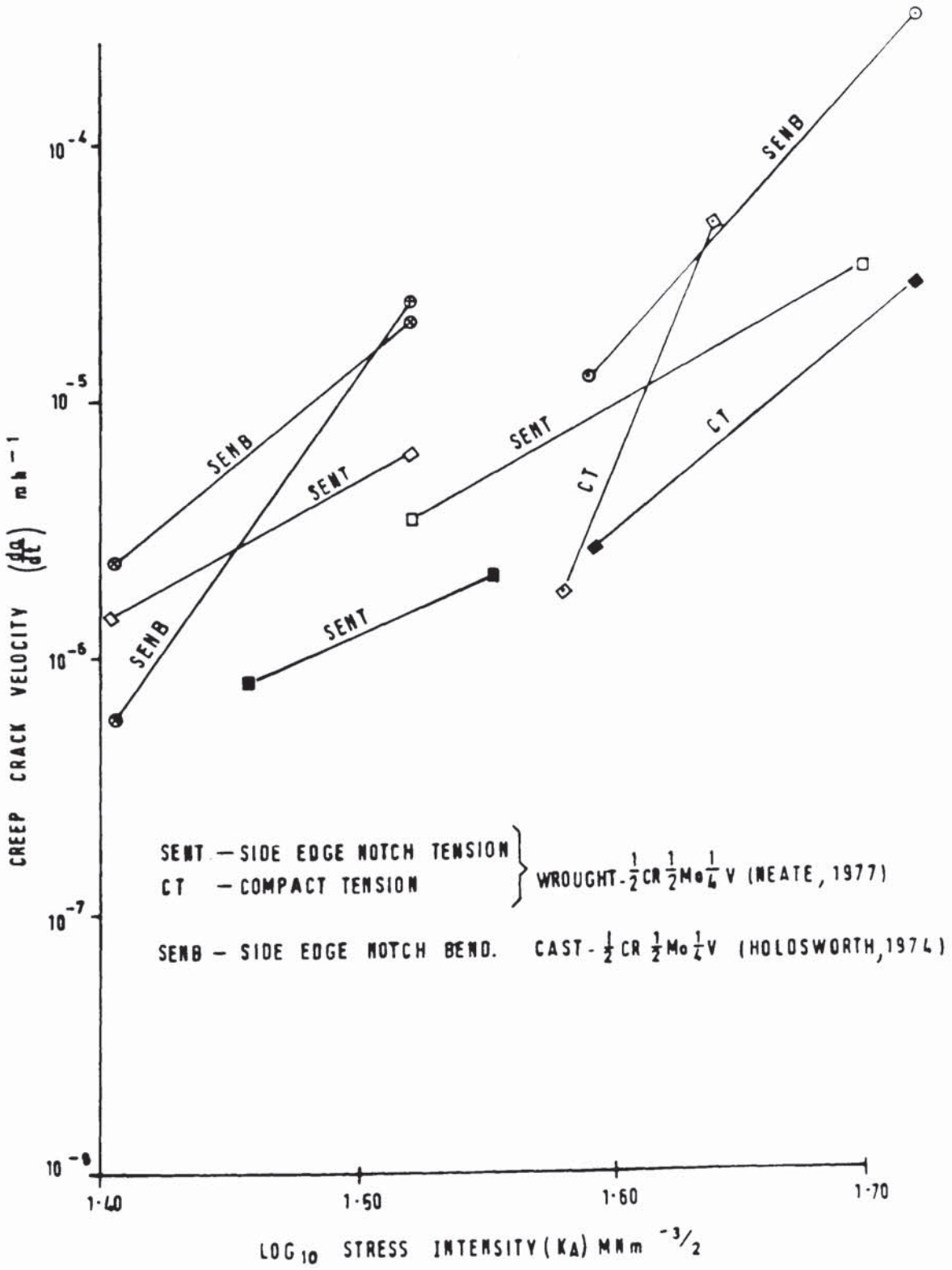

FIG. 96. DATA FROM FIG. 95 RE-PLOTTED IN TERMS OF EQUIVALENT FRACTURE STRESS.

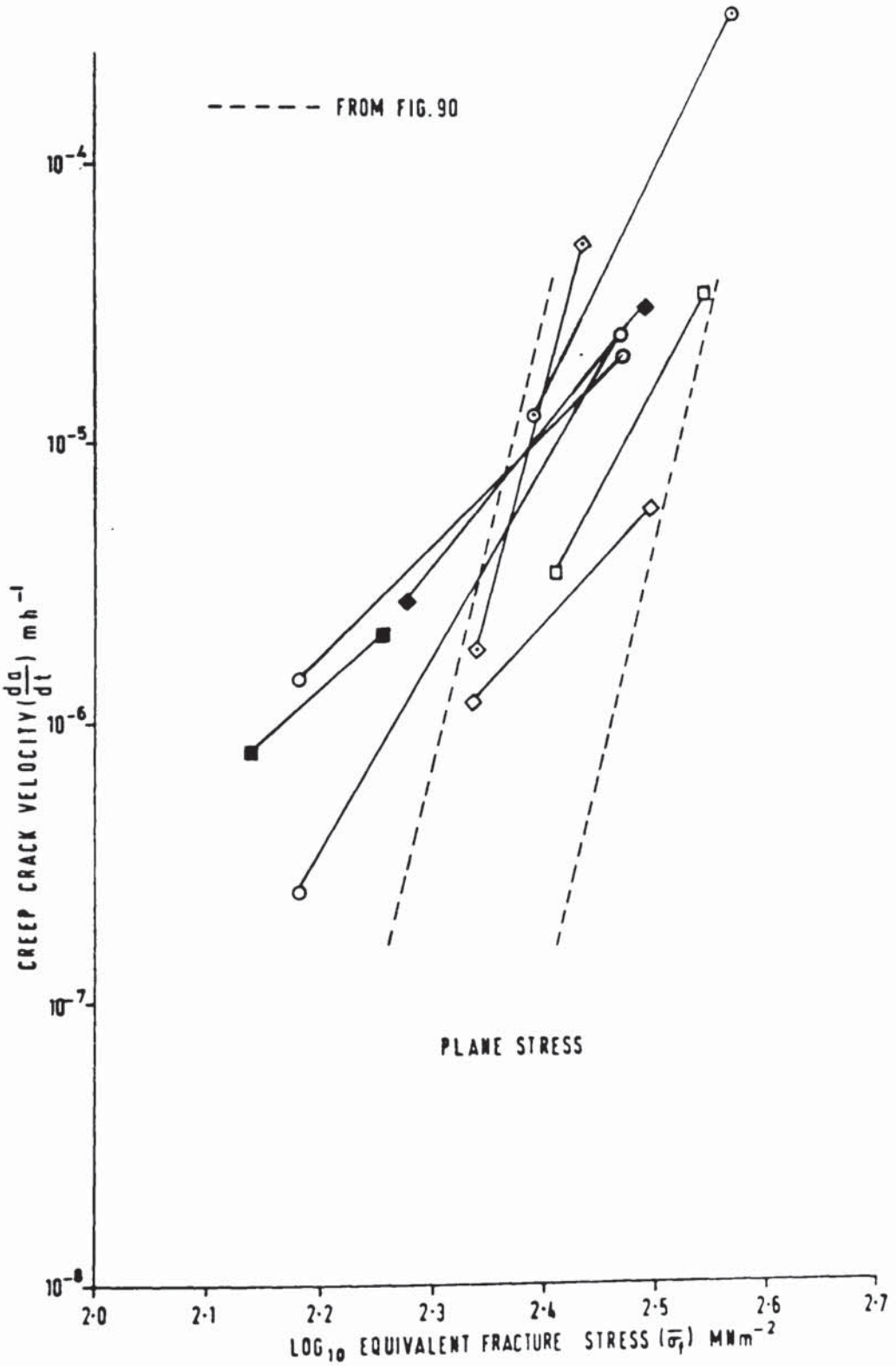

6.3 Application of Fracture Model to Service Problems

In order to ascertain the integrity of a defective component operating in the creep range it is necessary to know:

(a) The magnitude of the system stresses within the component.

(b) The components size and shape.

(c) The material creep laws. These normally take the form of empirically derived creep crack growth rate equations.

The system stresses can be thermally or mechanically induced, the proportion of which can vary from component to component. Residual stress fields can also be present. Thus, having established the nature and magnitude of the system stresses, they are then introduced into a geometrical model of the defective component in order to calculate the operative fracture stress. In cases where rapid defect assessments are required, it is usual to model components by using appropriate standard fracture toughness specimen geometries. This then allows crack tip stress fields to be calculated with comparative ease. More sophisticated finite element stress analysis techniques are generally reserved for the early stages of component design programmes. Both analytical techniques however, involve the problem of selecting an appropriate fracture stress and concomittant crack growth rate equation. The need for a pessimistic and hence safe life assessment has often meant that K_A and a growth rate equation based on the upper bound to the experimental data has been chosen. Unfortunately such an approach can result in high economic penalties when for example, generating plant is temporarily shut down or prematurely made obsolescent. An alternative approach is to adopt the near tip equivalent fracture stress concept as derived in this Thesis. It has been demonstrated that this stress ($\bar{\sigma}_f$) is capable of rationalising macroscopic creep fracture behaviour in CrMoV alloy steels when subjected to either plane stress or plane strain deformation. Clearly the selective nature of $\bar{\sigma}_f$ will allow the appropriate creep crack growth equation to be used for thick

or thin section components and as a consequence, reduce the level of the economic penalties.

In general, empirically derived creep crack growth laws (see Section 2.7.1) assume that a double log plot of creep crack velocity and the 'fracture stress' is a straight line. This assumption has been shown to be erroneous for the specific case of the normalised and tempered alloys when in the form of a C.T. specimen. For this case, two basic equations would need to be derived, one covering the initial stage of crack growth (Stage I) and the other the middle stage (Stage II). Of the two, an equation including $\bar{\sigma}_f$ and covering Stage II growth will be more realistic in practical situations as it covers that stage of growth where the crack is fully developed. Experience in manipulating crack growth equations of the form $\frac{da}{dt} = C\,\bar{\sigma}_f^{\,p}$ has shown that problems often become more tractable if stress exponents are small. The lower the stress exponent the more tolerant becomes the analytical procedure to errors in system stress calculations. These errors often originate from a lack of detailed knowledge of the level of the residual stress or its contribution to the fracture process. In this context, the service investigator or component designer will be at an advantage if he uses creep crack growth equations based on Stage II growth.

To date, all creep crack growth equations in ferrous and non-ferrous materials have been generated by time consuming and expensive experimental creep programmes. Ideally, if a method could be found of producing crack growth data which does not require a specialised testing programme and uses the plethora of published uniaxial creep data, the results would be economically rewarding. Such a method is suggested by the fracture model discussed in Section 6.2.2. By mathematically modelling the advance of a macroscopic creep crack by the successive rupture of elements which fracture upon accumulating the appropriate amount of strain, and by using a time hardening law to calculate the creep rupture time of each element, it is

possible to construct crack velocity/ $\bar{\sigma}_f$ plots from which crack growth rate equations can be derived. The model relies on the concept of cumulative damage in each element ahead of the advancing crack tip.

6.4 Cumulative Damage Creep Fracture Model

The assumptions on material behaviour and conditions for growth of a macroscopic creep crack are as follows.

6.4.1 At the instant of crack initiation the equivalent strain profile in the uncracked ligament along the projected cracking plane in the cast CrMoV alloy steels is as shown in Figures 78 and 79.

6.4.2 The critical equivalent fracture strain ($\bar{\varepsilon}_f$) is the strain that has accumulated at the tip of the pre-existing crack during the incubation period (Figures 78 and 79).

6.4.3 Following an infinitesimal amount of creep cracking at the end of the incubation period, the crack advances when the accumulated strain in the element adjacent to the crack tip attains the value $\bar{\varepsilon}_f$. The former strain will be composed of strain that has accumulated during the incubation period ($\bar{\varepsilon}_A$, Figures 78 and 79) which is taken to be the average strain in the element, and strain that has developed following crack initiation (i.e. the material ahead of the advancing crack tip will have a strain history).

6.4.4 Equivalent strain develops in the elements under the action of the equivalent stress distributions which are described in Section 6.2.2. The active stress in each element is taken to be that lying mid-way across the element. Figure 97 shows schematically the first and subsequent equivalent stress distributions ahead ofan advancing crack. In element 1, the strain $\bar{\varepsilon}_A^1$ will develop under the action of the steady state stress $\bar{\sigma}_1$. This element will rupture when the total accumulated strain $\left(\bar{\varepsilon}_A^1 + \bar{\varepsilon}_A\right)$ attains the value $\bar{\varepsilon}_f$. Element 2 will rupture in a similar manner following the action of the stresses $\bar{\sigma}_{21}$ and $\bar{\sigma}_2$. $\bar{\sigma}_{21}$ is the active stress in element 2 during the rupture process of the first element and will

FIG. 97. SCHEMATIC EQUIVALENT STRESS PROFILES AND ACTIVE STRESSES.

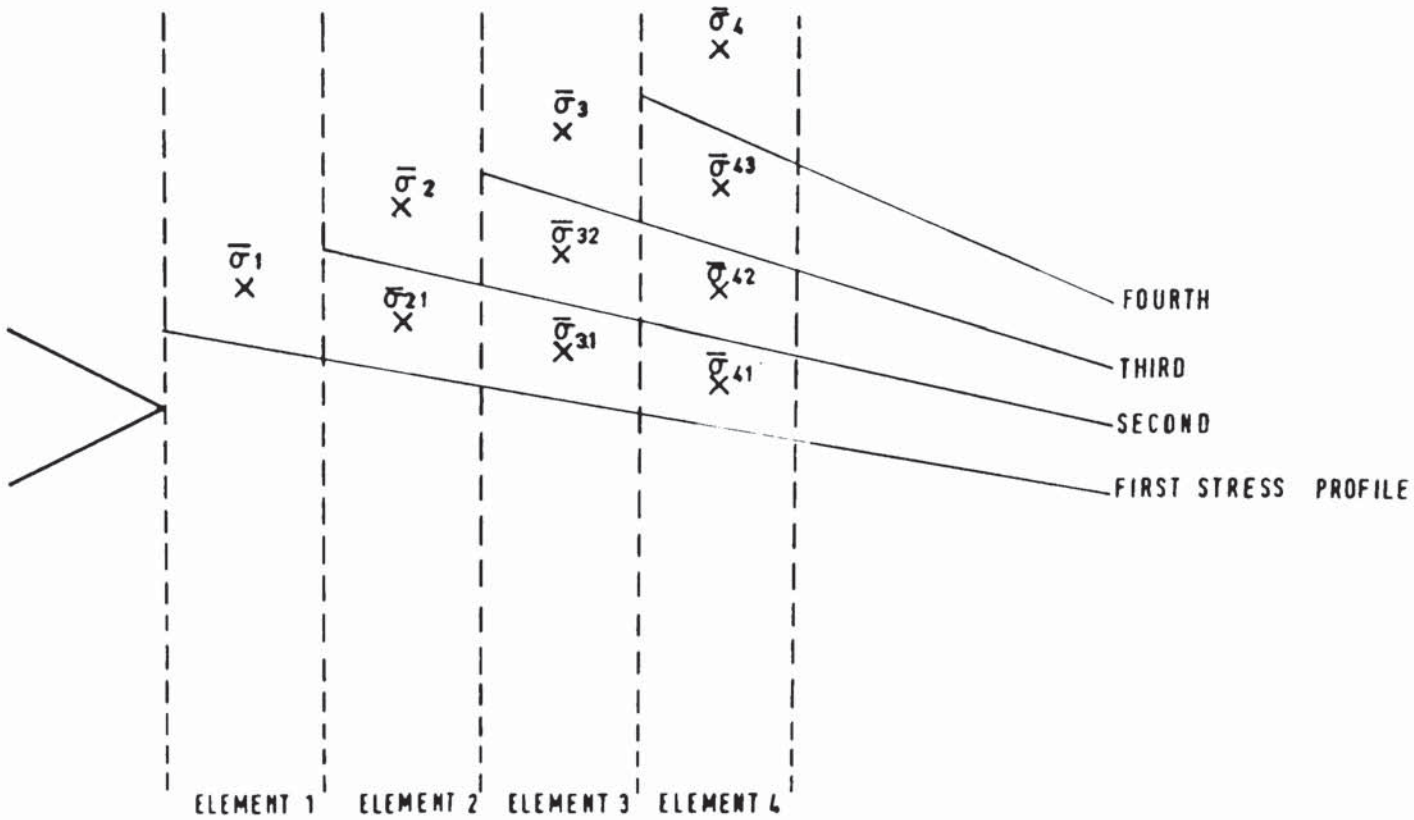

RC/SSR/A4/91

generate the strain $\bar{\varepsilon}_A^{21}$. The magnitude of this strain will depend on the time taken to rupture the first element since $\bar{\sigma}_{21}$ will cease to 'exist' when this element ruptures. $\bar{\sigma}_2$ is the active stress in element 2 following the rupture of the first element and will generate the strain $\bar{\varepsilon}_A^2$. Element 2 will rupture when the total accumulated strain $\bar{\varepsilon}_A^{21} + \bar{\varepsilon}_A^2 + \bar{\varepsilon}_A = \bar{\varepsilon}_f$. The development of strain in the other elements will follow an identical pattern.

6.4.5 Equivalent strain develops according to a time hardening creep law which from Equations 73 and 74 can be expressed as

$$\bar{\varepsilon} = B\ \bar{\sigma}^y t^z \tag{87}$$

Thus, the time (t) taken to generate a given amount of creep strain($\bar{\varepsilon}$) in any element subjected to either a main equivalent stress ($\bar{\sigma}_1$ type) or a secondary stress ($\bar{\sigma}_{21}$ type) can be obtained by rearranging Equation (87) to give

$$t = \left(\bar{\varepsilon}\ B^{-1}\ \bar{\sigma}_f^{-y} \right)^{\frac{1}{z}} \tag{88}$$

or

$$t_f = \left(\bar{\varepsilon}_f\ B^{-1}\ \bar{\sigma}_f^{-y} \right)^{\frac{1}{z}} \tag{89}$$

where t_f is the element rupture time and $\bar{\sigma}_f$ is the equivalent fracture stress which is equivalent to a main stress. Equation (89) will only apply when an element has no strain history. However, when a strain history as described in Section 6.4.4 is present, the expression for element rupture time will be

$$t_f = \left[\left(\bar{\varepsilon}_f - \bar{\varepsilon}_A \right) B^{-1}\ \bar{\sigma}_f^{-y} \right]^{\frac{1}{z}} = \left[\bar{\varepsilon}_A^1\ B^{-1}\ \bar{\sigma}_f^{-y} \right]^{\frac{1}{z}} \quad \text{for the first element}$$

and

$$t_f = \left[\left(\bar{\varepsilon}_f - \bar{\varepsilon}_A - \bar{\varepsilon}_A^{21} \right) B^{-1}\ \bar{\sigma}_f^{-y} \right]^{\frac{1}{z}} = \left[\bar{\varepsilon}_A^2\ B^{-1}\ \bar{\sigma}_f^{-y} \right]^{\frac{1}{z}} \quad \text{for the second element}$$

or in general terms for any element n

$$t_f = \left[\bar{\varepsilon}_A^n\ B^{-1}\ \bar{\sigma}_f^{-y} \right]^{\frac{1}{z}} \tag{90}$$

where $\bar{\sigma}_f$ is the appropriate equivalent fracture stress in element n and $\bar{\varepsilon}_A^n$ is the difference between $\bar{\varepsilon}_f$ and the previously accumulated strain.

6.4.6 Analytical Procedure and Results

Crack length/time plots were constructed using equations of the type 87 and 90, material creep laws as defined by Equations 73 and 74, the equivalent stress profiles (Section 6.2.2) and the corresponding equivalent strain profiles (Figures 78 and 79). These plots were in turn used to construct traces of crack velocity against $\bar{\sigma}_f$.

Figure 98 compares predicted plane strain crack velocity data and the experimental results from a 50mm thick C.T. specimen. It is clear that the two traces are almost identical in terms of shape and position on the plot. The ability to predict so accurately Stage I and Stage II type crack growth behaviour suggests that the cumulative damage model is both basically sound in its assumptions and realistic in its interpretation of material behaviour. In going through the iterative procedure of calculating accumulated creep strain, it appeared that the observed high rates of acceleration in creep crack growth tests could be explained by the presence of high incubation strains in the crack tip regions. Apparently, very little additional creep strain is required to fracture those elements lying within the crack tip region and under these circumstances the crack will accelerate rapidly from its initial stationary state (Stage I). Eventually however, the crack tip will run into less damaged material which together with the relatively low section stresses and hence low rate of creep strain accumulation, will result in a period of decreasing acceleration. This in turn leads to a stage where the combination of increasing stress, the stress and time dependence of the strain, and the strain history, causes the crack tip to move such that a constant gradient exists between its velocity and the fracture stress. This pattern of behaviour has been observed in the 1CrlMo¼V alloy in both heat treated forms.

The sensitivity of the model to changes in the value of the constant and the stress and time exponents in the creep law is small. In general, batch to batch variations in creep properties are only reflected in the

FIG. 98. COMPARISON OF PREDICTED AND EXPERIMENTAL EQUIVALENT STRESS/CRACK VELOCITY PLOT. FOR NORMALISED AND TEMPERED 1CR 1Mo 1/4 V, PLANE STRAIN DEFORMATION.

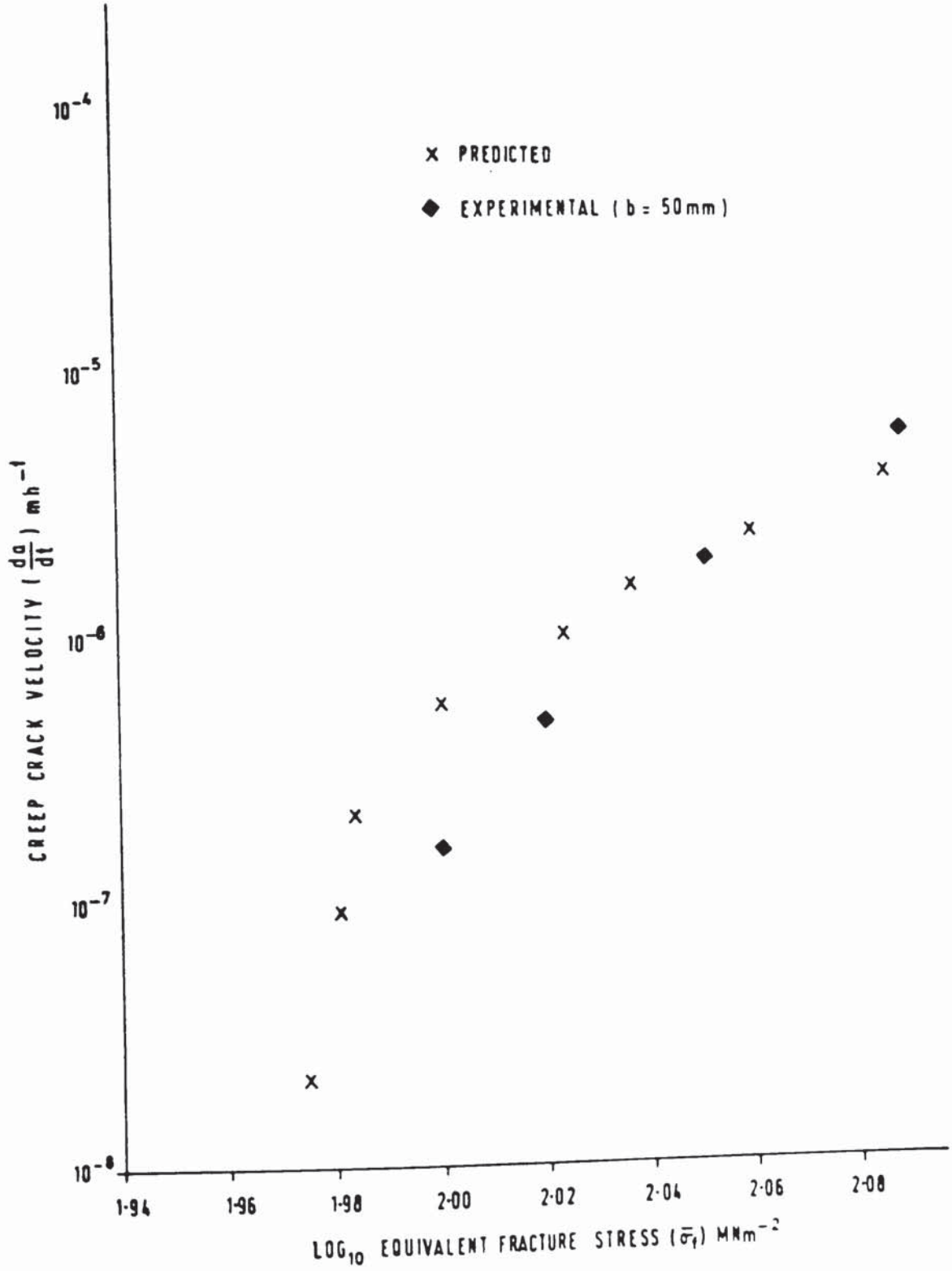

constant and not the exponents (Townley, 1972). For a ± 20% variation in the value of the constant, predicted crack velocities only change by ±0.1 log cycle. Thus the relationship between the predicted and experimental results shown in Figures 89 and 92 will be effectively unchanged.

The comparative ease with which creep crack growth behaviour can be predicted without recourse to complicated laboratory test programmes is encouraging and warrants further work. The technique can be refined by improving the continuity equations describing material behaviour in the uncracked ligament and by using more sophisticated creep laws. In addition, an understanding of the relationship between equivalent fracture strain and experimentally measurable fracture parameters, would enable data such as that given in Figures 60 and 61 to be used in the analysis. The work in this Thesis has shown that thickness is very important and several ways have been suggested in which constraint effects can be generalised. Ideally, if plane specimen creep ductility data could be used to predict the behaviour of thick section components, there would be no need to perform notched creep tests. At present this cannot be done and so we are limited to predicting only the behaviour of thin components.

The application of this cumulative damage model is not however, restricted to just cast CrMoV alloy steels. Providing the mechanisms of creep in a material can be classified as deformation controlled as opposed to diffusion controlled, the model can be used. There are several alloy steels presently in use in the CEGB which fall within the former category, for which little or no creep crack growth data is available. A possible solution is to compile a library of BERSAFE creep results covering all relevant component geometries, and combine this with an analytical cumulative damage creep fracture model.

6.5 Closing Statement

The work has shown that $\bar{\sigma}$ can describe macrosocpic creep fracture in cast CrMoV alloy steels whose creep stress exponents lie between 3.7 and 5.8 (Equations 73 and 74). For these materials and for the specimen geometries examined, the amount of near crack tip stress relaxation is such that neither K_A nor σ_R can describe the steady state stress distribution. The use of $\bar{\sigma}$ is not however, confined to describing creep fracture in alloy steels whose creep stress exponents lie within the above limits. $\bar{\sigma}$ can still be used to describe the stress distribution for the limiting case where the exponent tends to unity and a K correlation can be used, and where the exponent tends to infinity and a reference or net section stress correlation is applicable (Barnby and Nicholson, 1977).

The incorporation of the Von Mises equivalent stress into a model of macroscopic creep fracture is a new concept which has yet to be tried and tested. This Thesis has shown that the concept is scientifically sound and offers considerable advantages to the investigator and component designer, over existing theories. Whether it will complement or supplant present theories will depend primarily on its ability to underwrite component integrity to the satisfaction of all. Probably the most appropriate course of action to take is to re-analyse component case histories using the new concept to see whether known behaviour patterns could have been predicted. If the results are affirmative, then it could be gradually phased into existing defect assessment procedures.

Conclusions

1. In tests on C.T. and C.C.P. specimens of normalised and tempered, and quenched and tempered cast $\frac{1}{2}Cr\frac{1}{2}Mo\frac{1}{4}V$ and $1Cr1Mo\frac{1}{4}V$ steel at 550°C, it is found that a satisfactory correlation between creep crack velocity and the apparent stress intensity factor K_A or reference stress σ_R can only be achieved under very limited testing conditions. In the general case where initial crack length or applied loads are varied, neither stress function correlates the velocity data.

2. A double log plot of creep crack velocity and stress intensity or reference stress for the materials under investigation is not a straight line. A better description is provided either by a curve whose gradient decreases as the creep crack develops or alternatively, by two straight lines.

3. The development of creep cracks appears to fall into two distinct stages. In Stage I, immediately after crack initiation, crack velocity is low but acceleration high. In Stage II, the crack velocity continues to increase while acceleration decreases.

4. It is observed in all tests in the cast CrMoV alloys that a certain minimum displacement must be achieved for creep crack initiation and propagation. The displacement associated with initiation has been measured in terms of the crack opening displacement δ_i while for propagation, the crack aspect ratio $\frac{1}{\omega}$ has been used. Since δ_i and $\frac{1}{\omega}$ are measures of ductility, it is found that they both vary with applied load in a similar manner to the fracture strain of smooth bar creep rupture specimens. It is also found that both δ_i and $\frac{1}{\omega}$ in tests at constant initial K_A, σ_R and thickness, is invariant with crack length in all the materials and specimen geometries investigated.

5. Creep crack ductility at constant initial K_A or σ_R in the C.T. and C.C.P. geometries, as measured by δ_i or $\frac{1}{\omega}$, is found to decrease with increasing crack tip constraint in both the normalised and tempered, and quenched and tempered 1Cr1Mo¼V alloy. The variation of creep crack velocity with degree of constraint was less conclusive.

6. The creep crack ductility as measured by the crack velocity, δ_i and $\frac{1}{\omega}$ in C.T. and C.C.P. tests of the 1Cr1Mo¼V is found to be comparable.

7. The creep ductility of the ½Cr½Mo¼V alloy as measured by K_A, σ_R, δ_i and $\frac{1}{\omega}$, has been found to be greater than that of the 1Cr1Mo¼V alloy. This phenomenon is considered to be a reflection of the inherently more ductile microstructure of the ½Cr½Mo¼V alloy.

8. Optical metallography revealed that creep cracking in both the 1Cr1Mo¼V and ½Cr½Mo¼V alloy was intergranular and occurred primarily along the ferrite grain boundaries. Macrocracks formed by the nucleation and linkage of 'r' type cavities.

9. By using a numerical finite element creep stress analysis programme based on the classic theories of plastic flow, it has been shown that the local stress field ahead of an incubating creep crack in the two CrMoV alloys when in the form of a C.T. or C.C.P. specimen cannot be described by K_A. Neither can σ_R describe the steady state stress distribution in the C.T. geometry for either heat treated form of the 1Cr1Mo¼V alloy. The numerical analysis has also shown that the amount of stress relaxation ahead of an incubating creep crack is very dependent on constraint and material creep properties. A shift from plane stress deformation to plane strain deformation, and a decrease in the creep stress exponent in the material creep law, both result in lower amounts of stress relaxation.

10. By reasoning that the mechanism of creep fracture in the macroscopic crack tip zone is controlled by the local stress field which requires a deviatoric stress component ($\bar{\sigma}$) and a dilatational or normal stress (σ_{11}) component in its description, it has been found that the numerical stress analysis results can be used to rationalise the experimental observations on creep ductility. Since in CrMoV alloys, the nucleation and growth of cavities and consequently the development of macrocracks is dependent upon $\bar{\sigma}$ and $\bar{\sigma}_{11}$, it has been reasoned that creep cracks will develop relatively faster during plane strain deformation and when creep stress exponents are low.

11. From a development of the effect of $\bar{\sigma}$ and $\bar{\sigma}_{11}$ on the creep fracture process in cast CrMoV alloys, it has been found that creep crack growth in the C.T. and C.C.P. geometries can be described in terms of a near tip equivalent fracture stress ($\bar{\sigma}_f$). By assuming that the numerical predictions of the functional relationship between the stress field components and distance ahead of an incubating creep crack holds when the crack starts to grow, it is found that $\bar{\sigma}_f$ can rationalise all of the experimental crack velocity data. Neither K_A nor σ_R can do this.

12. A fracture model which is based on the concept of cumulative damage, uses $\bar{\sigma}_f$ and assumes a critical equivalent fracture strain ($\bar{\varepsilon}_f$) for crack growth, has been developed and found to be capable of predicting the behaviour of propagating creep cracks in cast CrMoV C.T. and C.C.P. specimens undergoing plane stress or plane strain deformation. In its present form, the model can only predict crack velocities in thin section components. Further knowledge on the effect of constraint on $\bar{\varepsilon}_f$ is required before the model can be used on large section components.

ACKNOWLEDGEMENTS

I would like to thank my supervisors, Professor J. T. Barnby, Dr. C. L. Formby and Dr. E. Taylor, for their guidance and encouragement during the course of this work. I am indebted to my colleagues for numerous discussions.

The work was carried out at the North Western Region Scientific Services Laboratories of the Central Electricity Generating Board. I wish to thank Dr. G. Oates, the Research Manager, for providing the facilities, and Mr. W. F. Cusworth, the Director-General, for permission to embark upon this work.

APPENDIX

Calculation of Outer Fibre Equivalent Elastic Stress

1. Side Edge Notch Tension Geometry (Neate, 1977)

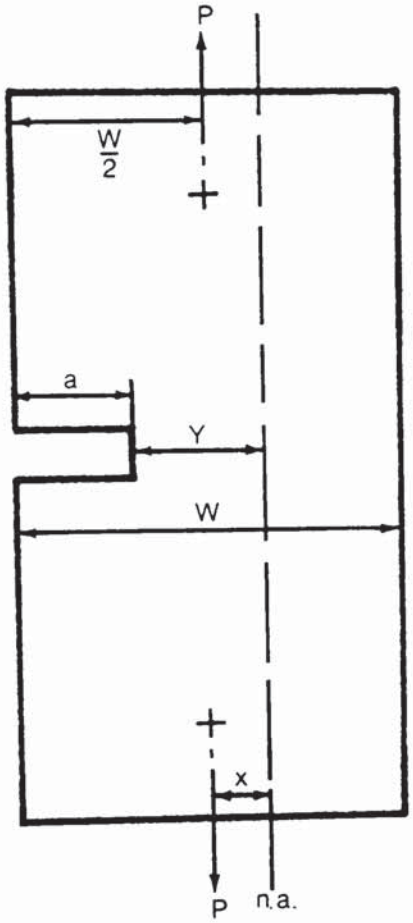

P - Load
W - Width
b - Breadth
a - Crack Length

In bending, the moment M about the neutral axis = Px

$$= P\left[\frac{W}{2} - \left(\frac{W - a}{2}\right)\right]$$

$$= \frac{Pa}{2} \qquad (A1.1)$$

For the outer fibre, $Y = \left(\frac{W - a}{2}\right)$ (A1.2)

The second moment of inertia $I = \frac{b\,(W - a)^3}{12}$ (A1.3)

Thus, from Equations A1.1, A1.2 and A1.3, the outer fibre bending stress $\sigma_B = \frac{MY}{I}$

$$= \frac{3\ Pa}{b\ (W-a)^2} \qquad \text{(A1.4)}$$

The direct stress component ahead of the notch, $\sigma_D = \frac{P}{b\ (W-a)}$ (A1.5)

Adding Equations A1.4 and A1.5 gives the total outer fibre stress

$$\sigma_T = \frac{3\ Pa + P(W-a)}{b\ (W-a)^2} \qquad \text{(A1.6)}$$

Thus, from Equations A1.6, 87 and 88, the outer fibre equivalent elastic stress $\bar{\sigma}_E$ is:

For Plane Stress, $\bar{\sigma}_E = \left[\frac{3\ Pa + P(W-a)}{b\ (W-a)^2}\right]$ (A1.7)

For Plane Strain, $\bar{\sigma}_E = \frac{1}{2.6}\left[\frac{3\ Pa + P(W-a)}{b\ (W-a)^2}\right]$ (A1.8)

2. Three Point Bend Side Edge Notch Geometry. (Holdsworth, 1974)

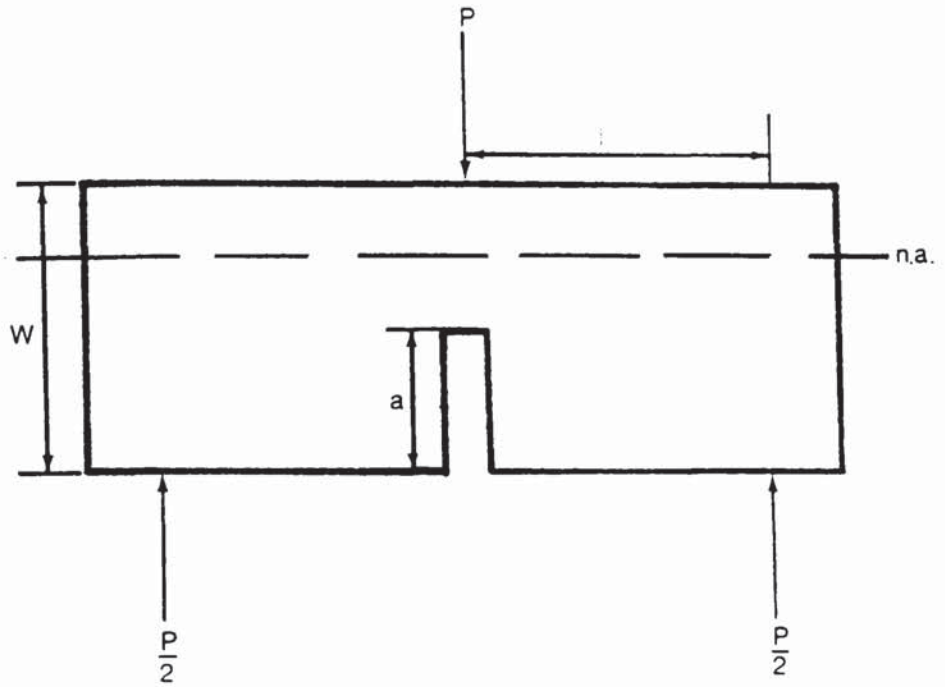

For the case of simple supports, it is assumed that there is no direct stress component ahead of the notch. Thus, the outer fibre stress is equivalent to the maximum bending stress σ_B. In accordance with the previous section,

$$\sigma_B = \frac{MY}{I} = \frac{P1\ (W - a)}{2} \cdot \frac{12}{2\ b\ (W - a)^3}$$

$$= \frac{3\ P1}{b\ (W - a)^2} \qquad (A1.9)$$

A comparison of the maximum shear stress and bending stress components ahead of the notch gives:

$$\frac{P/2\ (W - a)\ b}{3\ P1/b\ (W - a)^2} = \frac{(W - a)}{6\ 1} \qquad (A1.10)$$

For Holdsworth's work, Equation A1.10 indicates that the magnitude of the maximum shear stress will be less than 7% of the outer fibre bending stress. This figure is considered to be insignificant. As a consequence, the shear stresses have been ignored.

Thus, from Equations A1.9, 87 and 88, the outer fibre equivalent elastic stress $\bar{\sigma}_E$ is:

For Plane Stress, $$\bar{\sigma}_E = \left[\frac{3Pl}{b(W - a)^2}\right] \quad (A1.11)$$

For Plane Strain, $$\bar{\sigma}_E = \frac{1}{2{\cdot}6}\left[\frac{3Pl}{b(W - a)^2}\right] \quad (A1.12)$$

REFERENCES

Ashby, M. F., 1969, Scripta Met. 3, 837.

Ashby, M. F., 1972, Surface Sci., 31, 498.

Ashby, M. F. and Raj, R., 1975, Proc. Conf. 'The Mechanics and Physics of Fracture', Cambridge.

Ashby, M. F., Raj, R. and Gifkins, R. C., 1970, Scripta Met., 4, 737.

Bailey, R. W., 1935, Proc. Inst. of Mech. Eng., 131.

Baird, J. D., Jamieson, A., Preston, R. R. and Cochrane, R. C., 1972, Proc. of a Meeting on 'Creep Strength in Steel and High Temperature Alloys', I.S.I. at University of Sheffield, 207.

Baker, T. J. and Charles, J. A., 1973, J.I.S.I., 187.

Baluffi, R. W. and Seigle, L. L., 1955, Acta Met., 3, 170.

Baluffi, R. W. and Seigle, L. L., 1957, Acta Met., 5, 449.

Barnby, J. T., 1974, Eng. Fract. Mech., Vol. 6, 627.

Barnby, J. T., 1975, Eng. Fract. Mech., Vol. 7, 299.

Barnby, J. T. and Nicholson, R. D., 1977, J. Mat. Sci., 12, 2099.

Batte, A. D., 1975, C. A. Parsons Report MET 75-128.

Bilby, B. A., Cottrell, A. H. and Swinden, K. H., 1963, Proc. Roy. Soc., A272, 304.

Bleakney, H. H., 1952, Canadian J. Tech., 30, 340.

Boettner, R. C. and Robertson, W. D., 1961, Trans. A.I.M.E. 221, 613.

Bolton, C. J., 1977, C.E.G.B. Report RD/B/N4182.

Boniszweski, T. and Eaton, N. F., 1969, Met. Sci. J., 3, 103.

Bowring, P., Davies, P.W. and Wilshire, B., 1968, Met. Sci. J., 2, 168.

Branch, G.D., Carlton, R. G. and Murphy, M. C., 1973, Int. Conf. on 'Creep and Fatigue in Elevated Temperature Applications', Philadelphia/Sheffield, Paper C224/73.

British Standards, B.S.1500: 1958.
B.S.1515: 1965.
B.S.3915: 1965.
B.S.5500: 1976.
B.S.3100: 1976.
B.S.1504: 1976.

British Steel Corporation, 1970, Physical Met.Research Group, Report No. PM.6041/-/70/A.

Brookes, P. E., Kirby, N. and Burke, W.T., 1959-60, J.I.M., 88, 500.

Brown Jnr., W. G. and Sachs, G., 1951, N.A.C.A. Tech. Note 2433.

Brown Jnr., W. F. and Srawley, J. E., 1966, A.S.T.M. S.T.P.410.

Brown Jnr., W. F., Jones, M. H. and Newman, D. P., 1952, A.S.T.M. S.T.P.128.

Cane, B. J., 1974, C.E.G.B. Report RD/L/R1892.

Cane, B. J., 1976, Conference on Grain Boundaries, Jersey, Paper E7.

Cane, B. J., 1978, C.E.G.B. Report RD/L/R1979.

C.E.G.B. Standard 66011, Issue 3, 1974.

Chan, R., 1978, to be published.

Chang, H. C. and Grant, N. J., 1956, Trans. A.I.M.E., 206, 544.

Chen, C. W. and Machlin, E. S., 1956, Acta Met., 4, 655.

Chitty, A. and Duval, D., 1963, A.S.M.E./A.S.T.M./I.Mech.E., Joint Int. Conference on Creep, New York/London, Paper 2.

Coble, R. L., 1963, J. Appl. Phys., 34, 1679.

Cocks, G. J. and Taplin, D. M. R., 1967, Metallurgia, 75, 229.

Cottrell, A. H., 1961, I.S.I. Spec. Rep. 69, 281; I.S.I. Symposium 'Structural Processes in Creep', London.

Crossland, I. G., 1974, Phs. Stat. Sol., 23, 231; 1975, 'Proc. Int. Conf. on Phy. Met. of Reactor Fuel Elements', B.N.L.

Crossland, I. G. and Clay, B. D. 1977, Acta Met., Vol. 25, 929.

Davies, E. A., 1960, Trans. A.I.M.E. J. Basic Eng. 82, No.2.

Davies, E. A. and Manjoine, M. J., 1953, A.S.T.M. S.T.P. 128, 67.

Davies, C. K. L., Davies, P. W. and Wilshire, B., 1965, Phil. Mag. 12, 827.

Davies, P. W. and Wilshire, B., 1961, I.S.I. Symposium 'Structural Processes in Creep', London.

Davies, P. W. and Wilshire, B., 1965, Phil. Mag. 11, 189.

Davies, P. W. and Dutton, R., 1966, Acta Met. 14, 1138.

Davies, P. W. and Williams, K. R., 1969, Met. Sci. J., 3, 48.

Diehl, H., Granacher, J. and Wiegand, H., 1975, Arch. Eisenhuttenwes, 46(7), 461.

Dimelfi, R. J. and Nix, W. D., 1977, Int. J. of Frac. 13, 341.

Dobes, F. and Cadek, J., 1970, Scripta Met. 4, 1005.

Dugdale, D. S., 1960, J. Mech. Phys. Solids, 8, 100.

Dunlop, G. L., Edmonds, D. V. and Honeycombe, R. W. K., 1972, Proc. of a Meeting on 'Creep Strength in Steel and High Temperature Alloys', I.S.I. at University of Sheffield, 222.

Dunlop, G. L. and Honeycombe, R. W. K., 1976, Metal Science, 124; 1977, Metal Science, 495.

Durelli, A. J. and Murray, W. M., 1943, Proc. S.E.S.A. Vol. 1, No. 1.

Dyson, B. F. and McLean, D., 1972, Metal Sci. J., 6,220.

Dyson, B. F., Gibbons, T. B. and McLean, D., 1975, N.P.L. Report IMS30.

Dyson, B. F. and Taplin, D. M. R., 1976, Conference on Grain Boundaries, Jersey, Paper E23.

Dyson, B. F. and Rodgers, M. J., 1977, to be published.

Dyson, B. F. and McLean, D., 1977a, Metal Sci. J., 37.

Eborall, R., 1954, Proc. Symposium on 'Creep and Fracture of Metals at High Temperature', Teddington.

E.R.A. Report 2A/470; 1974.

Ellison, E. G. and Walton, D., 1973, Int. Conf. on 'Creep and Fatigue in Elevated Temperature Applications', Philadelphia/Sheffield, Paper C173/73.

Ellison, E. G. and Neate, G. J., 1976, Conference on 'Failure of Components Operating in the Creep Range', I. Mech. E., Paper C110/76.

Ellison, E. G. and Harper, M. P., 1978, J. of Strain Analysis, Vol. 13, 1.

Eshelby, J. D., Frank, F. C. and Nabarro, F. R. N., 1951, Phil. Mag., 42, 351.

Evans, H. E., 1969, Met. Sci. J., 3, 33.

Ewing, D. J. F. and Richards, C. E., 1973, C.E.G.B. Report RD/L/N237/72.

Ewing, D. J. F., 1977, C.E.G.B. Report RD/L/N233/76.

Featherstone, P. F., Procter, E. and Hother-Lushington, S., 1973, Int. Conf. on 'Creep and Fatigue in Elevated Temperature Applications', Philadelphia/Sheffield, Paper C189/73.

Findlay, G. E., 1973, ibid, Paper C223/73.

Fleck, R. G., Beevers, C. J. and Taplin, D.M.R., 1975, Met. Sci. J., 9, 49.

Floreen, S., 1975, Met. Trans. A., Vol. 6A.

Formby, C. L., 1972, C.E.G.B. Report RD/B/R2067.

Freed, C. N. and Krafft, J. M., 1966, J. Materials, 1, No.4, 770.

Freeman, B. L., 1977, C.E.G.B. Report SSD/MID/R54/77.

Garofalo, F., 1959, Proc. A.S.T.M., 957.

Garofalo, F., 1965, 'Fundamentals of Creep and Creep Rupture in Metals', MacMillan, New York.

Gifkins, R. C., 1959, 'Fracture', M.I.T. Press and Wiley, New York.

Gifkins, R. C., 1965, Proc. Conf. on Fracture, Tewkesbury.

Gittins, A., 1967, Met. Sci. J. 1, 214.

Gittins, A. and Williams, H. D., 1967, Phil. Mag. 16, 142.

Glen, J. and Barr, R. R., 1966, Proc. of 'High Temperature Properties of Steels', B.I.S.R.A./I.S.I. Conference, Eastbourne, 225.

Goldhoff, R. M. and Brothers, A. J., 1968, A.S.M.E. J. Basic Eng. 37.

Goldhoff, R. M., 1963, Proc. Joint Int. Conf. on Creep, London/New York.

Goodall, I. W. and Chubb, E. J., 1974, C.E.G.B. Report RD/B/N3227.

Goodall, I. W. and Chubb, E. J., 1976, Int. J. of Fracture, Vol. 12, No.2.

Goodier, J. N. and Field, F. A., 1963, 'Fracture of Solids', ed. Druckner and Gilman, New York (Academic Press), 103.

Grant, N. J., 1971, 'Fracture An Advanced Treatise Vol. III', Academic Press, New York/London.

Greenfield, P. and Vickers, W., 1967, J. Nucl. Mat., 22, 77.

Greenhough, A. P., 1952, Phil. Mag., 43, 1075.

Greenwood, G. W., 1969, Phil. Mag., 19, 423.

Greenwood, G. W., 1973, Int. Conf. on Metals, Cambridge, 91.

Greenwood, G. W., Fracture 1977, (ed. D.M.R. Taplin) Vol. 1, University of Waterloo Press, Canada.

Greenwood, J. N., 1952, J.I.S.I., 171, 380.

Greenwood, J. N., Miller, D. R. and Suiter, J. W., 1954, Acta Met., 2, 150.

Griffith, A. A., 1920, Phil. Trans. R. Soc. A221, 163.

Griffiths, J.R., Owen, D.R.J., 1971, J. Mech. Phys. Solids, 19, 419.

Haigh, J. R., 1973, C.E.G.B. Report RD/L/R1833.

Haigh, J. R., 1974, C.E.G.B. Report RD/L/N118/74.

Haigh, J. R. and Laidler, W., 1975, C.E.R.L. Lab. Memo. LM/MATS/011.

Haigh, J. R. and Laidler, W., 1978, C.E.G.B. Report RD/L/N174/77.

Haigh, J. R. and Richards, C. E., 1974, C.E.G.B. Report RD/L/M461.

Hanink, D. K. and Vorhees, H. R., 1962, A.S.M.E. J. Basic Eng., 84, 233.

Harper, P., 1968, C.E.G.B. Report.

Harper, M. P. and Ellison, E. G., 1977, J. of Strain Analysis, Vol. 12, No.3.

Harris, J. E., Haddrell, V. J. and Rickards, G. A., 1962, J. Nuclear Mats., 6, 144.

Harris, J. E., 1965, Trans. A.I.M.E. 233, 1509.

Harris, J. E., Tucker, M. O. and Greenwood, G. W., 1973, CEGB Report RD/B/N2873.

Harris, J. E., Tucker, M. O. and Greenwood, G. W., 1974, Met. Sci. J., 8, 310

Harrison, C. B. and Sandor, G. N., 1971, Eng. Frac. Mech.

Heald, P. T., Spink, G. M. and Worthington, P. J., 1972, Metal Sci. and Eng., 10.

Heaton, M. D. and Chan, R., 1976, C.E.G.B. Report NW/SSD/RN/91/76.

Heaton, M. D., 1978, to be published.

Hellan, K., 1975, Int. J. Mech. Science, 17, 369.

Henderson, J. and Snedden, J. D., 1972, J. Inst. Met., 100, 163.

Henderson, J. and Ferguson, F. R., 1977, Metals Technology, 296.

Hensler, J. H. and Cullen, G. V., 1964, J. Australian Inst. Met., 9, 38.

Herring, C., 1950, J. Appl. Phys., 21, 437.

Highton, J., 1978, Private Communication.

Hirth, J. P. 1972, Met. Trans. Vol. 3, 3047.

Holdsworth, S. R., 1974, G.E.C. Turbine Gen. Ltd. Report W/QM/1974/19.

Holdsworth, S. R., 1977, ibid.

Hondros, E. D. and McLean, D., 1976, 'Grain Boundary Structure and Properties', Academic Press.

Hoznek, J., 1967, Vasipari Kutato Intezet Evkonyve, 3, 223.

Hull, D. and Rimmer, D. E., 1959, Phil. Mag., 4, 673.

Inglis, C. E., 1913, Trans. Instn. Nav. Archit., LV, 1, 219.

I.S.O. Standard ISO/TC 17/SC 10.

I.S.O. Standard 3755, 1976.

Intrater, J. and Machlin, E. S., 1959, Acta Met. 7, 140.

Irwin, G. R., 1957, J. Appl. Phys., 24, 361.

Irwin, G. R., 1964, Appl. Mat. Res., 3, 65.

Ivanova, V. S. and Oding, L. A., 1955, Dokl. Acad. Nauk. U.S.S.R., 103, 77.

Jackson, R. H., 1973, C.E.G.B. Report SSD/MID/N11/73.

James, L. A., 1972, Int. J. of Frac. Mech. 8.

James, L. A., 1976, Atomic Energy Review, 14, 1.

Jamieson, A., Gulvin, T. F., Baird, J. D., Barr, R. R. and Preston, R. R., 1972, Proc. of a Meeting on 'Creep Strength in Steel and High Temperature Alloys', I.S.I. at University of Sheffield, 207.

Jenkins, C. H. M., Bucknall, E. H. and Jenkinson, E. A., 1944, J.I.M. 70, 657.

Jenkins, C. H. M., 1954, Proc. Symposium on 'Creep and Fracture of Metals at High Temperature', Teddington.

Johanneson, T. and Tholen, A., 1972, Met. Sci. J. 6, 189.

Johnson, A. E., Henderson, J. and Khan, B., 1962, 'Complex Stress Creep Relaxation and Fracture of Metallic Alloys', H.M.S.O., Edinburgh.

Johnson, A. E. and Henderson, J., 1962, ibid.

Johnson, A. E. and Khan, B., 1965, Metallurgia, 72, (430), 55.

Johnson, A. E., 1967, 'Recent Progress in Applied Mechanics', ed. B. Broberg, 289, John Wiley.

Johnson, R. F. and Glen, J., 1972, Proc. of a Meeting on 'Creep Strength in Steel and High Temperature Alloys', I.S.I. at University of Sheffield, 207.

Kachanov, M., 1958, Izr. Adad. Nauk., 555R OTN, No.8, 26.

Kaufman, J. G., Bogardus, K. O., Mauney, D. A. and Malcolm, R. C., 1976, A.S.T.M. S.T.P.590.

Kawasaki, T. and Horiguchi, M., 1977, Eng. Frac. Mech. Vol.9, 879.

Kenyon, J. L., 1973, Int. Conf. on 'Creep and Fatigue in Elevated Temperature Applications', Philadelphia/Sheffield, Paper C156/73.

Kirsch, B., 1898, Z, VDI.

Kolorz, A. and Orths, K., 1965, Giesserei, 52, (18), 542.

Kolosoff, G., 1910, Dissertation, St. Petersburg.

Kooistra, L. F., Tucker, J. T. and Coulter, E. E., 1960, Trans. A.S.M.E. J. Basic Eng., 82.

Koterazawa, R., 1975, Int. J. of Frac. 11, 1060.

Kramer, D. and Machlin, E. S., 1958, Acta Met., 6, 454.

Laidler, W., Whatmough, I. G. and Gray, I., 1974, C.E.G.B. Report NW/SSD/SR/373/74.

Laidler, W. and Haigh, J. R., 1976, C.E.R.L. Lab. Memo LM/MATS/049.

Landes, J. D. and Begley, J. A., 1976, A.S.T.M. S.T.P.590.

Lewis, D. J. and Hellen, T. K., 1973, C.E.G.B. Report RD/B/N2870.

Machlin, E. S., 1956, Trans. A.I.M.E. 206, 106.

Manjoine, M. J., 1962, A.S.M.E. J. Basic Eng. 220.

Manjoine, M. J., 1963, Proc. Joint Int. Conf. on Creep, London/New York.

Martin, D. C. and Blomfield, J. A., 1974, C.E.G.B. Report SSD/SW/M577.

Mellor, H. G., 1975, C.E.G.B. Report 443/75/M.

Mindlin, R. G., 1948, Proc. S.E.S.A. Vol.5, No.2.

Mirkin, I. L., Trusov, L. P. and Petropavlovskaya, Z. N., 1965, Metal Science and Heat Treatment, (11-12), 704.

Money, H. A. and Neate, G. J., 1971, C.E.G.B. Report SSD/MID/N/107/71.

Mullendore, A. W. and Grant, N. J., 1954, J. Metals, 6, (9), 973.

Mullendore, A. W. and Grant, N. J., 1961, 'Structural Processes in Creep', Special Rep. No. 70, I.S.I., London.

Murphy, M. C. and Branch, G. D., 1969, J.I.S.I., 207, (10), 1347.

McCann, J., Boardman, J. W. and Norton, J. F., 1973, J.I.S.I., 64.

McEvily, A. J. and Wells, C. H., 1973, Int. Conf. on 'Creep and Fatigue in Elevated Temperature Applications', Philadelphia/Sheffield, Paper C230/73.

McIntyre, P. and Priest, A. H., 1970, B.I.S.R.A. Report MG/ES/274/70.

McLean, D., 1957, "Grain Boundaries in Metals", O.U.P., London.

McLean, D., 1963, J. Australian Inst. of Metals, 8, 45.

McLean, D., Dyson, B. F. and Taplin, D.M.R., 1977, Fracture, Vol. I, ICF4, Waterloo, Canada.

McLintock, F., 1968, Int. J. Frac. Mech. 4, 101.

Nabarro, F.R.N., 1948, 'Strength of Solids', (London : The Physical Society), 75.

Nabarro, F.R.N., 1967, Phil. Mag., 16, 231.

Neale, B. K., 1972, C.E.G.B. Report RD/B/N2432.

Neate, G. J. and Siverns, M. J., 1973, Int. Conf. on 'Creep and Fatigue in Elevated Temperature Applications', Philadelphia/Sheffield, Paper C234/73.

Neate, G. J., 1974, C.E.G.B. Report SSD.MIR/R. 12/74.

Neate, G. J., 1975, C.E.G.B. Report 407/75/T.

Neate, G. J., Staddon, R. W., Procter, E., Mitchell, D. H. and Williams, H. D., 1976, C.E.G.B. Report SSD/MID/R14/76.

Neate, G. J., 1977, C.E.G.B. Report SSD/MID/M57/77.

Needham, N. G. and Greenwood, G. W., 1975, Met. Sci. J. 9, 258.

Nicholson, R. D., 1975, Ph.D. Thesis, University of Aston in Birmingham.

Nicholson, R. D. and Formby, C. L., 1975, Int. J. of Frac. Vol.11, No.4.

Nicholson, R. D. and Formby, C. L., 1976, C.E.G.B. Report RD/B/R2838.

Nikbin, K. M., Webster, G. A. and Turner, C. E., 1976, A.S.T.M. S.T.P.601.

Ohtani, R., Doi, K., Nakamura, S. and Nitta, A., 1973, J. Soc. Mat. Sci., Japan, 22, 291.

Paris, P. C. and Sih, G. C., 1964, A.S.T.M. S.T.P.381.

Penny, R. K. and Marriott, D. L., 1971, 'Design for Creep', McGraw-Hill.

Peterson, R. E., 1953 and 1975, 'Stress Concentration Design Factors', John Wiley & Sons Inc.

Pilkington, R., Hutchinson, D. and Jones, C. L., 1974, Metal Science, Vol.8.

Plumbridge, W. J. and Miller, K. J., 1972, Proc. of a Meeting on 'Creep Strength in Steel and High Temperature Alloys', I.S.I. at University of Sheffield, 207.

Pranatis, A. L. and Pound, G. M., 1955, Trans. A.I.M.E., 203, 664.

Prandtl, L., 1924, Proc. 1st Int. Congr. App. Mech., Delft, 43.

Presland, A. E. B. and Hutchinson, R. I., 1961-62, J.I.M., 90, 239.
ibid 1963-64, 92, 264.
idem 1962, 5th Int. Conf. on Electron Microscopy, New York, Paper J15.

Price, A. T., Hall, H. A. and Greenhough, A. P., 1964, Acta Met., 12, 49.

Purushothaman, P. and Tien, J. K., 1976, Scripta Metall., 10, 663.

Rao, P., Rao, V. V. P. and Pandey, M. C., 1973, J.I.S.I., 211, 801.

Ratcliffe, R. T. and Greenwood, G. W., 1965, Phil. Mag. 12, 59.

Raj, R. and Ashby, M. F., 1971, Met. Trans., 2, 1113.

Raj, R. and Ashby, M. F., 1975, Acta Met. Vol.23.

Resnick, R. and Seigle, L. L., 1955, Acta Met. 3, 605.

Reuss, A., 1930, Z. ang. Math. Mech., 10, 266.

Rice, J. R., 1968, 'Fracture - An Advanced Treatise', Academic Press, New York.

Robson, K., 1972, Conf. on 'Properties of Creep Resistant Steels', Dusseldorf, Paper 4.5.

Roes, H. L. and Witte, W., 1967, 33rd International Foundry Congress, New Delhi, Paper 11.

Rukweid, A., 1972, Met. Trans., 3, 3009.

Sachs, G. and Brown, W. F., 1953, A.S.T.M. S.T.P.128.

Sachs, G., Sessler, J. G. and Brown, W. F., 1959, A.S.T.M. S.T.P.260.

Sadananda, K. and Shaninian, P., 1978, Met. Trans. A., Vol. 9A, 79.

Sautter, F. K. and Chen, E. S., 1968, 'Oxide Dispersion Strengthening', ed. Ansell, C. S., Forden and Breach.

Schmeider, A. K., 1975, A.S.T.M. S.T.P. 125.

Seigfried, W., 1945, A.S.T.M. S.T.P. 260.

Seigfried, W., 1953, A.S.T.M. S.T.P. 128.

Sellars, C. M., 1972, Proc. of a Meeting on 'Creep Strength in Steel and High Temperature Alloys', I.S.I. at University of Sheffield, 20.

Servi, I. S. and Grant, N. J., 1951, Trans. A.I.M.E., 191, 909.

Sikka, V. K., Swinderman, R. W. and Brinkman, C. R., 1977, Met. Trans. A, Vol. 8A, 1117.

Simonen, F. A., 1973, Int. Conf. on 'Creep and Fatigue in Elevated Temperature Applications', Philadelphia/Sheffield, Paper C177/73.

Sinton, W., 1960, Electrical World, October.

Siverns, M. J. and Price, A. T., 1970, Nature, Vol. 228.

Skelton, R. P., 1975, Met. Sci. J., 9, 92.

Smith, A. I. and Murray, D., 1963, E.R.A. Report 2A/68 (Series X48).

Smith, E. and Nutting, J., 1957, J.I.S.I., 314.

Smithells, 1955, Metals Reference Book, Butterworths.

Soderberg, R., 1969, Proc. 2nd Int. Conf. on Fracture, Brighton.

Soo, J., 1974, C.E.G.B. Report RD/L/N182/74.

Soo, J., 1975, C.E.G.B. Report RD/L/N59/75.

Speight, M. V. and Harris, J. E., 1967, Met. Sci. J., 1, 83.

Speight, M. V. and Beere, W., 1975, Met. Sci. J., 9, 190.

Stroh,A. N., 1954, Proc. Roy. Soc. A233, 404.

Taira, S. and Ohtani, R., 1968, Bull. J. S. M. E., 11, No.46.

Taira, S., Ohtani, R. and Ito, T., 1971, Proc. 14th Japan Conf. on Materials Research, Kyoto, 158.

Taira, S. and Ohtani, R., 1971, 'Advances in Creep Design', Applied Science Pub. Ltd., London.

Taira, S. and Ohtani, R., 1973, Int. Conf. on 'Creep and Fatigue in Elevated Temperature Applications', Philadelphia/Sheffield, Paper C213/73.

Taplin, D. M. R., 1965, J. Aust. Inst. Met., 10, 336.

Taplin, D. M. R. and Barker, L. J., 1966, Acta Met. 14, 1527.

Taplin, D. M. R. and Gifkins, R. C., 1967, Acta Met. 15, 1967.

Taplin, D. M. R., 1969, Phil. Mag. 20, 1079.

Thornton, D. V., 1972, Conf. on 'Properties of Creep Resistant Steels', Dusseldorf, Paper 6.5.

Tipler, H. R., Taylor, L. H. and Hopkins, B. E., 1970, Metal Sci. J., 4, 167.

Tipler, H. R. and Hopkins, B. E., 1976, Metal Science, 10, (2), 47.

To, K. C., 1975, Int. J. of Frac. Mech., Vol. 11, No.4.

Toft, L. H. and Yeldham, D. E., 1976, Conf. on 'Components Operating in the Creep Range', I. Mech. E., Paper C107/76.

Townley, C. H. A., 1972, C.E.G.B. Report RD/B/N2292.

Townsend, R. D., 1971, C.E.G.B. Report RD/L/R1740.

Tuppeny, W. H., 1973, Int. Conf. on 'Creep and Fatigue in Elevated Temperature Applications', Philadelphia/Sheffield, Paper C184/73.

Van Leeuwen, H. P., 1977, Eng. Frac. Mech., Vol.9, 951.

Venkiteswaran, P. K., Bright, M. W. A. and Taplin, D. M. R., 1973, Mat. Sci. and Eng., 11, 255.

Vitek, V., 1976, C.E.G.B. Report RD/L/N34/76.

Vitek, V., 1978, C.E.G.B. Report RD/L/R1970.

Vitovec, F. H., 1972, J. Mat. Sci. 7, 615.

Voorhees, H. R. and Freeman, J. W., 1960, W.A.D.C. Report 59-470.

Voorhees, H. R., Freeman, J. W. and Herzog, J. A., 1962, J. Basic Eng., 84, 207.

Waddington, J. S. and Williams, J. A., 1967, Acta Met. 15, 1563.

Walker, E. F. and May, M. J., 1967, B.I.S.R.A. Report MG/E/307/67.

Weaver, C. W., 1958, J.I.M., 87, 126.

Weaver, C. W., 1959-60, J.I.M., 88, 296.

Webster, G. A., 1975, Conference on 'Mechanics and Physics of Fracture', Inst. of Phys., Cambridge.

Weertman, J., 1973, Scripta Met. 7, 1129.

Weertman, J., 1974, Met. Trans. Vol. 5, 1743.

Wells, A. A., 1961, Crack Propagation Symposium Proc., Cranfield College of Aeronautics, 1, 210.

Wells, A. A. and McBride, F. H., 1967, Canadian Met. Quart., Vol.6, No.4.

Westergaard, H. M., 1939, J. Appl. Mech. A49.

Williams, J. A., 1967, Phil. Mag. 15, 1289.

Williams, J. A., 1975, Proc. Conf. 'The Mechanics and Physics of Fracture', Cambridge.

Williams, J. A. and Price, A. T., 1975, Trans. A.S.M.E.

Wingrove, A. L. and Taplin, D. M. R., 1969, J. Mat. Sci., 4, 789.

Zener, C., 1948, 'Fracturing of Metals', A.S.M., Cleveland.